SOLVENT SELECTION METHODS IN AROMATIC EXTRACTION PROCESSES TOWARDS OPTIMAL AND SUSTAINABLE DESIGN CHOICES

by

Nivaar Brijmohan Pr. Eng.

(BSc Eng., MSc Eng)
University of KwaZulu-Natal

Submitted in fulfilment of the academic requirements for
the degree of Doctor of Philosophy (Chemical Engineering) in the School
of Engineering, University of KwaZulu-Natal

Durban
2023

ABSTRACT

This study presents a novel process decision-making framework that amalgamates Computer-Based Molecular Design (CAMD) of solvents using group contribution methods and artificial neural network Quantitative Structure Property Relationship (QSPR) models with Health, Safety, and Environmental (HSE) impacts using a rating-based risk assessment method. These then culminate in integrated solvent selections and process designs with relatively fixed configurations that capture the interaction of solvent choice on design alternatives, with the incorporation of sustainability measures. The objectives are to provide a platform based on systematic methods on which engineers can optimize solvent extraction processes by simultaneously considering all interlinking steps of process systems engineering from molecular design and selection to the optimization of the economics of large-scale processes, in the larger context of sustainable development.

In applying the proposed framework to the liquid-liquid extraction of aromatics from aliphatics, a selection of organic chemicals was proposed for further study as replacement solvents that meet the technological requirements for the process of aromatics extraction from alkanes and have not been conventionally considered previously for this application. Organic chemicals were screened with the use of a search algorithm based on process requirements in terms of physical properties, capacity, selectivity, and performance index, using UNIFAC-LLE. A risk assessment was constructed to further screen the identified new potential solvents using a ratings-based structure using HSE data. Thus, solvent impact in terms of sustainability were systematized in a manner that related thermodynamic theoretical predictions using molecular knowledge to that of HSE risk assessments using a benchmarking rating system.

Limitations in the group contribution models led to the need for concurrent screening methods to be used as a supplement to the predictions of UNIFAC-LLE in order to improve the robustness of the approach. As a result, a QSPR model was developed using artificial neural networks to estimate the binary interaction parameters for the temperature-dependent form of the NRTL model with the objective of using it to complement group contribution methods in the screening of potential solvents for liquid-liquid extraction processes. Parameters were regressed using experimental LLE

and VLE data and checked for consistency. Molecule structures were drawn, and descriptors determined with the use of Materials Studio. The QSPR model uses 31 descriptors as input and produced absolute average deviations of 0.23 and 0.19 for each pair of the NRTL dimensionless interaction parameterss τ_{ij} and τ_{ji} respectively. A novel method of solvent screening using these *a priori* NRTL interaction parameters is also presented in which a ratio is defined that incorporates values of the interaction parameters based on extent of ideality in relation to phase equilibria for the various binary pairs in a ternary mixture.

Validation of CAMD solvent screening results were done with the use of novel experimentally measured liquid-liquid equilibrium (LLE) phase compositions that were thermodynamically modelled for the ternary systems *n*-heptane + toluene + (butane-1,4-diol or glycerol) and *n*-nonane + *o*-xylene + (butane-1,4-diol or glycerol) at 298.2, 313.2 and 333.2 K and 0.1 MPa. *n*-Heptane represents the alkane component and toluene the aromatic component. The selectivity for the solvents studied were found to be comparable or superior to conventional solvents, but results of the ternary systems indicated that solvent capacities were poor, motivating for the use of a co-solvent to reduce solvent-to-feed ratios.

The use of 2-methyl-2,4-pentanediol as a potential co-solvent to butane-1,4-diol and glycerol was then studied in order to investigate its impact on solvent capacity in the separation of toluene from *n*-heptane via liquid-liquid extraction. To this end, quaternary liquid-liquid equilibrium (LLE) data was experimentally measured for the system *n*-heptane + toluene + (butane-1,4-diol or glycerol) + 2-methyl-2,4-pentanediol at 298.2 and 313.2 K and 0.1 MPa.

All measurements were conducted in a double-walled glass cell using the direct analytical method, and phase compositions were analysed via gas chromatography. The data was correlated using the NRTL and UNIQUAC models, which were able to suitably represent the tie-line compositions. At different molar ratios of solvent to co-solvent, the selectivity and solvent capacity were calculated and compared to that of using pure butane-1,4-diol or glycerol. It was ascertained that the pseudo ternary systems possess type I or type II behaviours depending on the molar ratio. It was observed that solvent capacity is not appreciatively improved for molar ratios that exhibit type II behaviour.

However significant increases in capacity were noted for high molar ratios producing a type I system.

Process designs were developed with the use of ASPEN Plus V10 in order to ascertain the effects of solvent choice on process economics via the use of total annual costs. The screening process in this work produced significant insights due to its holistic approach. The incorporation of factors such as solvent price, solvent loss, utilities, capital costs, health and environmental impact, showed that several of the solvents identified may be sustainable and cost-effective alternatives to conventionally used solvents. Conversion of energy sources and consumptions to equivalent carbon emissions closes the sustainability loop and associates solvent selection directly with large-scale environmental impact. In this manner, all steps of Process Systems Engineering (PSE) are combined in an approach that relates molecular solvent design with sustainable development and large-scale process optimization in a decision-making framework that may be effectively used to determine optimal design choices and inform efficient process retrofitting.

PREFACE

The research outcomes presented in this dissertation were achieved by work performed at the University of KwaZulu-Natal from January 2020 to February 2023. The work was supervised by Professor K. Moodley and Professor C. Narasigadu. This thesis is submitted as the full requirement for the degree Doctor of Philosophy (Chemical Engineering). I declare that:

1. The research reported in this thesis, except where otherwise indicated, is my original research.
2. This thesis has not been submitted for any degree or examination at any other university.
3. This thesis does not contain other persons' data, pictures, graphs or other information, unless specifically acknowledged as being sourced from other persons.
4. This thesis does not contain other persons' writing, unless specifically acknowledged as being sourced from other researchers. Where other written sources have been quoted, then:
   i. Their words have been re-written but the general information attributed to them has been referenced
   ii. Where their exact words have been used, then their writing has been placed in italics and inside quotation marks, and referenced.
5. This thesis does not contain text, graphics or tables copied and pasted from the internet, unless specifically acknowledged, and the source being detailed in the thesis and in the References sections.
6. As this thesis is submitted in the journal manuscript format, under Rule DR9 c) and d) of the University of KwaZulu-Natal, only manuscript versions of published or unpublished work are presented. These citations for these publications are listed under "Contributions to publications" and their description are outlined in the Introduction section.

N. Brijmohan

As supervisor of this candidate, I approve this thesis for submission:

Professor K. Moodley

Professor C. Narasigadu

CONTRIBUTION TO PUBLICATIONS

Details of contribution to publications and manuscripts: I designed all studies, conducted all experimental measurements, performed all calculations, wrote and submitted all manuscripts, and did all peer-reviewed corrections with suggestions and guidance from Professor Moodley and Professor Narasigadu.

1. Brijmohan, N., Moodley, K., & Narasigadu, C. (2021). Identification and Screening of Potential Organic Solvents for the Liquid–Liquid Extraction of Aromatics. *Org. Process Res. Dev.*, 25, 2230–2248. https://doi.org/10.1021/acs.oprd.1c00106

2. Brijmohan, N., Moodley, K., & Narasigadu, C. (2022a). Ternary Liquid–Liquid Equilibrium Data for the *n*-Heptane + Toluene + (Butane-1,4-diol or Glycerol) Systems at 298.2, 313.2, and 333.2 K and 0.1 MPa. *J. Chem. Eng. Data*, 67, 975–983. https://doi.org/10.1021/acs.jced.2c00011

3. Brijmohan, N., Moodley, K., & Narasigadu, C. (2022b). Liquid–Liquid Extraction of Toluene from *n*-Heptane Using Butane-1,4-diol + 2-Methyl-pentane-2,4-diol Liquid Mixtures. *J. Chem. Eng. Data*, 67, 3177–3185. https://doi.org/10.1021/acs.jced.2c00498

4. Brijmohan, N., Moodley, K., & Narasigadu, C. (2022c). Ternary Liquid–Liquid Equilibrium Data for the *n*-Nonane + o-Xylene + (Butane-1,4-diol or Glycerol) Systems at (298.2, 313.2, 333.2) K and 0.1 MPa. *J. Chem. Eng. Data*, 67, 3468–3475. https://doi.org/10.1021/acs.jced.2c00530

5. Brijmohan, N., Moodley, K., & Narasigadu, C. (2023a). Use of Glycerol + 2-Methylpentane-2,4-diol Liquid Mixtures in the Separation of Toluene from *n*-Heptane via Liquid–Liquid Extraction. *J. Chem. Eng. Data.* https://doi.org/10.1021/acs.jced.3c00041

6. Brijmohan, N., Moodley, K., & Narasigadu, C. (2023b). Technoeconomic Analysis and Feasibility of Co-Solvent Mixtures in the Liquid-Liquid Extraction of Aromatics. *Manuscript final revision submitted for publication together with peer reviewed minor corrections*.

7. Brijmohan, N., Moodley, K., & Narasigadu, C. (2023c). The *A Priori* Screening of Potential Organic Solvents Using Artificial Neural Networks. *Fluid Phase Equilib*, 577, 113960. https://doi.org/10.1016/j.fluid.2023.113960

ACKNOWLEDGEMENTS

The following people are acknowledged for their contribution to this work:

- My supervisors, Professor K. Moodley and Professor C. Narasigadu for their expert knowledge, guidance, and support.

- The technical staff at the School of Chemical Engineering, University of KwaZulu-Natal (UKZN) for their work done on the equipment used in this project.

- Dr Madison Lasich for including this work as part of Research Programme CHEM1028 which allowed me access to a high performance computer cluster.

- The Centre for High Performance Computing (CHPC) for access to the software Materials Studio.

- Fellow UKZN colleagues and postgrad students for their encouragement and assistance.

- Parents (Santash and Kala) and sibling (Nivedita) for a lifetime of support and motivation.

- My wife Tarana for her love, care, patience, and inspiration.

TABLE OF CONTENTS

ABSTRACT i

PREFACE iv

CONTRIBUTION TO PUBLICATIONS v

ACKNOWLEDGEMENTS vii

LIST OF FIGURES xii

LIST OF TABLES xxiii

NOMENCLATURE xxvi

CHAPTER ONE 1

Introduction and Background 1

1.1. Research Vision 1

1.2. Research Scope and Objectives 2

1.3. Organization of Thesis 6

1.4. Aromatic Compounds 7

1.5. Aromatic Production Processes 9

1.5.1 Azeotropic Distillation 10

1.5.2 Extractive Distillation 10

1.5.3 Liquid-Liquid Extraction 10

1.6. Commercial Liquid-Liquid Extraction Processes 11

1.7 Characterization of Solvents 13

1.7.1 Potential Solvent Screening 15

1.8 Thermodynamics Review 16

1.8.1 Phase Equilibrium 17

1.8.2 Thermodynamic Models 20

1.8.3 Limiting Activity Coefficients 24
1.9. Liquid-Liquid Equilibrium (LLE) Representation 25
1.9.1 Type 1 and 2 Systems 27
1.9.2 Type 3 Systems 28
1.9.3 Identification of Plait Point 29
1.10 LLE Measurements in Literature 30
1.11. LLE Measurement Techniques 32
1.11.1. Direct Analytical Method 32
1.11.2 Turbidity method 32
1.11.3 Titration method 33
1.11.4 Continuous Measurement Method 33
1.12. References 34
CHAPTER TWO 40
The Identification and Screening of Potential Organic Solvents for the Liquid-Liquid Extraction of Aromatics 40
2.1. Introduction 41
2.2. Identification of Potential Solvents 43
2.2.1 Physical Property Screening 43
2.2.2 Solvent Identification Results 47
2.3. Risk Assessment 56
2.3.1 Health, Safety and Environmental Impact Benchmarking 56
2.3.2 Risk Assessment Results 57
2.4. Process Economics 65
2.4.1 Process Design 65
2.4.2 Process Economics 78

2.5. Conclusion 84

2.7. Declaration 85

2.8. References 85

CHAPTER THREE 91

Experimental Liquid-Liquid Equilibrium Data for Alkane and Aromatic Mixtures in Solvent and Co-Solvent Mixtures 91

3.1. Introduction 92

3.2. Theory 96

3.2.1 Data Correlation 96

3.2.2 Selectivity and Distribution Coefficient. 99

3.3 Material and Methods 99

3.3.1 Chemicals 99

3.3.2 Equipment. 100

3.4. Results and Discussion 102

3.5. Conclusion 158

3.7. References 159

CHAPTER FOUR 165

Technoeconomic Analysis and Feasibility of Co-Solvent Mixtures in the Liquid-Liquid Extraction of Aromatics 165

4.1. Introduction 165

4.2. Solvent Extraction – Co-Solvent Mixtures 168

4.2.1 Process Design 168

4.2.2 Thermodynamic Modeling 173

4.2.3 Process Economics 178

4.3. Conclusion 184

4.6. References 184

CHAPTER FIVE 188

The *A Priori* Screening of Potential Organic Solvents Using Artificial Neural Networks 188

5.1. Introduction 188

5.2. Nonrandom Two-Liquid Activity Coefficient Model 191

5.3. Prediction of Interaction Parameters for Solvent Screening 192

5.3.1 Creation of Database and Regression of Binary Interaction Parameters 192

5.3.2 Calculation and Reduction of Descriptors 196

5.3.3 Development of QSPR Model and Artificial Neural Network 202

5.4. Model Results and Discussion 204

5.5. Conclusion 214

5.6. Acknowledgements 215

5.7. Declaration 215

5.8. References 215

CHAPTER SIX 220

CULMINATING DISCUSSION 220

CHAPTER SEVEN 225

CONCLUSIONS 225

CHAPTER EIGHT 228

RECOMMENDATIONS 228

APPENDIX A 229

APPENDIX B 252

LIST OF FIGURES

Figure 1.1: Dimensions of Sustainable Development (Ruiz-Mercado et al., 2012) 5
Figure 1.2: Uses of BTEX chemicals (Wiley Critical Content, 2007) 8
Figure 1.3: Illustration of the various elements in a liquid – liquid extraction system..... 11
Figure 1.4: Generic process flow diagram of the sulfolane process; E – extraction; ED – extractive distillation; RC – recovery column (Kaiser et al., 2019) 12
Figure 1.5: Composition plotting on a ternary LLE diagram (Treybal, 1963). 26
Figure 1.6: Type 1 ternary system in equilibrium (Treybal, 1963). 27
Figure 1.7 Type 2 ternary system in equilibrium (Treybal, 1963)..... 28
Figure 1.8: Type 3 ternary system in equilibrium (Treybal, 1963). 28
Figure 1.9: The plait point determined from graphical Coolidge method (Treybal, 1963). 29
Figure 2.1. Search algorithm to determine solvent suitability in terms of physical properties, selectivity, and capacity. 46
Figure 2.2. Solvent capacity comparison at 298.15 K and 101.33 kPa with respect to toluene content in the raffinate phase for conventional solvents from literature against new potential solvents predicted with UNIFAC-LLE, for the ternary system *n*-heptane (1) /toluene (2) / solvent (3). × – NMP (Nagpal & Rawat, 1981); ▲ – Sulfolane (Tripathi et al., 1975); + – NFM (DongChu, HongQi, & Hao, 2007); ■ – DMSO (Farghi & Kaddami, 2008); ● – Ethyl Cyanoacetate (Predicted); △ – Diethylenetriamine (Predicted); ● – 2-Methyl-2,4-pentanediol (Predicted); ● – 3-Hydroxypropanenitrile (Predicted); ● – 1,3-Butanediol (Predicted), partially obscured by diethanolamine; ◇ – 1,4-Butanediol (Predicted); ● – Diethanolamine (Predicted); ● – Glycerol (Predicted). 50
Figure 2.3. Selectivity comparison at 298.15 K and 101.33 kPa with respect to toluene content in the raffinate phase for conventional solvents from literature against new potential solvents predicted with UNIFAC-LLE, for the ternary system *n*-heptane (1) /toluene (2) / solvent (3). × – NMP (Nagpal & Rawat, 1981); ▲ – Sulfolane (Tripathi et al., 1975); + – NFM (DongChu, HongQi, & Hao, 2007); ■ – DMSO (Farghi & Kaddami, 2008); ● – Ethyl Cyanoacetate (Predicted); △ – Diethylenetriamine (Predicted); ● – 2-Methyl-2,4-pentanediol (Predicted); ● – 3-Hydroxypropanenitrile (Predicted); ● – 1,3-Butanediol (Predicted); ◇ – 1,4-Butanediol (Predicted); ● – Diethanolamine (Predicted); ● – Glycerol (Predicted)..... 51

Figure 2.4. Performance index comparison at 298.15 K and 101.33 kPa with respect to toluene content in the raffinate phase for conventional solvents from literature against new potential solvents predicted with UNIFAC-LLE, for the ternary system *n*-heptane (1) /toluene (2) / solvent (3). × – NMP (Mohsen-Nia et al., 2005); ▲ – Sulfolane (Tripathi et al., 1975); + – NFM (DongChu, HongQi, & Hao, 2007); ■ – DMSO (Farghi & Kaddami, 2008); ● – Ethyl Cyanoacetate (Predicted); ● – Diethylenetriamine (Predicted); ● – 2-Methyl-2,4-pentanediol (Predicted); ● – 3-Hydroxypropanenitrile (Predicted); ● – 1,3-Butanediol (Predicted); ◇ – 1,4-Butanediol (Predicted); ● – Diethanolamine (Predicted); ● – Glycerol (Predicted). 52
Figure 2.5. Solvent capacity comparison at 313.15 K and 101.33 kPa with respect to toluene content in the raffinate phase for conventional solvents from literature against new potential solvents predicted with UNIFAC-LLE. × – NMP (Nagpal & Rawat, 1981); ▲ – Sulfolane (Tripathi et al., 1975); + – NFM (DongChu, HongQi, & Hao, 2007); ■ – Tetraethylene Glycol (Saha et al., 1998a); ● – Ethyl Cyanoacetate (Predicted); △ – Diethylenetriamine (Predicted); ● – 2-Methyl-2,4-pentanediol (Predicted); ● – 3-Hydroxypropanenitrile (Predicted); ● – 1,3-Butanediol (Predicted), partially obscured by diethanolamine; ◇ – 1,4-Butanediol (Predicted); ● – Diethanolamine (Predicted); ● – Glycerol (Predicted). 53
Figure 2.6. Selectivity comparison at 313.15 K and 101.33 kPa with respect to toluene content in the raffinate phase for conventional solvents from literature against new potential solvents predicted with UNIFAC-LLE, for the ternary system *n*-heptane (1) /toluene (2) / solvent (3). × – NMP (Nagpal & Rawat, 1981); ▲–Sulfolane (Tripathi et al., 1975); + – NFM (DongChu, HongQi, & Hao, 2007); ■ – Tetraethylene Glycol (Saha et al., 1998a); ● – Ethyl Cyanoacetate (Predicted); △ – Diethylenetriamine (Predicted); ● – 2-Methyl-2,4-pentanediol (Predicted); ● – 3-Hydroxypropanenitrile (Predicted); ● – 1,3-Butanediol (Predicted); ◇ – 1,4-Butanediol (Predicted); ● – Diethanolamine (Predicted); ● – Glycerol (Predicted)..... 54
Figure 2.7. Performance index comparison at 313.15 K and 101.33 kPa with respect to toluene content in the raffinate phase for conventional solvents from literature against new potential solvents predicted with UNIFAC-LLE, for the ternary system *n*-heptane (1) /toluene (2) / solvent (3). × – NMP (Nagpal & Rawat, 1981); ▲–Sulfolane (Tripathi et al., 1975); + – NFM (DongChu, HongQi, & Hao, 2007); ■ – Tetraethylene Glycol (Saha et al., 1998a); ● – Ethyl Cyanoacetate (Predicted); △ – Diethylenetriamine (Predicted); ● – 2-Methyl-2,4-pentanediol (Predicted); ● –

3-Hydroxypropanenitrile (Predicted); ● – 1,3-Butanediol (Predicted); ◇ – 1,4-Butanediol (Predicted); ● – Diethanolamine (Predicted); ● – Glycerol (Predicted)..... 55
Figure 2.8. Overall scores of conventional solvents and new potential solvents, consisting of individual scores for health, safety, and environment. 63
Figure 2.9. Solvent capacity comparison at 298.15 K and 101.33 kPa with respect to toluene content in the raffinate phase for conventional solvents from literature against glycerol and glycerol + ethanol mixtures to demonstrate the increase in solvent capacity; predicted with UNIFAC-LLE for the ternary system *n*-heptane (1) /toluene (2) / solvent (3). × – NMP (Nagpal & Rawat, 1981); ▲–Sulfolane (Tripathi et al., 1975); + – NFM (DongChu, HongQi, & Hao, 2007); ■ – DMSO (Farghi & Kaddami, 2008); ● – Glycerol + Ethanol (Predicted); ● – Glycerol (Predicted)..... 65
Figure 2.10. Literature LLE data, × (Řehák & Dreiseitlová, 2006), ▲ (Gao et al., 2015), for the system toluene + ethylene glycol at 101.33 kPa compared to UNIFAC (LL) predictions (■). ... 68
Figure 2.11. Literature LLE data, × (Lesek & Mandík, 1982), for the system toluene + diethylene glycol at 101.33 kPa compared to UNIFAC (LL) predictions (■)..... 68
Figure 2.12. Literature LLE data, ▲ (Folas et al., 2006), for the system toluene + triethylene glycol at 101.33 kPa compared to UNIFAC (LL) predictions (■)..... 69
Figure 2.13. Isobaric vapor-liquid equilibrium data (x-y) at 101.33 kPa for the systems: (a) Toluene + Sulfolane, (b) Toluene + NFM (Huang et al., 2008), (c) Toluene + DMSO (Zhao et al., 2014), (d) Toluene + Glycerol (UNIFAC), (e) Toluene + Ethanol (Oracz & Kolasińska, 1987), (f) Toluene + 2-Methyl-2,4-pentanediol (UNIFAC), (g) Toluene + 1,4-Butanediol (UNIFAC). 72
Figure 2.14. Flowsheet for the optimized extraction process with the use of sulfolane as the solvent. 73
Figure 2.15. Flowsheet for the optimized extraction process with the use of NFM as the solvent. 73
Figure 2.16. Flowsheet for the optimized extraction process with the use of DMSO as the solvent. 74
Figure 2.17. Flowsheet for the optimized extraction process with the use of hexylene glycol as the solvent. 75
Figure 2.18. Flowsheet for the optimized extraction process with the use of 1,4-butanediol as the solvent. 75

Figure 2.19. Flowsheet for the optimized extraction process with the use of glycerol as the solvent. 76
Figure 2.20. T-*x*,*y* data for the toluene + ethanol system at (a) 0.1 atm and (b) 5 atm. 77
Figure 2.21. Flowsheet for the optimized extraction process with the use of glycerol + ethanol as the solvent. 78
Figure 2.22. Comparison of capital costs and payback times for the conventional and potential solvents. 81
Figure 2.23. Comparison of operating costs for the conventional and potential solvents. 82
Figure 2.24. Comparison of total annual cost (TAC) for the conventional and potential solvents 83
Figure 2.25. Comparison of CO_2 emissions for each solvent using coal or natural gas as an energy source with heat recovery potential 84
Figure 3.1. Comparison of the mutual solubility (mole basis) with reference data for the systems: (a) toluene (1) + 1,4-butanediol (2); ☐ – this work; × - ref (Lesek & Mandík, 1982), ▲ – ref (Fan et al., 2020). (b) toluene (1) + glycerol (2); ☐ – this work; ▲ – ref (Fan et al., 2020)..... 104
Figure 3.2. Binary liquid-liquid equilibrium data (mole basis) for the systems: (a) *o*-xylene (1) + butane-1,4-diol (2); ☐ – this work; (b) *o*-xylene (1) + glycerol (2); ☐ – this work..... 105
Figure 3.3. Liquid-liquid equilibrium mole composition data for the *n*-heptane (1) + toluene (2) + 1,4-butanediol (3) system at 298.2 K and 0.1 MPa. × – experimental (this study); -●- – NRTL model; ■ – tie -line feed composition 117
Figure 3.4. Liquid-liquid equilibrium mole composition data for the *n*-heptane (1) + toluene (2) + 1,4-butanediol (3) system at 313.2 K and 0.1 MPa. × – experimental (this study); -●- – NRTL model; ■ – tie -line feed composition 118
Figure 3.5. Liquid-liquid equilibrium mole composition data for the *n*-heptane (1) + toluene (2) + 1,4-butanediol (3) system at 333.2 K and 0.1 MPa. × – experimental (this study); -●- – NRTL model; ■ – tie -line feed composition 119
Figure 3.6. Liquid-liquid equilibrium mole composition data for the *n*-heptane (1) + toluene (2) + glycerol (3) system at 298.2 K and 0.1 MPa. × – experimental (this study); -●- – NRTL model; ■ – tie-line feed composition..... 120

Figure 3.7. Liquid-liquid equilibrium mole composition data for the *n*-heptane (1) + toluene (2) + glycerol (3) system at 313.2 K and 0.1 MPa. × – experimental (this study); -●- – NRTL model; ■ – tie-line feed composition..... 121
Figure 3.8. Liquid-liquid equilibrium mole composition data for the *n*-heptane (1) + toluene (2) + glycerol (3) system at 333.2 K and 0.1 MPa. × – experimental (this study); -●- – NRTL model; ■ – tie-line feed composition..... 122
Figure 3.9. Ternary liquid-liquid equilibrium data (mole basis) for the *n*-nonane (1) + *o*-xylene (2) + butane-1,4-diol (3) system at 298.2 K and 0.1 MPa. × – experimental (this study); -○- – NRTL model; ■ – tie -line feed composition 123
Figure 3.10. Ternary liquid-liquid equilibrium data (mole basis) for the *n*-nonane (1) + *o*-xylene (2) + butane-1,4-diol (3) system at 313.2 K and 0.1 MPa. × – experimental (this study); -○- – NRTL model; ■ – tie -line feed composition..... 124
Figure 3.11. Ternary liquid-liquid equilibrium data (mole basis) for the *n*-nonane (1) + *o*-xylene (2) + butane-1,4-diol (3) system at 333.2 K and 0.1 MPa. × – experimental (this study); -○- – NRTL model; ■ – tie -line feed composition..... 125
Figure 3.12. Ternary liquid-liquid equilibrium data (mole basis) for the *n*-nonane (1) + *o*-xylene (2) + glycerol (3) system at 298.2 K and 0.1 MPa. × – experimental (this study); -○- – NRTL model; ■ – tie-line feed composition 126
Figure 3.13. Ternary liquid-liquid equilibrium data (mole basis) for the *n*-nonane (1) + *o*-xylene (2) + glycerol (3) system at 313.2 K and 0.1 MPa. × – experimental (this study); -○- – NRTL model; ■ – tie-line feed composition 127
Figure 3.14. Ternary liquid-liquid equilibrium data (mole basis) for the *n*-nonane (1) + *o*-xylene (2) + glycerol (3) system at 333.2 K and 0.1 MPa. × – experimental (this study); -○- – NRTL model; ■ – tie-line feed composition 128
Figure 3.15. Pseudo ternary liquid -liquid equilibrium mole composition data for the *n*-heptane (1) + toluene (2) + 1,4-butanediol (3) + 2-methyl-2,4-pentanediol (4) system at 298.2 K and 0.1 MPa for 3:1 solvent: co-solvent ratio. × – experimental (this study); -●- – NRTL model; ■ – tie -line feed composition..... 129
Figure 3.16. Pseudo ternary liquid -liquid equilibrium mole composition data for the *n*-heptane (1) + toluene (2) + 1,4-butanediol (3) + 2-methyl-2,4-pentanediol (4) system at 313.2 K and 0.1 MPa

for 3:1 solvent: co-solvent ratio. × – experimental (this study); -●- – NRTL model; ■ – tie -line feed composition 130
Figure 3.17. Pseudo ternary liquid -liquid equilibrium mole composition data for the *n*-heptane (1) + toluene (2) + 1,4-butanediol (3) + 2-methyl-2,4-pentanediol (4) system at 298.2 K and 0.1 MPa for 1:1 solvent: co-solvent ratio. × – experimental (this study); -●- – NRTL model; ■ – tie -line feed composition 131
Figure 3.18. Pseudo ternary liquid -liquid equilibrium mole composition data for the *n*-heptane (1) + toluene (2) + 1,4-butanediol (3) + 2-methyl-2,4-pentanediol (4) system at 313.2 K and 0.1 MPa for 1:1 solvent: co-solvent ratio. × – experimental (this study); -●- – NRTL model; ■ – tie -line feed composition 132
Figure 3.19. Pseudo ternary liquid -liquid equilibrium mole composition data for the *n*-heptane (1) + toluene (2) + 1,4-butanediol (3) + 2-methyl-2,4-pentanediol (4) system at 298.2 K and 0.1 MPa for 1:3 solvent: co-solvent ratio. × – experimental (this study); -●- – NRTL model; ■ – tie-line feed composition; ▲ - plait point 133
Figure 3.20. Pseudo ternary liquid-liquid equilibrium mole composition data for the *n*-heptane (1) + toluene (2) + 1,4-butanediol (3) + 2-methyl-2,4-pentanediol (4) system at 313.2 K and 0.1 MPa for 1:3 solvent: co-solvent ratio. × – experimental (this study); -●- – NRTL model; ■ – tie-line feed composition; ▲ - plait point 134
Figure 3.21. Liquid-liquid equilibrium (pseudo ternary) mole composition data for the system *n*-heptane (1) + toluene (2) + glycerol (3) + 2-methyl-2,4-pentanediol (4) at 298.2 K and 0.1 MPa for 3:1 solvent: co-solvent ratio. × – experimental (this study); -○- – NRTL model; △ - UNIQUAC model; ■ – tie -line feed composition 135
Figure 3.22. Liquid-liquid equilibrium (pseudo ternary) mole composition data for the system *n*-heptane (1) + toluene (2) + glycerol (3) + 2-methyl-2,4-pentanediol (4) at 313.2 K and 0.1 MPa for 3:1 solvent: co-solvent ratio. × – experimental (this study); -○- – NRTL model; △ - UNIQUAC model; ■ – tie -line feed composition 136
Figure 3.23. Liquid-liquid equilibrium (pseudo ternary) mole composition data for the system *n*-heptane (1) + toluene (2) + glycerol (3) + 2-methyl-2,4-pentanediol (4) at 298.2 K and 0.1 MPa for 1:1 solvent: co-solvent ratio. × – experimental (this study); -○- – NRTL model; △ - UNIQUAC model; ■ – tie -line feed composition 137

Figure 3.24. Liquid-liquid equilibrium (pseudo ternary) mole composition data for the system *n*-heptane (1) + toluene (2) + glycerol (3) + 2-methyl-2,4-pentanediol (4) at 313.2 K and 0.1 MPa for 1:1 solvent: co-solvent ratio. × – experimental (this study); -○- – NRTL model; △ - UNIQUAC model; ■ – tie -line feed composition 138
Figure 3.25. Liquid-liquid equilibrium (pseudo ternary) mole composition data for the system *n*-heptane (1) + toluene (2) + glycerol (3) + 2-methyl-2,4-pentanediol (4) at 298.2 K and 0.1 MPa for 1:3 solvent: co-solvent ratio. × – experimental (this study); -○- – NRTL model; △ - UNIQUAC model; ■ – tie-line feed composition; ▲- plait point 139
Figure 3.26. Liquid-liquid equilibrium (pseudo ternary) mole composition data for the system *n*-heptane (1) + toluene (2) + glycerol (3) + 2-methyl-2,4-pentanediol (4) at 313.2 K and 0.1 MPa for 1:3 solvent: co-solvent ratio. × – experimental (this study); -○- – NRTL model; △ - UNIQUAC model; ■ – tie-line feed composition; ▲- plait point 140
Figure 3.27. Selectivity comparison with respect to toluene content in the alkane-rich phase for the ternary system *n*-heptane (1) + toluene (2) + solvent (3) at:..... 142
Figure 3.28. Solvent capacity comparison with respect to toluene content in the alkane-rich phase for the ternary system *n*-heptane (1) + toluene (2) + solvent (3) at: 144
Figure 3.29. Selectivity comparison for the ternary systems:..... 146
Figure 3.30. Distribution coefficient (capacity) comparison for the ternary systems: 148
Figure 3.31. Selectivity comparison for the *n*-heptane (1) + toluene (2) + 1,4-butanediol (3) + 2-methyl-2,4-pentanediol (4) system with respect to toluene content in the alkane-rich phase at (a) 298.2 K and 0.1 MPa, and (b) 313.2 K and 0.1 MPa; ✳ - pure 1,4-butandiol (this work), ○ - 3:1 ratio (this work); □ - 1:1 ratio (this work); △ - 1:3 ratio (this work)..... 149
Figure 3.32. Distribution coefficient comparison for the *n*-heptane (1) + toluene (2) + 1,4-butanediol (3) + 2-methyl-2,4-pentanediol (4) system with respect to toluene content in the alkane-rich phase at (a) 298.2 K and 0.1 MPa, and (b) 313.2 K and 0.1 MPa; ✳ - pure 1,4-butandiol (this work), ○ - 3:1 ratio (this work); □ - 1:1 ratio (this work); △ - 1:3 ratio (this work)..... 150
Figure 3.33. Comparison of selectivities for the system *n*-heptane (1) + toluene (2) + glycerol (3) + 2-methyl-2,4-pentanediol (4) at (a) 298.2 K and 0.1 MPa, and (b) 313.2 K and 0.1 MPa; ✳ - pure glycerol (this work); × – NMP (Nagpal & Rawat, 1981); ▲–Sulfolane (Tripathi et al., 1975); + – NFM (DongChu, HongQi, & Hao, 2007); ■ – DMSO (Farghi & Kaddami, 2008); ● -

[mebupy]BF_4 (Meindersma et al., 2006); ▬ - [emim]$C_2H_5SO_4$ (Meindersma et al., 2006); ▭ - [mmim]$C_2H_5SO_4$ (Meindersma et al., 2006); ○ - 3:1 ratio (this work); □ - 1:1 ratio (this work); △ - 1:3 ratio (this work) 151
Figure 3.34. Comparison of distribution coefficients for system the *n*-heptane (1) + toluene (2) + glycerol (3) + 2-methyl-2,4-pentanediol (4) at (a) 298.2 K and 0.1 MPa, and (b) 313.2 K and 0.1 MPa; ✳ - pure glycerol (this work); × – NMP (Nagpal & Rawat, 1981); ▲–Sulfolane (Tripathi et al., 1975); + – NFM (DongChu, HongQi, & Hao, 2007); ■ – DMSO (Farghi & Kaddami, 2008); ● -[mebupy]BF_4 (Meindersma et al., 2006); ◇ - [emim]$C_2H_5SO_4$ (Meindersma et al., 2006); ▭ - [mmim]$C_2H_5SO_4$ (Meindersma et al., 2006); ○ - 3:1 ratio (this work); □ - 1:1 ratio (this work); △ - 1:3 ratio (this work) 152
Figure 4.1. Flowsheet for the optimized extraction process with the use of 1,4-butanediol + hexylene glycol as the solvent mixture; compositions reported as wt%. 171
Figure 4.2. Flowsheet for the optimized extraction process with the use of glycerol + hexylene glycol as the solvent mixture; compositions reported as wt%. 171
Figure 4.3. Comparison of experimental selectivity data for the systems: 175
Figure 4.4. Comparison of experimental capacity data for the systems: 176
Figure 4.5. Validation of Sulfolane process by comparison of ASPEN Plus V10 simulated data against experimental data for the system *n*-heptane + toluene + sulfolane at 298.2 K and 101.3 kPa; × - Ashcroft et al. (1982); ▲ - Tripathi et al. (1975); ○ - ASPEN simulated extraction column profile 177
Figure 4.6. Payback times and capital costs for proposed co-solvent mixtures with conventional solvents. 180
Figure 4.7. Total annual costs and utilities (operating costs) for proposed co-solvent mixtures with conventional solvents prior to heat integration. 182
Figure 4.8. Total annual costs and utilities (operating costs) for proposed co-solvent mixtures with conventional solvents. 182
Figure 4.9. Energy intensity (kJ/kg) for proposed co-solvent mixtures with conventional solvents 183
Figure 4.10. Carbon emissions associated with energy consumption together with heat recovery potential for co-solvent and conventional solvents. 183

Figure 5.1: Regressed binary interaction parameters of the final dataset represented on miscible and partly miscible regions; solid line indicates phase boundary separation. 195
Figure 5.2: Percentage distribution of functional groups for compounds in database..... 196
Figure 5.3: Percentage area projection of molecule onto the *x*-*y* plane 198
Figure 5.4: Comparison of binary interaction parameter (τ_{ij}) determined from experimental data to correlated parameters 209
Figure 5.5: Residuals of correlated binary interaction parameter (τ_{ij}) against parameters determined from experimental data 209
Figure 5.6: Comparison of binary interaction parameter (τ_{ji}) determined from experimental data to correlated parameters 210
Figure 5.7: Residuals of correlated binary interaction parameter (τ_{ji}) against parameters determined from experimental data 210
Figure 5.8: Comparison of binary interaction parameter (τ_{ij}) for cross-validated subset (external test set) 211
Figure 5.9: Comparison of binary interaction parameter (τ_{ji}) for cross-validated subset (external test set) 211
Figure 5.10: Comparison of τ_{ij} R^2 and correlation coefficient (unpermuted and permuted) for randomized vector output of 40 trials 212
Figure 5.11: Comparison of τ_{ji}, R^2 and correlation coefficient (unpermuted and permuted) for randomized vector output of 40 trials 213
Figure 6.1.: Flowchart illustrating the process synthesis framework that captures the interaction of solvent choice on design alternatives with the incorporation of sustainability measures..... 221
Figure A1: Temperature calibration plot of cell 1 temperature sensor. 229
Figure A2: Temperature deviation plot of cell 1 temperature sensor. 230
Figure A3: GC detector calibration graph of *n*-heptane (1) + toluene (2) (*n*-heptane dilute region) 234
Figure A4: GC detector calibration graph of *n*-heptane (1) + toluene (2) (toluene dilute region) 234
Figure A5: Composition deviation plot for the *n*-heptane (1) + toluene (2) system 235
Figure A6: GC detector calibration graph of toluene (1) + 1,4-butanediol (2) (toluene dilute region) 235

Figure A7: GC detector calibration graph of toluene (1) + 1,4-butanediol (2) (1,4-butanediol dilute region) 236
Figure A8: Composition deviation plot for the toluene (1) + 1,4-butanediol (2) system 236
..... 237
Figure A9: GC detector calibration graph of toluene (1) + glycerol (2) (toluene dilute region) 237
Figure A10: GC detector calibration graph of toluene (1) + glycerol (2) (glycerol dilute region) 237
Figure A11: Composition deviation plot for the toluene (1) + glycerol (2) system 238
Figure A12: GC detector calibration graph of *n*-nonane (1) + *o*-xylene (2) (*n*-nonane dilute region) 238
Figure A13: GC detector calibration graph of *n*-nonane (1) + *o*-xylene (2) (*o*-xylene dilute region) 239
Figure A14: Composition deviation plot for the *n*-nonane (1) + *o*-xylene (2) system 239
Figure A15: GC detector calibration graph of *o*-xylene (1) + 1,4-butanediol (2) (*o*-xylene dilute region) 240
Figure A16: GC detector calibration graph of *o*-xylene (1) + 1,4-butanediol (2) (1,4-butanediol dilute region) 240
Figure A17: Composition deviation plot for the *o*-xylene (1) + 1,4-butanediol (2) system 241
Figure A18: GC detector calibration graph of *o*-xylene (1) + glycerol (2) (*o*-xylene dilute region) 241
Figure A19: GC detector calibration graph of *o*-xylene (1) + glycerol (2) (glycerol dilute region) 242
Figure A20: Composition deviation plot for the *o*-xylene (1) + glycerol (2) system 242
Figure A21: GC detector calibration graph of *n*-heptane (1) + toluene (2) (*n*-heptane dilute region) 243
Figure A22: GC detector calibration graph of *n*-heptane (1) + toluene (2) (toluene dilute region) 243
Figure A23: Composition deviation plot for the *n*-heptane (1) + toluene (2) system 244
Figure A24: GC detector calibration graph of toluene (1) + 1,4-butanediol (2) (toluene dilute region) 244

Figure A25: GC detector calibration graph of toluene (1) + 1,4-butanediol (2) (1,4-butanediol dilute region) 245
Figure A26: Composition deviation plot for the toluene (1) + 1,4-butanediol (2) system 245
Figure A27: GC detector calibration graph of toluene (1) + 2-methyl-2,4-pentanediol (2) (toluene dilute region) 246
Figure A28: GC detector calibration graph of toluene (1) + 2-methyl-2,4-pentanediol (2) (2-methyl-2,4-pentanediol dilute region) 246
Figure A29: Composition deviation plot for the toluene (1) + 2-methyl-2,4-pentanediol (2) system 247
Figure A30: GC detector calibration graph of *n*-heptane (1) + toluene (2) (n-heptane dilute region) 247
Figure A31: GC detector calibration graph of *n*-heptane (1) + toluene (2) (toluene dilute region) 248
Figure A32: Composition deviation plot for the *n*-heptane (1) + toluene (2) system 248
Figure A33: GC detector calibration graph of toluene (1) + glycerol (2) (toluene dilute region) 249
Figure A34: GC detector calibration graph of toluene (1) + glycerol (2) (glycerol dilute region) 249
Figure A35: Composition deviation plot for the toluene (1) + glycerol (2) system 250
Figure A36: GC detector calibration graph of toluene (1) + 2-methyl-2,4-pentanediol (2) (toluene dilute region) 250
Figure A37: GC calibration graph of toluene (1) + 2-methyl-2,4-pentanediol (2) (2-methyl-2,4-pentanediol dilute region) 251
Figure A38: Composition deviation plot for the toluene (1) + 2-methyl-2,4-pentanediol (2) system 251

LIST OF TABLES

Table 1.1: Summary of existing separation techniques (Weissermel & Arpe, 2003)..... 9
Table 1.2: Processes used for extraction of aromatics (Lo & Baird, 2000)..... 13
Table 1.3: List of experimental measurements available in literature..... 30
Table 1.4: Acronyms used in Table 1.3..... 31
Table 2.1. Feedstock components to aromatics extraction unit with selected physical properties. 43
Table 2.2. Comparison of physical properties of conventional solvents to new potential solvents at 298.15 K and 101.33 kPa (Aspen Plus, 2004; Canales and Brennecke, 2016; Green and Perry, 2008; Yaws, 2014, 2015). 48
Table 2.3. Summary of occupational health, safety, and environmental hazards of conventional and potential solvents. 59
Table 2.4. Solvent prices determined from market trends and bulk supplier quotations..... 79
Table 3.1. Chemical purity analysis. 100
Table 3.2. Experimental liquid-liquid equilibrium data (mole basis) for the *n*-heptane (1) + toluene (2) + 1,4-butanediol (3) system at (298.2, 313.2 and 333.2) K and 0.1 MPa.[a] 106
Table 3.3. Experimental liquid-liquid equilibrium data (mole basis) for the *n*-heptane (1) + toluene (2) + glycerol (3) system at (298.2, 313.2 and 333.2) K and 0.1 MPa.[a] 107
Table 3.4. Experimentally determined liquid-liquid equilibrium data (mole basis) for the *n*-nonane (1) + *o*-xylene (2) + butane-1,4-diol (3) system at (298.2, 313.2 and 333.2) K and 0.1 MPa.[a].. 108
Table 3.5. Experimentally determined liquid-liquid equilibrium data (mole basis) for the *n*-nonane (1) + *o*-xylene (2) + glycerol (3) system at (298.2, 313.2 and 333.2) K and 0.1 MPa.[a] 109
Table 3.6. Experimental liquid-liquid equilibrium data (mole basis) for the *n*-heptane (1) + toluene (2) + 1,4-butanediol (3) + 2-methyl-2,4-pentanediol (4) system at 298.2 K and 0.1 MPa.[a]..... 110
Table 3.7. Experimental liquid-liquid equilibrium data (mole basis) for the *n*-heptane (1) + toluene (2) + 1,4-butanediol (3) + 2-methyl-2,4-pentanediol (4) system at 313.2 K and 0.1 MPa.[a]..... 111
Table 3.8. Experimentally determined liquid-liquid equilibrium data (mole basis) for the system *n*-heptane (1) + toluene (2) + glycerol (3) + 2-methyl-2,4-pentanediol (4) at 298.2 K and 0.1 MPa.[a] 112

Table 3.9. Experimentally determined liquid-liquid equilibrium data (mole basis) for the system *n*-heptane (1) + toluene (2) + glycerol (3) + 2-methyl-2,4-pentanediol (4) at 313.2 K and 0.1 MPa.[a] 113
Table 3.10. NRTL and UNIQUAC T-dependent interaction parameters and root mean square deviations (RMSD) for the *n*-heptane (1) + toluene (2) + 1,4-butanediol (3) system at (298.2, 313.2 and 333.2) K and 0.1 MPa. 114
Table 3.11. NRTL and UNIQUAC T-dependent interaction parameters and root mean square deviations (RMSD) for the *n*-heptane (1) + toluene (2) + glycerol (3) system at (298.2, 313.2 and 333.2) K and 0.1 MPa. 114
Table 3.12. T-dependent binary interaction parameters for the NRTL and UNIQUAC models with root mean square deviations (RMSD) for the *n*-nonane (1) + *o*-xylene (2) + butane-1,4-diol (3) system at (298.2, 313.2 and 333.2) K and 0.1 MPa. 114
Table 3.13. T-dependent binary interaction parameters for the NRTL and UNIQUAC models with root mean square deviations (RMSD) for the *n*-nonane (1) + o-xylene (2) + glycerol (3) system at (298.2, 313.2 and 333.2) K and 0.1 MPa. 115
Table 3.14. NRTL and UNIQUAC T-dependent interaction parameters and root mean square deviations (RMSD) for the *n*-heptane (1) + toluene (2) + 1,4-butanediol (3) + 2-methyl-2,4-pentanediol (4) system at (298.2 and 313.2) K and 0.1 MPa..... 115
Table 3.15. NRTL and UNIQUAC model T-dependent interaction parameters together with root mean square deviations (RMSD) for the system *n*-heptane (1) + toluene (2) + glycerol (3) + 2-methyl-2,4-pentanediol (4) at (298.2 and 313.2) K and 0.1 MPa. 116
Table 3.16. Structural parameters for the UNIQUAC model: r (relative molecular volume) together with q (relative molecular surface area)..... 116
Table 3.17. Comparison of binary interaction parameters from binary, ternary, and quaternary data for the NRTL and UNIQUAC models for at 298.2 K for the system *n*-heptane (1) + toluene (2) + glycerol (3)..... 117
Table 4.1: Comparison of Simulation Results for Co-Solvent Mixtures and Conventional Solvents 170
Table 4.2: Equipment Specifications of Solvent Extraction and Distillation (Recovery) Columns 172
Table 4.3: Equipment Specifications of Heat Exchangers..... 173

Table 4.4: Binary interaction parameters for the NRTL model 178
Table 5.1: Correlation matrix of descriptors used as the input vector to the QSPR model 200
Table 5.2: Final list of descriptors used as input to ANN model with definitions 206
Table 5.3: Statistical parameters of AAN model; CV – cross validation 212
Table 5.4: Calculated δ values for the system *n*-heptane (1)-toluene (2)-solvent (3) 214
Table B1: Artificial neural network hidden layer weightings for τ_{ij} 252
Table B2: Artificial neural network hidden layer weightings for τ_{ji} 254
Table B3: Artificial neural network output layer weightings 256
Table B4: QSPR descriptors for chemicals used in input vector 257

NOMENCLATURE

English Letters

A_i*	Peak area response as determined through gas chromatography analysis.
D*	Required parameter in Renon and Prausnitz's (1968) LLE charts
F_i	Response factor
f	Fugacity [kPa]
$\hat{f}_i$	Fugacity in solution for component i [kPa]
G	Specific or molar Gibbs energy [J/mol]
$\overline{G}$	Partial molar Gibbs energy [J/mol]
G_{ij}	Parameter in Renon and Prausnitz's (1968) NRTL activity coefficient model
g_{ij} - g_{ii}	Energy interaction parameter between components in Renon and Prausnitz's (1968) NRTL model [J/mol]
H	Enthalpy [J/mol]
l_i	Parameter in Abrams and Prausnitz's (1975) UNIQUAC activity coefficient model
K	Distribution coefficient
M	Denotes a thermodynamic property in general
n	Number of moles
P	Pressure of the system [kPa]
PI	Performance index
q_i	Area parameter of a pure component in Abrams and Prausnitz's (1975) UNIQUAC activity coefficient model
q'_i	Area parameter of a pure component in Anderson and Prausnitz's (1978) modified UNIQUAC activity coefficient model
R	Universal gas constant [J/mol.K]
r_i	Volume parameter of a pure component in Abrams and Prausnitz's (1975) UNIQUAC activity coefficient model

rmsd	Root mean squared deviation
S	Entropy [J/mol.K]
*S**	Required parameter in Renon and Prausnitz's (1968) LLE charts
S_{ij}	Selectivity
S_P	Solvent capacity
T	Temperature of the system [^{0}C or K]
u_{ij} - u_{ii}	Energy interaction parameter between components in Abrams and Prausnitz's (1975) UNIQUAC activity coefficient model [J/mol]
V	Specific or molar volume [cm^3/mol]
X	Composition or mole fraction in the liquid phase
Y	Composition or mole fraction in the vapour phase
Z	Coordination number in Abrams and Prausnitz's (1975) UNIQUAC activity coefficient model

Greek Letters

α_{ij}	Parameter signifying non-randomness in Renon and Prausnitz's (1968) NRTL activity coefficient model
δ	Characterizes a residual (e.g. δP)
Γ_i	Constant of integration that is temperature dependent
γ	Activity coefficient
∞	Infinite dilution
μ_i	Chemical potential of component *i*
θ_i	Area fraction in Abrams and Prausnitz's (1975) UNIQUAC activity coefficient model
θ'_i	Area fraction in Anderson and Prausnitz's (1978) modified UNIQUAC activity coefficient model
τ_{ij}	Dimensionless interaction parameter in Renon and Prausnitz's (1968) NRTL activity coefficient model

Subscript

1	Represents component 1
2	Represents component 2
3	Represents component 3
Ad	Represents an absolute deviation
C	Represents a critical property
Calc	Represents a calculated value
Exp	Represents an experimental value
R	Represents a reduced property

Superscripts

C	Signifies a combinatorial property for the UNIQUAC model of Abrams and Prausnitz's (1975) UNIQUAC activity coefficient model
E	Represents an excess property
L	Represents a liquid phase
α	Represents a particular thermodynamic phase
β	Represents a particular thermodynamic phase or separation factor
π	Represents a particular thermodynamic phase

1

CHAPTER ONE

Introduction and Background

1.1. Research Vision

The work of chemical engineers has historically been most concentrated at the latter stages of the Process Systems Engineering (PSE) framework. The role of transforming the findings of chemists with regards to molecular structures and lab-scale synthesis methods into large-scale production and manufacturing processes occupies a significant part of the domain of chemical engineering. However, each step of PSE such as product development, lab-scale experimental results, pilot studies, market research, process design, computer simulations, logistical considerations, and finally macro-scale production, are explicably linked. The focus of chemical engineering as a discipline on process design, simulation, and optimization may result in industrial operational strategies that are suboptimal. It would greatly benefit industrial practitioners to function within decision-making frameworks in which all steps of PSE are considered simultaneously. Grossmann & Westerberg (2000) have established the necessity of chemical engineers being able to link computer-aided process design and operation at an industrial level, to that of research and development at the molecular level.

Group contribution methods are common empirical and semi-empirical models that are used to relate microscopic behaviour to macroscopic levels, which allow for the prediction of physical properties and thermodynamic quantities, which are then used in process development as the bridge between chemistry and engineering. The development of process units is done with the

view to conform to governmental regulations and societal expectations regarding health, safety, and environmental impact.

The aim of this thesis is the development of a novel integrated decision-making framework that encompasses the core aspects of PSE with regards to solvent selection and identification of new solvents, linking molecular design with process operations. There is considerable interaction between choice of solvent and industrial process design and development. It is required that there be efficient and reliable methods of screening solvents, considering the vast number of existing solvents, and the potential solvents that have yet to be studied, in order to improve the sustainability of chemical processes. The ACS Green Chemistry Institute has identified optimal solvent selection, and detection of new alternatives, as part of the top five priorities of green chemistry research (Henderson et al., 2011). The case considered for exploration of the integrated decision-making framework centres around the classic problem of reducing the energy requirements for the separation of aliphatics from aromatics in petroleum processing.

1.2. Research Scope and Objectives

The purpose of a solvent in general terms is to act as an agent for the selective dissolution of a particular solute. Industrial processes use millions of tons of solvents worldwide in numerous industries that encompass the petrochemical, pharmaceutical, biotechnology, and chemical process industries, with demand steadily increasing. Solvents are used in numerous applications that include fluid separations (liquid-liquid extraction, gas absorption, extractive distillation), crystallization, dissolution and separation of solid components, and the facilitation of chemical reactions (reaction equilibrium conversion improvement, increasing of reaction rate).

Solvents are commonly classified depending on their chemical make-up, with molecular solvents forming the bulk of industrial applications, mainly consisting of water and organic compounds such as ketones, alcohols, esters, amines and nitriles. These solvents are further categorized depending on whether the molecule is polar or nonpolar, with the definition being extended to polar protic solvents such as water and methanol, and polar aprotic solvents such as acetonitrile.

Another category of solvents is that of switchable solvents, where the polarity and physical characteristics of the solvents are changed through a reversible process. Supercritical CO_2 and gas

expanded liquids are examples of switchable solvents (Jessop & Subramaniam, 2007). Ionic liquids are another class of solvents that have been widely studied as a separation agent, which exist as molten salt at room temperature, and are made up of a cation and anion.
The search for alternative solvents is motivated by the need to improve economic performance in terms of capital and operating costs, as well as reduce the impact on the environment, while complying with stricter regulations with regards to health and safety.

Liquid-liquid extraction is a technique that strongly depends on a variety of solvent characteristics on a molecular level to achieve a particular separation objective, that is interlinked with macro-scale process considerations such as operating costs, energy consumption, health, safety, and environmental impact. Developing a decision-making structure for this application is motivated by the strong interconnections in each step of PSE by the impact of solvent selection. The focus in this thesis is therefore on liquid-liquid extraction as the primary application to which a solvent selection structure is developed. The case study to which this decision-making framework will be applied is that of the separation of aromatics from aliphatics, which appears to be the most studied context of liquid-liquid extraction in the open literature, with suitable solvents being studied since the 1960s. This case study allows for a variety of comparisons to be made due to the wide availability of literature data, and therefore serves as a benchmark and effective illustration for the solvent selection and identification of new solvents decision-making structure.

The increasing focus on the replacement of commonly used solvents in liquid-liquid extraction processes with environmentally friendly solvents plays an important role in improving process sustainability. Ionic liquids have generally been proposed as a more environmentally friendly alternative to volatile organic solvents, however, there have been engineering challenges related to industrial application and adoption (Meindersma et al., 2010). In this regard, the proposal of replacing existing solvents requires a methodology and system of assessing what constitutes a sustainable solvent within the context of PSE. Generally, the sustainability of solvents can be considered in terms of EHS (environmental, health, and safety), the production of solvents from renewable materials (e.g., bioalcohols), or the use of supercritical fluids that have little direct environmental impact.

Modifications to liquid-liquid extraction processes may return economic benefits if the choice of the replacement solvent results in lower recirculation rates with the same process yield. This manifests as reduced heating and cooling requirements in various utility consumers such as heat exchangers. This reduction in process energy streams can then be related upstream to energy resources e.g. the fuel or electricity used in steam generation in boilers. Ultimately, this would constitute to less environmentally friendly practice as these energy savings manifest in reduced carbon emissions.

Thus, organizations that utilize solvent extraction processes can benefit from the adoption of a structure that assesses the sustainability of utilizing alternative technologies. Replacing existing solvents with environmentally friendly alternatives is a step towards embracing sustainability. It is postulated that the process of solvent extraction and recovery can be assessed in the broader framework of sustainability. Sustainability benchmarks give organizations this capacity to evaluate current performance, and thereby set targets to ascertain if the impact of process and equipment modifications are increasing sustainable development. Azapagic & Perdan (2000) defined 35 metrics to classify sustainability into three main areas: environment, society, and the economy. Figure 1.1 illustrates sustainable development as being the intersection of these dimensions.

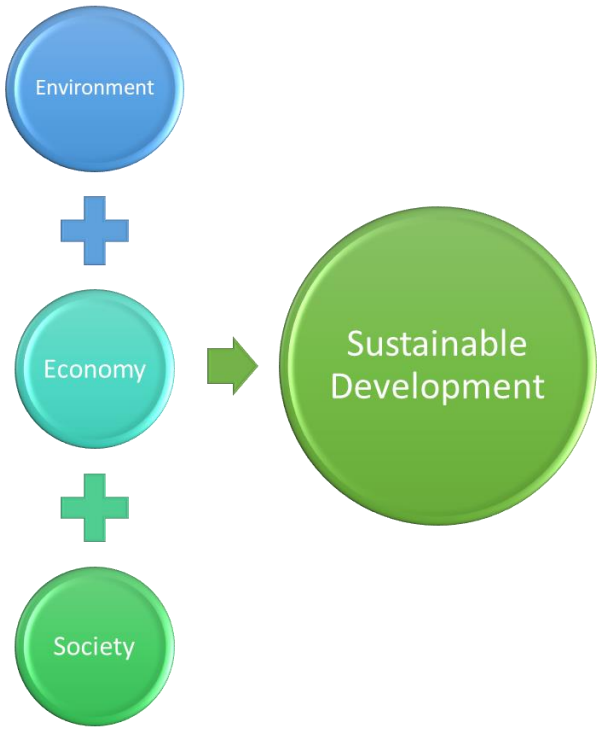

Figure 1.1: Dimensions of Sustainable Development (Ruiz-Mercado et al., 2012)

An overall perspective on the environmental impact can then be taken by combining the EHS analysis with a life-cycle analysis taken with a variety of solvents. Capello et al. (2007) performed this comparison on 26 solvents – one of which was dimethylformamide (DMF), which is used extensively in aromatics extraction. There does not appear to be a definitive study comparing the environmental impact of the spectrum of solvents used in the extraction of aromatics.

Research on various solvent types in reaction engineering and separation technologies have been ongoing for decades. The use of computer-based methods involving search algorithms have been steadily growing as a tool used to enhance solvent selection methods. Computer-based Molecular Design (CAMD) is widely used with solvents being considered in various separation methods (Ng et al., 2015; Zhou et al., 2016).

In view of the above points, the objectives of this work are to develop novel systematic methods that involved CAMD for the screening of solvents for liquid-liquid extraction processes applied to the extraction of aromatics from aliphatics. This considers existing solvents and identify new potential solvents, taking into account the strong interdependence of solvent selection on process

operation, enabling engineers to concurrently consider all PSE levels, within the context of sustainability benchmarking.

1.3. Organization of Thesis

The thesis consists of eight chapters which includes this introductory chapter – the rest of which focuses on a review of aromatic compounds and the production of aromatics from the separation from intermediate petroleum streams. Also included is a review of separation techniques and commercial liquid-liquid extraction processes, which is followed by a characterization of solvents based on physical properties. Thereafter a review of the required thermodynamic background is presented together with the representation of liquid-liquid equilibrium and a literature review of published data, followed by a review of experimental methods.

The second chapter is a publication that considers each step of PSE for the extraction of aromatics, by constructing a solvent screening procedure for new potential solvents that begins with identification via physical properties and group contribution methods. The next step is a rating-based risk assessment of the identified solvents that takes into consideration numerous HSE metrics. The final step is the development of process designs using ASPEN Plus for the new potential solvents compared to existing solvents. In this manner, the economic performance of a design choice is linked to molecular design at the first stage, with sustainability benchmarking built into the framework by consideration of the carbon emissions associated with each solvent choice and the impact of each in terms of HSE.

In Chapter 3, an amalgamation of four recent publications from this work is presented that addresses the verification of the PSE solvent screening framework with new experimental data for the new potential solvents identified that were not previously considered, and had no data available in the open literature for the systems measured as follows:

- Ternary LLE data for the system *n*-heptane + toluene + 1,4-butanediol at 298.2 K, 313.2 K, 333.2 K and 0.1 MPa
- Ternary LLE data for the system *n*-heptane + toluene + glycerol at 298.2 K, 313.2 K, 333.2 K and 0.1 MPa

- Ternary LLE data for the system *n*-nonane + *o*-xylene + 1,4-butanediol at 298.2 K, 313.2 K, 333.2 K and 0.1 MPa
- Ternary LLE data for the system *n*-nonane + *o*-xylene + glycerol at 298.2 K, 313.2 K, 333.2 K and 0.1 MPa
- Quaternary LLE data for the system *n*-heptane + toluene + 1,4-butanediol + 2-methyl-2,4-pentanediol at 298.2 K, 313.2 K and 0.1 MPa at various molar ratios of solvent:co-solvent
- Quaternary LLE data for the system *n*-heptane + toluene + glycerol + 2-methyl-2,4-pentanediol at 298.2 K, 313.2 K and 0.1 MPa at various molar ratios of solvent:co-solvent

Chapter 4 is a publication that re-evaluates the process designs in Chapter 2 using the measured equilibrium data in Chapter 3 from which an optimal solvent configuration is determined (co-solvent mixture).
Chapter 5 is the seventh and final publication in this work, and serves to address certain limitations in the systematic methods developed, with the use of a novel QSPR artificial neural network that seeks to complement the group contribution methods used in the initial stages by improving the robustness of the process. Chapters 6, 7 and 8 conclude the thesis by summarizing the main findings, achievements, and limitations of this work, and provides future directions.

1.4. Aromatic Compounds

Benzene, toluene, ethylbenzene, and xylenes (BTEX) are an important group of chemicals known as aromatics. These compounds are large-scale feedstocks and are typically obtained from gasoline streams such as petroleum naphtha, coking naphtha, and pyrolysis gasoline (Chen et al., 2017). Aromatics constitute a part of reformate, which is a desired pre-processed form of gasoline due it's high octane rating.

BTEX components are not merely regarded as petroleum by-products, and are considered important enough in the manufacturing process to justify its own treatment facility. This is due to the fact that BTEX chemicals form the basis of a number of consumer products, such as solvents, plastics, fibres and films (Wiley Critical Content, 2007). The economic value of benzene and xylenes (particularly *p*-xylene) is higher than that of toluene, and as such several processes have

been commercialized to convert toluene to benzene (hydrodealkylation) (Kaiser et al., 2019). Figure 1.2 illustrates the uses of BTEX chemicals.

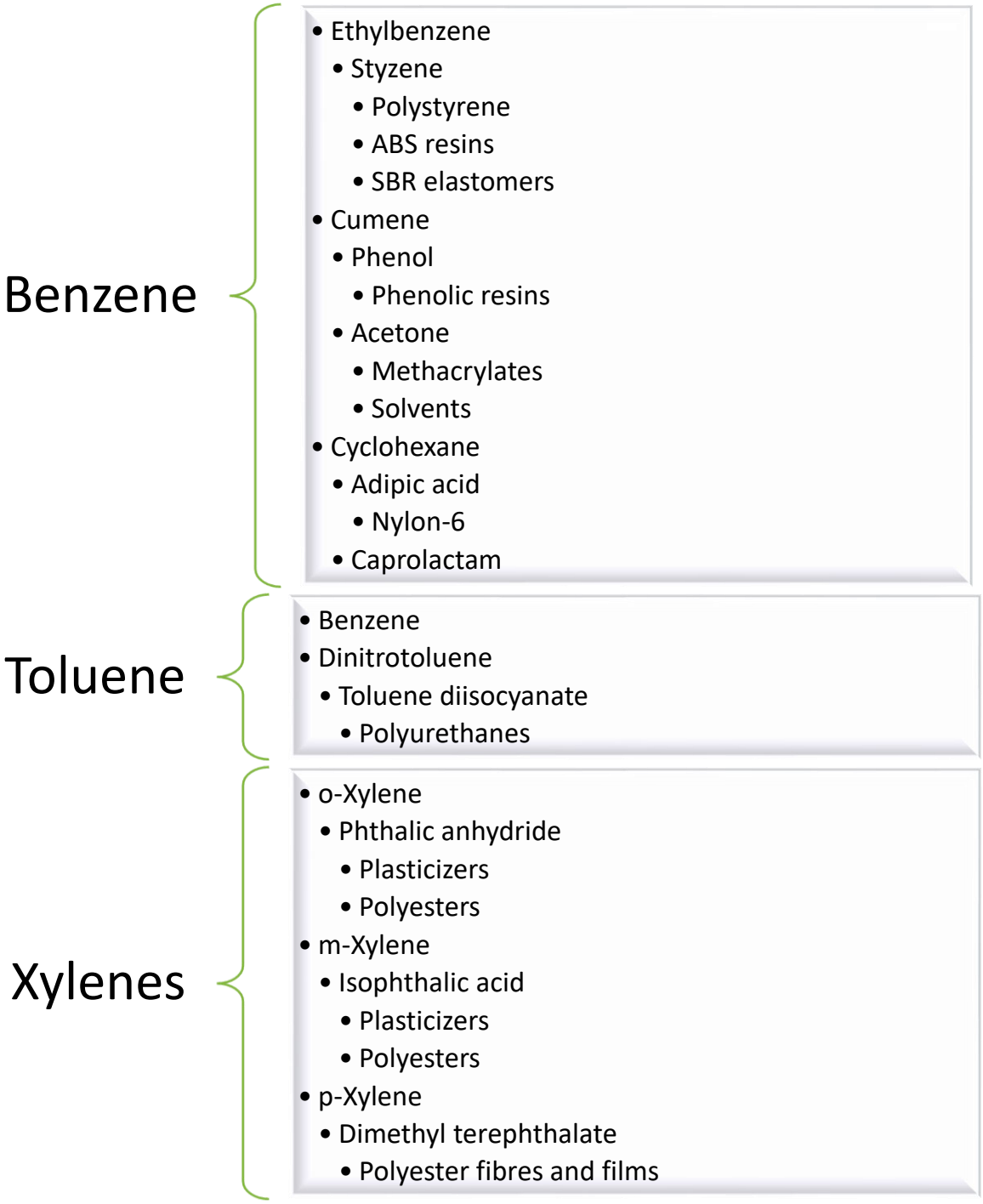

Figure 1.2: Uses of BTEX chemicals (Wiley Critical Content, 2007)

1.5. Aromatic Production Processes

Aromatic groups can be industrially produced through catalytic reformation, hydrocarbon pyrolysis, and coal pyrolysis. The manner in which aromatics are separated from these process streams depends on the concentration of aromatics therein. If the concentration is small, conventional distillation is regarded as being sufficient. With larger concentration of aromatics, the separation via conventional distillation becomes more difficult to effect due to the similarities in boiling point between the paraffinic, aromatic, and other hydrocarbon groups; as well as the formation of various azeotropes. As such, the separation design strategy depends on feed aromatic content and boiling point ranges. Table 1.1 gives an outline of separation techniques used at varying process conditions. The initialism BTX refers to mixtures of benzene, toluene, and isomers of xylene.

Table 1.1: Outline of industrial separation methods (Weissermel & Arpe, 2003).

Process	Separation Problem	Operational Requirements
Azeotropic Distillation	BTX separation from pyrolysis gasoline	High aromatic content (>90%)
Extractive Distillation	BTX separation from pyrolysis gasoline	Medium aromatic content (65–90%)
Liquid-Liquid Extraction	BTX separation from reformate gasoline	Lower aromatic content (20-65%)
Crystallization by Freezing	Isolation of *p*-xylene from *m*/*p*-mixtures	Distillate pre-separation of o-xylene and ethylbenzene from C_8 aromatic fractions
Adsorption on Solids	Isolation of *p*-xylene from C_8 aromatic fractions	Continuous, reversible, and selective adsorption

1.5.1 Azeotropic Distillation

As indicated in Table 1-1, azeotropic distillation is effective when aromatic feedstocks are greater than 90% in aromatic content. Separation of smaller boiling point azeotropes relating to cycloalkanes and alkanes are enabled by polar solvents such as amines and water.

1.5.2 Extractive Distillation

When feedstocks are of medium aromatic content (65-90%), extractive distillation can be utilized effectively. The solvent is mixed with the feed to increase the volatilities of naphthenes or aliphatics compared to aromatics, as well as volatile paraffins compared with olefins, naphthenes, alkynes and diolefins (Lei et al., 2005). This reduces the operational demands of distillation and improves economics. The feed together with the solvent is supplied to a sequence of columns in which the aliphatics are drawn as the top product in the first column and the solvent and aromatic components in the bottom and thereafter separated in subsequent columns.

1.5.3 Liquid-Liquid Extraction

Solvent extraction (liquid-liquid extraction) is used when the aromatic content in the feed is low (20-65%), but significant. The process consists of the addition of a solvent to the feed in a packed or trayed column to allow for the splitting of components amongst two immiscible phases. During blending, mass transfer occurs between a solute (aromatic compound) and the solvent. Generally, the two output streams from the extraction column are representative of the two phases formed. As illustrated in Figure 1.3, The bottom product is known as the extract and is rich in the aromatic and solvent components. The top product is the raffinate and is the residual feed rich in the non-aromatic components (Delancey, 2013).

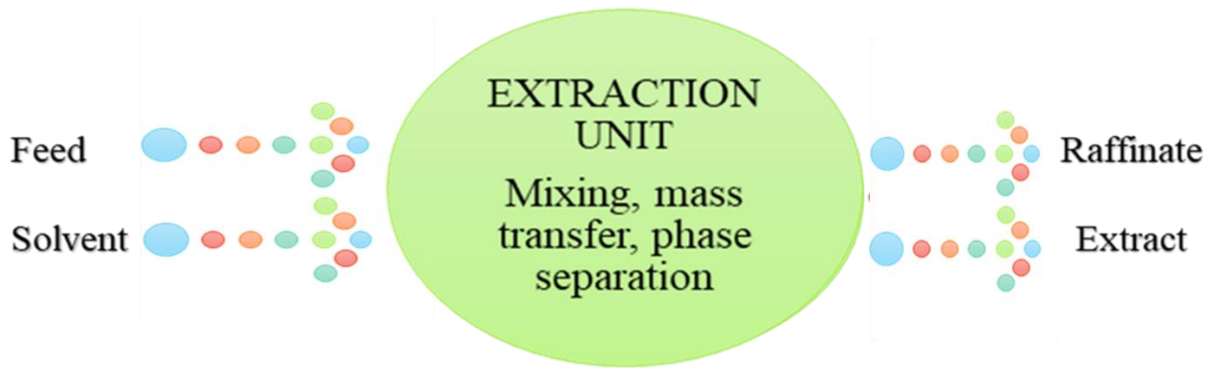

Figure 1.3: Illustration of the various elements in a liquid – liquid extraction system

1.6. Commercial Liquid-Liquid Extraction Processes

There are several types of commercial liquid-liquid extraction processes which follow a structure of liquid extraction and thereafter solvent recovery via distillation. The distinction between these processes is the type of solvent used.

Initial commercial liquid-liquid extraction processes such as the UOP Udex process (which is still used) utilized a glycol solvent (Wiley Critical Content, 2007). Diethylene and dipropylene glycol were originally used in the process, with triethylene glycol used later on as it improved solvent performance. Tetraethylene glycol was used as a further improvement.

The Shell Sulfolane process is most commonly used due to a good balance in the solvent's (sulfolane) properties (Meyers, 2016). The high density and high boiling point enables easier separation between hydrocarbon streams. Figure 1.4 gives the general process flow of the sulfolane process.

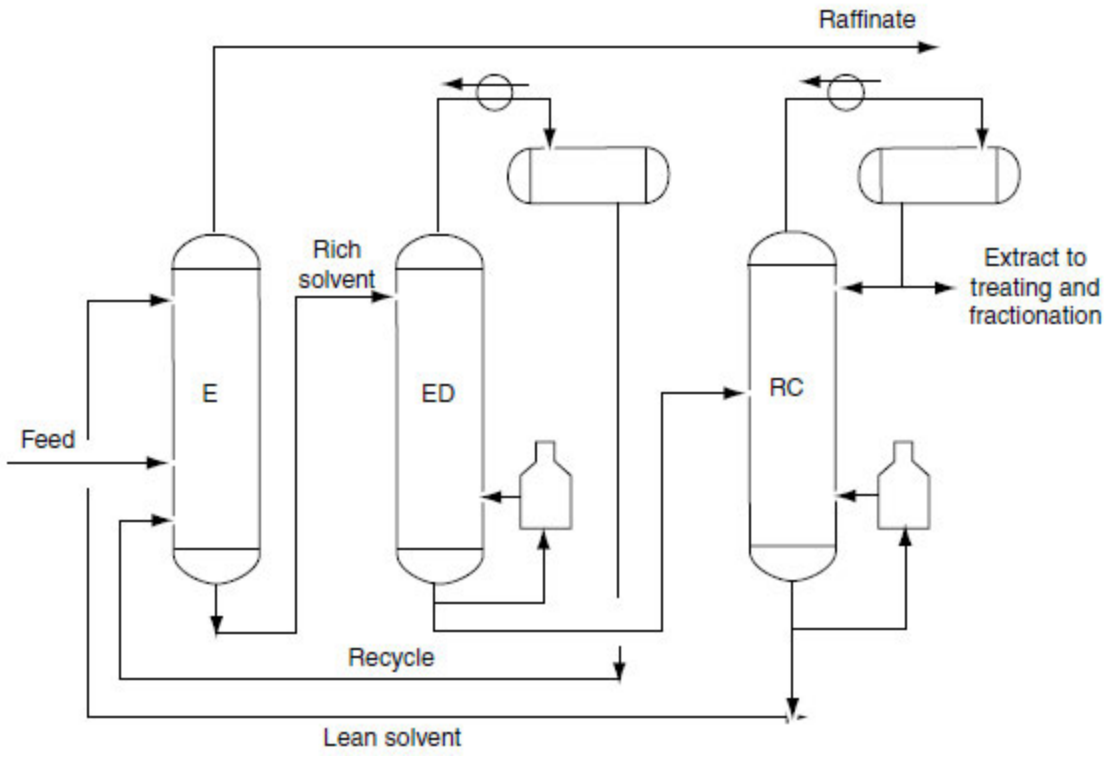

Figure 1.4: Generic process flow diagram of the sulfolane process; E – extraction; ED – extractive distillation; RC – recovery column (Kaiser et al., 2019)

The feed enters the extraction column and flows counter-currently with the solvent, which typically enters at the top. The feedstock to the aromatic extraction unit can be different types of refinery streams including straight-run, cracked or reformed naphtha. The raffinate exits at the top for further downstream processing, while the solvent-rich extract is sent to the top of an extractive distillation column. As the concentration of aromatics increases in the raffinate, the ability of the solvent to absorb aromatics decreases, resulting in a carry-over of aliphatics to the extract. Thus, the extract also contains traces of lighter aliphatic and other non-aromatic components present in the feed. Each phase is contaminated with all components, and the process is designed to minimize this effect, utilizing recycles and additional separation steps. The impurities from each phase are separated and recycled to the liquid-liquid extraction column. The bottoms from the extractive distillation column contains almost pure solvent and aromatic components only. The solvent is thereafter recovered via distillation in the third column and is recycled to the liquid-liquid extraction column.

1.7 Characterization of Solvents

Most liquid-liquid extraction processes use the basic processing sequence highlighted in Figure 1-3, with the distinction being the usage of different solvents. Various solvents such as sulfolane, morpholine-4-carbaldehyde (NFM), 1-methylpyrrolidin-2-one (NMP), 2,2′-oxydiethanol (DEG) , triethylene glycol, tetraethylene glycol, dimethylsulfoxide (DMSO), dimethylformamide (DMF) and propylene carbonate have been studied with the aim of optimizing the extraction process, and selection of the suitable solvent is dependent on the inherent advantages and disadvantages of each.

To date, potential solvents were identified based on desired physical properties and two important parameters known as selectivity and capacity. Selectivity of the solvent is an important factor because it gives an indication of the extent to which the solvent is able to distinguish between aromatics and non-aromatics, and capacity is important because it gives an indication of the maximum volume of aromatics that the solvent is able to extract. A detailed treatment of selectivity and capacity is given in subsequent sections. Table 1.2 lists the patented aromatic extraction processes developed with different solvents, with the advantages of each.

Table 1.2: Processes used for extraction of aromatics (Lo & Baird, 2000)

Process	Solvent	Operating Conditions	Comments
Shell Process Universal Oil Products	Sulfolane	120 ℃	High selectivity and capacity resulting in low solvent to feed ratios
Udex Process Universal Oil Products	Diethylene – glycol/water mixture	150 ℃	The co-solvent mixture significantly improves capacity. The recovery of

			BTX is a two-step process.
Union Carbide Corporation	Tetraethylene glycol	100 ℃	Process does not require intermediate recovery of aliphatics from the extract of the primary extractor.
Institut Francis du Petrole	DMSO	Ambient	The solvent is non-toxic and has a low freezing point, as well as being noncorrosive.
Arosolvan Process, Lurgi	NMP	NMP – ethylene glycol (40 – 50 wt%), 60 ℃	Either ethylene glycol or water is used as a co-solvent with NMP. The solvent to co-solvent ratio is dependent on the feed aromatics content.
		NMP – water (12 – 20 wt%), 35 ℃	
Formex Process, SNAM Progetti	NFM	40 ℃	Noncorrosiveness of the solvent means that carbon steel can be used for the equipment.

Petroleum Technology (2007) describes the trade-off between capacity and selectivity as follows: "*Capacity, defined as the quantity of material that is extracted from the feed by a given quantity of solvent, must be balanced against selectivity, defined as the degree to which the solvent extracts the aromatics in the feed in preference to paraffins and other materials. Most high capacity*

solvents have low selectivity." The ideal solvent therefore would possess the characteristic of high capacity and high selectivity.

Sulfolane being the most commonly employed solvent offers a good balance between selectivity and capacity, thus offering low solvent to feed ratios; this was generally an improvement over the processes using diethylene, triethylene, and tetraethylene glycols with water. DMSO offers economic benefits because the extraction is conducted at ambient conditions, due to the solvent's good properties of high density and low freezing point. NMP is utilized with ethylene glycol or water to improve selectivity and decrease boiling point, however at the cost of capacity. These combinations serve as co-solvents. Generally, the volume of co-solvent used depends on feed characteristics such as aromatic content. Due to the variety of solvents available and the need to continually improve process economics and environmental impact, it is of value to continually search for alternative solvents.

1.7.1 Potential Solvent Screening

As stated in the previous section, a solvent should essentially have a high affinity for aromatics (high selectivity), and a low selectivity for non-aromatics. Kaiser et al. (2019) gives the following important requirements for a solvent:

- Must be more selective to aromatics
- Needs to have a high capacity (solubility) for aromatics
- Able to form two phases
- Capable of rapid phase separation
- Must be stable in a range of temperatures
- Must be nonreactive with other components and noncorrosive
- Must be cheap to handle

A higher capacity is desired; e.g. at a fixed selectivity the capacity of sulfolane is double that of triethylene glycol. This would manifest as lower solvent demand flowrates and therefore lower operating costs.

Physical properties of the solvent play an important role in solvent selection. (Müller et al. (2000) gives the following desired physical properties.

Boiling point: solvents should not have a boiling point that is too close to the boiling point of the feed, as this will make the solvent difficult to recover. The current solvents utilized have much higher boiling points than aromatics. The boiling point between the aromatic and solvent components must differ significantly to enable separation by simple distillation.

Temperature of miscibility: solvent extraction is a process that relies on the formation of two phases, thus necessitating that the separation be to effected at temperatures below the miscibility temperature.

Polarity: solvents must be polar as this is a factor that influences solubility and therefore selectivity. Polar aprotic solvents have significant dipole moments with which the pi electrons in aromatics can interact favourably with.

Viscosity: low solvent viscosities are desired to facilitate better mixing, and also reduce pumping energy requirements in the plant.

Surface tension: high surface tensions reduce the likelihood of the formation of emulsions.

Vapour pressure: lower vapour pressures are desired as it is indicative of reduced rates of solvent loss which implies reduced solvent makeup requirements. In striving for minimal solvent loss, raw material and operating costs are reduced.

Density: solvent density must be higher than the aromatic and aliphatic components by virtue of the extraction process in order to form the extract phase.

1.8 Thermodynamics Review

The design of solvent extraction systems is highly dependent on the selective solubility of aromatic components. The information required to effectively and optimally design these units is at chemical equilibrium, which is indicative of the point at which the maximum volume of aromatics that a solvent can extract at certain conditions is reached. The interaction between these systems results in the formation of distinct phases, and an understanding of the behaviour of these phases can greatly influence the economic viability of large-scale extraction units. A review of the manner in which phase equilibrium is defined is thus conducted, and the context to which it is applied to solvent extraction is outlined.

1.8.1 Phase Equilibrium

The phase equilibrium criterion is ascertained from the definition of the Gibbs energy in terms of pressure and temperature for a closed system:

$$d(nG) = (nV)dP - (nS)dT \tag{1.1}$$

Where G is the molar Gibbs energy, n is number of moles, T is temperature, P is pressure, V is molar volume, and S is specific entropy.

Thereafter, the assumption that no chemical reactions is applied which leads to the implication of a constant composition system resulting in the following deductions:

$$\left[\frac{\partial(nG)}{\partial P}\right]_{T,n} = nV \tag{1.2}$$

$$\left[\frac{\partial(nG)}{\partial T}\right]_{P,n} = -nS \tag{1.3}$$

The subscript variables are those properties which are kept constant, with n representing the quantity in terms of moles of that specific chemical in the system.

While the Gibbs energy is dependent on pressure and temperature, it is also contingent on the number of moles, if broadly considered for an open system. This is the relation in Equation (1.4).

$$nG = g(P,T,n) \tag{1.4}$$

Applying the differential form of Equation (1.4) results in:

$$d(nG) = (nV)dP - (nS)dT + \sum_i \mu_i dn_i \tag{1.5}$$

For species i in the mixture, the chemical potential (μ_i) was thereafter applied in Equation (1.5) and is defined as follows:

$$\mu_i = \left[\frac{\partial(nG)}{\partial n_i} \right]_{P,T,n_j} \tag{1.6}$$

A theoretical closed system is now defined considering two phases (α and β) in contact with each other as two open systems. This allows for incorporating the interaction between the phases in terms of mass transfer. After applying the constraint of constant pressure and temperature, Equation (1.6) is now expressed for each phase in terms of this scenario as follows:

$$d(nG)^{\alpha} = (nV)^{\alpha} dP - (nS)^{\alpha} dT + \sum_i \mu_i^{\alpha} dn_i^{\alpha} \tag{1.7}$$

$$d(nG)^{\beta} = (nV)^{\beta} dP - (nS)^{\beta} dT + \sum_i \mu_i^{\beta} dn_i^{\beta} \tag{1.8}$$

The total Gibbs energy for the overall system can be expressed as follows:

$$nM = (nM)^{\alpha} + (nM)^{\beta} \tag{1.9}$$

In Equation (1.9), *M* may represent any number of extensive thermodynamic properties. Application of Equation (1.9) results in the following:

$$d(nG) = (nV)dP - (nS)dT + \sum_i \mu_i^{\alpha} dn_i^{\alpha} + \sum_i \mu_i^{\beta} dn_i^{\beta} \tag{1.10}$$

Since this is a closed system, Equation (1.10) can be applied to Equation (1.9), with the following implication:

$$\sum_i \mu_i^{\alpha} dn_i^{\alpha} + \sum_i \mu_i^{\beta} dn_i^{\beta} = 0 \tag{1.11}$$

The terms dn_i^{α} and dn_i^{β} represent changes in the quantity of moles as a result of the transfer of particles between phases. For a non-reactive system, the law of mass conservation requires that $dn_i^{\alpha} = -dn_i^{\beta}$, since a closed system is being considered. Hence equation 1.11 results in the following:

$$\sum_i (\mu_i^{\alpha} - \mu_i^{\beta}) dn_i^{\alpha} = 0 \tag{1.12}$$

Equation (1.12) becomes zero primarily when the bracketed term is zero, for which the conclusion is now characterized as follows:

$$\mu_i^{\alpha} = \mu_i^{\beta} \tag{1.13}$$

A generalized form of Equation (1.13) is achieved upon extension to multiple phases. For a closed system consisting of π phases at the same pressure and temperature and *N* chemical species, the following results:

$$\mu_i^{\alpha} = \mu_i^{\beta} = \ldots = \mu_i^{\pi} \tag{1.14}$$

where $i = 1, 2, \ldots, N$.

Therefore, for a closed system containing many phases at the same pressure and temperature, the criterion for equilibrium is that the chemical potential is the same in all phases for each component (Smith et al., 2001).

A shortcoming of the above definition is that chemical potential is a quantity not easily measurable. Fugacity is a concept more useful as it is defined in terms of pressure, and can be used to characterize chemical potential. Thus expressing Equation (1.14) in terms of fugacity results in the following:

$$\hat{f}_i^{\alpha} = \hat{f}_i^{\beta} = \hat{f}_i^{\pi} \tag{1.15}$$

where $i = 1, 2, 3 \ldots N$ and $\hat{f}_i$ is the fugacity in solution of component *i*.

In the context of liquid-liquid extraction, the phases are two liquids and the non-idealities can be quantified with the use of the activity coefficient – defined as follows:

$$\gamma_i = \frac{\hat{f}_i}{x_i f_i} \tag{1.16}$$

After applying Equation (1.16) to a liquid-liquid system comprising two phases (*I* and *II*), expressing the equilibrium criterion in terms of activity coefficients, and cancelling the common pure component fugacities, the equilibrium criterion can be expressed as indicated in Equation (1.17):

$$x_i^I \gamma_i^I = x_i^{II} \gamma_i^{II} \tag{1.17}$$

1.8.2 Thermodynamic Models

Characterization of the phase equilibrium behaviour of the solvent in a mixture of aromatic and hydrocarbon components is necessary to evaluate the performance of the solvent. Activity coefficient models serve to provide predicted LLE (liquid-liquid equilibrium) data for the required systems and thereby give an indication of solvent performance in terms of capacity and selectivity. The Non-Random-Two-Liquid (NRTL) local composition model (Renon & Prausnitz, 1968), and quasi chemical theory models UNIQUAC (Abrams & Prausnitz, 1975), and UNIFAC (Fredenslund et al., 1975), are generally used to model LLE due to a fairly good representation of aromatic-hydrocarbon-solvent systems. These models require specification of binary interaction parameters, acquired by regression of experimentally measured LLE data. A detailed discussion of the NRTL model is presented in Chapters 3 and 5, while the UNIQUAC and UNIFAC models are described herewith.

1.8.2.1 The UNIQUAC (UNIversal QUasi-Chemical) Model

The UNIQUAC (UNIversal QUasi-Chemical) model results from the idea of local composition and a two-liquid model. It is composed of two parts: a combinatorial term and a residual term, and is expressed in Equation (1.22).

$$\frac{G^E}{RT} = \left(\frac{G^E}{RT}\right)_{combinatorial} + \left(\frac{G^E}{RT}\right)_{residual} \tag{1.22}$$

The combinatorial term represents the variations in molecular structure, while the residual term represents the differences in intermolecular forces between molecules. Equations (1.23) and (1.24) give the mathematical definitions of the combinatorial and residual terms.

$$\left(\frac{G^E}{RT}\right)_{combinatorial} = \sum_{i=1}^{n} x_i \ln\frac{\Phi_i^*}{x_i} + \frac{z}{2}\sum_{i=1}^{n} q_i x_i \ln\frac{\theta_i}{\Phi_i^*} \tag{1.23}$$

$$\left(\frac{G^E}{RT}\right)_{reesidual} = -\sum_{i=1}^{n} q_i x_i \ln\left(\sum_{j=1}^{n} \theta_j^{'} \tau_{ji}\right) \tag{1.24}$$

The co-ordination number (z) is generally attributed a value of 10, while the area fractions (θ, θ') and segment fraction (Φ^*) are expressed in Equations (1.25) to (1.27):

$$\Phi_i^* = \frac{r_i x_i}{\sum_{j=1}^{n} r_j x_j} \tag{1.25}$$

$$\theta_i = \frac{q_i x_i}{\sum_{j=1}^{n} q_j x_j} \tag{1.26}$$

$$\theta_i^{'} = \frac{q_i^{'} x_i}{\sum_{j=1}^{n} q_j x_j} \tag{1.27}$$

The parameters q, q' and r take into consideration molecular structure in terms of external surface area of the molecules and size of the molecules respectively. The parameter q' was introduced by Anderson & Prausnitz (1978) as a modification for better model results for water as well as smaller chain alcohols. The original UNIQUAC equation is used by specifying the condition of $q = q'$.

The characteristic energies ($u_{ij} - u_{jj}$) parameters are adjustable and dependent on the components of the system, thereafter used to determine parameter τ_{ij} as follows:

$$\tau_{ij} = \exp\left(-\left[\frac{u_{ij} - u_{jj}}{RT}\right]\right) \tag{1.28}$$

The above equations can be represented in terms of activity coefficients for component *i* as follows:

$$\ln\gamma_i = \ln\gamma_i^C + \ln\gamma_i^R \tag{1.29}$$

$$\ln\gamma_i^C = \ln\frac{\Phi_i}{x_i} + \frac{z}{2}q_i\ln\frac{\theta_i}{\Phi_i} + l_i - \frac{\Phi_i}{x_i}\sum_{j=1}^{n}x_j l_j \tag{1.30}$$

$$\ln\gamma_i^R = -q_i^{'}\ln\left(\sum_{j=1}^{n}\theta_j^{'}\tau_{ji}\right) + q_i^{'} - q_i^{'}\sum_{j=1}^{n}\frac{\theta_j^{'}\tau_{ij}}{\sum_{k=1}^{n}\theta_k^{'}\tau_{kj}} \tag{1.31}$$

where $$l_i = \frac{z}{2}(r_i - q_i) - (r_i - 1) \tag{32}$$

The UNIQUAC model can represent non-electrolyte systems fairly accurately, and can be used in the design of liquid-liquid extraction systems with the availability of the characterizing binary interaction parameters.

1.8.2.3 The UNIFAC (UNIQUAC Functional-group Activity Coefficients) Model

The UNIFAC model results from the idea of the solution of functional groups, to create an activity coefficient model stemming from the quasi-chemical theory of liquid mixtures. It comprises two adjustable parameters per functional group pair. The general idea of the UNIFAC model is to use

experimental phase equilibrium data to predict the equilibrium behaviour for systems that have no data available.

The mathematical definition of the UNIFAC model in terms of activity coefficients is the same as that of the UNIQUAC model (Equation 1.22), consisting of a combinatorial and residual term. The combinatorial term is the same as that for UNIQUAC (Equation 1.23), and requires only pure component properties. The residual term is the distinction between UNIQUAC and UNIFAC, and involves the interactions between groups as given in Equation (1.33):

$$\ln \gamma_i^R = \sum_k v_k^{(i)} \left[\ln \Gamma_k - \ln \Gamma_k^{(i)} \right] \tag{1.33}$$

$\Gamma_k^{(i)}$ is the residual activity coefficient of group *k* for molecules of type *i* in a reference solution, while Γ_k is the group residual activity coefficient. The number of groups of type *k* in molecule *i* is denoted by $v_k^{(i)}$. Γ_k is the group activity coefficient and is given in Equation (1.34) as follows:

$$\ln \Gamma_k = Q_k \left[1 - \ln \left(\sum_m \Theta_m \Psi_{mk} \right) - \sum_m \left(\frac{\Theta_m \Psi_{mk}}{\sum_n \Theta_n \Psi_{nm}} \right) \right] \tag{1.34}$$

$\ln \Gamma_k^{(i)}$ can also be in the form of Equation (1.34). Θ_m is the area fraction of group *m*, and is the summation of different groups, as expressed in Equation (1.35).

$$\Theta_m = \frac{Q_m X_m}{\sum_n Q_n X_n} \tag{1.35}$$

Where X_m is the mole fraction of that specific group in the mixture. The group interaction parameter Ψ_{nm} is given by Equation (1.36) as follows:

$$\Psi_{nm} = \exp\left(- \left[\frac{U_{nm} - U_{nn}}{RT} \right] \right) \equiv \exp\left(- \frac{a_{nm}}{T} \right) \tag{1.36}$$

Where U_{nm} is a measure of the energy of interaction between groups *n* and *m*, and are regressed from experimental phase equilibrium data.

1.8.3 Limiting Activity Coefficients

Where LLE experimental data is not available, infinite dilution activity coefficients may be used to evaluate the efficacy of a potential solvent. These limiting activity coefficients give an insight into the behaviour of a solution with a low concentration of an important component, which enables an assessment of the recoverability and separability of that specific component. The activity coefficient at infinite dilution describes the behaviour of the aromatic component surrounded by excess solvent, which represents an environment of maximum non-ideality. This characterization enables calculation of a limiting selectivity as indicated in Equation (1.46):

$$S_{ij}^{\infty} = \left(\frac{\gamma_j^{\infty}}{\gamma_i^{\infty}}\right)^{I}\left(\frac{\gamma_i^{\infty}}{\gamma_j^{\infty}}\right)^{II} \tag{1.46}$$

Deal and Derr (1964) determined that the non-polar phase approaches unity at infinite dilution, thus reducing Equation (1.46) as follows:

$$S_{ij}^{\infty} \cong \left(\frac{\gamma_j^{\infty}}{\gamma_i^{\infty}}\right)^{I} \tag{1.47}$$

This also results in a simplification of the solvent capacity at infinite dilution, as illustrated in Equation (1.48).

$$S_P \cong \left(\frac{1}{\gamma_i^{\infty}}\right)^{I} \tag{1.48}$$

The performance index as defined in Equation (1.45), can thus be represented in terms of infinite dilution activity coefficients as indicated in Equation (1.49):

$$PI^{\infty} = \left(\frac{\gamma_j^{\infty}}{\left(\gamma_i^{\infty}\right)^2} \right)^I \tag{1.49}$$

Deal & Derr (1964) listed potential solvents in terms of infinite dilution activity coefficients using hexane and benzene. Selectivity and capacity were related in this manner for a range of solvents from 25 – 100 ℃. Selectivity was found to decrease with increasing temperature for the majority of solvents studied.

Infinite dilution activity coefficients were characterized by Rawat et al. (1976) for sulfolane and a variety of sulphur group solvents such as 2-4-dimethyl sulfolane, vinyl sulfone, tetramethlyene sulfoxide, and glycol sulphite. Sulfone and sulfoxide groups were observed to display superior solvent characteristics in terms of capacity and selectivity.

1.9. Liquid-Liquid Equilibrium (LLE) Representation

Liquid-liquid equilibrium data is important to understand the behaviour of the system under consideration, as it provides key characteristics necessary for the design of extraction systems. Additionally, the data is necessary for the regression of interaction parameters for predictive models (as discussed in the previous section), as well as for determining solvent selectivities and capacities. Binary, ternary, and quaternary data of systems consisting of aliphatics and aromatics for a range of solvents are available in the open literature.

Ternary data is generally most commonly measured to determine the behaviour and interaction of an aliphatic-aromatic-solvent system. While the feed to the extraction unit comprises many light and heavy components, assessing the behaviour of each component with an aromatic and solvent allows for the interaction parameters to be determined; this gives an indication of the extent to which each component will split between the extract and raffinate phases, allowing for an iterative design procedure to reach the desired process yields. It is thus important to review the manner in which LLE data is analysed in the context of aromatics extraction.

An equilateral triangle may be used to evaluate the phase equilibrium behaviour of ternary systems. Figure 1.5 demonstrates the way in which compositions are plotted on an equilateral triangle chart:

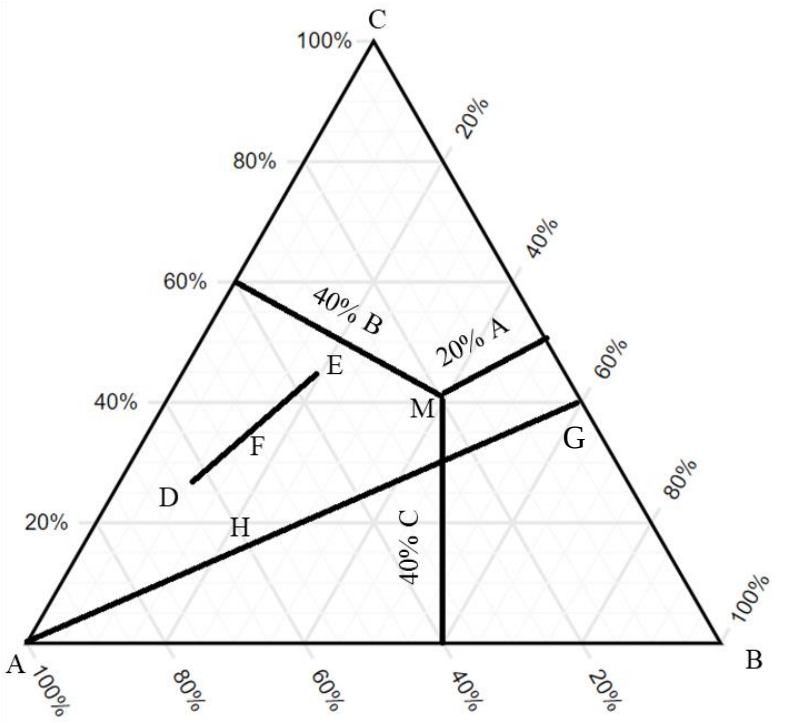

Figure 1.5: Composition plotting on a ternary LLE diagram (Treybal, 1963)**.**

Point M represents a mixture consisting of 20% A, 40% B, and 40% C. The apex of an axis is indicative of a pure component, while the vertical distance from a point to the axis across from the apex indicates the composition of that specific component. The straight line DFE represents ternary compositions with point F resulting from mixing liquids with compositions shown at D and E. Line AG shows the composition range of mixtures with constant ratios of component A added successively.

As the concept of liquid-liquid extraction is dependent on the separation of phases, understanding of the immiscibility regions is the primary consideration. Treybal (1963) presented the following categorization of immiscibility regions of ternary systems:

- Type 1: creation of one pair of partially miscible liquids

- Type 2: creation of two pairs of partially miscible liquids
- Type 3: creation of three pairs of partially miscible liquids

1.9.1 Type 1 and 2 Systems

In Type 1systems, 2 out of 3 binary pairs of each component are miscible in all ratios at constant pressure and temperature. The plait point P represents the composition at which all three components are entire miscible and form a single phase. Figure 1.6 illustrates the isotherm of this particular system:

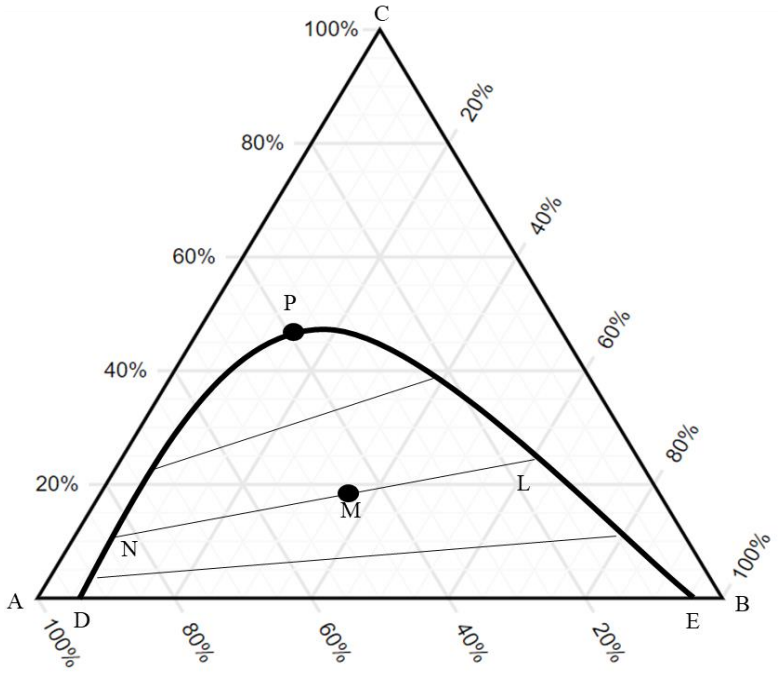

Figure 1.6: Type 1 ternary system in equilibrium (Treybal, 1963).

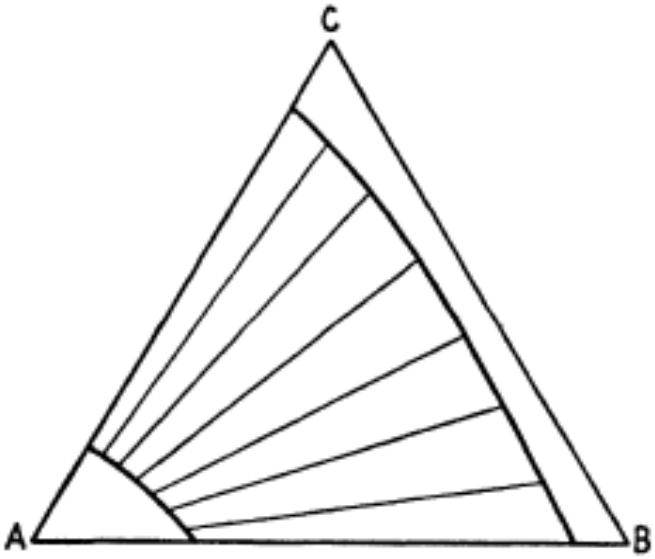

Figure 1.7 Type 2 ternary system in equilibrium (Treybal, 1963).

In type 2 systems, a single component pair forms a homogeneous liquid across the composition range (points C to B), while two pairs of binary components are partially miscible (A-C and A-B). The area between the two binodal curves represent liquids that form two immiscible phases, and there is no plait point.

1.9.2 Type 3 Systems

Type 3 systems are quite rare, and are formed when there is mutual partial miscibility between all three components, as illustrated in Figure 1.8.

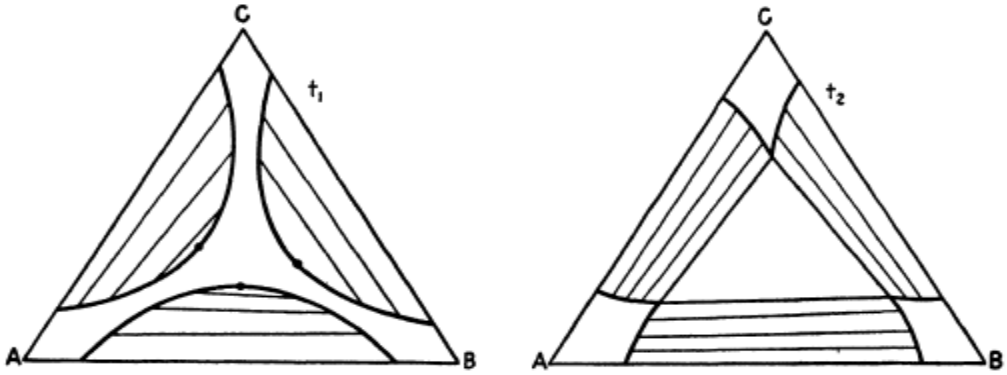

Figure 1.8: Type 3 ternary system in equilibrium (Treybal, 1963).

Upon changing the temperature from t_1 to t_2, an intersection of the three binodal curves forms, which results in a three-liquid region at constant pressure and temperature.

Other types of LLE systems with variations on the triangular diagrams are reviewed in greater detail by Novák et al. (1987) and Sørensen et al. (1979).

1.9.3 Identification of Plait Point

Treybal (1963) outlines a widely used method of ascertaining the plait point, known as the Coolidge method. This method is demonstrated for a Type 1 system in Figure 1.9.

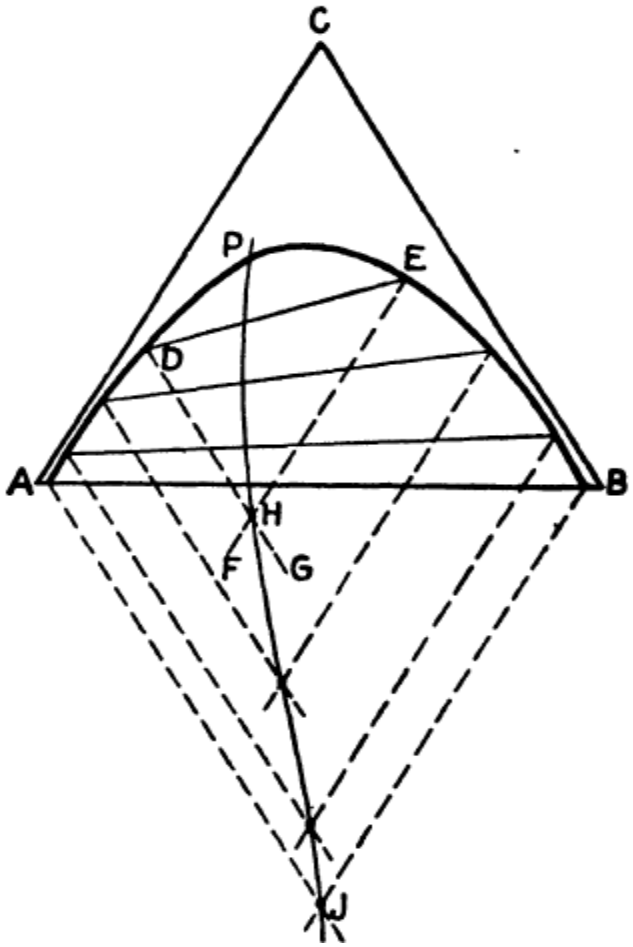

Figure 1.9: The plait point determined from graphical Coolidge method (Treybal, 1963).

The tie line DE is used as an example. Lines parallel to AC and CB are drawn with an intersection at point H. These construction lines are then drawn for all tie lines until the curve JHP results. The plait point is characterized as the intersection with the binodal curve.

1.10 LLE Measurements in Literature

As sulfolane is the most commonly used solvent, it is the most widely studied in terms of phase equilibrium with aliphatic and aromatic compounds. However, LLE data has been published for other solvents such as NFM, NMP etc, with combinations of aromatic components. Table 1.3 lists the experimental measurements currently available in the open literature for binary and ternary systems. The acronyms used in Table 1.3 are listed in Table 1.4.

Table 1.3: List of experimental measurements available in literature

Aliphatic	Aromatic + Solvent
n-Pentane	B+S (Cassell, Dural, et al., 1989), T+S (Cassell, Dural, et al., 1989), NFM (Ko et al., 2002)
2,2,4-trimethylpentane	NFM, EB+NFM (Wang et al., 2012)
Cyclopentane	NFM (Ko, Na, Lee, et al., 2003)
2-Methyl-pentane	T+S (Garduno et al., 1991)
3-Methyl-pentane	NFM (Wang et al., 2012)
Methylcyclopentane	NFM (Ko, Na, Kwon, et al., 2003)
n-Hexane	T+S (Cassell, Hassan, & Junes, 1989), X+S (J. Chen, Duan, et al., 2000), T+NMP (Letcher & Naicker, 1998), B+NFM (Mahmoudi & Lotfollahi, 2010), B+(S+NFM) (Mahmoudi & Lotfollahi, 2010)
1-Hexene	T+S (Garduno et al., 1991), B+S (de Fré & Verhoeye, 1976)
Cyclohexane	T+S (Garduno et al., 1993), pX+S (Rappel et al., 2002), B+S (De Fré and Verhoeye, 1976), B+NFM (Seyedein Ghannad et al., 2011), NFM (Ko, Na, Lee, et al., 2003), B+EG (Ghannad et al., 2011), T+PC (Ali et al., 2003)
Methylcyclohexane	NFM (Ko, Na, Kwon, et al., 2003)
Ethylcyclohexane	NFM (Ko, Na, Kwon, et al., 2003)
n-Heptane	T+S (Cassell, Hassan, & Hines, 1989), X+S (Cassell, Hassan, & Hines, 1989), B+S (Letcher et al., 1996), pX+S (Letcher et al., 1996), T+NMP (Nagpal & Rawat, 1981), T+(10% NMP & 20%H_2O) (Nagpal and Rawat, 1981), B+(EG+NMP) (Nagpal and Rawat, 1981), B+NMP (Blanco et al., 2002), B+NFM (DongChu, HongQi, & Hao, 2007), T+NFM (DongChu et al., 2007), X+NFM (DongChu et al., 2007), B+pX (Cincotti et al., 1999),

	(EG+DMF) (Radwan et al., 1997), EB+EG (Radwan et al., 1997), T+TEG (Saha et al., 1998a), T+(NFM+TEG) (Saha et al., 1998), T+(NMP+TEG) (Saha et al., 1998), NFM (Wang et al., 2012)
Methylcyclohexane	B+NFM (Chen et al., 2007), T+NFM (DongChu, HongQi, & Wu, 2007)
1,2-Dimethylcyclohexane	T+S (Sun & Xiang, 2014)
n-Octane	B+S, T+S, X+S (Chen et al., 2000), NFM (Ko et al., 2002), T+EG (Mohsen-Nia et al., 2008), T+DEG (Lababidi et al., 2006), (DEG+PC) (Lababidi et al., 2006), EB+PC (Ali et al., 2003)
Cyclooctane	NFM (Ko, Na, Lee, et al., 2003)
n-Nonane	T+NMP (Letcher and Naicker, 1998), NFM (Wang et al., 2012) T+NFM (Brijmohan & Narasigadu, 2020)
i-Nonane	NFM (Cincotti, 1999)
n-Decane	B+S (Letcher et al., 1996), T+NFM (Brijmohan & Narasigadu, 2020)
Tetradecane	PB+NMP (Fandary et al., 2006), T+NMP (Letcher and Naicker, 1998)
Hexadecane	T+NMP (Letcher and Naicker, 1998), (o-p-m)X+NMP (Letcher and Naicker, 1998), M+NMP (Letcher and Naicker, 1998), EB+NMP (Letcher and Naicker, 1998)
Heptadecane	PB+NMP (Fandary et al., 2006)
Dodecane	B+S (Letcher et al., 1996), EB+DMF (Radwan et al., 1997), B+DMF (Radwan et al., 1997)

Table 1.4: Acronyms used in Table 1.3

Aromatic	**Solvent**
Benzene (B)	Sulfolane (S)
Toluene (T)	N-Methyl-2-pyrrolidone (NMP)
Xylene (X)	N-Formylmorpholine (NFM)
Ethylbenzene (E)	Ethylene Glycol (EG)
o-Xylene (oX)	Diethylene Glycol (DEG)
p-Xylene (pX)	Tetraethylene Glycol (TEG)
m-Xylene (mX)	Propylene Carbonate (PC)
Xylene (X) – isomer not stated	Dimethylsulfoxide (DMSO)
Pentylbenzene (PB)	Dimethylformamide (DMF)
Mesitylene (M)	

1.11. LLE Measurement Techniques

Liquid-liquid equilibrium phase behaviour requires measurement of variables such as temperature, pressure, and phase composition. Any method requires measurement of phases at the condition of equilibrium. The direct analytical method (used in this work) will be presented, together with the turbidity method, titration method, the continuous measurement method, and laser-light scattering method.

1.11.1. Direct Analytical Method

The direct analytical method is a highly effective method of performing LLE measurements and widely used to determine phase compositions (Moriyoshi et al., 1989). The chemicals under consideration are charged to an equilibrium cell that is maintained at constant temperature with the assistance of a recirculation bath or through submersion in a bath. After the chemicals are charged, the contents are stirred such that there is good mixing between phases, and then left to settle until equilibrium is reached. Samples for each phase are then withdrawn and analyzed using gas chromatography (GC). The binodal curve can be generated by taking the collection of phase compositions forming the tie-lines, which can be determined across the entire composition range by appropriate choice of overall composition (Novák et al., 1987). For ternary and multicomponent systems, only the analytical method can be used to determine tie-lines. Details of the equipment used in this study are given in Chapter 3.

1.11.2 Turbidity method

The turbidity method involves initially charging an equilibrium cell with a particular chemical, at a fixed temperature. For a binary system, another chemical is then added in known quantities until the disappearance or onset of another phase is noted. The accuracy of this method depends on the visible inspection of different phases, and the quantities of the second chemical added. There is no analysis of phase compositions. A variation of the method for binary systems includes preparing a fixed synthetic mixture and varying the temperature until turbidity is observed/eliminated. Practical application of the turbidity method is based on constant temperature and is restricted to

binary systems. For a review of this method and the cells that have demonstrated its use, the reader is referred to Muhlbauer & Raal (1998).

1.11.3 Titration method

The principle behind this method entails the constant addition of a particular component to a mixture that has been pre-charged to an equilibrium cell or stirred vessel at a fixed temperature. The addition of this component occurs until the onset or disappearance of another phase is noted. The titration method is a variant of the turbidity method, in which an amount of one component is changed at constant temperature. The binodal curve is generated by measurement of the phase compositions using density or refractive index measurements. This method avoids the use of analysis by GC for chemicals that pose difficulty with GC operational conditions (such as residence times). The tie-lines are then determined after the binodal curve using the calibration done with the binodal curve measurements. In this part there is no onset or disappearance observed but each phase is analyzed. The technique is confirmed when a straight line is observed for the extract, raffinate and feed compositions. Further detailed reviews of the method may be obtained from Letcher et al. (1989).

1.11.4 Continuous Measurement Method

Reinhardt et al. (1969) developed the continuous measurement method, which entails two liquids being contacted in a chamber and thereafter thoroughly mixed and finally separated into two exiting phases with the use of a centrifuge, with phase recirculation also occurring. The compositions of the phases are determined via an online detector which depends on the type of chemicals used. This method is not frequently used due to the costly nature of the required equipment.

1.12. References

Abrams, D. S., & Prausnitz, J. M. (1975). Statistical Thermodynamics of Liquid Mixtures: A New Expression for the Excess Gibbs Energy of Partly or Completely Miscible Systems. *AIChE J, 21*, 116–118.

Ali, S. H., Lababidi, H. M. S., Merchant, S. Q., & Fahim, M. A. (2003). Extraction of aromatics from naphtha reformate using propylene carbonate. *Fluid Phase Equilib.*, *214*, 25–38. https://doi.org/10.1016/S0378-3812(03)00323-6

Anderson, T. F., & Prausnitz, J. M. (1978). Application of the UNIQUAC Equation to Calculation of Multicomponent Phase Equilibria. 1. Vapor-Liquid Equilibria. *Industrial & Engineering Chemistry Process Design and Development*, *17*, 552–561. https://doi.org/10.1021/i260068a028

Azapagic, A., & Perdan, S. (2000). Indicators of Sustainable Development for Industry. *Process Safety and Environmental Protection*, *78*, 243–261. https://doi.org/10.1205/095758200530763

Blanco, B., Sanz, M. T., Beltrán, S., Cabezas, J. L., & Coca, J. (2002). Vapor−Liquid Equilibria of the Ternary System Benzene + n-Heptane + N-Methylpyrrolidone (NMP) at 101.33 kPa. *J. Chem. Eng. Data*, *47*, 1167–1170. https://doi.org/10.1021/je020007r

Brijmohan, N., & Narasigadu, C. (2020). Ternary Liquid–Liquid Equilibrium Data for the N-Formylmorpholine + Toluene + {n-Nonane or n-Decane} Systems at (303.2, 323.2, and 343.2) K and 101.3 kPa. *J. Chem. Eng. Data*, *65*, 788–792. https://doi.org/10.1021/acs.jced.9b01011

Capello, C., Fischer, U., & Hungerbühler, K. (2007). What is a green solvent? A comprehensive framework for the environmental assessment of solvents. *Green Chemistry*, *9*, 927–934. https://doi.org/10.1039/b617536h

Cassell, G. W., Dural, N., & Hines, A. L. (1989). Liquid-Liquid Equilibrium of Sulfolane-Benzene-Pentane and Sulfolane-Toluene-Pentane. *Ind. Eng. Chem. Res, 28*, 1369−1374.

Cassell, G. W., Hassan, M. M., & Hines, A. L. (1989). Correlation of the Phase Equilibrium Data for the Heptane-Toluene-Sulfolane and Heptane-Xylene-Sulfolane Systems. *J. Chem. Eng. Data*, *34*, 434−438.

Cassell, G. W., Hassan, M. M., & Junes, A. L. (1989). Phase Equilibria of the Cylohexane-Toluene-Sulfolane and Hexane-Toluene-Sulfolane Ternary Systems. *Chem. Eng. Commun*, *85*, 233−243.

Chen, D., Ye, H., & Wu, H. (2007). Liquid–liquid equilibria of methylcyclohexane–benzene–N-formylmorpholine at several temperatures. *Fluid Phase Equilib.*, *255*, 115–120. https://doi.org/10.1016/j.fluid.2007.03.013

Chen, J., Duan, L. P., Mi, J. G., Fei, W. Y., & Li, Z. C. (2000). Liquid-liquid equilibria of multi-component systems including n-hexane, n-octane, benzene, toluene, xylene and sulfolane at 298.15 K and atmospheric pressure. *Fluid Phase Equilib*, *173*, 109−119.

Chen, Q. L., Wang, Q., Zhang, B. J., He, C., & He, C. C. (2017). Optimal Design of a New Aromatic Extractive Distillation Process Aided by a Co-Solvent Mixture. *Energy Procedia*, *105*, 4927–4934.

Cincotti, A., Murru, M., Cao, G., Marongiu, B., Masia, F., & Sannia, M. (1999). Liquid−Liquid Equilibria of Hydrocarbons with N-Formylmorpholine. *J. Chem. Eng. Data*, *44*, 480–483. https://doi.org/10.1021/je980168o

De Fré, R. M., & Verhoeye, L. A. (1976). Phase Equilibria in Systems Composed of an Aliphatic and an Aromatic Hydrocarbon and Sulpholane. *J. Appl. Chem. Biotechnol*, *26*, 469−487.

Deal, C. H., & Derr, E. L. (1964). Selectivity and Solvency in Aromatics Recovery. *Ind. Eng. Chem. Proc. Des. Dev.*, *3*, 394–399. https://doi.org/10.1021/i260012a022

Delancey, G. (2013). *Principles of Chemical Engineering Practice*. John Wiley & Sons.

DongChu, C., HongQi, Y., & Hao, W. (2007). (Liquid + liquid) equilibria of three ternary systems: (heptane + benzene + N-formylmorpholine), (heptane + toluene + N-formylmorpholine), (heptane + xylene + N-formylmorpholine) from T = (298.15 to 353.15) K. *J. Chem. Thermodyn*, *39*, 1182−1188.

DongChu, C., HongQi, Y., & Wu, H. (2007). Measurement and Correlation of Liquid−Liquid Equilibria of Methylcyclohexane + Toluene + N-Formylmorpholine at (293, 303, 313, and 323) K. *J. Chem. Eng. Data*, *52*, 1297–1301. https://doi.org/10.1021/je700036v

Fandary, M. S., Al-Jimaz, A. S., Al-Kandary, J. A., & Fahim, M. A. (2006). Extraction of pentylbenzene from high molar mass alkanes (C14 and C17) by N-methyl-2-pyrrolidone. *J. Chem. Thermodyn*, *38*, 455–460. https://doi.org/10.1016/j.jct.2005.06.012

Fredenslund, A., Jones, R. L., & Prausnitz, J. M. (1975). Group-contribution estimation of activity coefficients in nonideal liquid mixtures. *AIChE Journal*, *21*, 1086–1099. https://doi.org/10.1002/aic.690210607

Grossmann, I. E., & Westerberg, A. W. (2000). Research challenges in process systems engineering. *AIChE Journal*, *46*, 1700–1703. https://doi.org/10.1002/aic.690460902

Henderson, R. K., Jiménez-González, C., Constable, D. J. C., Alston, S. R., Inglis, G. G. A., Fisher, G., Sherwood, J., Binks, S. P., & Curzons, A. D. (2011). Expanding GSK's solvent selection guide – embedding sustainability into solvent selection starting at medicinal chemistry. *Green Chem.*, *13*, 854. https://doi.org/10.1039/c0gc00918k

Jessop, P. G., & Subramaniam, B. (2007). Gas-Expanded Liquids. *Chemical Reviews*, *107*, 2666–2694. https://doi.org/10.1021/cr040199o

Kaiser, M. J., Klerk, A. de, Gary, J. H., & Hwerk, G. E. (2019). *Petroleum Refining* (6th ed.). CRC Press. https://doi.org/10.1201/9780429188893

Ko, M., Lee, S., Cho, J., & Kim, H. (2002). Liquid−Liquid Equilibria for Binary Systems Containing N-Formylmorpholine. *J. Chem. Eng. Data*, *47*, 923–926. https://doi.org/10.1021/je010328n

Ko, M., Na, S., Lee, S., & Kim, H. (2003). Liquid−Liquid Equilibria for the Binary Systems of N-Formylmorpholine with Cycloalkanes. *J. Chem. Eng. Data*, *48*, 249–252. https://doi.org/10.1021/je020089j

Ko, Na, S., Kwon, S., Lee, S., & Kim, H. (2003). Liquid−Liquid Equilibria for the Binary Systems of N-Formylmorpholine with Branched Cycloalkanes. *J. Chem. Eng. Data*, *48*, 699–702. https://doi.org/10.1021/je020208v

Lababidi, H. M. S., Ali, S. H., & Fahim, M. A. (2006). Optimization of Aromatics Extraction of Naphtha Reformate by Propylene Carbonate/Diethylene Glycol Mixed Solvent. *Industrial & Engineering Chemistry Research*, *45*, 5086–5097. https://doi.org/10.1021/ie050537r

Lei, Z., Chen, B., & Ding, Z. (2005). *Special distillation processes* (B. Chen & Z. Ding, Eds.; 1st ed.). Elsevier. https://www.sciencedirect.com/science/book/9780444516480

Letcher, T. M., Redhi, G. G., Radloff, S. E., & Domańska, U. (1996). Liquid−Liquid Equilibria of the Ternary Mixtures with Sulfolane at 303.15 K. *J. Chem. Eng. Data*, *41*, 634–638. https://doi.org/10.1021/je950308j

Letcher, T. M., Siswana, P. M., Van Der Watt, P., & Radloff, S. (1989). Phase equilibria for (an alkanol + p-xylene + water) at 298.2 K. *J. Chem. Thermodyn.*, *21*, 1053–1060. https://doi.org/10.1016/0021-9614(89)90091-8

Lo, T. C., & Baird, M. H. I. (2000). Extraction, Liquid–Liquid. In *Kirk-Othmer Encyclopedia of Chemical Technology*. John Wiley & Sons, Inc. https://doi.org/10.1002/0471238961.120917211215.a01

M. Letcher, T., & K. Naicker, P. (1998). Ternary Liquid−Liquid Equilibria for Mixtures of an n-Alkane + an Aromatic Hydrocarbon + N-Methyl-2-pyrrolidone at 298.2 K and 1 atm. *J. Chem. Eng. Data*, *43*, 1034–1038. https://doi.org/10.1021/je980114e

Mahmoudi, J., & Lotfollahi, M. N. (2010). (Liquid+liquid) equilibria of (sulfolane+benzene+n-hexane), (N-formylmorpholine+benzene+n-hexane), and (sulfolane+N-formylmorpholine+benzene+n-hexane) at temperatures ranging from (298.15 to 318.15)K: Experimental results and correlation. *J. Chem. Thermodyn.*, *42*, 466–471. https://doi.org/10.1016/j.jct.2009.10.010

Meindersma, G. W., Hansmeier, A. R., & de Haan, A. B. (2010). Ionic Liquids for Aromatics Extraction. Present Status and Future Outlook. *Ind. Eng. Chem. Res.*, *49*, 7530–7540. https://doi.org/10.1021/ie100703p

Mohammad Reza Seyedein Ghannad, S., Lotfollahi, M. N., & Asl, A. H. (2011). (Liquid+liquid) equilibria for mixtures of (ethylene glycol+benzene+cyclohexane) at temperatures (298.15, 308.15, and 318.15)K. *J. Chem. Thermodyn.*, *43*, 329–333. https://doi.org/10.1016/j.jct.2010.10.003

Mohsen-Nia, M., Mohammad Doulabi, F. S., & Manousiouthakis, V. I. (2008). (Liquid+liquid) equilibria for ternary mixtures of (ethylene glycol+toluene+n-octane). *J. Chem. Thermodyn.*, *40*, 1269–1273. https://doi.org/10.1016/j.jct.2008.03.014

Mondragón-Garduño, M., Romero-Martínez, A., & Trejo, A. (1991). Liquid—liquid equilibria for ternary systems. I. C6-isomers + sulfolane + toluene at 298.15 K. *Fluid Phase Equilib.*, *64*, 291–303. https://doi.org/10.1016/0378-3812(91)90020-8

Moriyoshi, T., Uosaki, Y., Sakamoto, T., & Hayashi, Y. (1989). (Liquid + liquid) equilibria of (water + ethanol + 2,6-dimethyl-4-heptanone) from 0.1 to 200 MPa at 298.15 and 323.15 K. *J. Chem. Thermodyn.*, *21*, 219–224. https://doi.org/10.1016/0021-9614(89)90133-X

Muhlbauer, A. L., & Raal, J. D. (1998). *Phase Equilibria*. Routledge. https://doi.org/10.1201/9780203743621

Müller, E., Berger, R., Blass, E., & Sluyts, D. (2000). Liquid-Liquid Extraction. In *Ullmann's Encyclopedia of Industrial Chemistry*. Wiley-VCH Verlag GmbH & Co. KGaA. https://doi.org/10.1002/14356007.b03_06

Nagpal, J. M., & Rawat, B. S. (1981). Liquid-Liquid Equilibria for Toluene-Heptane-N-Methyl Pyrrolidone and Benzene-Heptane Solvents. *J. Chem. Technol. Biotechnol*, *31*, 146−150.

Ng, L. Y., Chong, F. K., & Chemmangattuvalappil, N. G. (2015). Challenges and opportunities in computer-aided molecular design. *Computers & Chemical Engineering*, *81*, 115–129. https://doi.org/10.1016/j.compchemeng.2015.03.009

Novák, J. P., Matouš, J., & Pick, J. (1987). *Liquid-Liquid Equilibria*. Elsevier: Amsterdam.

Radwan, G. M., Al-Muhtaseb, S. A., & Fahim, M. A. (1997). Liquid-liquid equilibria for the extraction of aromatics from naphtha reformate by dimethylformamide/ethylene glycol mixed solvent. *Fluid Phase Equilib.*, *129*, 175–186. https://doi.org/10.1016/S0378-3812(96)03179-2

Rappel, R., de Góis, L. M. N., & Mattedi, S. (2002). Liquid–liquid equilibria data for systems containing aromatic + nonaromatic + sulfolane at 308.15 and 323.15 K. *Fluid Phase Equilib.*, *202*, 263–276. https://doi.org/10.1016/S0378-3812(02)00138-3

Rawat, B. S., Gulati, I. B., & Mallik, K. L. (1976). Study of some sulphur-group solvents for aromatics extraction by gas chromatography. *J. Appl. Chem. Biotechnol.*, *26*, 247–252. https://doi.org/10.1002/jctb.5020260504

Reinhardt, H., Rydberg, J., Liljenzin, J. O., Reinhardt, H., Rydberg, J., & Craig, J. C. (1969). Solvent Extraction Studies by the AKUFVE Method. II. A New Centrifuge for Absolute Phase Separation. *Acta Chemica Scandinavica*, *23*, 2773–2780. https://doi.org/10.3891/acta.chem.scand.23-2773

Renon, H., & Prausnitz, J. M. (1968). Local Compositions in Thermodynamic Excess Functions for Liquid Mixtures. *AIChE J*, *14*, 135–144.

Ruiz-Mercado, G. J., Smith, R. L., & Gonzalez, M. A. (2012). Sustainability Indicators for Chemical Processes: I. Taxonomy. *Ind. Eng. Chem. Res.*, *51*, 2309–2328. https://doi.org/10.1021/ie102116e

Saha, M., Rawat, B. S., Khanna, M. K., & Nautiyal, B. R. (1998). Liquid−Liquid Equilibrium Studies on Toluene + Heptane + Solvent. *J. Chem. Eng. Data*, *43*, 422−426.

Seyedein Ghannad, S. M., Lotfollahi, M. N., & Haghighi Asl, A. (2011). Measurement of (liquid + liquid) equilibria for ternary systems of (N-formylmorpholine + benzene + cyclohexane) at temperatures (303.15, 308.15, and 313.15) K. *J. Chem. Thermodyn*, *43*, 938−942.

Smith, J. M., Van Ness, H. C., & Abbott, M. M. (2001). *Introduction to Chemical Engineering Thermodynamics* (6th edition). McGraw-Hill.

Sørensen, J. M., Magnussen, T., Rasmussen, P., & Fredenslund, A. (1979). Liquid—liquid equilibrium data: Their retrieval, correlation and prediction Part II: Correlation. *Fluid Phase Equilib.*, *3*, 47–82. https://doi.org/10.1016/0378-3812(79)80027-8

Sun, X., & Xiang, S. (2014). Liquid–Liquid Equilibria of Ternary Systemscis-1,2-Dimethylcyclohexane+Toluene+Sulfolane. *Chinese Journal of Chemical Engineering*, *22*, 1298–1301. https://doi.org/10.1016/j.cjche.2013.05.003

Treybal, R. E. (1963). *Liquid Extraction* (2nd ed.). McGraw-Hill: New York.

Wang, Z., Xia, S., & Ma, P. (2012). (Liquid + Liquid Equilibria for the Ternary System of (N-Formylmorpholine + Ethylbenzene + 2,2,4-Trimethylpentane) at Temperatures (303.15 , 313.15, and 323.15) K. *Fluid Phase Equilib*, *328*, 25−30.

Weissermel, K., & Arpe, H. (2003). *Industrial Organic Chemistry*. Wiley. https://doi.org/10.1002/9783527619191

Wiley Critical Content. (2007). *Petroleum Technology*. John Wiley & Sons, Inc, New Jersey.

Zhou, T., Wang, J., McBride, K., & Sundmacher, K. (2016). Optimal design of solvents for extractive reaction processes. *AIChE Journal*, *62*, 3238–3249. https://doi.org/10.1002/aic.15360

2

CHAPTER TWO

The Identification and Screening of Potential Organic Solvents for the Liquid-Liquid Extraction of Aromatics

Abstract

There is increasing focus on the replacement of commonly used solvents in the liquid-liquid extraction of aromatics with solvents that result in improved process economics as well as reduced risk in terms of health, safety, and environment. In this work a selection of organic chemicals is proposed for further study as replacement solvents that meet the technological requirements for the process of aromatics extraction from alkanes, and have not been conventionally considered previously for this application. There were 52654 organic chemicals screened with the use of a search algorithm based on the process requirements in terms of physical properties, capacity, selectivity, and performance index. Nine organic chemicals were identified (not being previously considered) that met all the criteria imposed by the search algorithm. A risk assessment further screened the identified chemicals, filtering out the potential solvents with adverse impacts on health, safety, and the environment. Process designs were developed with the use of ASPEN Plus V10 in order to ascertain the effects of solvent choice on process economics via the use of total annual costs. The screening process in this work produced significant insights due to its holistic approach. The incorporation of factors such as solvent price, solvent loss, utilities, capital costs, health and environmental impact, showed that several of the solvents identified may be sustainable and cost effective alternatives to conventionally used solvents. This highlights the need for a robust and broad perspective in considering the impact of solvent choice.

2.1. Introduction

There is a group of aromatic chemicals, called BTEX (benzene, toluene, ethylbenzene, and xylene) compounds, which are utilized for a variety of purposes – including being used as a feedstock to the plastic and fibers industry (Chen et al., 2017). These chemicals are produced by the petroleum industry and can be regarded as byproducts, albeit significant byproducts.

Processes in the petroleum industry such as catalytic reformation, hydrocarbon pyrolysis, and coal pyrolysis contain streams with varying concentrations of aromatic compounds. Generally, the method of aromatics production is separation from these intermediate petroleum streams. The type of separation depends on the concentration of the aromatics in these streams (Wiley Critical Content, 2007). Traditional distillation is not used because the boiling points of the aromatic compounds are very close to the other hydrocarbon groups in the mixture (primarily aliphatics). Liquid-liquid extraction with a polar solvent is used for aromatic content between 20-65%, whereas extractive and azeotropic distillation are used for higher concentrations (Firnhaber et al., 2000; Weissermel & Arpe, 2003).

A common solvent extraction system involves contacting the aromatic feedstock with a solvent in a packed or trayed column to form two immiscible phases. There is a distribution of components between the two phases via mass transfer from the solute (aromatics) to the solvent and the result is two streams – one rich in solvent and aromatics (extract), and the other rich in the remaining non-aromatic components (raffinate). The aromatics are then separated from the extract via conventional distillation and the solvent is recycled back to the extraction column (Delancey, 2013; Kaiser et al., 2019).

This process (in the context of the solvent used) has been widely studied; and a variety of liquid-liquid equilibrium (LLE) data has been published for mixtures containing alkanes, aromatics, and certain solvents for more than 50 years. Glycol solvents were used since the early 1950's in the UOP Udex process (Rawat & Prasad, 1980). This process used diethylene and dipropylene glycol as the solvent, with triethylene and tetraethylene glycol later adopted due to superior solvent performance (Delancey, 2013; Rawat & Prasad, 1980). Since the early 1960's, the Sulfolane process became more commonly used due to the observation that the solvent sulfolane demonstrated improved solvent characteristics (Ashcroft et al., 1982; Cassell, Dural, et al., 1989; Cassell, Hassan, & Hines, 1989; Cassell, Hassan, & Junes, 1989; J. Chen, Duan, et al., 2000; J. Chen, Li, et al., 2000; de Fré & Verhoeye, 1976; Mohsen-Nia et al., 2005). Other organic chemicals were then studied in the following decades as potential solvents such as 1-

methylpyrrolidin-2-one (NMP) (Alkhaldi et al., 2009; Al-Zayied et al., 1990; Ferreira et al., 1984), morpholine-4-carbaldehyde (NFM) (D. Chen, Ye, & Hao, 2007; Seyedein Ghannad et al., 2011; Wang et al., 2012), N,N-dimethylmethanamide (DMF) (Li et al., 2014), and dimethyl sulfoxide (DMSO) (Saha et al., 1998a).

It is important to continually search for new solvents with the aim of decreasing risks to health, safety, and environment, as well as improving process economics. An environmentally friendly solvent would ideally be biodegradable, with low volatility and toxicity (Canales & Brennecke, 2016). The focus in recent times has been on ionic liquids as an environmentally friendly alternative to volatile organic solvents (Canales & Brennecke, 2016; de Riva et al., 2016; Ferro et al., 2015; Huddleston et al., 1998; Meindersma, 2005). However, there are challenges in replacing conventional organic solvents due to the difficulty and cost associated with the large-scale production of ionic liquids. Additionally, some ionic liquids are not necessarily considered intrinsically "green" for a variety of reasons – among them being the non-renewable feedstock used for production and the disposal method utilized (Werner et al., 2010). Deep Eutectic Solvents (DES) have also been studied extensively, analogously to ionic liquids, as potential replacement solvents due to benefits in terms of environmental impact and costs. Many are based on choline chloride and levulinic acid, combined with urea, glycerol, and ethylene glycol (Hadj-Kali et al., 2017). Some difficulties identified with the large-scale adoption of deep eutectic liquids are the high melting points, and solvent recovery via distillation as the temperature profiles are close to the thermal stability boundaries (Larriba et al., 2018). A recent promising development is the use of cyclic carbonates due to good solvent properties, use of CO_2, simple synthesis route, and comparable extraction ability to sulfolane and NFM (Hernández et al., 2021).

The objective of this work is to propose a series of organic chemicals for further study as new potential aromatic extraction solvents, that have not been widely considered for usage in the solvent extraction of aromatics in the published literature, to the best of the knowledge of the authors. The identification of new potential solvents was conducted in three phases. The first was determining a series of chemicals that could theoretically be used by meeting the physical and thermodynamic requirements of the process. The second phase was a risk assessment of the chemicals identified in the first phase to determine their suitability in terms of occupational health, safety, and environmental impact. The third phase is an assessment of the process economics of the chemicals screened in the first two phases with respect to

solvent rates, solvent cost, energy consumption, capital costs, operating costs, and total annual costs (TAC).

2.2. Identification of Potential Solvents

2.2.1 Physical Property Screening

A search algorithm using physical property requirements based on the extraction process was developed to identify organic chemicals for further study as potential solvents. Table 2.1 lists constituents of the feed to the process, with selected physical properties. It is assumed that despite variations in composition between the types of feedstock that could be used (reformate or pyrolysis gasoline intermediates), the feedstock would consist of a combination of the alkanes and aromatics listed in Table 2.1.

Table 2.1. Feedstock components to aromatics extraction unit with selected physical properties.

Component (Firnhaber et al., 2000; Meindersma & de Haan, 2008)	**Boiling Point at 101.33 kPa** (Carl. L. Yaws, 2015)	**Density at 298.15 K (g/cm^3)** (C. Yaws, 2014)
i-Pentane	309.21	0.621
n-Pentane	300.98	0.616
Cyclopentane	322.40	0.750
2,3-Dimethylbutane	331.13	0.658
2-Methylpentane	333.36	0.648
3-Methylpentane	336.42	0.660
n-Hexane	341.86	0.656
Methylcyclopentane	345.00	0.745
Benzene	353.22	0.873
Cyclohexane	353.90	0.773
2-Methylhexane	363.20	0.674
3-Methylhexane	365.00	0.684
n-Heptane	371.53	0.682
Methylcyclohexane	374.00	0.766
Toluene	383.75	0.865
2-Methylheptane	390.80	0.696
1,3-Dimethylcyclohexane	393.00	0.767

n-Octane	398.77	0.699
Ethylcyclohexane	405.00	0.784
2,6-Dimethylheptane	408.36	0.706
Ethyl benzene	409.35	0.865
p-Xylene	411.51	0.858
m-Xylene	412.27	0.861
3-Methyloctane	417.38	0.717
o-Xylene	417.58	0.876
n-Nonane	423.91	0.715
n-Decane	447.20	0.728
i-Decane	440.15	0.723

As the solvent is desired in the heavier extract phase, it is important that the solvent possesses a density larger than that of the heaviest aromatic, which is 0.873 g/cm^3 as seen in Table 2.1. The recovery of the solvent is done via distillation, necessitating that the boiling point of the solvent be significantly higher than that of highest-boiling aromatic – which as seen in Table 2.1 is 417.58 K. Other desired physical properties are that of low viscosities, high surface tension, and low vapour pressure (Müller et al., 2000). Additionally, it would be important for the solvent to be stable in a range of temperatures, nonreactive with the other components, and noncorrosive to equipment. The solvent should also possess a melting point lower than the operating temperatures of the process.

Two important characteristics of measuring solvent performance is that of capacity and selectivity. Selectivity gives an indication of the affinity of the solvent to solubilize aromatics, and capacity indicates the maximum volume of aromatics that the solvent is able to extract (solubility). An ideal solvent would therefore possess a high selectivity for aromatics, low selectivity for non-aromatics, and a high capacity for aromatics. Generally, most solvents would have a trade-off between selectivity and capacity, with better performing solvents demonstrating good selectivity and capacity.

Capacity is represented mathematically as the distribution coefficient of the aromatic component (K_A) between the two immiscible phases.

$$K_A = \frac{x_i^I}{x_i^{II}} \tag{2.1}$$

K_A is the solvent capacity, x the phase composition, subscript 'i' the aromatic component, and superscripts I and II the solvent-rich and aliphatic-rich phases respectively.

Selectivity is represented mathematically as the ratio of distribution coefficients between the aromatic (i) and non-aromatic (j) component.

$$S_{ij} = \frac{K_i}{K_j} = \frac{x_i^I x_j^{II}}{x_i^{II} x_j^I} \tag{2.2}$$

The distribution coefficient of the aromatic should exceed that of the non-aromatic components, and as such for the solvent to be effective, the selectivity must exceed 1.

The thermodynamic criterion for a liquid-liquid system comprising two phases (I and II), can be expressed in terms of activity coefficients (γ) as indicated in Equation (2.3) (Smith et al., 2001).

$$x_i^I \gamma_i^I = x_i^{II} \gamma_i^{II} \tag{2.3}$$

This allows for expression of the capacity and selectivity in terms of activity coefficients as shown in Equations (2.4) and (2.5) respectively.

$$K_i = \frac{\gamma_i^{II}}{\gamma_i^I} \tag{2.4}$$

$$S_{ij} = \frac{\gamma_i^{II} \gamma_j^I}{\gamma_i^I \gamma_j^{II}} \tag{2.5}$$

Brignole et al. (1986) proposed a performance index (Equation 2.6) that incorporates both selectivity and capacity.

$$PI = S_{ij} \times K_i \tag{2.6}$$

The activity coefficients were estimated with the use of the UNIFAC (LLE) model (Fredenslund et al., 1975). A search algorithm was implemented to determine potential organic solvents, illustrated in Figure 2.1.

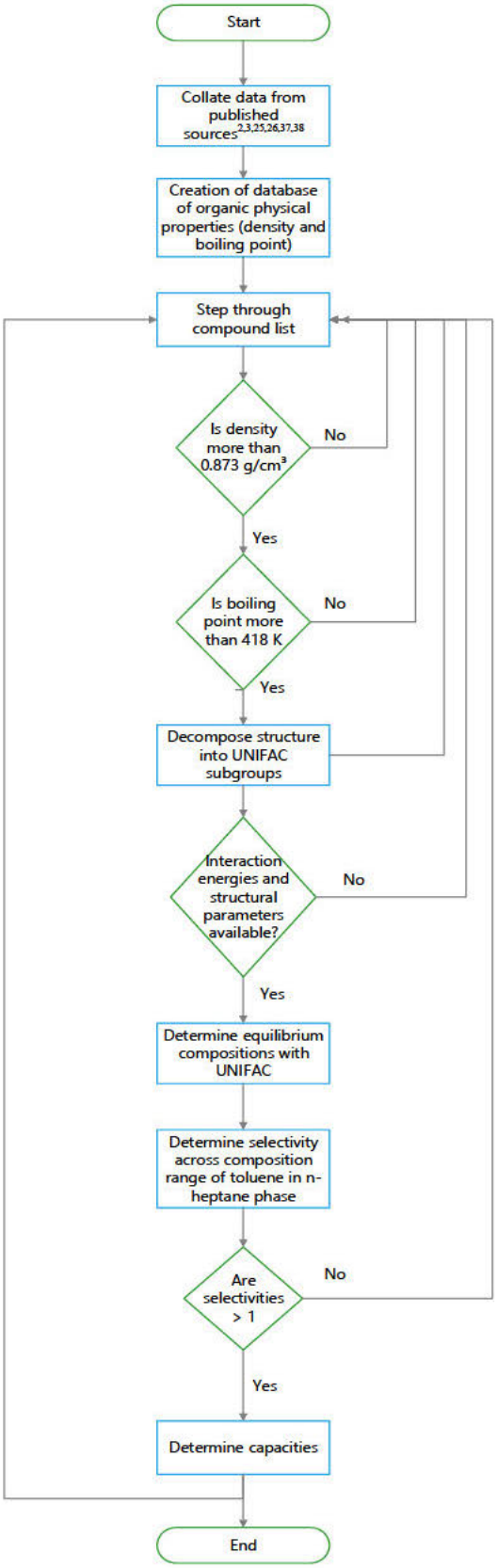

Figure 2.1. Search algorithm to determine solvent suitability in terms of physical properties, selectivity, and capacity.

2.2.2 Solvent Identification Results

The suitability of the new potential solvents resulting from the methodology in the preceding section are discussed in terms of their physical properties by comparison against the existing conventional solvents. This gives an indication of how likely such solvents would be able to easily integrate within existing processes should they demonstrate improved feasibility over existing solvents. Thereafter, the capacity, selectivity, and performance index for the new potential solvents (determined from the UNIFAC model) are represented and discussed together with the capacity, selectivity, and performance index for the conventional solvents.

Table 2.2 lists the physical properties for conventional solvents with a comparison to the potential solvents identified in this work. There were 52654 organic chemicals screened and the compounds listed in Table 2.2 are identified as most promising for further study as new potential solvents. The conventional solvents listed in Table 2.2 have boiling points between 426.25 – 560.45 K, and the new solvents between 470.62 - 564.37 K which indicates that the probability is high that these chemicals could be more easily separated from the aromatic components via distillation.

The melting point of the conventional solvents vary between 212.75 – 301.55 K, and the new potential solvents 196.15 – 301.02 K. Sulfolane has the highest melting point just above room temperature, similarly to diethanolamine from the new set. The implication is that higher operating temperatures above room temperature would be required if a process were to use diethanolamine, analogous to the operating temperatures for sulfolane.

All of the new potential solvents possess densities greater than the heaviest aromatic component (0.92 – 1.26 g/cm^3). This allows for the solvent to form the extract phase containing the aromatic components for further separation.

Lower viscosities are desired to reduce the possibility of ineffective transfer of the solute (aromatic component) to the solvent-rich phase, and to reduce energy costs of fluid transport (Müller et al., 2000). Sulfolane has a viscosity of 10.26 mPa.s; while the list of new potential solvents, possess four compounds with significantly lower viscosities (2.19 – 5.65 mPa.s). On the other hand, four compounds demonstrate higher viscosities between 71.81 – 582.60 mPa.s. Higher viscosities are less preferable due to higher energy and pumping costs and lower column efficiencies.

Table 2.2. Comparison of physical properties of conventional solvents to new potential solvents at 298.15 K and 101.33 kPa (Aspen Plus, 2004; Canales and Brennecke, 2016; Green and Perry, 2008; Yaws, 2014, 2015)**.**

Conventional Solvents	**MW (g/mol)**	**T_b (K)**	**T_m (K)**	**ρ (g/cm^3)**	**μ (mPa.s)**	**P_{vap} (Pa)**	**σ ($mN.m^{-1}$)**
Sulfolane	120.17	560.45	301.55	1.27	10.26	1.46	51.3
Ethylene glycol (EG)	62.07	470.65	260.15	1.10	16.06	11.91	48.6
Diethylene glycol (EG)	106.12	518.65	262.85	1.11	30.2	2.32	27.93
N-Methyl-2-pyrrolidone (NMP)	99.13	475.05	248.75	1.03	1.67	50	40.25
N-Formylmorpholine (NFM)	115.13	513.15	296.15	1.15	7.67	5.77	45.86
Dimethylformamide (DMF)	73.09	426.25	212.75	0.94	0.9	370	35.83
Dimethyl sulfoxide (DMSO)	78.13	462.25	291.75	1.10	2	60	41.7
New Potential Solvents (Identified in this work)	**MW (g/mol)**	**T_b (K)**	**T_m (K)**	**ρ (g/cm^3)**	**μ (mPa.s)**	**P_{vap} (Pa)**	**σ ($mN.m^{-1}$)**
Ethyl cyanoacetate	113.12	479.16	246.81	1.06	2.19	4.65	35.55
Diethylenetriamine	106.12	518.61	262.85	1.11	5.65	2.00	41.64
2-Methyl-2,4-pentanediol	118.18	470.62	223.15	0.92	25.60	8.58	32.76
3-Hydroxypropanenitrile	71.08	493.81	228.20	1.04	3.57	15.64	58.03
1,3-Butanediol	90.12	481.38	196.15	1.00	98.30	6.51	37.80
1,4-Butanediol	90.12	502.80	293.58	1.01	71.81	1.17	44.20
Diethanolamine	105.14	542.02	301.02	1.09	553.64	0.10	49.57
Glycerol	92.09	564.37	290.83	1.26	582.60	0.03	63.05

Vapour pressure is an important factor to consider due to the role it plays in determining the rate of solvent loss (Müller et al., 2000). A lower vapour pressure is desired to limit these factors. Conventional solvents listed in Table 2.2 have vapour pressures between 1.46 – 370 Pa at ambient conditions, whereas the new potential solvents possess vapour pressures between 0.03 – 15.46 Pa. The vapour pressures of the new potential solvents appear to be lower overall.

A high surface tension for the solvent is desired to limit the formation of emulsions (Müller et al., 2000). There is no significant difference in the order of magnitude in terms of surface tension for the conventional solvents (27.93 – 51.3 $mN.m^{-1}$) compared to the new potential solvents (32.76 – 63.05 $mN.m^{-1}$). This would seemingly indicate that these chemicals are similar to the conventional solvents in their susceptibility to form emulsions.

Solvent performance is frequently established and reported in literature typically in the form of ternary liquid-liquid equilibrium (LLE) measurements. The ternary system consists of the solvent, a representative aromatic such as benzene or toluene, and a representative alkane such as *n*-heptane or *n*-hexane, as these components are higher in concentration than other aliphatics (Meindersma & de Haan, 2008). Literature data of different alkane chain lengths as well as branched-chain alkanes, with different aromatic compounds is also available and aids in the assessment of the phase behavior of the variety of compounds contained in feed mixtures as listed in Table 2.1. This data is often most successfully modeled with the Non-Random Two-Liquid (NRTL) (Renon & Prausnitz, 1968) and Universal QuasiChemical (UNIQUAC) (Abrams & Prausnitz, 1975) models, and regressed parameters can be used to design solvent extraction systems at conditions different to the conditions under which the equilibrium studies were conducted. The capacity and selectivity (defined in the preceding section) are useful indicators derived from the thermodynamic behavior that characterizes the capability of the solvent as an extractive agent.

If there is no experimental LLE data available for a potential solvent, then activity coefficients at infinite dilution can be used to investigate the solvent's efficacy in the required separation problem. These limiting activity coefficients give an insight into the behaviour of a solution with a low concentration of an important component, which enables an assessment of the recoverability and separability of that specific component. The activity coefficient at infinite dilution describes the behaviour of the aromatic component surrounded by excess solvent, which represents an environment of maximum non-ideality.

However, if there are no LLE nor infinite dilution activity coefficient data available, the only option is to use predictive methods to estimate the potential solvent's behaviour with the aromatic and aliphatic components. The potential solvents screened in this work do not have published LLE or limiting activity coefficient data, and as such the phase behaviour for the ternary systems *n*-heptane (1) / toluene (1) / solvent (3) were estimated with the use of the group contribution method UNIFAC (Fredenslund et al., 1975), where the solvent are chemicals listed in Table 2.1. Predictions were also made with the modified UNIFAC (Do) model (Weidlich & Gmehling, 1987), and good agreement was identified with the prediction from the UNIFAC (LLE) model for some systems that could be compared. The results reported in this work are only that of the UNIFAC (LLE) predictions due to the fact that there are more main group and sub-group parameters as well as interaction energies available for this model, allowing more chemicals to be screened. Of the 52654 compounds screened, there were an additional 117 chemicals that met the criteria based on physical properties but could not be evaluated in terms of selectivity and capacity due to lack of available of structural parameters.

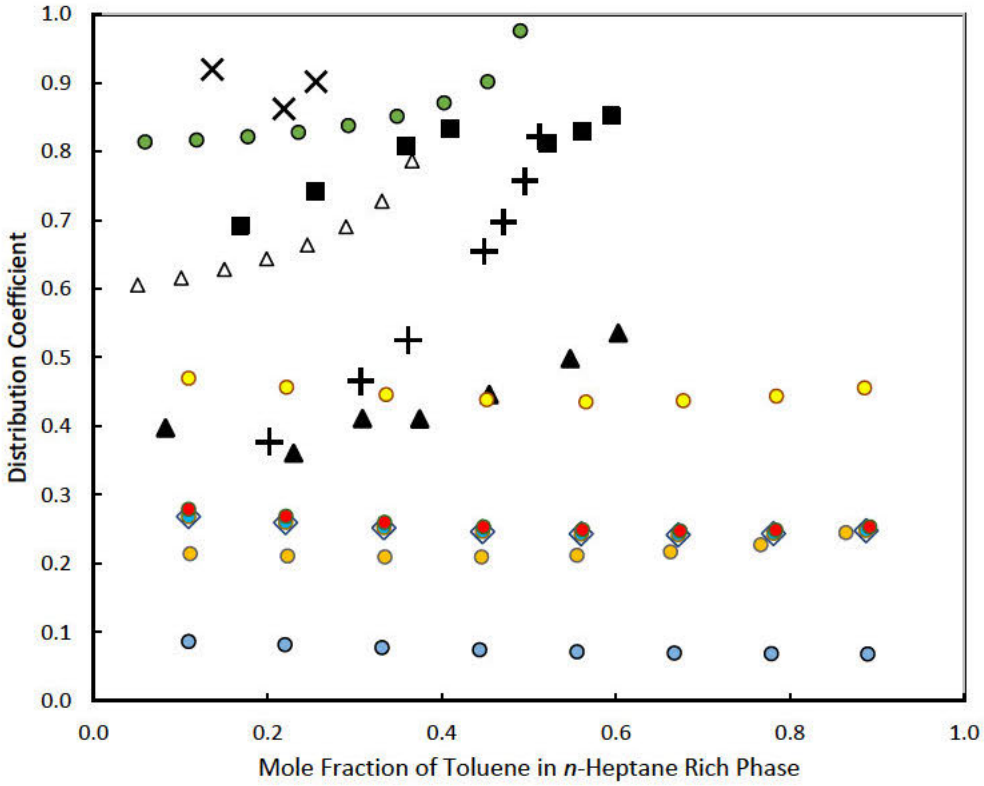

Figure 2.2. Solvent capacity comparison at 298.15 K and 101.33 kPa with respect to toluene content in the raffinate phase for conventional solvents from literature against new potential solvents predicted with UNIFAC-LLE, for the ternary system *n*-heptane (1) /toluene (2) / solvent (3). × – NMP (Nagpal & Rawat, 1981); ▲ – Sulfolane (Tripathi et al., 1975); + – NFM (DongChu, HongQi, & Hao, 2007); ■ – DMSO (Farghi & Kaddami, 2008); ● – Ethyl Cyanoacetate (Predicted); △ – Diethylenetriamine (Predicted); ● – 2-Methyl-2,4-pentanediol (Predicted); ● – 3-Hydroxypropanenitrile (Predicted); ● – 1,3-Butanediol (Predicted), partially obscured by diethanolamine; ◇ – 1,4-Butanediol (Predicted); ● – Diethanolamine (Predicted); ● – Glycerol (Predicted).

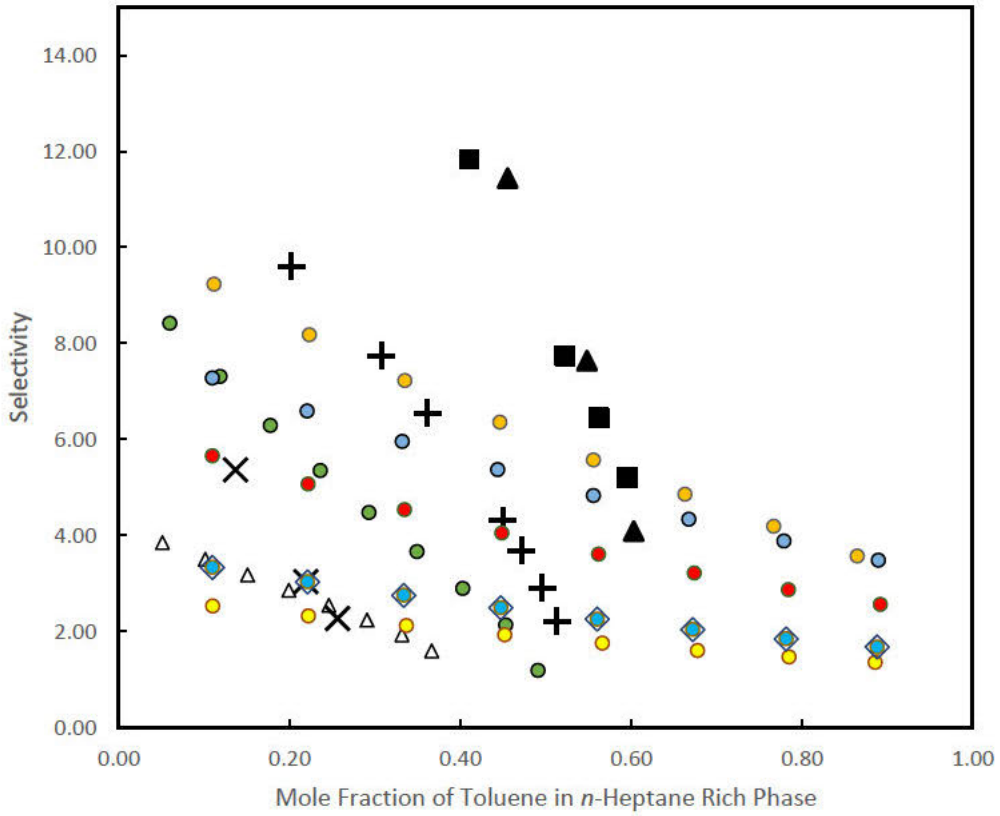

Figure 2.3. Selectivity comparison at 298.15 K and 101.33 kPa with respect to toluene content in the raffinate phase for conventional solvents from literature against new potential solvents predicted with UNIFAC-LLE, for the ternary system *n*-heptane (1) /toluene (2) / solvent (3). × – NMP (Nagpal & Rawat, 1981); ▲ – Sulfolane (Tripathi et al., 1975); + – NFM (DongChu, HongQi, & Hao, 2007); ■ – DMSO (Farghi & Kaddami, 2008); ● – Ethyl Cyanoacetate (Predicted); △ – Diethylenetriamine (Predicted); ● – 2-Methyl-2,4-pentanediol (Predicted); ● – 3-Hydroxypropanenitrile (Predicted); ● – 1,3-Butanediol (Predicted); ◇ – 1,4-Butanediol (Predicted); ● – Diethanolamine (Predicted); ● – Glycerol (Predicted).

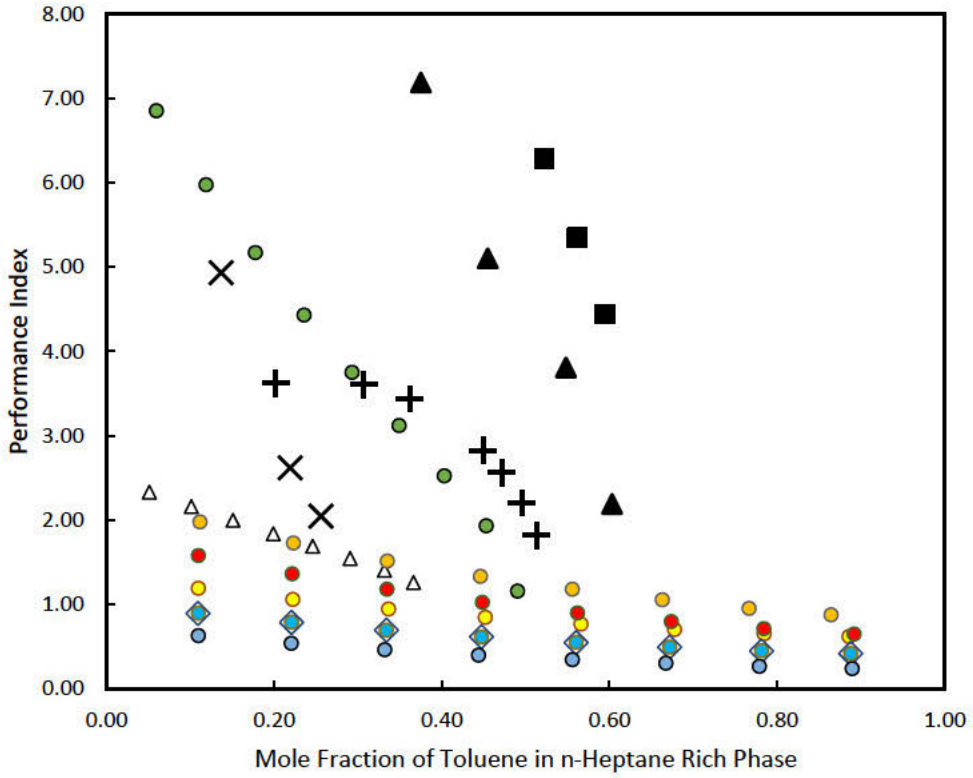

Figure 2.4. Performance index comparison at 298.15 K and 101.33 kPa with respect to toluene content in the raffinate phase for conventional solvents from literature against new potential solvents predicted with UNIFAC-LLE, for the ternary system *n*-heptane (1) /toluene (2) / solvent (3). × – NMP (Mohsen-Nia et al., 2005); ▲ – Sulfolane (Tripathi et al., 1975); + – NFM (DongChu, HongQi, & Hao, 2007); ■ – DMSO (Farghi & Kaddami, 2008); ● – Ethyl Cyanoacetate (Predicted); ● – Diethylenetriamine (Predicted); ● – 2-Methyl-2,4-pentanediol (Predicted); ● – 3-Hydroxypropanenitrile (Predicted); ● – 1,3-Butanediol (Predicted); ◇ – 1,4-Butanediol (Predicted); ● – Diethanolamine (Predicted); ● – Glycerol (Predicted).

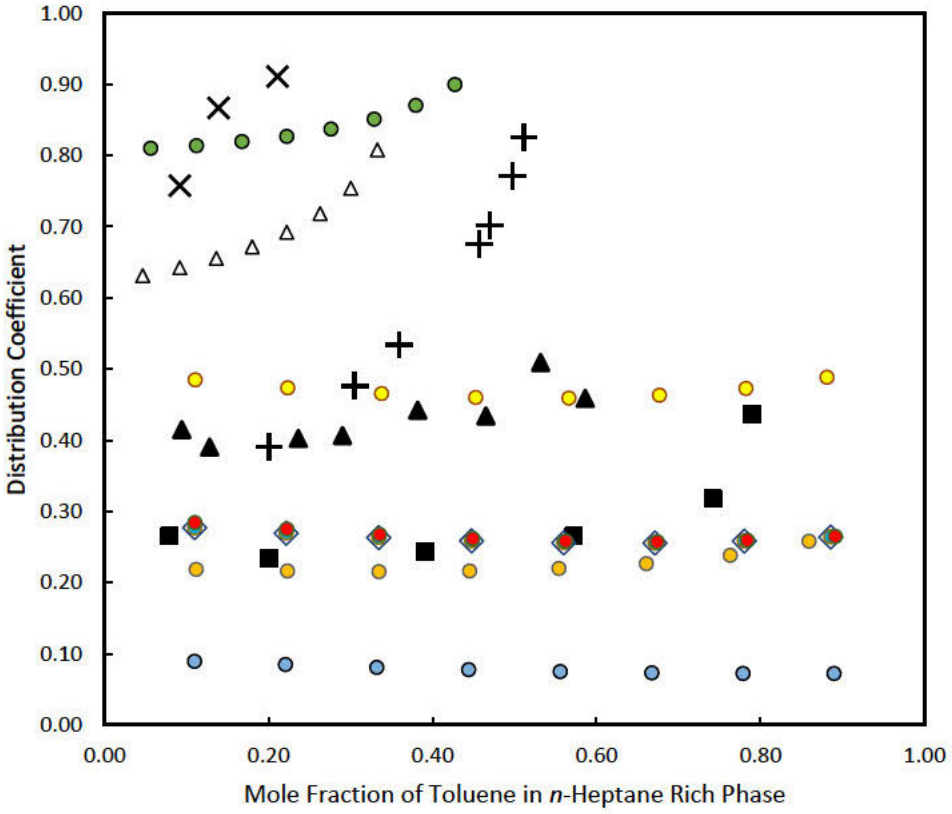

Figure 2.5. Solvent capacity comparison at 313.15 K and 101.33 kPa with respect to toluene content in the raffinate phase for conventional solvents from literature against new potential solvents predicted with UNIFAC-LLE. × – NMP (Nagpal & Rawat, 1981); ▲ – Sulfolane (Tripathi et al., 1975); **+ – NFM (DongChu, HongQi, & Hao, 2007); ■ – Tetraethylene Glycol** (Saha et al., 1998a); **● – Ethyl Cyanoacetate (Predicted); △ – Diethylenetriamine (Predicted); ○ – 2-Methyl-2,4-pentanediol (Predicted); ○ – 3-Hydroxypropanenitrile (Predicted); ○ – 1,3-Butanediol (Predicted), partially obscured by diethanolamine; ◇ – 1,4-Butanediol (Predicted); ● – Diethanolamine (Predicted); ○ – Glycerol (Predicted).**

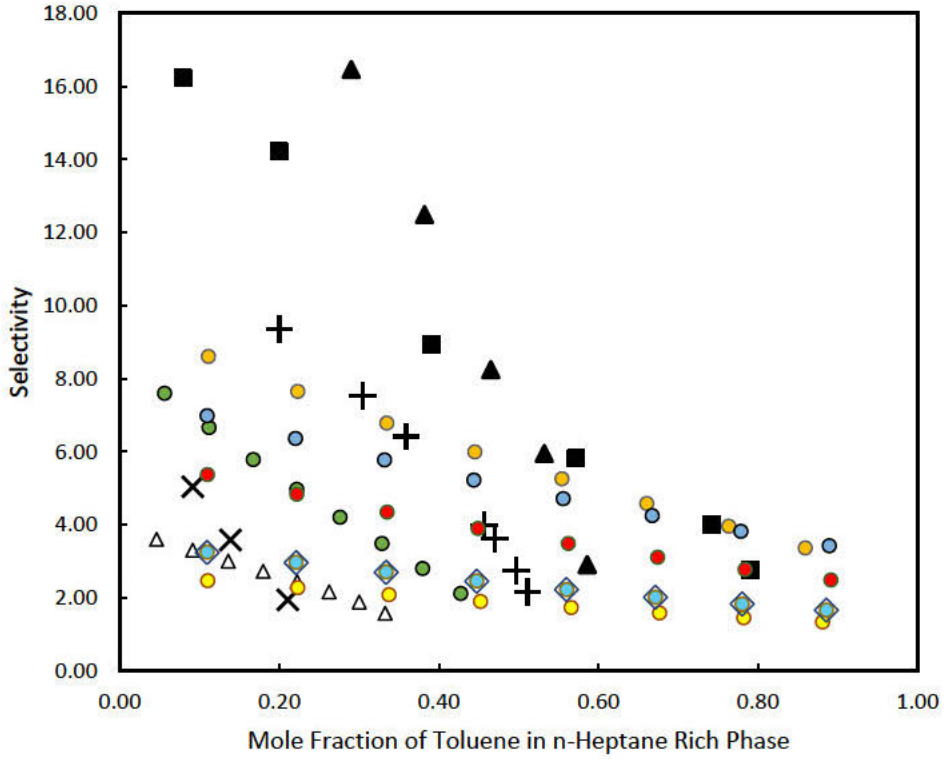

Figure 2.6. Selectivity comparison at 313.15 K and 101.33 kPa with respect to toluene content in the raffinate phase for conventional solvents from literature against new potential solvents predicted with UNIFAC-LLE, for the ternary system *n*-heptane (1) /toluene (2) / solvent (3). × – NMP (Nagpal & Rawat, 1981); ▲–Sulfolane (Tripathi et al., 1975); + – NFM (DongChu, HongQi, & Hao, 2007); ■ – Tetraethylene Glycol (Saha et al., 1998a); ● – Ethyl Cyanoacetate (Predicted); △ – Diethylenetriamine (Predicted); ● – 2-Methyl-2,4-pentanediol (Predicted); ● – 3-Hydroxypropanenitrile (Predicted); ● – 1,3-Butanediol (Predicted); ◇ – 1,4-Butanediol (Predicted); ● – Diethanolamine (Predicted); ● – Glycerol (Predicted).

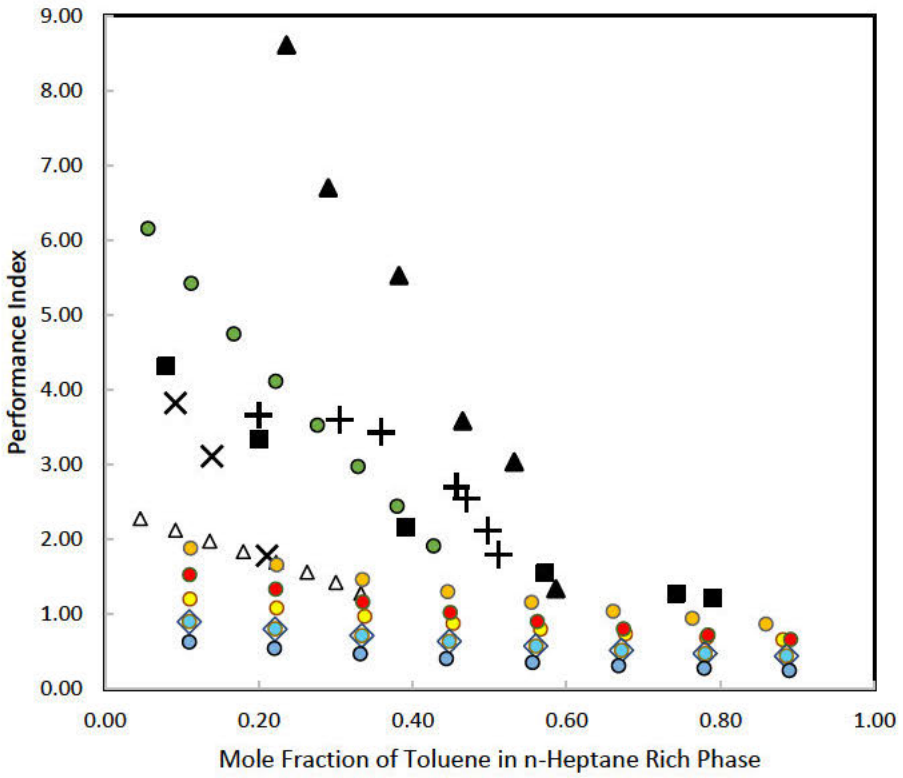

Figure 2.7. Performance index comparison at 313.15 K and 101.33 kPa with respect to toluene content in the raffinate phase for conventional solvents from literature against new potential solvents predicted with UNIFAC-LLE, for the ternary system *n*-heptane (1) /toluene (2) / solvent (3). × – NMP (Nagpal & Rawat, 1981); ▲–Sulfolane (Tripathi et al., 1975); + – NFM (DongChu, HongQi, & Hao, 2007); ■ – Tetraethylene Glycol (Saha et al., 1998a); ● – Ethyl Cyanoacetate (Predicted); △ – Diethylenetriamine (Predicted); ● – 2-Methyl-2,4-pentanediol (Predicted); ● – 3-Hydroxypropanenitrile (Predicted); ● – 1,3-Butanediol (Predicted); ◇ – 1,4-Butanediol (Predicted); ● – Diethanolamine (Predicted); ● – Glycerol (Predicted).

Figures 2.2 – 2.4 represent the capacity, selectivity, and performance index predictions for the system *n*-heptane (1) / toluene (2) / solvent (3) at 298.15 K and 101.33 kPa. The solvents are the compounds listed in Table 2.2 that met the criteria represented in Figure 2.1. These predictions are compared on the same axis to phase equilibrium measurements of conventional solvents at the same conditions available in literature. Figures 2.5 – 2.7 are the capacity, selectivity, and performance index predictions as well as literature data at 313 K and 101.33 kPa. These parameters are presented relative to varying concentrations of aromatic (toluene) in the aliphatic-rich phase.

The UNIFAC predictions for capacity in Figures 2.2 and 2.5 suggest that ethyl cyanoacetate appears to possess a capacity for aromatics superior to that of sulfolane, NFM, and DMSO; while being comparative to the conventional solvent with the best capacity (NMP). Diethylenetriamine appears to have promising capacities superior to NFM and DMSO in a range of toluene concentrations, with 2-methyl-2,4-pentanediol (hexylene glycol) possessing capacities similar to sulfolane.

Figures 2.3 and 2.6 indicate that all of the selectivities predicted for the new potential solvents are greater than unity, suggesting that separation with these chemicals is possible. These are worse than sulfolane and DMSO, but similar to NFM and NMP in differing ranges of toluene concentrations. The performance indices shown Figures 2.4 and 2.7 mirror the trends for selectivities highlighted in Figures 2.3 and 2.6. This is due to the fact that this index is the product of selectivity and capacity, as discussed in the preceding section.

2.3. Risk Assessment

2.3.1 Health, Safety and Environmental Impact Benchmarking

A risk assessment in terms of health, safety, and environment (HSE) was conducted on the new potential solvents to determine their suitability as a sustainable alternative in an industrial setting compared to the conventional solvents. A variety of solvent selection guides based on HSE considerations have been published (Alfonsi et al., 2008; Curzons et al., 1999; Henderson et al., 2011; Prat et al., 2013, 2014; Slater & Savelski, 2007). These guides rate solvents into categories such as ‘preferred’ or ‘recommended’, ‘usable’, ‘hazardous’, ‘highly hazardous’ or ‘not recommended’. While the HSE impact for conventional solvents can be determined from said guides, some of the new potential solvents are chemicals that have not been previously considered in this context and are not rated. Therefore, it was necessary to benchmark the HSE impact of the potential solvents relative to the conventional solvents. The general methodology of most solvent selection guides is similar in that each attribute scores to the solvents within various HSE criteria, with the subsequent ranking determining the category a solvent falls in. This method has been applied to the chemicals considered in this study. This risk assessment does not serve as a framework for general solvent selection, but rather as a benchmarking mechanism to compare the health, safety, and environmental impact of the new potential solvents against that of conventional solvents for this specific industrial application.

Occupational health risk was scored between 1 to 5 based on the number of hazards as well as impact associated with a particular chemical. A score of 5 indicates a significant health risk as a result of high

acute and chronic toxicity to humans, while a score of 1 represents low acute toxicity. More serious cases of acute toxicity were allocated scores of 2 to 3, while serious chronic cases created by prolonged or repeated exposure were given a score of 4.

With respect to safety, the fire and explosion potential was evaluated by consideration of the flash points and autoignition temperatures. Also considered were reactivity, stability, potential for decomposition, ability to form peroxides, and hazards associated with combustion products. Scoring was conducted based on the number, risk, and impact of particular hazards. If the safety hazard of a chemical was combustible only, then a score of 1 was given, while those which were flammable and had risks associated with reactivity and stability were given higher scores.

Environmental impact was assessed in terms of biodegradability and environmental toxicity. Biodegradation rates as well as the log octanol/water partition coefficient were considered to inform the scoring. A chemical that was not readily biodegradable, possessed high persistency, and was harmful to aquatic life with long lasting effects was attributed a score of 5, while a score of 1 was given to a chemical that could be discharged with minimal pollution risk.

The overall score was determined by summing the individual health, safety and environment scores with a maximum possible score of 15. The conventional and new potential solvents were then categorized using the overall score as follows:

1 to 6 – Preferred (green)

7 to 9 – Usable (orange)

10 to 15 – Undesirable (red)

The overall score highlights specific areas of concern with a view to objectively determine the suitability of the new potential solvents to be considered as sustainable alternatives.

2.3.2 Risk Assessment Results

The results of the benchmarking in terms of health, safety, and environment (HSE) serve to further screen the new potential solvents due to the fact that it is important for any new feasible alternative to be considered a sustainable replacement. Table 2.3 summarizes the main HSE risks and hazards identified for conventional and new potential solvents. The type, number, extent, and impact of the hazards determined the scoring, as highlighted in the preceding section. Figure 2.8 presents the overall and individual HSE scores for each solvent, as well as the category each solvent is placed in (preferred, usable, undesirable). This procedure was performed on the conventional solvents initially in order to set a baseline, to compare to their rating in published solvent guides (Alfonsi et al., 2008; Curzons et al., 1999;

Henderson et al., 2011; Prat et al., 2013, 2014; Slater & Savelski, 2007). The weighting and scoring systems between the guides are different, thus creating difficulties in making direct comparisons. Prat et al. (2014) have collated, combined, and transformed the HSE data in the various guides in order to make a consistent ranking comparison.

Table 2.3. Summary of occupational health, safety, and environmental hazards of conventional and potential solvents.

Conventional Solvents	Known Health Risks (GHS Statement)	Known Safety Risks	Known Environmental Risks
Sulfolane	Harmful if swallowed	Combustible Poisonous gases released in the event of a fire Hygroscopic Eventual degradation into acidic byproducts	Water pollution hazard with release to environment
Ethylene glycol (EG)	Harmful if swallowed May cause damage to organs through prolonged or repeated exposure	Combustible Hygroscopic May decompose at high temperatures	Water pollution hazard with release to environment
Diethylene glycol (EG)	Harmful if swallowed May cause damage to organs through prolonged or repeated exposure	Combustible Hygroscopic May decompose at high temperatures	Water pollution hazard with release to environment Dangerous to aquatic life in high concentrations
N-methyl-2-pyrrolidone (NMP)	Causes skin irritation. Causes serious eye irritation. May cause respiratory irritation. May damage fertility or unborn child.	Combustible Poisonous gases released in the event of a fire Hygroscopic	Water pollution hazard with release to environment

N-formylmorpholine (NFM)	May cause an allergic skin reaction	Combustible Poisonous gases released in the event of a fire	Water pollution hazard with release to environment
Dimethylformamide (DMF)	May damage the unborn child. Harmful in contact with skin or if inhaled. Causes serious eye irritation	Flammable liquid Poisonous gases released in the event of a fire Hygroscopic	Water pollution hazard with release to environment
Dimethyl sulfoxide (DMSO)	Causes skin irritation Causes serious eye irritation	Combustible Hygroscopic May decompose at high temperatures	Water pollution hazard with release to environment Dangerous to aquatic life in high concentrations.
New Potential Solvents			
Ethyl cyanoacetate	Causes serious eye irritation	Combustible Poisonous gases released in the event of a fire Violent reactions possible with strong acids and bases Unstable at elevated temperatures	Water pollution hazard with release to environment
Diethylenetriamine	Harmful if swallowed or in contact with skin. Causes severe skin burns and eye damage.	Combustible Hygroscopic Poisonous gases released in the event of a fire	Water pollution hazard with release to environment

	May cause an allergic skin reaction. Fatal if inhaled. May cause respiratory irritation.	Violent reactions possible with strong acids	
2-Methyl-2,4-pentanediol	Causes skin irritation. Causes serious eye irritation.	Combustible	Water pollution hazard with release to environment
3-Hydroxypropionitrile	Causes skin irritation. Causes serious eye irritation.	Combustible Poisonous gases released in the event of a fire Violent reactions possible with strong acids	Water pollution hazard with release to environment
1,3-Butanediol	Causes serious eye irritation.	Combustible	Water pollution hazard with release to environment
1,4-Butanediol	Harmful if swallowed May cause drowsiness or dizziness	Combustible	Water pollution hazard with release to environment
Diethanolamine	Harmful if swallowed. Causes skin irritation. Causes serious eye damage. May cause damage to organs through prolonged or repeated exposure if swallowed.	Combustible Poisonous gases released in the event of a fire Exothermic reaction with acids Hygroscopic Sensitive to air and light	Water pollution hazard with release to environment Harmful to aquatic life with long lasting effects

Glycerol	May cause mild skin irritation	Combustible Hygroscopic	Water pollution hazard with release to environment
Ethanol	Causes eye irritation	Flammable liquid and vapour Hygroscopic	Water pollution hazard with release to environment

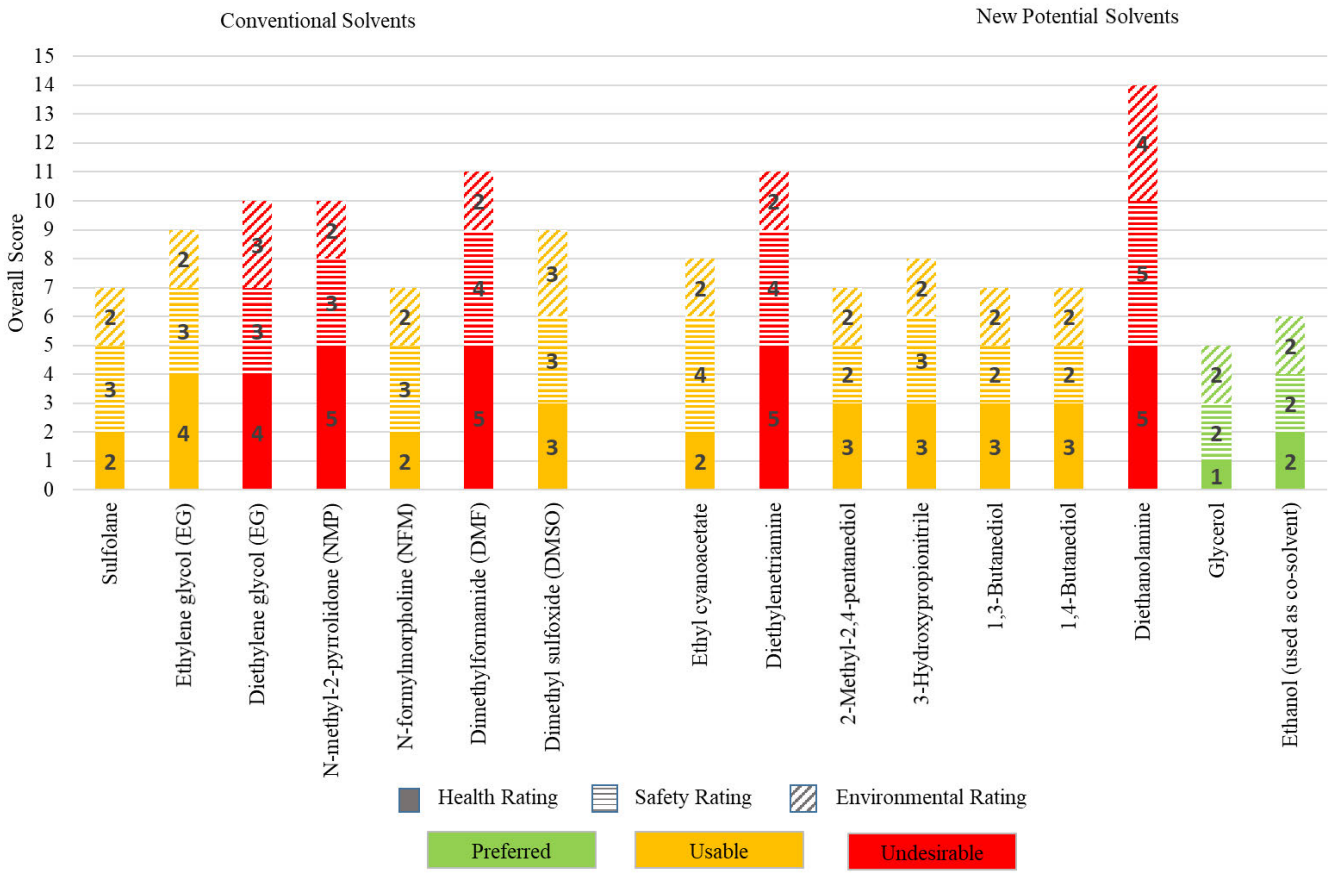

Figure 2.8. Overall scores of conventional solvents and new potential solvents, consisting of individual scores for health, safety, and environment.

In this work, dimethylformamide (DMF), and N-methyl-2-pyrrolidone (NMP) were ranked as 'Undesirable' with scores of 11 and 10, as a result of their acute and chronic toxicity hazards to humans. This corresponds with the relative ratings of Alfonsi et al. (2008) in which DMF and NMP are also rated as 'Undesirable', and Prat et al. (2013) who classified them as 'Substitution Required'. Sulfolane and N-formylmorpholine (NFM) are the best ranking conventional solvents in this study, with a score of 7 and rank as 'Usable'. NFM does not appear in the solvent selection guides, and sulfolane is ranked as 'substitute advised' by Prat et al. (2013). Ethylene glycol was ranked as 'Usable' in this study, which corresponds with its 'Usable' rating by Alfonsi et al. (2008). There is reasonable agreement between the ranking system developed in this work and the solvent selection guides available in literature.

Diethanolamine is ranked the worst from the new potential solvents with a score of 14 ('Undesirable'). This is due to the fact that it poses serious acute and chronic toxicity hazards to humans, is sensitive to air and light, and has long lasting harmful effects to aquatic life. Another that is ranked 'Undesirable' is diethylenetriamine since it causes severe skin burns and eye damage and is fatal if inhaled. Glycerol has the best score of 6 and is the only identified solvent to receive a 'Preferred' rating, as it presents little risk to occupational health and safety and is a renewable bioresource. 1,3-Butanediol, 1,4-butanediol, and 2-methyl-2,4-pentanediol (hexylene glycol) received the same rating as sulfolane and NFM, and as diols, can be produced in biologically sustainable processes.

While glycerol may be the most desirable due to its superior HSE impact rating, it has the lowest performance index (as seen in Figures 2.4 and 2.7). This is primarily due to exceptionally low solvent capacities as indicated in Figures 2.2 and 2.5, while possessing a reasonably good selectivity (as seen in Figures 2.3 and 2.6) superior to NMP and NFM across most of the composition range. Use of glycerol was then considered in conjunction with a co-solvent, which is frequently used to improve characteristics such as capacity or selectivity. The Arosolvan and Formex processes uses NMP and NFM respectively with water as the co-solvent (Weissermel & Arpe, 2003). A variety of commonly used chemicals that present little risk according to published solvent selection guides were considered as potential co-solvents to glycerol such as water, ethanol, *n*-propanol, and *n*-butanol. Ethanol was thereafter identified as a suitable co-solvent due to the good HSE rating, ability to form two phases in a mixture with glycerol and *n*-heptane, and improvement of overall solvent capacity (as highlighted in Figure 2.9). The improvement in capacity is significant with it being comparable to sulfolane and NFM for certain regions of the composition range.

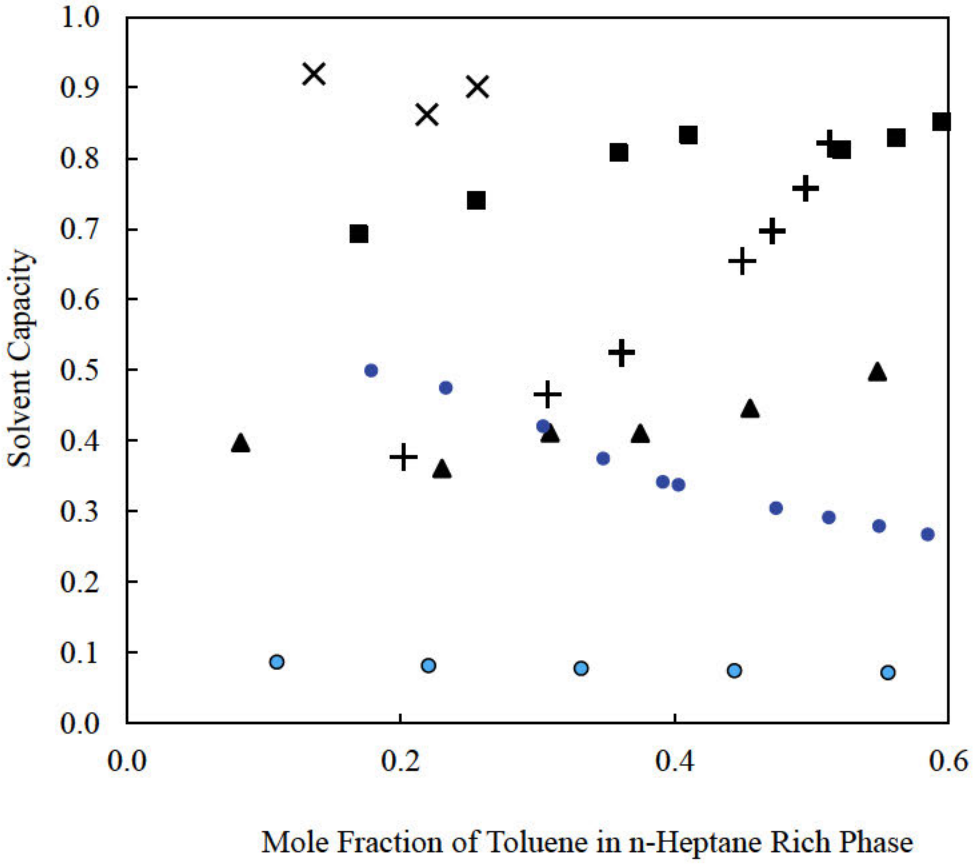

Figure 2.9. Solvent capacity comparison at 298.15 K and 101.33 kPa with respect to toluene content in the raffinate phase for conventional solvents from literature against glycerol and glycerol + ethanol mixtures to demonstrate the increase in solvent capacity; predicted with UNIFAC-LLE for the ternary system *n*-heptane (1) /toluene (2) / solvent (3). × – NMP (Nagpal & Rawat, 1981); ▲–Sulfolane (Tripathi et al., 1975); **+ – NFM (DongChu, HongQi, & Hao, 2007); ■ – DMSO (Farghi & Kaddami, 2008); ● – Glycerol + Ethanol (Predicted); ○ – Glycerol (Predicted).**

2.4. Process Economics

2.4.1 Process Design

The choice of solvent affects the process design in terms of infrastructure requirements thus increasing or decreasing capital costs. Also affected are utilities and other operating costs. It is

therefore necessary to have an indication of how solvent choice affects process economics. The potential solvents identified from the search algorithm were evaluated in conjunction with the conventional solvents to determine their comparative efficacy.

ASPEN Plus V10 was used to develop a conceptual design for each of the solvents tested to meet a specified recovery of at least 99% of aromatics from an aliphatic-aromatic feed. A process design was developed for the extraction and recovery processes for three conventional solvents to set a baseline feasibility to which the potential solvents will be compared. Sulfolane, NFM, and DMSO were chosen due to the high performance index determined from published phase equilibrium data as observed in Figures 2.2 – 2.7, as well as their relatively lower risk in terms of health, safety, and environment (Figure 2.8). 1,4-Butanediol and hexylene glycol were chosen due to their good performance index as discussed in the preceding section as well as HSE scores. Glycerol was chosen as it possesses the best HSE rating.

The process design was developed to separate a 1500 kg/hr feed stream at 25°C and 101.325 kPa, consisting of 70 wt % *n*-heptane and 30 wt % toluene, as this composition falls within the range to which liquid-liquid extraction is applied (Weissermel & Arpe, 2003). In order for the feasibility of the potential solvents to be fairly assessed, it is important that the input conditions under which the process is developed be kept consistent for the baseline and potential solvents. Therefore, the potential solvents must be able to produce relatively equivalent recoveries and purities as that of the baseline/conventional solvents, utilizing the same feed composition. This is necessary to ensure that any assessment made is due to the effect of solvent choice alone. Different refineries will have a range of feed conditions which would each require their own development of a baseline under those specific conditions. The purpose of this evaluation is to determine the effects of solvent choice on process economics to achieve a minimum aromatics recovery of 99 wt %.

The Non-Random Two Liquid (NRTL) (Renon & Prausnitz, 1968) equation was used to model the liquid phases, together with the Redlich-Kwong (Redlich & Kwong, 1949) equation of state for the vapour phase. The NRTL model is able to successfully represent deviations at low pressure, with numerous studies demonstrating the effectiveness of its representation of ternary phase equilibrium measurements consisting of aliphatic-aromatic-solvent mixtures (Alkhaldi et al.,

2009; Al-Zayied et al., 1990; Ashcroft et al., 1982; Cassell, Dural, et al., 1989; Cassell, Hassan, & Hines, 1989; Cassell, Hassan, & Junes, 1989; J. Chen, Duan, et al., 2000; J. Chen, Li, et al., 2000; de Fré & Verhoeye, 1976; Ferreira et al., 1984). The binary interaction parameters are automatically extracted from APV100 VLE-LIT and APV100 LLE-ASPEN databanks. The UNIFAC (LL) model was used to estimate missing parameters or model the liquid phases where no experimental data was available, which was the case with the potential solvents.

The glycols (hexylene glycol, 1,4-butanediol, glycerol) were the only chemicals from the potential solvents for which the use of UNIFAC can be reasonably validated. As the other chemicals (ethyl cyanoacetate, 3-hydroxypropanenitrile, diethylenetriamine, and diethanolamine) are not being considered further for health, safety, and environmental reasons as outlined in the previous section, only the glycols require model validation for further study in the ASPEN simulations. Figures 2.10 – 2.12 illustrate the literature liquid-liquid equilibrium (LLE) data for the systems toluene + ethylene glycol, diethylene glycol, and triethylene glycol respectively. The UNIFAC predictions are reasonably close to the experimental literature data in the temperature range under consideration, suggesting that UNIFAC is suitable for systems containing toluene and glycols under these conditions. The glycols considered in this study consist of longer chains, however UNIFAC accounts for this by including the higher number of CH_2 and OH subgroups in the relative molecular volume (R), and relative molecular surface area (Q) parameters. The use of predictive models is less accurate and reliable compared to using actual published data (Gmehling & Schedemann, 2014; Wittig et al., 2003). Known limitations of group contribution methods are that they do not account for isomeric effects, with difficulties observed in the prediction of systems containing water (Gmehling et al., 2019). The experimental data involving the glycols identified in this work is being measured at the Thermodynamics Research Unit and the data together with thermodynamic modeling is the subject of future publications. The nature of this work is intentional in showcasing a theoretical screening process, highlighting a robust and consolidated method that includes health, safety, environment, process simulations, energy analysis, and economics. The intention is to use the screening process to efficiently direct research focus (and subsequent experimental measurements) in a liquid-liquid extraction application.

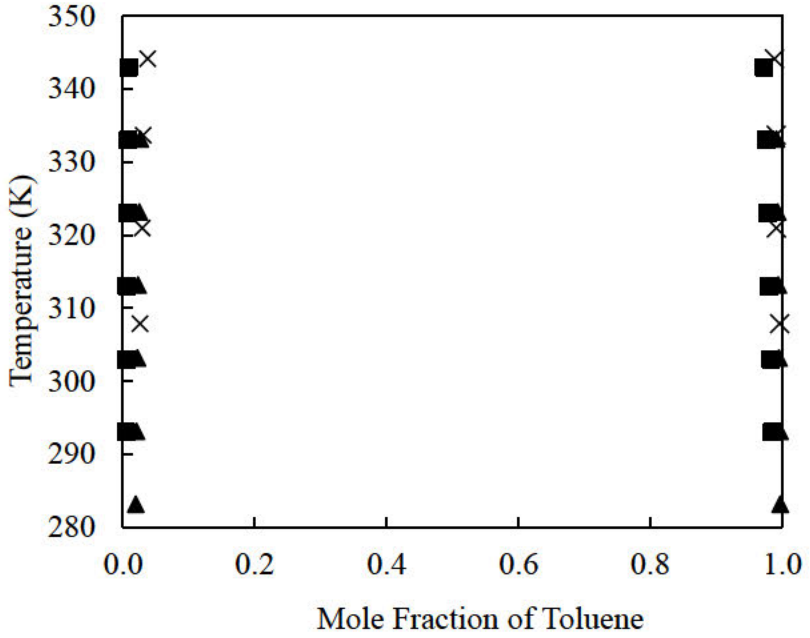

Figure 2.10. Literature LLE data, × (Řehák & Dreiseitlová, 2006), ▲ (Gao et al., 2015)**, for the system toluene + ethylene glycol at 101.33 kPa compared to UNIFAC (LL) predictions (■).**

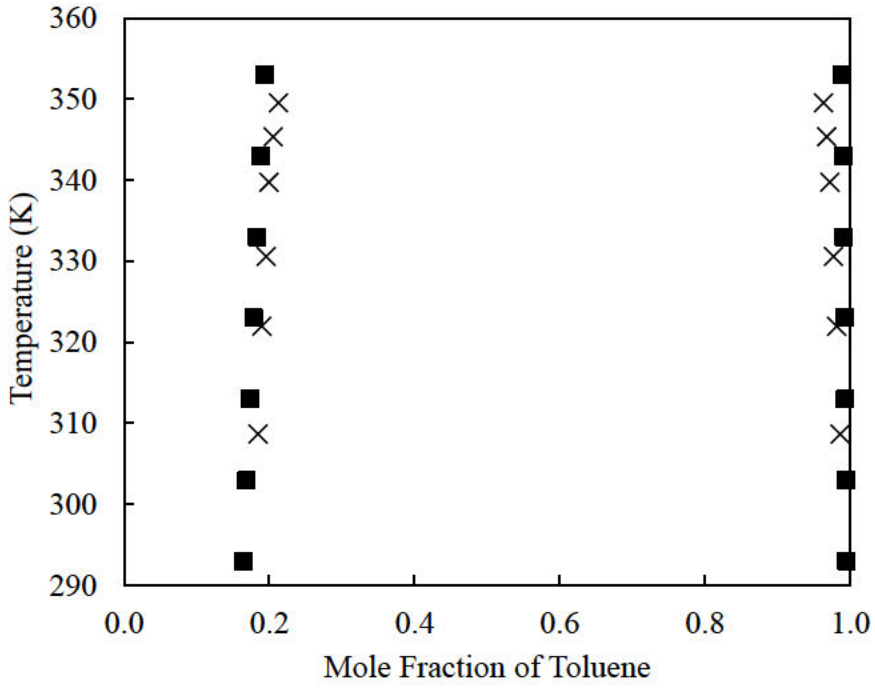

Figure 2.11. Literature LLE data, × (Lesek & Mandík, 1982), for the system toluene + diethylene glycol at 101.33 kPa compared to UNIFAC (LL) predictions (■)

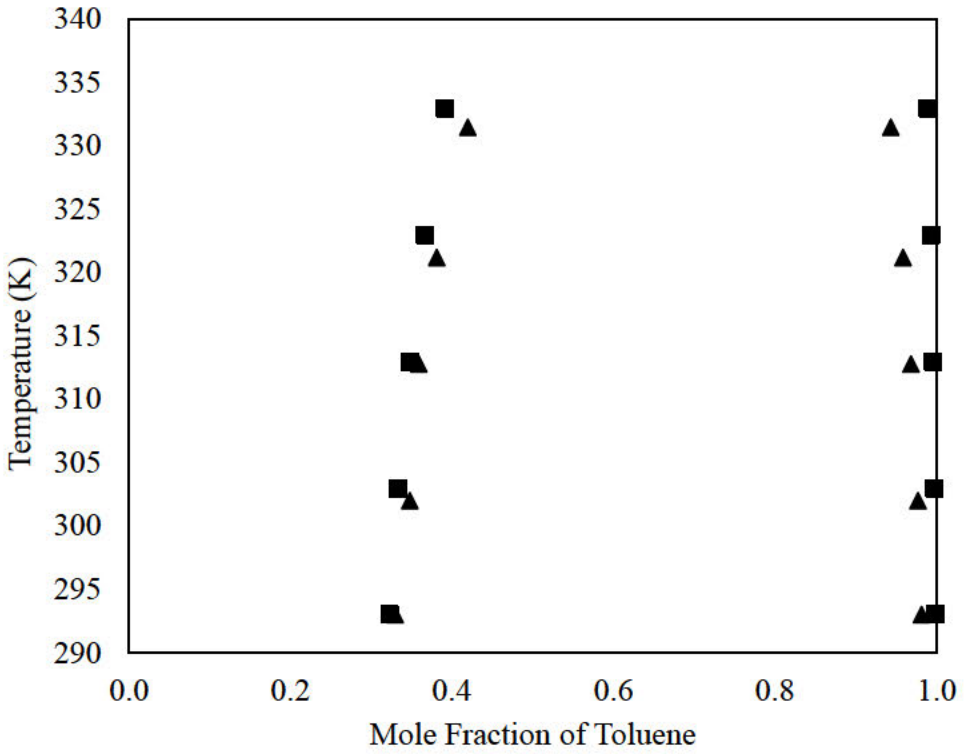

Figure 2.12. Literature LLE data, ▲ (Folas et al., 2006)**, for the system toluene + triethylene glycol at 101.33 kPa compared to UNIFAC (LL) predictions (■)**

A series of three columns were used to achieve the separation, consisting of a counter-current liquid-liquid extraction column followed by a stripper and the solvent recovery column. The rigorous 'Extract' column was used in ASPEN V10 with the feed entering at the bottom and the solvent at the top. The minimum solvent rate was determined with the use of a sensitivity analysis by varying the solvent rate and choosing the minimum flowrate which maximizes recovery of toluene and minimizes recovery of *n*-heptane in the extract. The solvent to feed ratio depends on the feed composition, particularly the aromatic content. As such, the selectivity profile varies across the column length. A large number of stages (50) was selected initially and thereafter optimized using a sensitivity analysis in the same manner as the optimization of the required solvent rate. The column was designed to operate isobarically and isothermally by specifying the temperature and pressure profiles to match the inlet feed conditions. It is unavoidable that there be carryover of *n*-heptane to the extract, due to the decrease in selectivity across the column. This

was addressed with the use of the stripper column to remove the lighter aliphatic component together with a portion of toluene as the distillate, to be recycled back to the extraction column near the fresh feed entry point. This allows for complete recovery of the valuable aliphatic component as the raffinate of the extraction column. The stripper was modeled with the rigorous Radfrac column. The number of stages in the stripper column was initially specified at 50 stages and later optimized with the sensitivity analysis. The boil-up ratio and distillate-to-feed ratio were optimized with the use of the *design spec* functionality in ASPEN V10, in which the desired recovery as well as purity of toluene was specified to be at least 99%. The bottoms of the second column contain the extracted aromatic and solvent, which is then sent to the solvent recovery column with the aim of separating and recycling the solvent to the extraction column. In keeping with industry practice, the solvent loss to the raffinate was addressed with use of another extractor using water as the solvent to capture solvent losses. The water and solvent mixture (extract) is separated in the downstream distillation column and decanter, and recycled to the respective extractors.

Figure 2.13 is the VLE *x-y* data for the aromatic and solvent system, required for the design of the solvent recovery system. Experimental data is available for the toluene + sulfolane (de Fré & Verhoeye, 1976), toluene + NFM (Huang et al., 2008), toluene + DMSO systems (Zhao et al., 2014), while UNIFAC was used to predict the phase behaviour of the potential solvents. The systems of toluene + glycerol, toluene + 2-methyl-2,4-pentanediol, toluene + 1,4-butanediol mirror the phase behaviour of the conventional solvents considered, thus indicating that recovery via conventional distillation can be achieved easily, with the exception of ethanol as a co-solvent.

Figures 2.14 – 2.16 are the simulation results for the base case simulations using sulfolane, NFM and DMSO. Stream flowrates, conditions, compositions, as well as column specs are highlighted. The toluene product flowrate as the distillate of the solvent recovery column is greater than 446 kg/hr for all solvents used, which meets the objective function of a desired recovery; the stream purity is greater than 99%. The desired recovery specification was met for the raffinate of the extraction column which is 99% *n*-heptane (greater than 1038 kg/hr). The feed temperatures of 100°C for sulfolane, 40°C for NFM and 25°C for DMSO were selected based on the actual operating conditions of the Sulfolane, Formex and DMSO processes (Lo & Baird, 2000). While

increasing the boil-up or reflux ratios for the columns increases the product purity, it also increases the heat duties of the condenser or reboiler. Therefore, these parameters were minimized in conjunction with the number of stages and feed stages, with a view towards minimizing capital and energy costs. The boil-up ratio was used for the stripper column because of the relatively small carryover of *n*-heptane, which implies a low distillate rate and therefore small reflux rates. Figures 2.14 – 2.16 also includes the heat duties of heaters, coolers, condensers and reboilers. It is assumed that the fresh feed is coming from intermediate storage at ambient conditions thus requiring preheating of the feed to the extraction column operating temperature in the case of sulfolane and NFM. From the base case simulations, sulfolane appears to have the largest solvent requirement of 4200 kg/hr. This is followed by NFM at 4000 kg/hr, and DMSO significantly lower at 3000 kg/hr. While NFM and DMSO offer lower solvent rates, the boil-up ratio and number of stages in the stripping and solvent recovery columns are higher. In the case of DMSO the reflux ratio is 0.85 compared to sulfolane's (0.4); the number of stages is 25 compared to the 16 required with sulfolane.

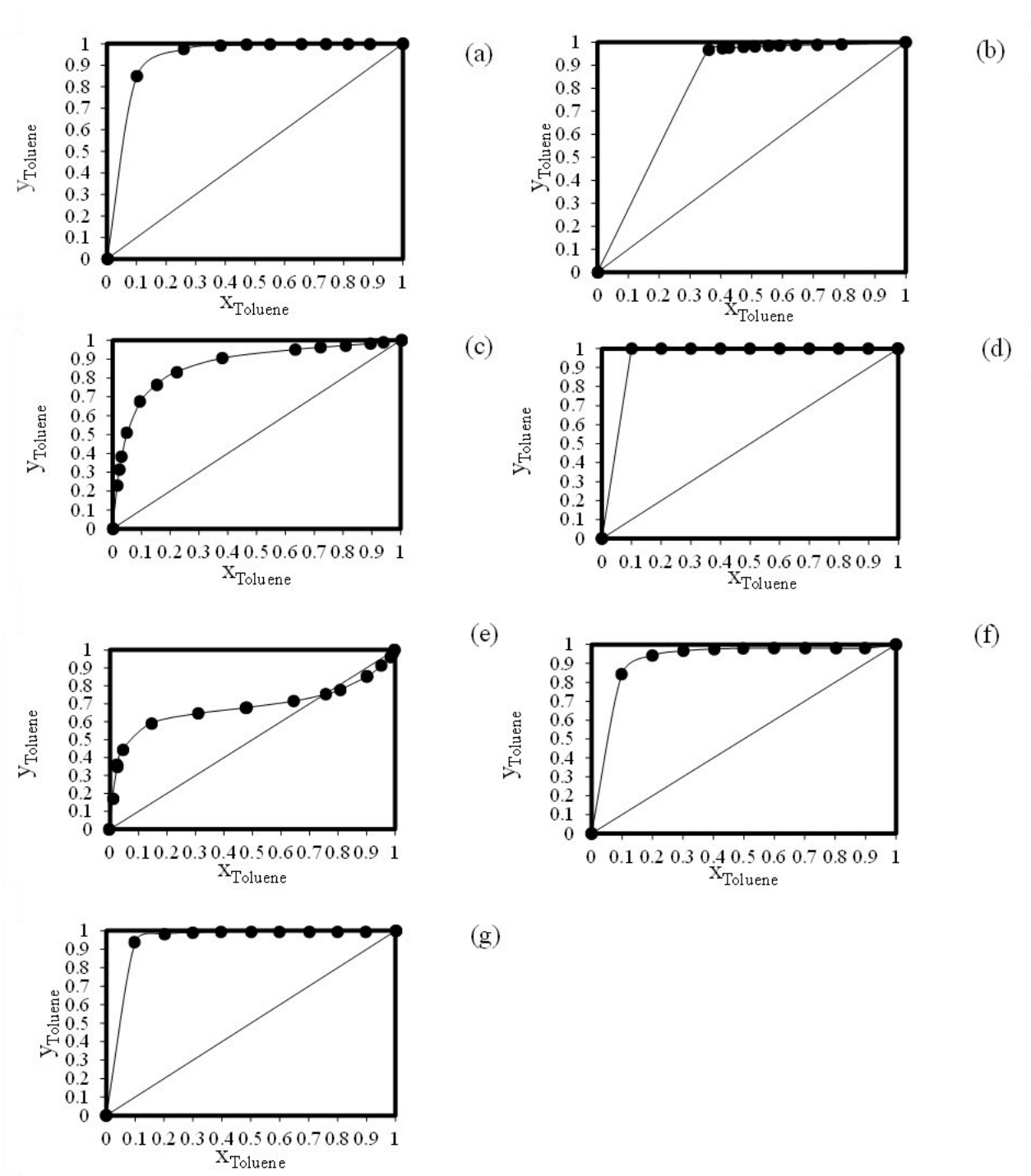

Figure 2.13. Isobaric vapor-liquid equilibrium data (x-y) at 101.33 kPa for the systems: (a) Toluene + Sulfolane, (b) Toluene + NFM (Huang et al., 2008)**, (c) Toluene + DMSO** (Zhao et al., 2014)**, (d) Toluene + Glycerol (UNIFAC), (e) Toluene + Ethanol (Oracz & Kolasińska, 1987), (f) Toluene + 2-Methyl-2,4-pentanediol (UNIFAC), (g) Toluene + 1,4-Butanediol (UNIFAC).**

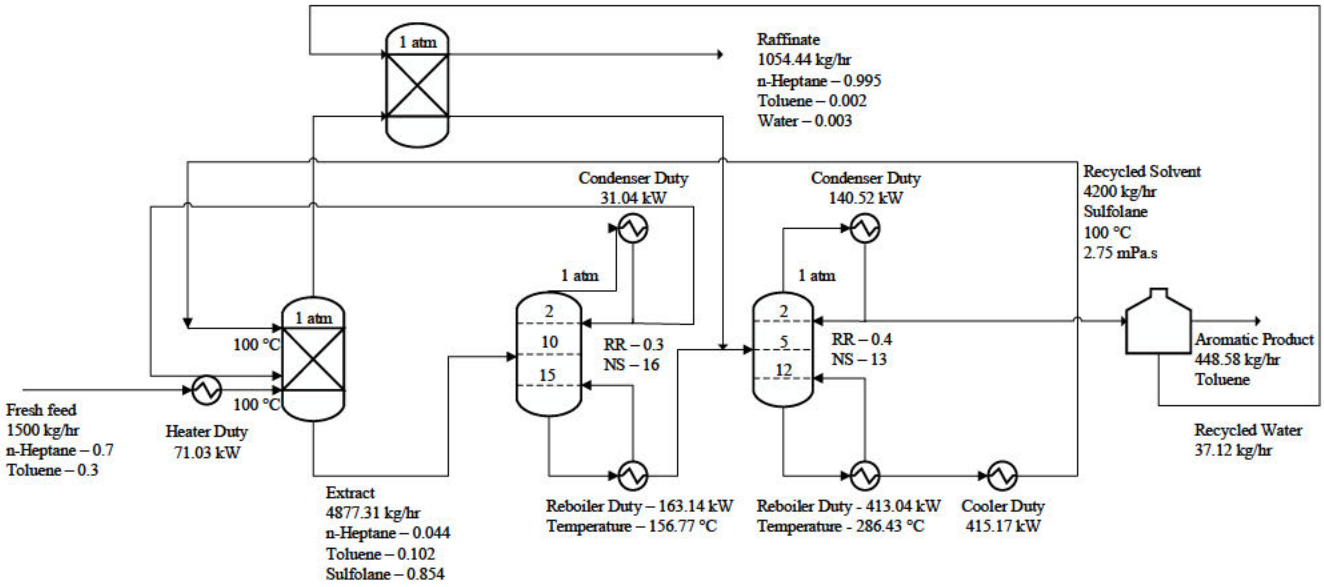

Figure 2.14. Flowsheet for the optimized extraction process with the use of sulfolane as the solvent.

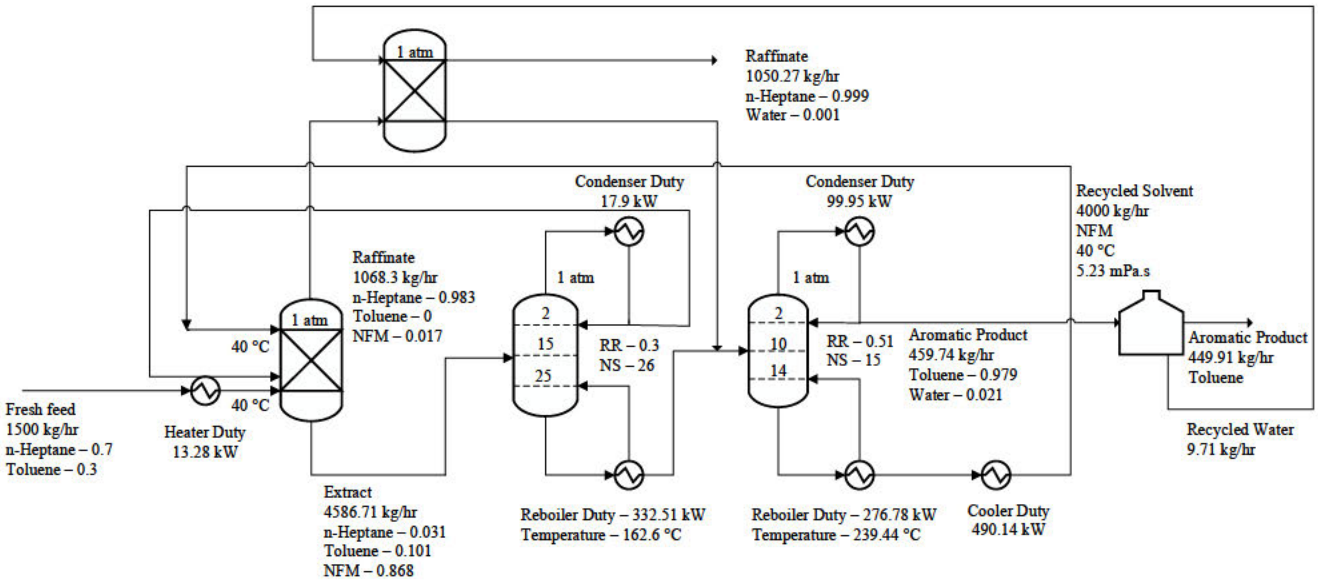

Figure 2.15. Flowsheet for the optimized extraction process with the use of NFM as the solvent.

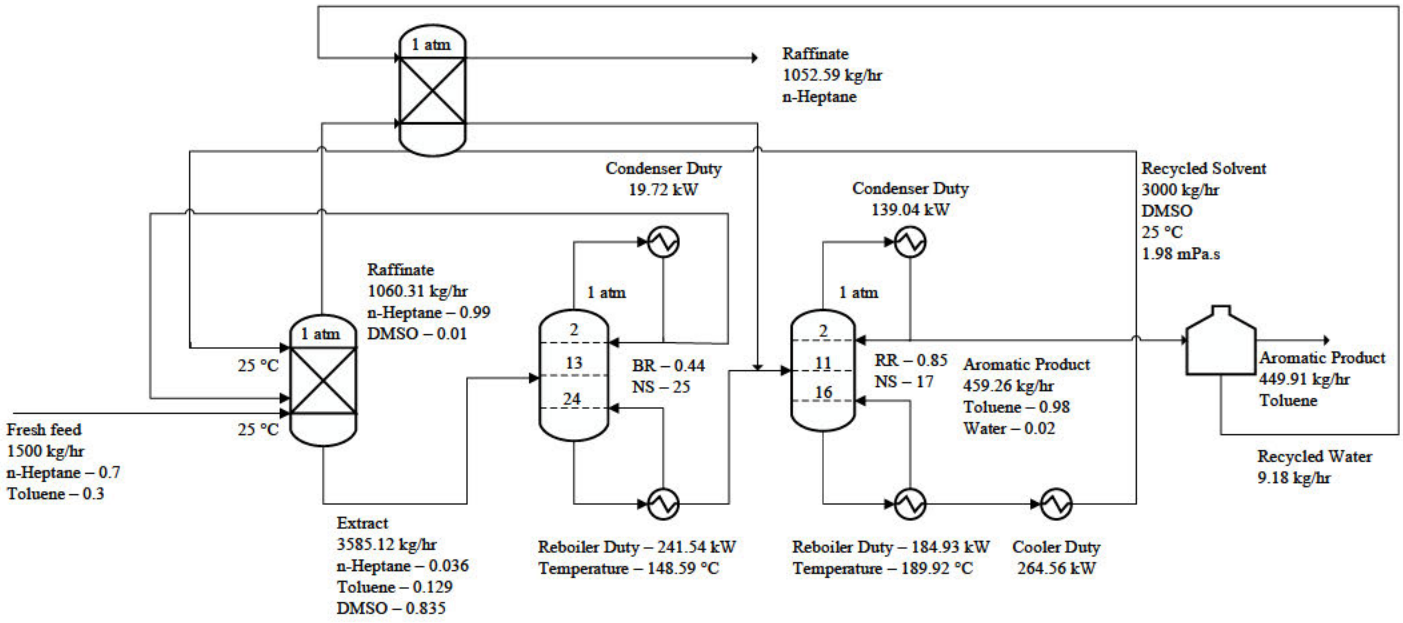

Figure 2.16. Flowsheet for the optimized extraction process with the use of DMSO as the solvent.

The simulation results for the potential solvents are given in Figures 2.17 – 2.19. Recoveries of toluene and *n*-heptane are greater than 99%, with product purity also greater than 99%. Since the primary results of the potential solvents match those of the baseline simulations, it is possible to make a reasonable comparison on the financial implications of solvent choice. The optimization procedure for potential solvents was the same as the baseline simulations, as the process design is inherently the same. The boil-up ratio, distillate to feed ratio, reflux ratio, number of stages, and feed stage position were optimized with the desired recoveries and purities as the objective function. Separation with hexylene glycol and 1,4-butanediol requires similar solvent rates to sulfolane at 4200 kg/hr and 3819 kg/hr respectively. The column variables are in similar ranges to separation with NFM and DMSO, with reflux ratios between 0.37 – 0.54. The commonalities in the values of the operating variables suggests that existing refineries could retrofit their processes to using hexylene glycol or 1,4-butanediol without significant equipment modifications.

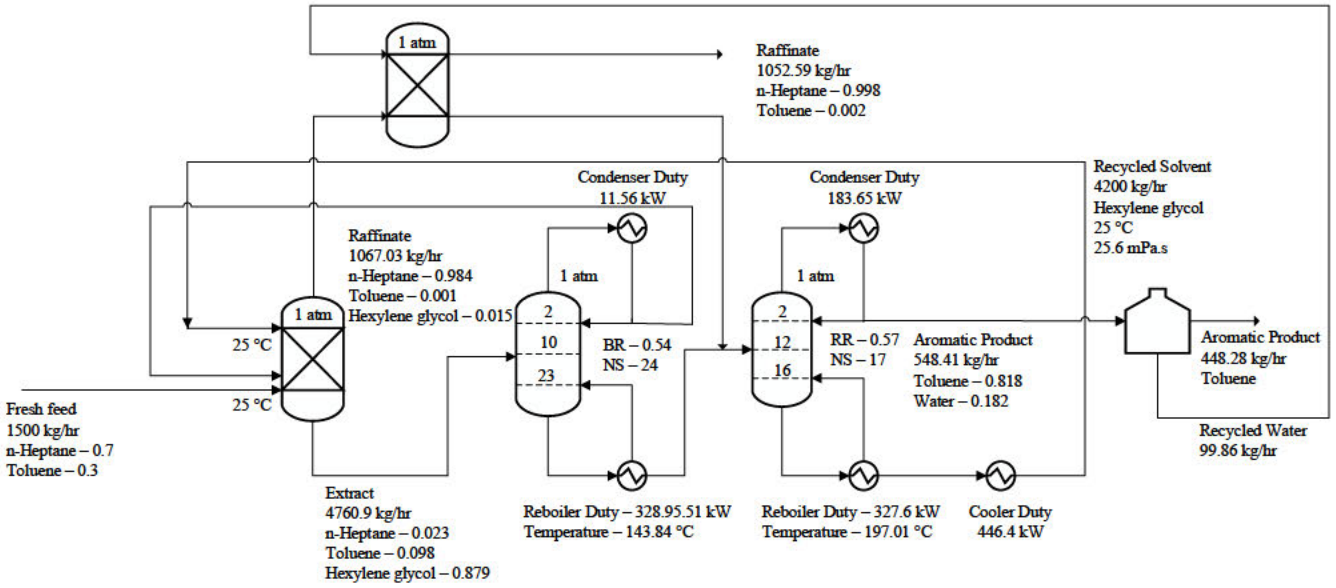

Figure 2.17. Flowsheet for the optimized extraction process with the use of hexylene glycol as the solvent.

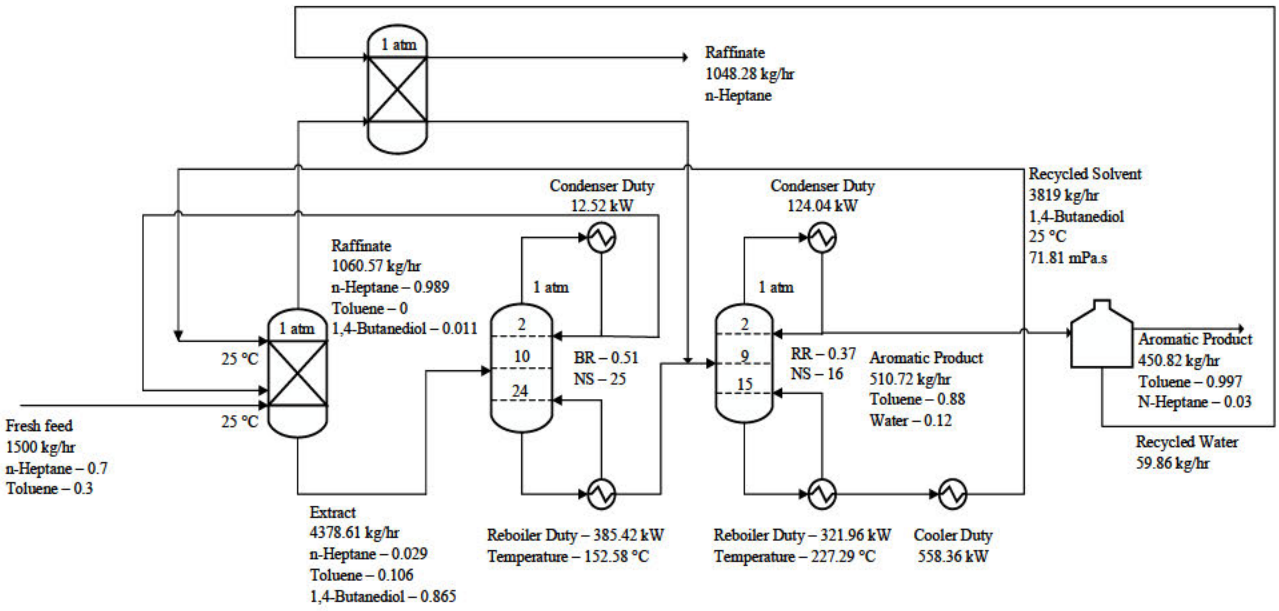

Figure 2.18. Flowsheet for the optimized extraction process with the use of 1,4-butanediol as the solvent.

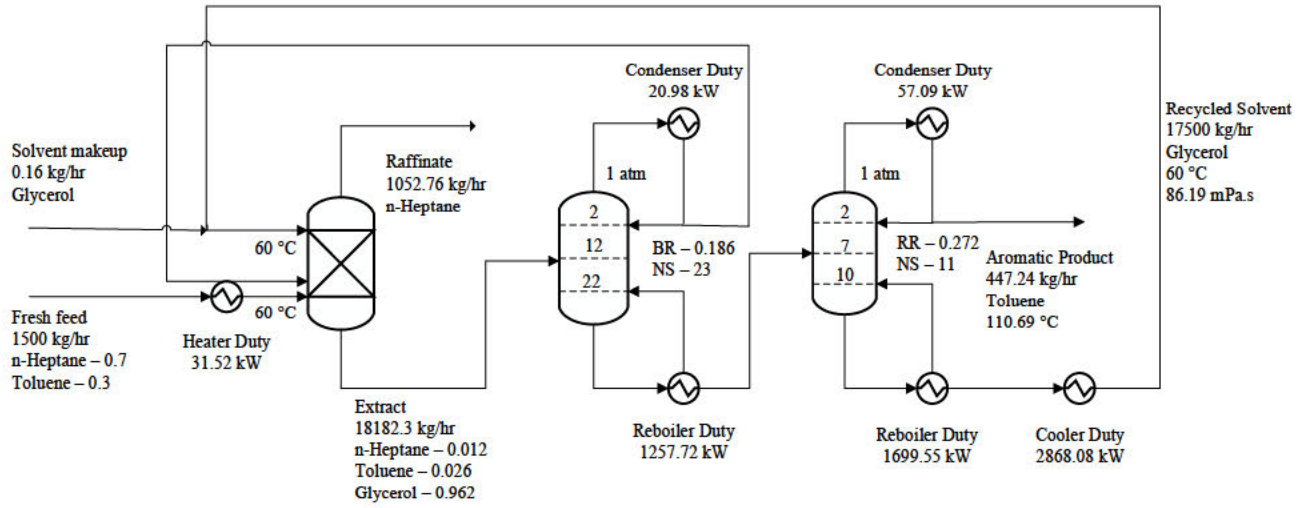

Figure 2.19. Flowsheet for the optimized extraction process with the use of glycerol as the solvent.

Due to the low capacity of glycerol, the required solvent feed rate is 17500 kg/hr which is substantially higher than that of the other solvents. This high solvent rate significantly increases the heating duties required by the reboilers in the stripper and solvent recovery columns, as well as the cooling duty required to return the solvent to the extraction temperature. As seen in Figure 19 the heating duties are 1257.72 kW in the stripper column, and 1699.55 kW in the solvent recovery column. The solvent cooler has a duty of 2868 kW. While these duties are substantially higher than those of the other solvents, the difference in duties between the reboilers and the cooler implies substantial opportunity for heat integration. Due to the low volatility of glycerol there is negligible solvent loss, which removes the additional step required to recover solvent losses using water.

The use of ethanol as a co-solvent to glycerol is complicated with the formation of an azeotrope between toluene and ethanol. This necessitates that an alternative separation scheme be considered in order to achieve the solvent recovery. It has been demonstrated via ASPEN V10 simulations that toluene and ethanol can be separated effectively with the use of pressure swing distillation (PSD) (Zhu et al., 2015). This process consists of two columns, one at low pressure (LP) and the other at high pressure (HP) in order to shift the azeotropic composition such that each component

is recovered separately from bottoms of each column. The advantage of this is that no other solvents are used, however it is likely that capital and utility costs are higher compared to the recovery of conventional solvents due to the additional column required. In the process design using glycerol and ethanol, the extraction and stripper columns are developed in the same manner as with the other solvents, with the single recovery column being replaced by the LP and HP columns. Ethanol and glycerol are recovered in the bottoms of the first column, while the distillate consisting of ethanol and toluene is pumped to the HP column where toluene is drawn off as the bottoms while the distillate at the azeotropic composition of the HP column is recycled to the feed of the LP column. The pressures of the two columns were chosen using a sensitivity analysis by varying column pressure and assessing the impact on the final recovery of toluene. Figure 2.20 indicates the azeotropes at the specified pressures, illustrating the distillate compositions in the LP and HP columns. The optimization of these columns was conducted in a sequential iterative procedure with the objective function being at least 99% recovery of aromatics. This is in order for the simulations to be comparable to the baseline simulations of the conventional solvents. The reflux ratios and distillate to feed ratios were then specified and optimized using the *design spec* functionality to achieve the desired recovery. Other column variables such as number of stages and feed stage were thereafter optimized with a sensitivity analysis. These parameters are given in Figure 2.21.

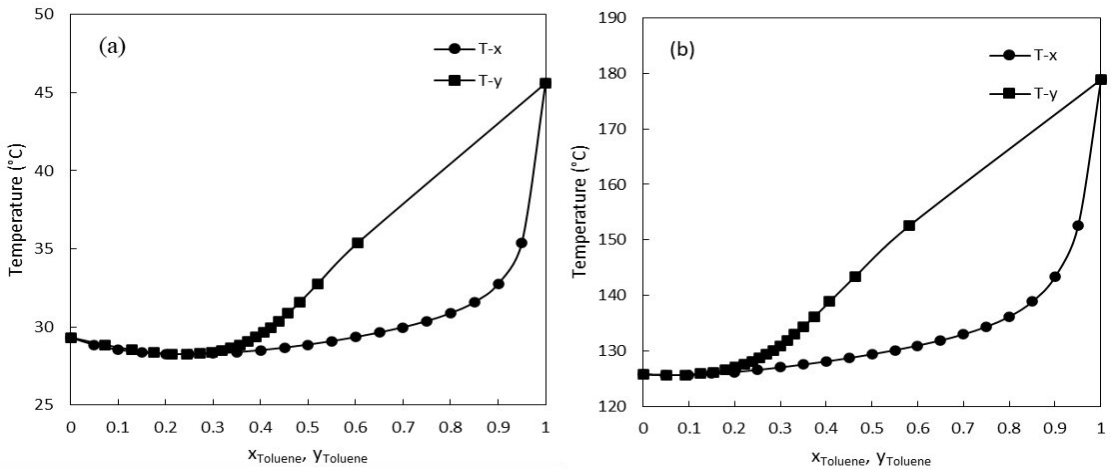

Figure 2.20. T-*x,y* data for the toluene + ethanol system at (a) 0.1 atm and (b) 5 atm.

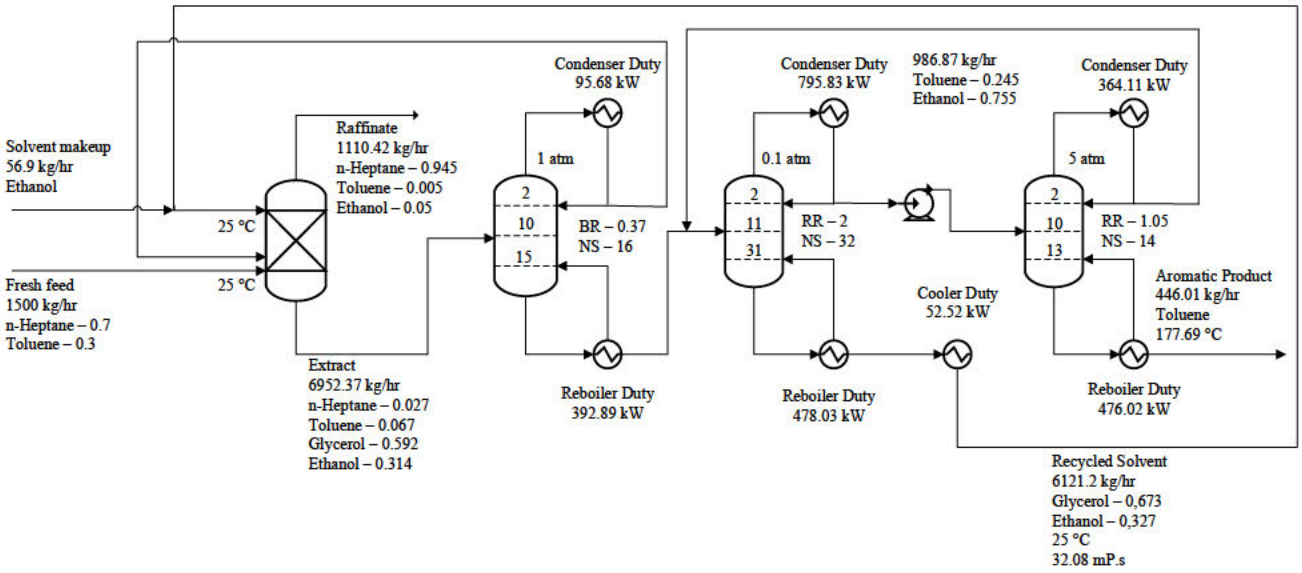

Figure 2.21. Flowsheet for the optimized extraction process with the use of glycerol + ethanol as the solvent.

2.4.2 Process Economics

Solvent selection affects the required solvent rate, which in turn influences equipment sizing as well as energy requirements. The extent to which energy consumption is affected also depends on the solvent's heat capacity as well as process operating conditions such as column temperatures and pressures. Ultimately, these factors have a collective influence on capital and operating costs, which can then be used as the mechanism to evaluate the overall impact of solvent choice.

The detailed costing of chemical processes is a specialized profession, and the entails significantly more considerations than the preliminary costing conducted in this study. Preliminary costing is a mechanism primarily to choose between different design alternatives. In this study, the aim is to gauge the impact of solvent choice in terms of the conventional and potential solvents on process economics. Aspen Process Economic Analyzer (APEA) was used to determine capital and operating costs. It is integrated within ASPEN V10, and uses data from equipment manufacturers as well as engineering, procurement, and construction companies (Haydary, 2018). The capital costs considered are the column costs of the extraction and distillation sections, feed preheaters, coolers, condensers and reboilers, reflux drums, and reflux pumps. These include the cost of the

purchased equipment as well as the installation costs. Indirect capital costs included are the costs associated with engineering and supervision, legal expenses, construction expenses and contractor's fees. After the process simulation is completed, APEA maps the flowsheet models to real world equipment. Thereafter, this equipment is sized based on the process conditions and specifications provided by the simulation. It is necessary to verify that the default mapping and sizing are correct to prevent errors resulting from implementing incorrect costing models. The economics are then calculated as the last evaluation step. Operating costs such as utilities are also determined by APEA, with the main contributions being electricity for the reflux pumps, cooling water for the condensers, and low pressure steam in the reboilers and preheaters. Solvent makeup is treated as an annual operating cost and is included by summing the solvent losses in the extraction column raffinate and recovery column distillate, and multiplying this with the bulk market price (listed in Table 2.4).

Table 2.4. Solvent prices determined from market trends and bulk supplier quotations

Solvent	Solvent Price ($/Ton)
Sulfolane	2400
NFM	4700
DMSO	2672
Hexylene glycol	1500
1,4-Butanediol	2029
Glycerol	746
Glycerol + Ethanol	866
Ethanol	1113

The capital and operating costs are used in the calculation of the Total Annual Cost (TAC) as shown in Equation (2.7):

$$\mathrm{TAC} = \frac{\mathrm{Capital\,Cost}}{\mathrm{Payback\,Time}} + \mathrm{Utilities} \tag{2.7}$$

Payback time is evaluated by determining the revenue from sales of the aromatic component using the aromatic recovery and bulk market price:

$$\text{Payback Time} = \frac{\text{Capital Cost}}{\text{Annual Aromatic Sales}} \tag{2.8}$$

Figure 2.22 reflects the capital costs associated with each solvent. Most of the conventional and potential solvents would require capital between \$5.5-6.5 million. Glycerol + ethanol has a higher capital requirement as there is an additional distillation column needed to be included as a result of the pressure-swing operation to address the formation of the azeotrope between ethanol and toluene. This also increases the payback time significantly as the product revenue of toluene from use of all solvents has been essentially designed to be the same, while glycerol + ethanol at the same time incurs an additional cost by the extra column. There does not appear to be a clear relationship between selectivity, capacity and capital costs. Although using glycerol would require a solvent feed more than triple that of sulfolane, its overall capital cost is the lowest as there is no need for additional process equipment to recover glycerol's negligible solvent losses. While this also causes the lowest payback time, it does not account for major operating costs such as utilities and pumping costs, which as a whole indicates that payback time on its own is not a rigorous or effective measure of feasibility in solvent choice. Transport costs are likely to be higher for the glycol solvents due to the higher viscosities at the required operating temperatures.

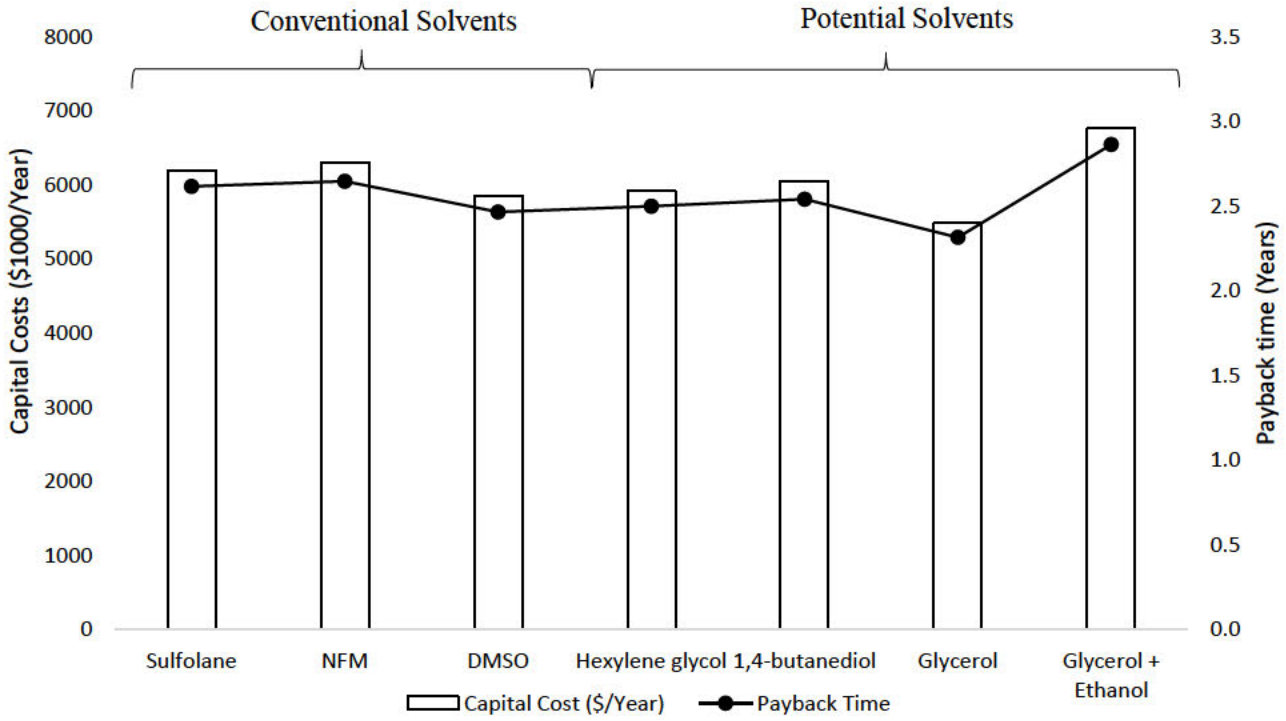

Figure 2.22. Comparison of capital costs and payback times for the conventional and potential solvents.

Figure 2.23 shows the operating costs, which are made up of primarily utility costs. Sulfolane, NFM, and DMSO have lower energy consumptions than all the potential solvents and therefore lower utility costs. This encompasses a number of factors, with the most significant being the higher solvent capacities at the specified feed conditions, the reduced heating and cooling duties as a result of the reduced solvent feed, the lower heat capacities, and the reflux ratios resulting from better relative volatilities in the solvent recovery column. The utility costs associated with glycerol are substantially higher due to the high solvent feed. Utility as well as solvent makeup costs are higher when ethanol is used as a co-solvent to glycerol due to the additional heating and cooling requirements in the extra column as well as the loss of ethanol to the raffinate, which cannot be easily recovered with water. However, the presence of ethanol (as a result of solvent loss) in the product reformate stream could holistically characterize the solvent extraction process as a possible blending point for ethanol-gasoline mixtures, with the stripper boil-up ratio controlling the raffinate ethanol content.

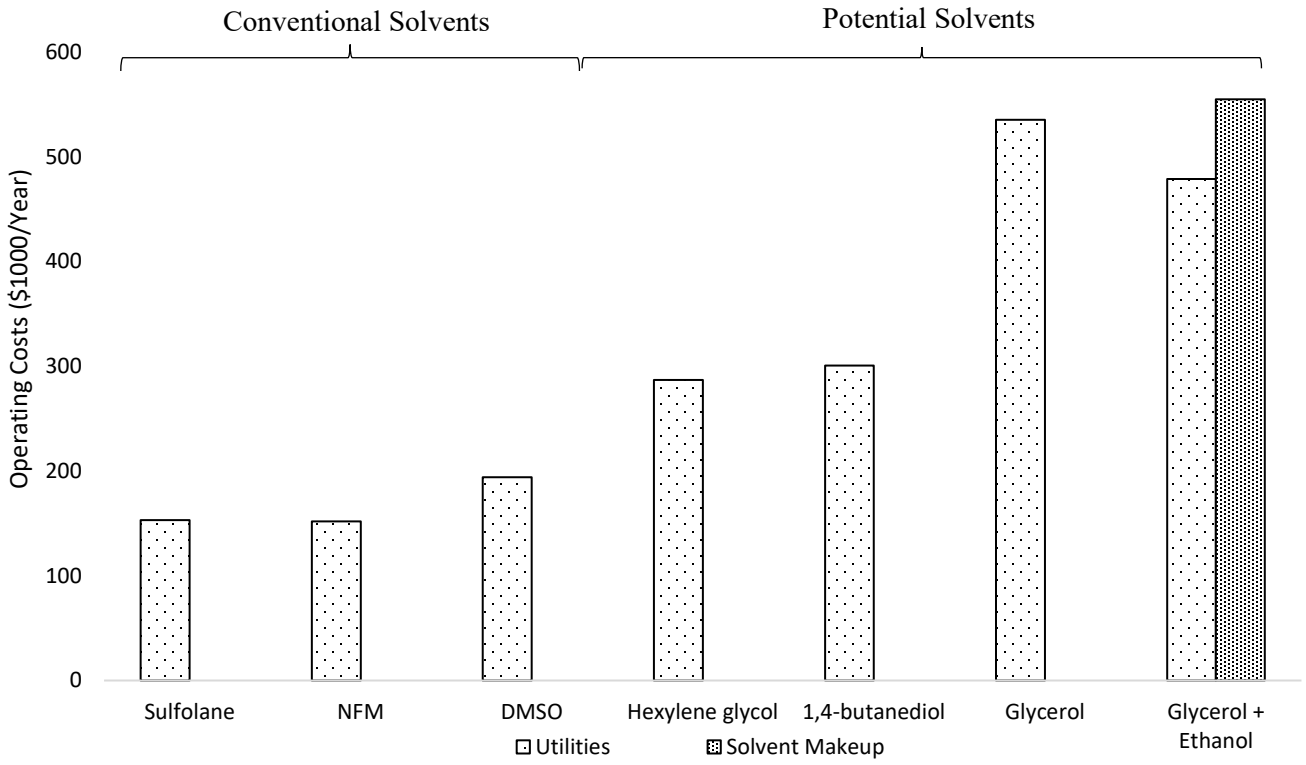

Figure 2.23. Comparison of operating costs for the conventional and potential solvents.

The total annual costs (TACs) are illustrated in Figure 2.24. All solvents considered, with the exception of glycerol + ethanol, have similar TACs between $2 – $3 million. 1,4-Butanediol and hexylene glycol produce the best TACs from the potential solvents studied. The reduced capital cost associated with glycerol is offset by the high operating costs. However, operating costs may change with the inclusion of heat integration, pumping and other variable costs.

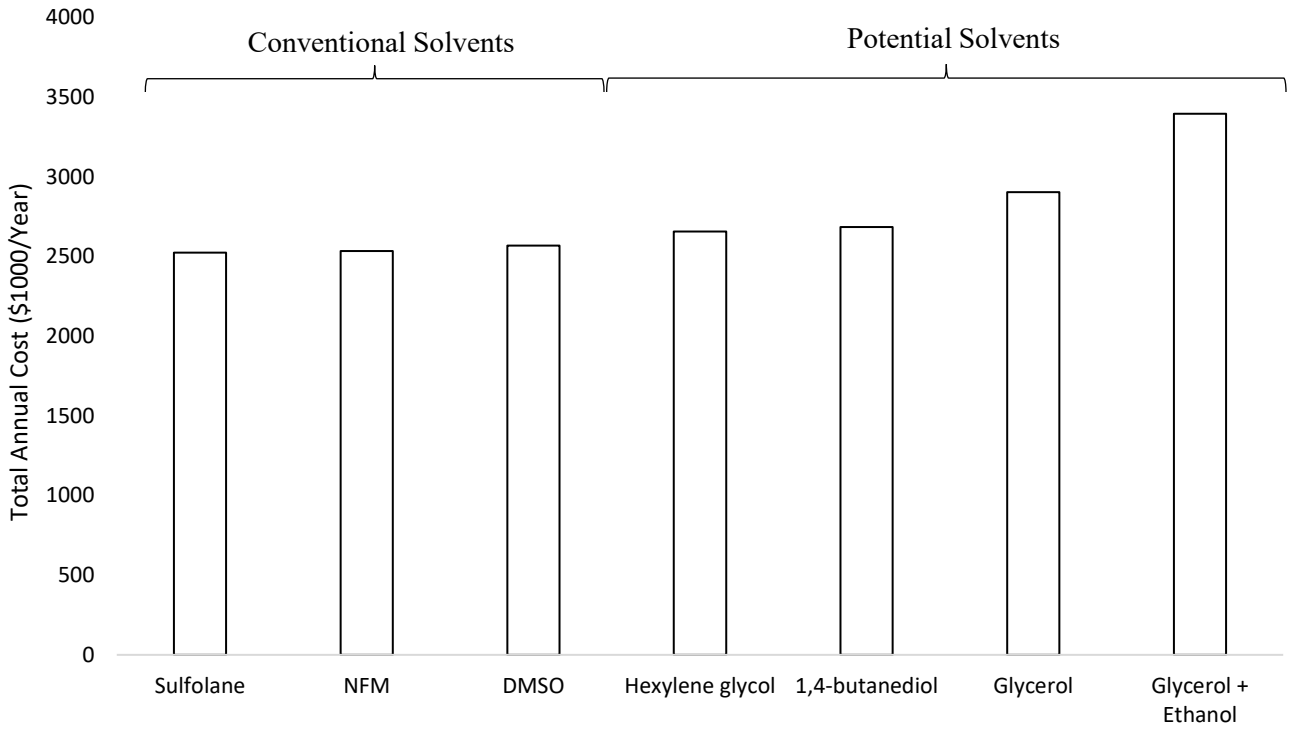

Figure 2.24. Comparison of total annual cost (TAC) for the conventional and potential solvents

Figure 2.25 illustrates the annual CO_2 emissions resulting from the heating utilities in each simulation. LP and MP steam is used to provide the heating utilities. The emissions were determined by converting the annual energy requirement into its coal or natural gas equivalent with the use of annual fuel utilization efficiencies, boiler efficiencies, and net heating values for both coal and natural gas as the energy source. Use of natural gas as the energy source generally resulted in lower emissions regardless of the solvent used due to higher net heating values and improved boiler technologies over traditional coal-fired heaters. The emissions with each solvent correspond well with the overall utility costs, with the higher utility requirements resulting in higher emissions; emissions for potential solvents are higher due to the higher utility requirements. The heat recovery potential is the percentage energy reduction possible with heat recovery. The solvents with higher utility emissions have more potential for heat integration due to the differences in heating and cooling requirements. Further research into identifying co-solvents in order to improve solvent capacity and viscosity will reduce utilities requirements and carbon emissions.

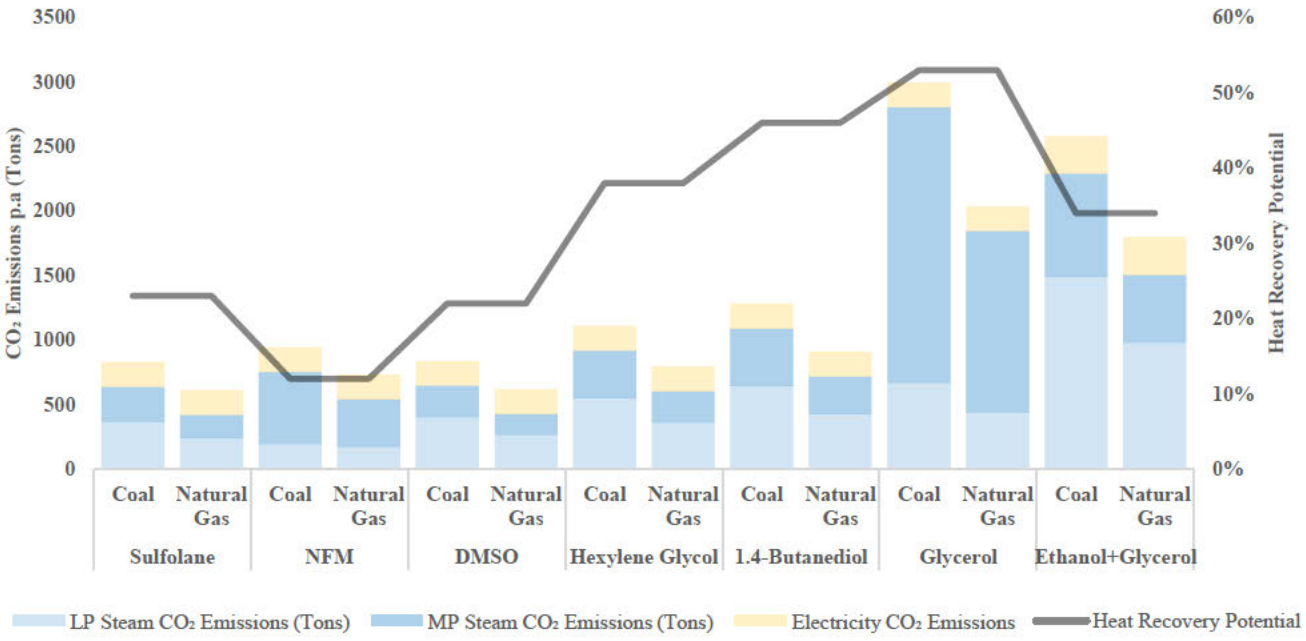

Figure 2.25. Comparison of CO_2 emissions for each solvent using coal or natural gas as an energy source with heat recovery potential

2.5. Conclusion

A search algorithm was employed to identify organic chemicals for further study as solvents for the extraction of aromatics. There were nine chemicals that met the criteria in terms of physical properties, capacity, selectivity, and performance index (predicted with the use of the UNIFAC-LLE model). A risk assessment showed that several potential solvents were similar to conventional solvents in terms of health, safety and environment. ASPEN V10 simulations indicated that process economics plays a significant role in solvent selection, with the total annual cost serving as a basis on which solvents can be assessed. The robust methodology highlights the need for an integrated holistic approach in the identification of potential solvents. Hexylene glycol, 1,4-butanediol, and glycerol may offer some advantages compared to conventional solvents in terms of health, safety, environment and solvent price, however conventional solvents may offer lower operating costs.

2.7. Declaration

The authors declare no competing financial interests.

2.8. References

Abrams, D. S., & Prausnitz, J. M. (1975). Statistical Thermodynamics of Liquid Mixtures: A New Expression for the Excess Gibbs Energy of Partly or Completely Miscible Systems. *AIChE J*, *21*, 116–118.

Alfonsi, K., Colberg, J., Dunn, P. J., Fevig, T., Jennings, S., Johnson, T. A., Kleine, H. P., Knight, C., Nagy, M. A., Perry, D. A., & Stefaniak, M. (2008). Green chemistry tools to influence a medicinal chemistry and research chemistry based organisation. *Green Chem.*, *10*, 31–36.

Alkhaldi, K. H. A. E., Fandary, M. S., Al-Jimaz, A. S., Al-Tuwaim, M. S., & Fahim, M. A. (2009). Liquid−liquid Equilibria of Aromatics Removal from Middle Distillate Using NMP. *Fluid Phase Equilib*, *286*, 190−195.

Al-Zayied, T. A., Al-Sahhaf, T. A., & Fahim, M. A. (1990). Measurement of Phase Equilibrium in Multicomponent Systems of Aromatics with N-Methylpyrrolidone and Predictions with Unifac. *Fluid Phase Equilib*, *61*, 131−144.

Ashcroft, S. J., Clayton, A. D., & Shearn, R. B. (1982). Liquid-Liquid Equilibriums for Three Ternary and Six Quaternary Systems Containing Sulfolane, N-Heptane, Toluene, 2-Propanol, and Water at 303.15 K. *J. Chem. Eng. Data*, *27*, 148–151.

Aspen Plus (No. 10). (2004). Aspen Technology Incorporation.

Brignole, E. A., Bottini, S., & Gani, R. (1986). A strategy for the design and selection of solvents for separation processes. *Fluid Phase Equilib.*, *29*, 125–132.

Canales, R. I., & Brennecke, J. F. (2016). Comparison of Ionic Liquids to Conventional Organic Solvents for Extraction of Aromatics from Aliphatics. *J. Chem. Eng. Data*, *61*, 1685–1699.

Cassell, G. W., Dural, N., & Hines, A. L. (1989). Liquid-Liquid Equilibrium of Sulfolane-Benzene-Pentane and Sulfolane-Toluene-Pentane. *Ind. Eng. Chem. Res*, *28*, 1369−1374.

Cassell, G. W., Hassan, M. M., & Hines, A. L. (1989). Correlation of the Phase Equilibrium Data for the Heptane-Toluene-Sulfolane and Heptane-Xylene-Sulfolane Systems. *J. Chem. Eng. Data*, *34*, 434−438.

Cassell, G. W., Hassan, M. M., & Junes, A. L. (1989). Phase Equilibria of the Cylohexane-Toluene-Sulfolane and Hexane-Toluene-Sulfolane Ternary Systems. *Chem. Eng. Commun*, *85*, 233−243.

Chen, D., Ye, H., & Hao, W. (2007). Liquid + Liquid Equilibria of heptane + Xylene + N-Formylmorpholine Ternary System. *J. Chem. Thermodyn*, *39*, 1571−1577.

Chen, J., Duan, L. P., Mi, J. G., Fei, W. Y., & Li, Z. C. (2000). Liquid-liquid equilibria of multi-component systems including n-hexane, n-octane, benzene, toluene, xylene and sulfolane at 298.15 K and atmospheric pressure. *Fluid Phase Equilib*, *173*, 109−119.

Chen, J., Li, Z., & Duan, L. (2000). Liquid−Liquid Equilibria of Ternary and Quaternary Systems Including Cyclohexane, 1-Heptene, Benzene, Toluene, and Sulfolane at 298.15 K. *J. Chem. Eng. Data*, *45*, 689−692.

Chen, Q. L., Wang, Q., Zhang, B. J., He, C., & He, C. C. (2017). Optimal Design of a New Aromatic Extractive Distillation Process Aided by a Co-Solvent Mixture. *Energy Procedia*, *105*, 4927–4934.

Curzons, A. D., Constable, D. C., & Cunningham, V. L. (1999). Solvent selection guide: a guide to the integration of environmental, health and safety criteria into the selection of solvents. *Clean Technol. Environ. Policy*, *1*, 82–90.

de Fré, R. M., & Verhoeye, L. A. (1976). Phase Equilibria in Systems Composed of an Aliphatic and an Aromatic Hydrocarbon and Sulpholane. *J. Appl. Chem. Biotechnol*, *26*, 469−487.

de Riva, J., Ferro, V. R., D. Moreno, I. Diaz, & J. Palomar. (2016). Aspen Plus supported conceptual design of the aromatic–aliphatic separation from low aromatic content naphtha using 4-methyl-N-butylpyridinium tetrafluoroborate ionic liquid. *Fuel Process. Technol.*, *146*, 29–38.

Delancey, G. (2013). *Principles of Chemical Engineering Practice*. John Wiley & Sons.

DongChu, C., HongQi, Y., & Hao, W. (2007). (Liquid + liquid) equilibria of three ternary systems: (heptane + benzene + N-formylmorpholine), (heptane + toluene + N-formylmorpholine), (heptane + xylene + N-formylmorpholine) from T = (298.15 to 353.15) K. *J. Chem. Thermodyn*, *39*, 1182−1188.

Farghi, F., & Kaddami, M. (2008). Phase Diagrams of Ternary and Quaternary Systems Containing Heptane, Toluene, Dimethylsulfoxide, Methanol, and Ethanol at 298.15 K. *Russ. J. Phys. Chem.*, *92*, 2502–2506.

Ferreira, P. O., Ferreira, J. B., & Medina, A. G. (1984). Liquid-liquid equilibria for the system N-methylpyrrolidone + toluene + n-heptane: UNIFAC interaction parameters for N-methylpyrrolidone. *Fluid Phase Equilib*, *16*, 369−379.

Ferro, V. R., de Riva, J., Sanchez, D., Ruiz, E., & Palomar, J. (2015). Conceptual design of unit operations to separate aromatic hydrocarbons from naphtha using ionic liquids. COSMO-based process simulations with multi-component "real" mixture feed. *Chem. Eng. Res. Des.*, *94*, 632–647.

Firnhaber, B., Emmrich, G., Ennenbach, F., & Ranke, U. (2000). Separation process for the recovery of pure aromatics. *Erdoel Erdgas Kohle, 116*, 254–260.

Folas, G. K., Kontogeorgis, G. M., Michelsen, M. L., Stenby, E. H., & Solbraa, E. (2006). Liquid−Liquid Equilibria for Binary and Ternary Systems Containing Glycols, Aromatic Hydrocarbons, and Water: Experimental Measurements and Modeling with the CPA EoS. *J. Chem. Eng. Data*, *51*, 977–983.

Fredenslund, A., Jones, R. L., & Prausnitz, J. M. (1975). Group-contribution estimation of activity coefficients in nonideal liquid mixtures. *AIChE Journal, 21*, 1086–1099.

Gao, X., Yang, Z., Xia, S., & Ma, P. (2015). Liquid–liquid equilibrium data for binary systems containing o-dichlorobenzene and nitrobenzene. *Fluid Phase Equilib., 385*, 175–181.

Gmehling, J., Kleiber, M., Kolbe, B., & Rarey, J. (2019). *Chemical Thermodynamics for Process Simulation*. Wiley.

Gmehling, J., & Schedemann, A. (2014). Selection of Solvents or Solvent Mixtures for Liquid–Liquid Extraction Using Predictive Thermodynamic Models or Access to the Dortmund Data Bank. *Ind. Eng. Chem. Res., 53*, 17794–17805.

Green, D. W., & Perry, R. H. (2008). *Perry's Chemical Engineers' Handbook, Eighth Edition*. McGraw-Hill Education.

Hadj-Kali, M. K., Salleh, Z., Ali, E., Khan, R., & Hashim, M. A. (2017). Separation of aromatic and aliphatic hydrocarbons using deep eutectic solvents: a critical review. *Fluid Phase Equilib*, *448*, 152–167.

Haydary, J. (2018). *Chemical Process Design and Simulation*. John Wiley & Sons, Inc.

Henderson, R. K., Jiménez-González, C., Constable, D. J. C., Alston, S. R., Inglis, G. G. A., Fisher, G., Sherwood, J., Binks, S. P., & Curzons, A. D. (2011). Expanding GSK's solvent selection

guide – embedding sustainability into solvent selection starting at medicinal chemistry. *Green Chem.*, *13*, 854.

Hernández, E., Santiago, R., Moya, C., Navarro, P., & Palomar, J. (2021). Multiscale evaluation of CO2-derived cyclic carbonates to separate hydrocarbons: Drafting new competitive processes. *Fuel Process Technol.*, *212*, 106–639.

Huang, X., Xia, S., Ma, P., Song, S., & Ma, B. (2008). Vapor–Liquid Equilibrium of N-Formylmorpholine with Toluene and Xylene at 101.33 kPa. *J. Chem. Eng. Data*, *53*, 252–255.

Huddleston, J. G., Willauer, H. D., Swatloski, R. P., Visser, A. E., & Rogers, R. D. (1998). Room temperature ionic liquids as novel media for 'clean' liquid–liquid extraction. *Chem. Commun.*, 1765–1766.

Kaiser, M. J., Klerk, A. de, Gary, J. H., & Hwerk, G. E. (2019). *Petroleum Refining* (6th ed.). CRC Press.

Larriba, M., Ayuso, M., Navarro, P., Delgado-Mellado, N., Gonzalez-Miquel, M., García, J., & Rodríguez, F. (2018). Choline Chloride-Based Deep Eutectic Solvents in the Dearomatization of Gasolines. *Sustainable Chem. Eng.*, *6*, 1039–1047.

Lesek, F., & Mandík, L. (1982). Liquid-liquid equilibrium in binary glycols-toluene and glycols-xylenes systems. *Collect. Czech. Chem. Commun*, *47*, 1686–1694.

Li, J., Zhao, Q., Tang, X., Xiao, K., & Yuan, J. (2014). Liquid−Liquid Equilibria for the Systems: Heptane + Benzene + Solvent (Propylene Carbonate, N,N-Dimethylformamide, or Mixtures) at Temperature from (303.2 to 323.2) K. *J. Chem. Eng. Data*, *59*, 3307−3313.

Lo, T. C., & Baird, M. H. I. (2000). Extraction, Liquid–Liquid. In *Kirk-Othmer Encyclopedia of Chemical Technology*. John Wiley & Sons, Inc.

Meindersma, G. W. (2005). *Extraction of aromatics from naphtha with ionic liquids: from solvent development to pilot RDC evaluation*. University of Twente.

Meindersma, G. W., & de Haan, A. B. (2008). Conceptual process design for aromatic/aliphatic separation with ionic liquids. *Chem. Eng. Res. Des.*, *86*, 745–752.

Mohsen-Nia, M., Modarress, H., Doulabi, F., & Bagheri, H. (2005). Liquid+liquid equilibria for ternary mixtures of (solvent+aromatic hydrocarbon+alkane). *J. Chem. Thermodyn.*, *37*, 1111–1118.

Müller, E., Berger, R., Blass, E., & Sluyts, D. (2000). Liquid-Liquid Extraction. In *Ullmann's Encyclopedia of Industrial Chemistry*. Wiley-VCH Verlag GmbH & Co. KGaA.

Nagpal, J. M., & Rawat, B. S. (1981). Liquid-Liquid Equilibria for Toluene-Heptane-N-Methyl Pyrrolidone and Benzene-Heptane Solvents. *J. Chem. Technol. Biotechnol, 31*, 146−150.

Oracz, P., & Kolasińska, G. (1987). Vapour-liquid equilibria—III. Total vapour pressure measurements for binary mixtures of methanol, ethanol, 1-propanol and 1-butanol with benzene, toluene and p-xylene at 313.15 K. *Fluid Phase Equilib., 35*, 253–278.

Prat, D., Hayler, J., & Wells, A. (2014). A survey of solvent selection guides. *Green Chem., 16*, 4546–4551.

Prat, D., Pardigon, O., Flemming, H.-W., Letestu, S., Ducandas, V., Isnard, P., Guntrum, E., Senac, T., Ruisseau, S., Cruciani, P., & Hosek, P. (2013). Sanofi's Solvent Selection Guide: A Step Toward More Sustainable Processes. *Org. Process Res. Dev., 17*, 1517–1525.

Rawat, B. S., & Prasad, G. (1980). Liquid-Liquid Equilibria for Benzene-N-Heptane Systems with Triethylene Glycol, Tetraethylene Glycol, and Sulfolane Containing Water at Elevated Temperatures. *J. Chem. Eng. Data*, *25*, 227−230.

Redlich, Otto., & Kwong, J. N. S. (1949). On the Thermodynamics of Solutions. V. An Equation of State. Fugacities of Gaseous Solutions. *Chem. Rev., 44*, 233–244.

Řehák, K., & Dreiseitlová, J. (2006). Binary liquid–liquid equilibrium in the systems containing monofunctional benzene derivates and 1,2-ethanediol. *Fluid Phase Equilib., 249*, 104–108.

Renon, H., & Prausnitz, J. M. (1968). Local Compositions in Thermodynamic Excess Functions for Liquid Mixtures. *AIChE J, 14*, 135–144.

Saha, M., Rawat, B. S., Khanna, M. K., & Nautiyal, B. R. (1998). Liquid−Liquid Equilibrium Studies on Toluene + Heptane + Solvent. *J. Chem. Eng. Data*, *43*, 422−426.

Seyedein Ghannad, S. M., Lotfollahi, M. N., & Haghighi Asl, A. (2011). Measurement of (liquid + liquid) equilibria for ternary systems of (N-formylmorpholine + benzene + cyclohexane) at temperatures (303.15, 308.15, and 313.15) K. *J. Chem. Thermodyn, 43*, 938−942.

Slater, C. S., & Savelski, M. (2007). A method to characterize the greenness of solvents used in pharmaceutical manufacture. *Environ. Sci. Health Part A, 42*, 1595–1605.

Smith, J. M., van Ness, H. C., & Abbott, M. M. (2001). *Introduction to Chemical Engineering Thermodynamics* (6th edition). McGraw-Hill.

Tripathi, R. P., Ram, A. R., & Rao, P. B. (1975). Liquid-Liquid Equilibriums in Ternary System Toluene-N-Heptane-Sulfolane. *J. Chem. Eng. Data*, *20*, 261−264.

Wang, Z., Xia, S., & Ma, P. (2012). (Liquid + Liquid Equilibria for the Ternary System of (N-Formylmorpholine + Ethylbenzene + 2,2,4-Trimethylpentane) at Temperatures (303.15 , 313.15, and 323.15) K. *Fluid Phase Equilib*, *328*, 25−30.

Weidlich, U., & Gmehling, J. (1987). A modified UNIFAC model. 1. Prediction of VLE, hE, and gamma infinity. *Ind. Eng. Chem. Res.*, *26*, 1372–1381.

Weissermel, K., & Arpe, H. (2003). *Industrial Organic Chemistry*. Wiley.

Werner, S., Haumann, M., & Wasserscheid, P. (2010). Ionic Liquids in Chemical Engineering. *Annu. Rev. Chem. Biomol. Eng*, *1*, 203–230.

Wiley Critical Content. (2007). *Petroleum Technology*. John Wiley & Sons, Inc, New Jersey.

Wittig, R., Lohmann, J., & Gmehling, J. (2003). Vapor−Liquid Equilibria by UNIFAC Group Contribution. 6. Revision and Extension. *Ind. Eng. Chem. Res.*, *42*, 183–188.

Yaws, C. (2014). *Thermophysical Properties of Chemicals and Hydrocarbons*. Elsevier.

Yaws, Carl. L. (2015). *The Yaws Handbook of Vapor Pressure*. Elsevier.

Zhao, S., Bai, P., & Sun, C. (2014). Isobaric vapor–liquid equilibrium for binary and ternary systems with toluene, 2-methoxyethanol and dimethyl sulfoxide at 101.3kPa. *Fluid Phase Equilib.*, *375*, 37–44.

Zhu, Z., Wang, L., Ma, Y., Wang, W., & Wang, Y. (2015). Separating an azeotropic mixture of toluene and ethanol via heat integration pressure swing distillation. *Comput. Chem. Eng.*, *76*, 137–149.

3

CHAPTER THREE

Experimental Liquid-Liquid Equilibrium Data for Alkane and Aromatic Mixtures in Solvent and Co-Solvent Mixtures

Abstract

Liquid-liquid equilibrium (LLE) phase compositions (tie-line data) were experimentally measured and thermodynamically modelled for the ternary systems *n*-heptane + toluene + (butane-1,4-diol or glycerol) and *n*-nonane + *o*-xylene + (butane-1,4-diol or glycerol) at 298.2, 313.2 and 333.2 K and 0.1 MPa. The use of 2-methyl-2,4-pentanediol as a potential co-solvent to butane-1,4-diol and glycerol was studied in order to investigate its impact on solvent capacity in the separation of toluene from *n*-heptane via liquid-liquid extraction. To this end, quaternary liquid-liquid equilibrium (LLE) data was experimentally measured for the system *n*-heptane + toluene + (butane-1,4-diol or glycerol) + 2-methyl-2,4-pentanediol at 298.2 and 313.2 K and 0.1 MPa. The measurements were conducted in a double-walled glass cell using the direct analytical method, and phase compositions were analysed via gas chromatography. The data was correlated using the NRTL and UNIQUAC models, which were able to suitably represent the tie-line compositions. The selectivity for the solvents studied were found to be comparable or superior to conventional solvents, but results of the ternary systems indicated that solvent capacities were poor, motivating use of a co-solvent to reduce solvent-to-feed ratios. At different molar ratios of solvent to co-solvent, the selectivity and solvent capacity were calculated and compared to that of using pure

butane-1,4-diol or glycerol. It was ascertained that the pseudo ternary systems possess type 1 or type 2 behaviour depending on the molar ratio. It was observed that solvent capacity is not appreciatively improved for molar ratios that exhibit type II behaviour, however significant increases in capacity were noted for high molar ratios producing a type I system.

3.1. Introduction

Knowledge of phase equilibrium behaviour is imperative in order to understand the effect of solvent type on capital and operating costs in liquid-liquid extraction. Solvent type affects column design which in turn determines capital costs, therefore access to liquid-liquid equilibrium (LLE) data is a necessity when studying the impact of solvent choice.

Aromatic compounds such as benzene, toluene, and xylene serve as feedstocks to the plastics industry and are produced in bulk from reformate and pyrolysis gasoline streams (Chen et al., 2017). These chemicals are removed from the hydrocarbon streams prior to final blending processes. The separation challenge presented by these chemicals is as a result of the azeotropes that form between the aromatic and alkane components. This prevents conventional distillation from being a suitable option for isolation. Various separation methods are utilized depending on the aromatic content in the feed, with liquid-liquid extraction used for aromatic content between 20-65%, and azeotropic and extractive distillation used for higher concentrations. With feedstocks that possess low to medium aromatic composition, solvent extraction is the method generally used to generate high purity aromatic streams, as a result of lower energy consumption, easy continuous operation and large production capacity (Cho et al., 2002; Weissermel & Arpe, 2003).

Liquid-liquid equilibrium is the phenomenon relevant to solvent extraction, and is the formation of two immiscible liquid phases resulting from the addition of a solvent to the feed mixture (Treybal, 1963). One phase is rich in the solvent while the other is rich in the carrier liquid. In this application, the solute is the aromatic component, and it is desired that it has a greater affinity for the solvent-rich phase (Delancey, 2013). Evaluation of the suitability of a liquid extraction system requires LLE experimental measurements. The direct method involves charging an equilibrium cell with the constituents, thoroughly mixing the phases, and then sampling each phase at equilibrium. The extract of the solvent column is rich in the solvent as well as the aromatic components, which can then be separated through traditional distillation. The search for solvents

is ongoing and considerable research efforts have been made to identify and study alternatives to conventional solvents.

By studying the liquid-liquid equilibrium phase behaviour of various combinations of alkanes, aromatics, and solvents, one is able to ascertain the effectiveness and suitability of a particular solvent. For several decades, there have been various studies reporting phase data for solvents such as sulfolane (Ashcroft et al., 1982; Cassell, Dural, et al., 1989; Cassell, Hassan, & Hines, 1989; Cassell, Hassan, & Junes, 1989; J. Chen, Duan, et al., 2000; J. Chen, Li, et al., 2000; de Fré & Verhoeye, 1976), tetraethylene glycol (Rawat & Prasad, 1980), 1-methylpyrrolidin-2-one (NMP) (Alkhaldi et al., 2009; Al-Zayied et al., 1990; Ferreira et al., 1984), morpholine-4-carbaldehyde (NFM) (D. Chen, Ye, & Hao, 2007; Seyedein Ghannad et al., 2011; Wang et al., 2012), N,N-dimethylmethanamide (DMF) (Li et al., 2014), and dimethyl sulfoxide (DMSO) (Saha et al., 1998b). A significant number of literature studies use alkanes such as *n*-heptane as a representation of the feed and benzene or toluene as the aromatic solute to be extracted (Al-Zayied et al., 1990; Ashcroft et al., 1982; Cassell, Hassan, & Hines, 1989; Cassell, Hassan, & Junes, 1989; D. Chen, Ye, & Hao, 2007; J. Chen, Duan, et al., 2000; J. Chen, Li, et al., 2000; de Fré & Verhoeye, 1976; Ferreira et al., 1984; Li et al., 2014; Rawat & Prasad, 1980; Saha et al., 1998b). Continuous improvement necessitates that research efforts focus on optimizing capital and operating costs with solutions that are more sustainable in reducing risks to health, safety and the environment.

Recent focus has been on ionic liquids as a less environmentally harmful alternative to volatile organic solvents. Replacing conventional organic solvents with ionic liquids is noted to be difficult due to the costs associated with the large-scale production, and the fact that some ionic liquids are not considered less environmentally harmful due to the non-renewable feedstock used for production and the disposal method utilized (Werner et al., 2010). Another class of compounds extensively studied is that of Deep Eutectic Solvents (DES). These are derived from levulinic acid and choline chloride, in addition to glycerol, ethylene glycol, and urea (Hadj-Kali et al., 2017). A challenge identified with using deep eutectic solvents commercially, is in solvent recovery via distillation due to the column temperature profiles being close to thermal stability boundaries, as well as high melting points (Larriba et al., 2018). The use of cyclic carbonates is an encouraging recent development due to the use of CO_2, good solvent properties, similar extraction ability to sulfolane and NFM, and a simple synthesis route (Hernández et al., 2021).

A consolidated, integrated approach that incorporates technical feasibility, as well as impact on sustainability is required to evaluate the suitability of various solvents. The authors here previously developed a comprehensive screening methodology that considered sustainability through numerous health, safety, environmental factors; feasibility was incorporated with the inclusion of factors such as solvent price, process utilities, physical properties, and capital costs (Brijmohan et al., 2021). The result of the screening process was that propane-1,2,3-triol (glycerol), as well as butane-1,4-diol were identified as potential commercial and sustainable alternatives. UNIFAC (LL) was the model used to estimate the selectivity of the chemicals in the database where there was no experimental data. Ternary liquid-liquid equilibrium (LLE) data for alkane and aromatic mixtures were measured using the aforementioned solvents. The experimental data affirmed that the solvents identified are potential commercial alternatives, however improvement to the solvent capacities are required in order to effectively compete with conventional solvents in terms of operating costs, as low capacities are associated with high solvent-feed ratios.

In practice, the feed stream consists of a variety of different alkanes, branched alkanes, as well as different aromatics. In an actual industrial liquid-liquid extraction unit, the system has to be able to separate the diverse range of alkanes and aromatics in the feedstock. The design of the unit has to be based on knowledge of phase behaviour for the variety of combinations of components in the feed in order for the system to be effective for a multi-component system. LLE phase behaviour of the new potential solvents with heavy alkanes and heavy aromatics was also investigated. This variation is necessary as it also serves as an indicator of the solvent performance on the heavier diesel fraction.

UNIFAC (LL) was found to have inaccurately predicted immiscibility between 2-methyl-2,4-pentanediol and *n*-heptane at all compositions, implying that UNIFAC (LL) is inappropriate for the system (Brijmohan et al., 2022a). It was thereafter experimentally noted that 2-methyl-2,4-pentanediol forms a two-phase region with longer chain alkanes while maintaining complete solubility with toluene. The authors thereafter hypothesised that 2-methyl-2,4-pentanediol may be used as a co-solvent to improve the solvent characteristics (specifically capacity) of 1,4-butanediol and glycerol (Brijmohan et al., 2023). In another study (Brijmohan et al., 2021), the authors presented and highlighted that 2-methyl-2,4-pentanediol has benefits in terms of health, safety, and the environment compared to conventional solvents. Sulfolane is harmful if swallowed and has safety risks such as the release of poisonous gases in the event of a fire, and eventually degrades

into acidic byproducts. NMP may cause respiratory irritation and damage fertility, and also may release poisonous gases. DMF is a flammable liquid and may also damage fertility. DMSO decomposes at high temperatures and is dangerous to aquatic life in high concentrations.

2-Methyl-2,4-pentanediol does not possess these safety and health risks, although may cause skin irritation. This motivates the need to understand the phase behaviour of the system in question with 2-methyl-2,4-pentanediol as a co-solvent. The effect of 2-methyl-2,4-pentanediol on the distribution coefficient of 1,4-butanediol and glycerol were then studied by measurement of quaternary LLE data. It was found that 2-methyl-2,4-pentanediol significantly improves the capacity of 1,4-butanediol and glycerol at high molar ratios of co-solvent to solvent mixtures.

The impact of 2-methyl-2,4-pentanediol on the capacity of glycerol was also investigated. To the extent that the authors are aware, experimental data for the systems studied were not previously available in the open literature. In summary, experimental equilibrium data is presented for the systems listed below (Brijmohan et al., 2022b, 2022c, 2022a, 2023).

- Ternary LLE data for the system *n*-heptane + toluene + 1,4-butanediol at 298.2 K, 313.2 K, 333.2 K and 0.1 MPa
- Ternary LLE data for the system *n*-heptane + toluene + glycerol at 298.2 K, 313.2 K, 333.2 K and 0.1 MPa
- Ternary LLE data for the system *n*-nonane + *o*-xylene + 1,4-butanediol at 298.2 K, 313.2 K, 333.2 K and 0.1 MPa
- Ternary LLE data for the system *n*-nonane + *o*-xylene + glycerol at 298.2 K, 313.2 K, 333.2 K and 0.1 MPa
- Quaternary LLE data for the system *n*-heptane + toluene + 1,4-butanediol + 2-methyl-2,4-pentanediol at 298.2 K, 313.2 K and 0.1 MPa at various molar ratios of solvent:co-solvent
- Quaternary LLE data for the system *n*-heptane + toluene + glycerol + 2-methyl-2,4-pentanediol at 298.2 K, 313.2 K and 0.1 MPa at various molar ratios of solvent:co-solvent

3.2. Theory

3.2.1 Data Correlation. At equilibrium, the thermodynamic criterion is expressed in terms of fugacity in solution ($\hat{f}_i$) and this was used to correlate the experimental data for each phase.

$$\left(\hat{f}_i\right)^I = \left(\hat{f}_i\right)^{II} \tag{3.1}$$

$$\left(x_i\gamma_i\right)^I = \left(x_i\gamma_i\right)^{II} \tag{3.2}$$

where γ represents the activity coefficient in each liquid phase, x is the liquid phase mole fraction, i represents species, and I and II denote each equilibrium phase. At moderate to low pressures, the activity coefficient is known not be appreciably dependent on pressure, which also does not have a discernible effect on the liquid phase mole fraction for multiple liquid phases (Moodley et al., 2018).

The measured data was correlated with the Nonrandom Two-Liquid (NRTL) (Renon & Prausnitz, 1968) and UNIversal QUasi-Chemical UNIQUAC (Abrams & Prausnitz, 1975) activity coefficient models using ASPEN Plus® Version 10 (*Aspen Plus*, 2004).

Renon and Prausnitz (1968) developed the NRTL model on the basis of the assumption of non-randomness.

$$\ln(\gamma_i) = \frac{\sum_{j=1}^{n}\tau_{ji}G_{ji}x_j}{\sum_{k=1}^{n}G_{ki}x_k} + \sum_{j=1}^{n}\frac{\sum_{j=1}^{n}G_{ij}x_j}{\sum_{k=1}^{n}G_{kj}x_k}\left(\tau_{ij} - \frac{\sum_{r=1}^{n}\tau_{rj}G_{rj}x_r}{\sum_{k=1}^{n}G_{kj}x_k}\right) \tag{3.3}$$

Where

$$G_{ij} = \exp(-\alpha_{ij}\tau_{ij}) \tag{3.4}$$

$$\tau_{ij} = \frac{g_{ij} - g_{ji}}{RT} \tag{3.5}$$

The level of randomness in the system is accounted for by the term α_{ij}, with 0 indicating a state of complete randomness. Different values may be used for different systems, with Renon and Prausnitz (1968) establishing that $\alpha_{ij} = \alpha_{ji}$ in their formulation. The parameters ($g_{ij} - g_{jj}$) and ($g_{ji} - g_{ii}$) are referred to as the binary interaction parameters and are included to consider the molecular interactions between components i and j. T is the system temperature, and R is the ideal gas constant.

The UNIQUAC model is derived on the basis of a two-liquid model using local composition theory. The model consists of two sections: a combinatorial term and a residual term. The combinatorial part (Equation 3.6) serves to account for the dissimilarities in molecular structure, while the residual term (Equation 3.7) describes the interactions between molecules in terms of intermolecular forces.

$$\ln \gamma_i^C = \ln \frac{\Phi_i}{x_i} + \frac{z}{2} q_i \ln \frac{\theta_i}{\Phi_i} + l_i - \frac{\Phi_i}{x_i} \sum_{j=1}^{n} x_j l_j \tag{3.6}$$

$$\ln \gamma_i^R = -q_i \ln \left(\sum_{j=1}^{n} \theta_j \tau_{ji} \right) + q_i - q_i \sum_{j=1}^{n} \frac{\theta_j \tau_{ij}}{\sum_{k=1}^{n} \theta_k \tau_{kj}} \tag{3.7}$$

$$\ln \gamma_i = \ln \gamma_i^C + \ln \gamma_i^R \tag{3.8}$$

Where

$$\Phi_i = \frac{r_i x_i}{\sum_{j=1}^{n} r_j x_j} \tag{3.9}$$

$$\theta_i = \frac{q_j x_j}{\sum_{j=1}^{n} q_j x_j} \tag{3.10}$$

$$l_i = \frac{z}{2}(r_i - q_i) - (r_i - 1) \tag{3.11}$$

$$\tau_{ij} = \exp\left(-\left[\frac{u_{ij} - u_{jj}}{RT} \right] \right) \tag{3.12}$$

The area fraction (θ) and the segment fraction (Φ) and are determined from Equations (3.9) and (3.10) while the co-ordination number (z) is commonly assignment a value of 10. The parameters *r* accounts for the size of the molecules while *q* accounts for the external surface area of the molecules. The parameter τ_{ij} is described by the characteristic energies ($u_{ij} - u_{jj}$), which varies based upon the components comprising the system.

The Britt-Luecke algorithm (Britt & Luecke, 1973) and Deming Initialisation method (Deming, 1943) was used together with a maximum likelihood objective function to conduct the regression. The interaction parameters were determined in the temperature-independent form (Equation 3.13)

for the quaternary data at each of the two isotherms, while the temperature-dependent (Equation 3.14) form was used for the ternary data collectively for the three isotherms.

$$\tau_{ij} = a_{ij} \tag{3.13}$$

$$\tau_{ij} = a_{ij} + \frac{b_{ij}}{T} \tag{3.14}$$

where τ_{ij} is the dimensionless interaction parameter, a_{ij} and b_{ij} are the regressed coefficients, and T is temperature in Kelvin.

The non-randomness parameter (α_{ij}) of the NRTL model was incorporated into the regression, with the range of values as suggested by Walas (1985). The regression was performed for various α_{ij} values in the suggested range, and then specified at the value that resulted in a minimal root mean square deviation (RMSD), which was used as an indicator of the accuracy of the fit of the experimental data to the NRTL and UNIQUAC models. The average absolute deviation (AAD) and percentage average absolute relative deviation (%AARD) was also determined and used to assess the suitability of the correlation.

$$\mathrm{RMSD} = \left\{ \frac{\sum_a \sum_b \sum_c \left\{ x_{abc}(\mathrm{exp}) - x_{abc}(\mathrm{calc}) \right\}^2}{8k} \right\}^{1/2} \tag{3.15}$$

$$AAD = \frac{1}{k} \sum_i \left| x_i(\mathrm{exp}) - x_i(\mathrm{calc}) \right| \tag{3.16}$$

$$\%AARD = \frac{100}{k} \sum_i \left| \frac{x_i(\mathrm{exp}) - x_i(\mathrm{calc})}{x_i(\mathrm{exp})} \right| \tag{3.17}$$

where exp denotes the experimental data, and calc refers to the calculated data. The liquid phase mole fraction is indicated by x, whereas k is the number of experimental points. The subscripts a, b, and c denote the component, phase, and tie-line correspondingly.

3.2.2 Selectivity and Distribution Coefficient. It is necessary for the selectivity to be greater than one for any solvent to be effective in a liquid-liquid extraction system. The selectivity is defined as the fraction of aromatics that disseminates in the solvent-rich phase (the extract) compared to the proportion of alkanes. It is the ratio of the distribution coefficient of the aromatics and the distribution coefficient of alkanes.

$$\text{Selectivity} = \frac{\text{Distribution coefficient for aromatic}}{\text{Distribution coefficient for non - aromatic}} \tag{3.18}$$

$$S_{ij} = \frac{K_i}{K_j} = \frac{x_i^I x_j^{II}}{x_i^{II} x_j^I} \tag{3.19}$$

The distribution coefficient is represented by *K*, and the phase composition by *x*. The subscripts '*i*' and '*j*' refer to the aromatic and non-aromatic components, while the superscripts *I* and *II* denote the solvent-rich and aliphatic-rich phases correspondingly.

The capacity of the solvent is the extent to which the aromatic component has transferred to solvent-rich phase, and is represented by the distribution coefficient itself. This characteristic plays a significant role in ascertaining the solvent to feed ratio, which impacts the energy consumption of the process in the solvent recovery section.

$$K_i = \frac{x_i^I}{x_i^{II}} \tag{3.20}$$

3.3 Material and Methods

3.3.1 Chemicals. The purities of all chemicals utilized in this study were verified with gas chromatography and refractive index measurements. The chemicals were purchased from Sigma-Aldrich®. An Atago model RX 7000α was the refractometer used, with an overall uncertainty of 0.0001. Table 1 summarizes the chemical purity analysis. As no significant impurities were detected, no further purification was performed for the chemicals involved in the study. Karl Fisher titration was used to verify that the water content was less than 0.005 mole fraction.

Table 3.1. Chemical purity analysis.

Chemical	CAS Reg. No.	GC Peak Area fraction	Mass fraction purity[a]	Measured n_D[b,c]	Literature (Lide, 2006) n_D
n-Heptane	142-82-5	0.997	> 0.99	1.3854[d]	1.3855
n-Nonane	95-47-6	0.997	> 0.99	1.4054	1.4058
Toluene	108-88-3	0.998	> 0.99	1.4955	1.4961
o-Xylene	111-84-2	0.998	>0.99	1.5055	1.5053
1,4-Butanediol	110-63-4	0.998	> 0.99	1.4461	1.4460
Glycerol	56-81-5	0.998	> 0.99	1.4748	1.4746
2-methyl-2,4-pentanediol	107-41-5	0.998	> 0.99	1.4273	1.4276

[a] As stated by supplier.

[b]n_D is the refractive index at T = 293.2 K, 0.1 MPa at sodium D-line = 589 nm. [c]Expanded uncertainties for n_D experiments are: U are $U(T)$ = 0.1 K, $U(n_D)$ = 0.0001 (0.95 level of confidence, k = 2) (Taylor & Kuyatt, 1994). [d]n_D is the refractive index at T = 298.2 K, 0.1 MPa at sodium D-line = 589 nm.

3.3.2 Equipment. The experimental measurements were performed using a double-walled glass cell and magnetic stirrer. The double-walled glass cell was used as the fluid recirculation in the inner wall allows for temperature control and measurements at various temperatures. The magnetic stirrer agitates the mixture for both phases, ensuring that there is mass transfer of all species between phases. The experimental method used to perform the measurements was the direct analytical method, which involves charging an equilibrium cell with the solvent and carrier liquid, and thereafter incrementally injecting solute into the system and determining the resulting tie lines. The equipment and the method were successfully used in several previous studies (Brijmohan & Narasigadu, 2020; Narasigadu et al., 2014). The experimental procedure followed the technique as suggested by Alders (1959). Initially, 30 cm^3 of the solvent mixture consisting of either 1,4--butanediol, glycerol, or 2-methyl-2,4-pentanediol was charged to a jacketed 100 cm^3 cell, together with 20 cm^3 of *n*-heptane or *n*-nonane. In order to generate the tie-line data, toluene or *o*-xylene was added incrementally in quantities between 2-5 cm^3 such that the phase behaviour was sufficiently represented across the entire two-phase region. The solution volumes in the cell were

determined by trial and error such that the sampling point of the solvent-rich phase was below the interface of the two phases. For the co-solvent mixtures, the solvent-rich phase was prepared by creating solvent mixtures of 1,4-butanediol/glycerol and 2-methyl-2,4-pentanediol comprising 0.75, 0.50, and 0.25 1,4-butanediol/glycerol (molar ratios 3:1, 1:1, and 1:3). The molar ratios were chosen in equal increments from pure solvent to pure co-solvent to ensure that the phase behaviour is fully understood and represented across the entire composition range. In order to ensure the phases were well-mixed and to expedite transfer of components between phases, a magnetic stirrer was used to agitate the cell-contents for at least an hour. The mixture was then left to settle overnight to allow for complete phase separation. Initially, the mixture was sampled after various settling times, and it was ascertained that there was little significant variations in composition after 5 hours. The mixing and settling time were determined by trial and error. Sampling of the individual phases occurred thereafter with a minimum of 3 samples drawn. The sampling continued until the calculated area ratios for each phase had a standard deviation that was within 1% of the mean for a minimum of three samples.

The Pt-100 temperature sensor was calibrated with a Wika CTB 9100 unit. The sensor and standard probe were immersed in an oil liquid bath for which the temperature was varied from 293.2 K to 373.2 K and back to 293.2 K in 5 K increments. The temperature readings were recorded at all setpoint temperatures, and the calibration curve was subsequently developed. The temperature measurement had an expanded uncertainty of 0.1 K (k = 2), where k is the number of standard deviations, indicating a 95% confidence interval (Taylor & Kuyatt, 1994). The compositions of each phase were analysed with the use of gas chromatography (GC). The GC type conditions for each collection of measurements are herewith summarized. The detector was calibrated with the area ratio method (Raal & Mühlbauer, 1998) in all instances to determine phase compositions.

Ternary measurements (*n*-heptane + toluene + 1,4-butanediol or glycerol):

A Shimadzu 2014 thermal conductivity unit using helium as the carrier gas was used. The column was a Poropak Q column (2 m × 2.2 mm) with the detector temperature at 523.15 K, the column temperature at 493.15 K and the carrier gas flow at 70 ml/min.

Ternary measurements (*n*-nonane + *o*-xylene + 1,4-butanediol or glycerol):

A 2010 flame ionization detector (FID) Shimadzu unit was used, in which the carrier gas was hydrogen. The detector temperature was at 523.15 K, the initial column temperature at 363.15 K, the initial pressure at 23 kPa and the carrier gas flow at 30 ml/min. The column was a Perkin Elmer capillary column (30 m × 0.25 mm). The column temperature was ramped to 493.15 K and pressure to 40 kPa after 5.7 minutes.

Quaternary measurements (*n*-heptane + toluene + 1,4-butanediol + 2-methyl-2,4-pentanediol):

A Shimadzu GC2014 thermal conductivity unit with helium as the carrier gas was used to perform the composition analysis. The unit had a packed column (Poropak Q) with dimensions 2 m × 2.2 mm. The detector temperature was set at 503.15 K, the column temperature at 493.15 K and the carrier gas flow 30 ml/min.

Quaternary measurements (*n*-heptane + toluene + glycerol + 2-methyl-2,4-pentanediol):

A Shimadzu GC2010 flame ionization detector (FID) unit was used with hydrogen as the carrier gas. The column was a Perkin Elmer capillary column (30 m × 0.25 mm) with the detector temperature at 513.2 K, the column temperature at 378.2 K, the pressure at 40 kPa and the carrier gas flow at 148.3 ml/min, with a split ratio of 210.

3.4. Results and Discussion

The mutual solubilities between toluene and 1,4-butanediol, as well as glycerol are displayed in Figures 3.1 and 3.2 and compared to literature. Departures from the literature data were noted to possibly be a result of different GC conditions, experimental measurement methods, as well as chemical purity.

Figures 3.3 – 3.8 graphically present the experimental and thermodynamically modelled LLE data for the *n*-heptane + toluene + (1,4-butanediol or glycerol) systems at (298.2, 313.2 and 333.2) K and 0.1 MPa. The ternary LLE data for the systems *n*-nonane + *o*-xylene + (butane-1,4-diol or glycerol) at (298.2, 313.2 and 333.2) K and 0.1 MPa are shown in Figures 3.9 – 3.14, together with the thermodynamically modelled data. The experimental LLE data for the *n*-heptane + toluene + 1,4-butanediol + 2-methyl-2,4-pentanediol system at (298.2 and 313.2) K and 0.1 MPa is represented in Figures 3.15 – 3.20 together with the correlated data. The quaternary system is represented as a pseudo ternary system with the solvent (1,4-butanediol) and co-solvent (2-methyl-

2,4-pentanediol) combined in one axis. Figures 3.21 – 3.26 illustrates the experimental and correlated LLE data for the system *n*-heptane + toluene + glycerol + 2-methyl-2,4-pentanediol at (298.2 and 313.2) K and 0.1 MPa. The third component is indicated as a pseudo-component in which the solvent (glycerol) and co-solvent (2-methyl-2,4-pentanediol) is amalgamated on one axis.

The experimental LLE data, including selectivity and distribution coefficients, are tabulated in Tables 3.2 to 3.9, whilst the correlated NRTL and UNIQUAC model parameters are reported in Tables 3.10 to 3.15. Table 3.16 lists the UNIQUAC structural parameters for each species. These parameters were obtained from ASPEN Plus® Version 10.

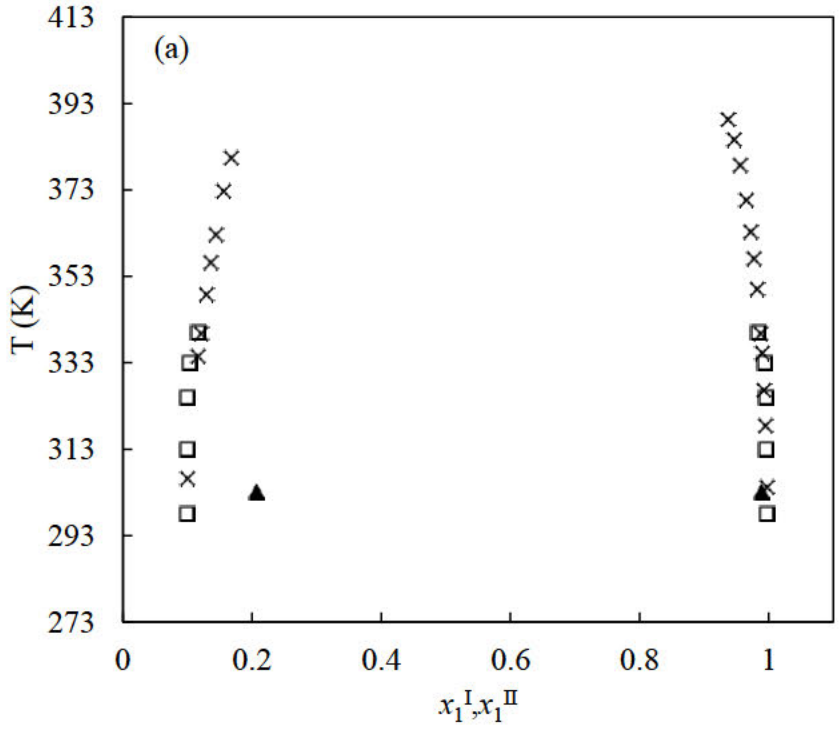

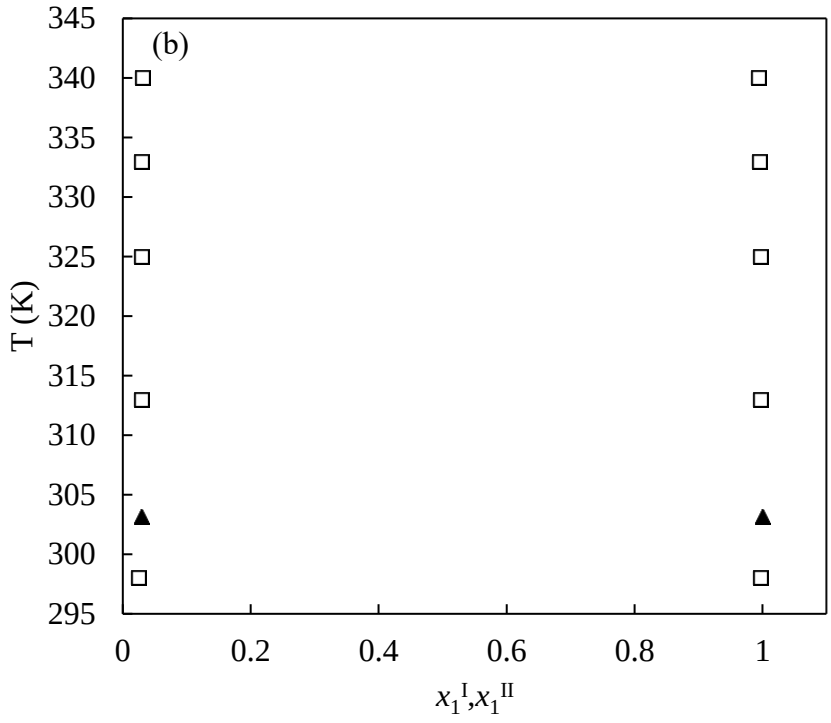

Figure 3.1. Comparison of the mutual solubility (mole basis) with reference data for the systems: (a) toluene (1) + 1,4-butanediol (2); □ – this work; × - ref (Lesek & Mandík, 1982), ▲ – ref (Fan et al., 2020)**. (b) toluene (1) + glycerol (2); □ – this work; ▲ – ref** (Fan et al., 2020)

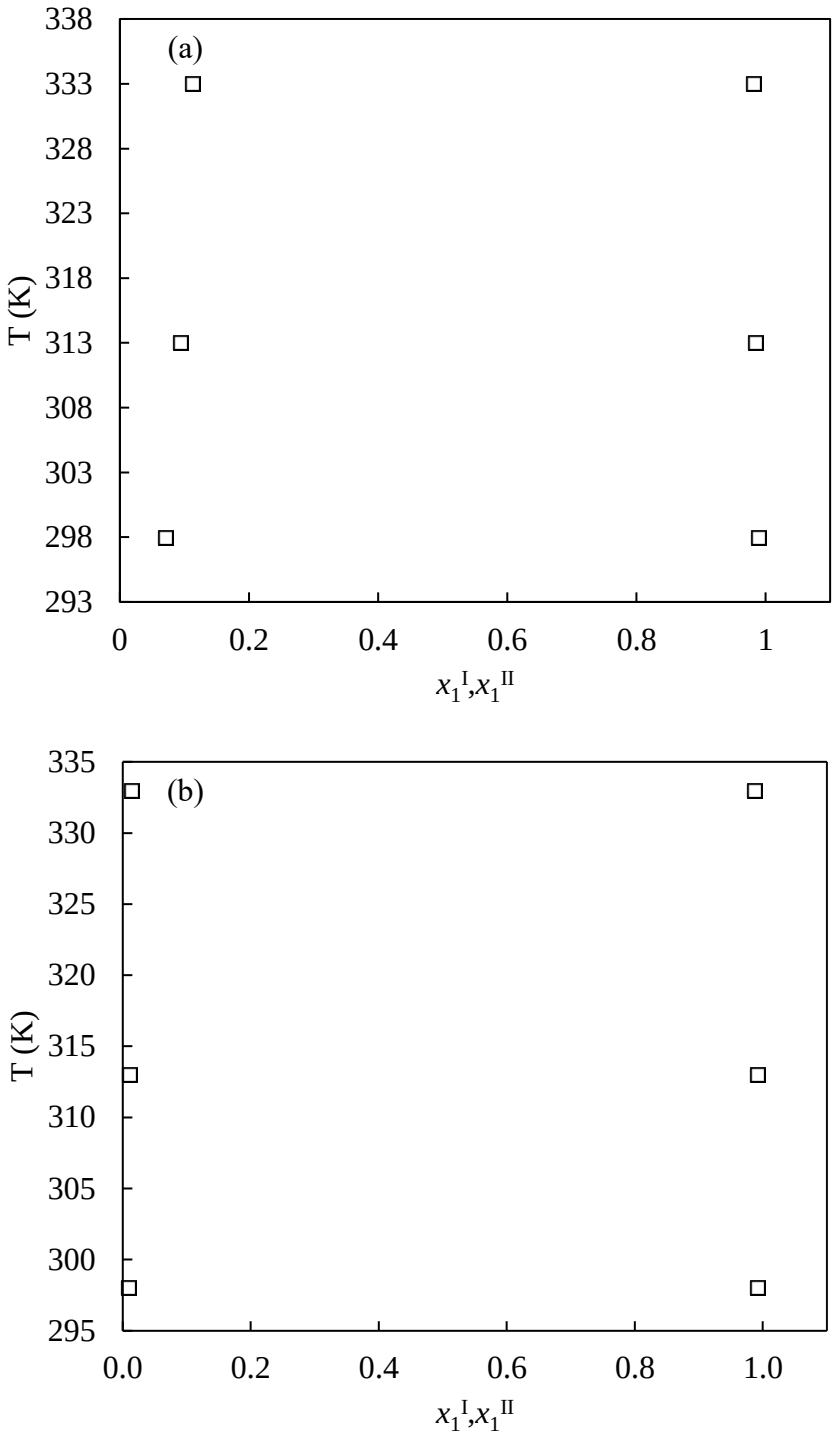

Figure 3.2. Binary liquid-liquid equilibrium data (mole basis) for the systems: (a) *o*-xylene (1) + butane-1,4-diol (2); □ – this work; (b) *o*-xylene (1) + glycerol (2); □ – this work

Table 3.2. Experimental liquid-liquid equilibrium data (mole basis) for the *n*-heptane (1) + toluene (2) + 1,4-butanediol (3) system at (298.2, 313.2 and 333.2) K and 0.1 MPa.[a]

solvent rich phase			alkane rich phase				
x_1	x_2	x_3	x_1	x_2	x_3	S	K
			T = 298.2 K				
0.009	0.014	0.977	0.855	0.141	0.004	9.433	0.099
0.008	0.033	0.959	0.675	0.321	0.004	8.674	0.103
0.008	0.043	0.949	0.554	0.443	0.003	6.722	0.097
0.007	0.052	0.941	0.466	0.531	0.003	6.519	0.098
0.006	0.059	0.935	0.386	0.611	0.003	6.212	0.097
0.005	0.065	0.930	0.311	0.685	0.004	5.902	0.095
0.003	0.084	0.913	0.156	0.841	0.003	5.194	0.100
0.000	0.099	0.901	0.000	0.997	0.003	-	-
			T = 313.2 K				
0.012	0.019	0.969	0.854	0.142	0.004	9.522	0.134
0.010	0.035	0.955	0.674	0.322	0.004	7.326	0.109
0.009	0.046	0.945	0.553	0.443	0.004	6.380	0.104
0.008	0.050	0.942	0.466	0.530	0.004	5.495	0.094
0.006	0.074	0.920	0.308	0.688	0.004	5.521	0.108
0.004	0.081	0.915	0.199	0.797	0.004	5.056	0.102
0.002	0.092	0.906	0.051	0.945	0.004	2.483	0.097
0.000	0.100	0.900	0.000	0.996	0.004	-	-
			T = 325.2 K				
0.000	0.100	0.900	0.000	0.995	0.005	-	-
			T = 333.2 K				
0.014	0.019	0.967	0.853	0.141	0.006	8.210	0.135
0.011	0.036	0.953	0.673	0.321	0.006	6.862	0.112
0.009	0.045	0.946	0.552	0.442	0.006	6.244	0.102
0.008	0.055	0.937	0.465	0.529	0.006	6.043	0.104
0.007	0.063	0.930	0.383	0.611	0.006	5.642	0.103
0.006	0.068	0.926	0.310	0.684	0.006	5.136	0.099
0.003	0.085	0.912	0.139	0.855	0.006	4.606	0.099
0.000	0.101	0.899	0.000	0.994	0.006	-	-
			T = 340.2 K				
0.000	0.1163	0.8837	0.000	0.9837	0.0163	-	-

[a] Expanded uncertainties U are $U(T)$ = 0.1 K, $U(P)$ = 1 kPa, $U(x_i)$ = 0.004 for the solvent-rich phase, and $U(x_i)$ = 0.006 for the alkane-rich phase (0.95 level of confidence, k = 2) (Taylor & Kuyatt, 1994)

Table 3.3. Experimental liquid-liquid equilibrium data (mole basis) for the *n*-heptane (1) + toluene (2) + glycerol (3) system at (298.2, 313.2 and 333.2) K and 0.1 MPa.[a]

solvent rich phase			alkane rich phase				
x_1	x_2	x_3	x_1	x_2	x_3	S	K
			T = 298.2 K				
0.003	0.008	0.989	0.830	0.167	0.003	13.25	0.048
0.001	0.022	0.977	0.333	0.664	0.003	11.03	0.033
0.001	0.024	0.975	0.226	0.771	0.003	7.035	0.031
0.001	0.022	0.977	0.115	0.883	0.002	2.865	0.025
0.002	0.016	0.982	0.589	0.408	0.003	11.55	0.039
0.001	0.022	0.977	0.092	0.905	0.003	2.236	0.024
0.001	0.022	0.977	0.157	0.841	0.002	4.107	0.026
0.000	0.024	0.976	0.000	0.997	0.003	-	-
			T = 313.2 K				
0.004	0.008	0.988	0.829	0.168	0.003	9.869	0.048
0.001	0.023	0.976	0.330	0.667	0.003	11.38	0.034
0.001	0.026	0.973	0.212	0.785	0.003	7.022	0.033
0.000	0.028	0.972	0.116	0.882	0.002	9.206	0.032
0.001	0.027	0.972	0.136	0.861	0.003	4.265	0.031
0.001	0.027	0.972	0.200	0.796	0.004	6.784	0.034
0.002	0.015	0.983	0.599	0.398	0.003	11.29	0.038
0.000	0.029	0.971	0.000	0.997	0.003	-	-
			T = 325.2 K				
0.000	0.028	0.972	0.000	0.997	0.003	-	-
			T = 333.2 K				
0.005	0.009	0.986	0.827	0.167	0.006	8.914	0.054
0.003	0.017	0.980	0.605	0.392	0.003	8.746	0.043
0.003	0.018	0.979	0.539	0.458	0.003	7.061	0.039
0.002	0.019	0.979	0.437	0.560	0.003	7.413	0.034
0.001	0.023	0.976	0.168	0.829	0.003	4.661	0.028
0.001	0.024	0.975	0.085	0.909	0.006	2.244	0.026
0.001	0.024	0.975	0.109	0.888	0.003	2.946	0.027
0.000	0.026	0.974	0.000	0.997	0.003	-	-
			T = 340.2 K				
0.000	0.031	0.969	0.000	0.994	0.006	-	-

[a] Expanded uncertainties U are $U(T)$ = 0.1 K, $U(P)$ = 1 kPa, $U(x_i)$ = 0.002 for the solvent-rich phase, and $U(x_i)$ = 0.006 for the alkane-rich phase (0.95 level of confidence, k = 2) (Taylor & Kuyatt, 1994)

Table 3.4. Experimentally determined liquid-liquid equilibrium data (mole basis) for the *n*-nonane (1) + *o*-xylene (2) + butane-1,4-diol (3) system at (298.2, 313.2 and 333.2) K and 0.1 MPa.[a]

solvent rich phase			alkane rich phase				
x_1	x_2	x_3	x_1	x_2	x_3	S	K
			T = 298.2 K				
0.008	0.029	0.963	0.887	0.111	0.002	28.97	0.261
0.008	0.041	0.951	0.796	0.202	0.002	20.20	0.203
0.006	0.046	0.948	0.679	0.318	0.003	16.37	0.145
0.005	0.053	0.942	0.554	0.441	0.005	13.32	0.120
0.004	0.061	0.935	0.486	0.508	0.006	14.59	0.120
0.003	0.064	0.933	0.263	0.729	0.008	7.696	0.088
0.001	0.068	0.931	0.114	0.879	0.007	8.819	0.077
0.000	0.071	0.929	0.000	0.989	0.011	-	-
			T = 313.2 K				
0.009	0.016	0.975	0.941	0.057	0.002	29.35	0.281
0.005	0.038	0.957	0.752	0.246	0.002	23.23	0.154
0.004	0.038	0.958	0.691	0.305	0.004	21.52	0.125
0.004	0.043	0.953	0.558	0.437	0.005	13.73	0.098
0.004	0.046	0.950	0.444	0.549	0.007	9.301	0.084
0.003	0.062	0.935	0.242	0.748	0.010	6.686	0.083
0.002	0.074	0.924	0.116	0.870	0.014	4.933	0.085
0.000	0.094	0.906	0.000	0.985	0.015	-	-
			T = 333.2 K				
0.007	0.012	0.981	0.921	0.076	0.003	20.78	0.158
0.006	0.032	0.962	0.777	0.219	0.004	18.92	0.146
0.004	0.039	0.957	0.651	0.345	0.004	18.40	0.113
0.004	0.041	0.955	0.553	0.441	0.006	12.85	0.093
0.004	0.049	0.947	0.472	0.518	0.010	11.16	0.095
0.003	0.068	0.929	0.247	0.743	0.010	7.535	0.092
0.002	0.081	0.917	0.106	0.879	0.015	4.884	0.092
0.000	0.112	0.888	0.000	0.981	0.019	-	-

[a] Expanded uncertainties U are $U(T)$ = 0.1 K, $U(P)$ = 1 kPa, $U(x_i)$ = 0.001 for the solvent-rich phase, and $U(x_i)$ = 0.003 for the alkane-rich phase (0.95 level of confidence, k = 2) (Taylor & Kuyatt, 1994)

Table 3.5. Experimentally determined liquid-liquid equilibrium data (mole basis) for the *n*-nonane (1) + *o*-xylene (2) + glycerol (3) system at (298.2, 313.2 and 333.2) K and 0.1 MPa.[a]

solvent rich phase			alkane rich phase				
x_1	x_2	x_3	x_1	x_2	x_3	S	K
			T = 298.2 K				
0.002	0.009	0.989	0.905	0.092	0.003	44.27	0.098
0.001	0.008	0.991	0.794	0.204	0.002	31.14	0.039
0.001	0.008	0.991	0.599	0.398	0.003	12.04	0.020
0.001	0.008	0.991	0.442	0.553	0.005	6.394	0.014
0.001	0.008	0.991	0.230	0.762	0.008	2.415	0.010
0.000	0.009	0.991	0.039	0.953	0.008	-	-
0.000	0.009	0.991	0.000	0.992	0.008	-	-
			T = 313.2 K				
0.002	0.009	0.989	0.875	0.123	0.002	32.01	0.073
0.002	0.008	0.990	0.792	0.205	0.003	15.45	0.039
0.002	0.008	0.990	0.635	0.361	0.004	7.036	0.022
0.001	0.009	0.990	0.467	0.528	0.005	7.960	0.017
0.001	0.009	0.990	0.396	0.599	0.005	5.950	0.015
0.002	0.008	0.990	0.232	0.764	0.004	1.215	0.010
0.000	0.009	0.991	0.055	0.937	0.008	-	-
0.000	0.010	0.990	0.000	0.991	0.009	-	-
			T = 333.2 K				
0.001	0.007	0.992	0.840	0.156	0.004	37.69	0.045
0.001	0.008	0.991	0.787	0.210	0.003	29.98	0.038
0.001	0.008	0.991	0.648	0.348	0.004	14.90	0.023
0.001	0.008	0.991	0.488	0.507	0.005	7.700	0.016
0.001	0.008	0.991	0.368	0.629	0.005	4.655	0.013
0.001	0.010	0.989	0.219	0.774	0.007	2.829	0.013
0.001	0.013	0.986	0.055	0.938	0.007	0.762	0.014
0.000	0.014	0.986	0.000	0.987	0.013	-	-

[a] Expanded uncertainties U are $U(T)$ = 0.1 K, $U(P)$ = 1 kPa, $U(x_i)$ = 0.0008 for the solvent-rich phase, and $U(x_i)$ = 0.001 for the alkane-rich phase (0.95 level of confidence, k = 2) (Taylor & Kuyatt, 1994)

Table 3.6. Experimental liquid-liquid equilibrium data (mole basis) for the *n*-heptane (1) + toluene (2) + 1,4-butanediol (3) + 2-methyl-2,4-pentanediol (4) system at 298.2 K and 0.1 MPa.[a]

solvent rich phase				alkane rich phase					
x_1	x_2	x_3	x_4	x_1	x_2	x_3	x_4	S	K
1,4-butanediol (3):2-methyl-2,4-pentanediol (4) = 3:1									
0.025	0.000	0.805	0.169	0.997	0.000	0.003	0.000	-	-
0.020	0.042	0.783	0.154	0.790	0.206	0.004	0.000	7.854	0.202
0.014	0.067	0.767	0.153	0.566	0.430	0.004	0.000	6.476	0.156
0.010	0.092	0.746	0.152	0.402	0.594	0.004	0.000	5.975	0.154
0.007	0.115	0.735	0.143	0.199	0.797	0.004	0.000	4.190	0.144
0.004	0.133	0.721	0.142	0.106	0.890	0.004	0.000	3.928	0.149
0.000	0.157	0.700	0.143	0.000	0.996	0.004	0.000	-	-
1,4-butanediol (3):2-methyl-2,4-pentanediol (4) = 1:1									
0.051	0.000	0.513	0.436	0.997	0.000	0.003	0.000	-	-
0.046	0.046	0.511	0.398	0.865	0.131	0.004	0.000	6.524	0.348
0.037	0.083	0.502	0.379	0.715	0.280	0.005	0.000	5.760	0.295
0.031	0.131	0.497	0.342	0.565	0.430	0.005	0.000	5.589	0.304
0.025	0.152	0.489	0.334	0.417	0.550	0.029	0.003	4.537	0.276
0.020	0.171	0.480	0.329	0.251	0.690	0.055	0.004	3.138	0.248
0.012	0.187	0.476	0.325	0.124	0.807	0.065	0.004	2.369	0.232
0.000	0.234	0.473	0.293	0.000	0.921	0.075	0.004	-	-
1,4-butanediol (3):2-methyl-2,4-pentanediol (4) = 1:3									
0.052	0.000	0.337	0.610	0.997	0.000	0.003	0.000	-	-
0.065	0.048	0.326	0.561	0.840	0.155	0.005	0.000	3.966	0.308
0.074	0.079	0.313	0.533	0.770	0.223	0.007	0.000	3.708	0.356
0.091	0.140	0.308	0.462	0.682	0.301	0.012	0.005	3.493	0.464
0.098	0.195	0.284	0.423	0.580	0.372	0.027	0.021	3.088	0.524
0.111	0.246	0.266	0.376	0.407	0.429	0.092	0.072	2.096	0.574

[a] Expanded uncertainties U are $U(T)$ = 0.1 K, $U(P)$ = 1 kPa, $U(x_i)$ = 0.007 for the solvent-rich phase, and $U(x_i)$ = 0.002 for the alkane-rich phase (0.95 level of confidence, k = 2) (Taylor & Kuyatt, 1994)

Table 3.7. Experimental liquid-liquid equilibrium data (mole basis) for the *n*-heptane (1) + toluene (2) + 1,4-butanediol (3) + 2-methyl-2,4-pentanediol (4) system at 313.2 K and 0.1 MPa.[a]

solvent rich phase				alkane rich phase					
x_1	x_2	x_3	x_4	x_1	x_2	x_3	x_4	S	K
1,4-butanediol (3):2-methyl-2,4-pentanediol (4) = 3:1									
0.043	0.000	0.743	0.214	0.995	0.000	0.005	0.000	-	-
0.034	0.033	0.738	0.195	0.865	0.130	0.005	0.000	6.442	0.253
0.032	0.048	0.735	0.185	0.653	0.343	0.004	0.000	2.897	0.141
0.025	0.063	0.730	0.181	0.534	0.462	0.004	0.000	2.899	0.137
0.016	0.096	0.728	0.159	0.329	0.666	0.005	0.000	2.919	0.144
0.008	0.120	0.721	0.151	0.206	0.789	0.005	0.000	3.740	0.152
0.005	0.140	0.717	0.138	0.115	0.881	0.004	0.000	3.875	0.159
0.000	0.169	0.695	0.135	0.008	0.987	0.005	0.000	-	-
1,4-butanediol (3):2-methyl-2,4-pentanediol (4) = 1:1									
0.045	0.000	0.532	0.423	0.995	0.000	0.005	0.000	-	-
0.043	0.032	0.522	0.403	0.887	0.109	0.004	0.000	6.101	0.294
0.037	0.063	0.521	0.379	0.723	0.273	0.004	0.000	4.470	0.231
0.032	0.096	0.504	0.368	0.571	0.424	0.005	0.000	4.023	0.227
0.023	0.120	0.491	0.366	0.431	0.564	0.005	0.000	4.009	0.213
0.017	0.191	0.479	0.314	0.212	0.726	0.059	0.004	3.339	0.263
0.000	0.259	0.452	0.289	0.000	0.811	0.107	0.083	-	-
1,4-butanediol (3):2-methyl-2,4-pentanediol (4) = 1:3									
0.072	0.000	0.367	0.560	0.995	0.000	0.005	0.000		
0.086	0.050	0.344	0.519	0.835	0.153	0.009	0.003	3.175	0.328
0.114	0.101	0.325	0.460	0.674	0.265	0.028	0.034	2.232	0.379
0.131	0.147	0.297	0.424	0.547	0.340	0.039	0.073	1.804	0.433
0.148	0.199	0.282	0.371	0.470	0.370	0.059	0.100	1.714	0.539
0.154	0.252	0.272	0.322	0.363	0.394	0.136	0.108	1.511	0.641

[a] Expanded uncertainties U are $U(T)$ = 0.1 K, $U(P)$ = 1 kPa, $U(x_i)$ = 0.006 for the solvent-rich phase, and $U(x_i)$ = 0.002 for the alkane-rich phase (0.95 level of confidence, k = 2) (Taylor & Kuyatt, 1994)

Table 3.8. Experimentally determined liquid-liquid equilibrium data (mole basis) for the system *n*-heptane (1) + toluene (2) + glycerol (3) + 2-methyl-2,4-pentanediol (4) at 298.2 K and 0.1 MPa.[a]

solvent rich phase				alkane rich phase					
x_1	x_2	x_3	x_4	x_1	x_2	x_3	x_4	S	K
glycerol (3):2-methyl-2,4-pentanediol (4) = 3:1									
0.0000	0.0034	0.9733	0.0233	0.0000	0.6129	0.0724	0.3147	-	-
0.0004	0.0043	0.9468	0.0485	0.1467	0.5299	0.0527	0.2707	2.976	0.008
0.0008	0.0042	0.9391	0.0560	0.4518	0.3557	0.0322	0.1603	6.668	0.012
0.0009	0.0041	0.9314	0.0636	0.5199	0.2971	0.0243	0.1587	7.972	0.014
0.0014	0.0043	0.9282	0.0860	0.6564	0.2060	0.0154	0.1222	9.787	0.021
0.0018	0.0048	0.8919	0.1014	0.8550	0.0995	0.0068	0.0386	22.91	0.048
0.0022	0.0048	0.8724	0.1206	0.9389	0.0460	0.0018	0.0132	44.53	0.104
glycerol (3):2-methyl-2,4-pentanediol (4) = 1:1									
0.0000	0.0050	0.9347	0.0604	0.0000	0.4478	0.1320	0.4201	-	-
0.0010	0.0064	0.9137	0.0789	0.2225	0.3407	0.1030	0.3338	4.180	0.019
0.0013	0.0057	0.9180	0.0750	0.2944	0.3158	0.0973	0.2924	4.087	0.018
0.0013	0.0058	0.9273	0.0656	0.3595	0.2904	0.0816	0.2685	5.523	0.020
0.0020	0.0060	0.9172	0.0748	0.4907	0.2432	0.0514	0.2147	6.053	0.025
0.0022	0.0059	0.9249	0.0670	0.5804	0.2029	0.0352	0.1815	7.671	0.029
0.0035	0.0064	0.9107	0.0794	0.6734	0.1677	0.0235	0.1353	7.343	0.038
0.0046	0.0065	0.9063	0.0826	0.7742	0.1238	0.0131	0.0889	8.837	0.053
0.0050	0.0070	0.8904	0.0977	0.8765	0.0685	0.0067	0.0483	17.91	0.102
glycerol (3):2-methyl-2,4-pentanediol (4) = 1:3									
0.1998	0.0933	0.2798	0.4271	0.6576	0.1773	0.0448	0.1203	1.732	0.526
0.1684	0.0775	0.3184	0.4356	0.7075	0.1609	0.0205	0.1112	2.024	0.482
0.1475	0.0582	0.3827	0.4117	0.7470	0.1357	0.0154	0.1019	2.172	0.429
0.0841	0.0372	0.4637	0.4151	0.7948	0.1150	0.0071	0.0831	3.057	0.323
0.0336	0.0119	0.5402	0.4143	0.8420	0.0915	0.0044	0.0621	3.259	0.130
0.0103	0.0030	0.5517	0.4349	0.9459	0.0508	0.0013	0.0020	5.423	0.059

[a] Expanded uncertainties U are $U(T)$ = 0.1 K, $U(P)$ = 1 kPa, $U(x_i)$ = 0.002 for the solvent-rich phase, and $U(x_i)$ = 0.005 for the alkane-rich phase (0.95 level of confidence, k = 2) (Taylor & Kuyatt, 1994)

Table 3.9. Experimentally determined liquid-liquid equilibrium data (mole basis) for the system *n*-heptane (1) + toluene (2) + glycerol (3) + 2-methyl-2,4-pentanediol (4) at 313.2 K and 0.1 MPa.[a]

solvent rich phase				alkane rich phase					
x_1	x_2	x_3	x_4	x_1	x_2	x_3	x_4	S	K
glycerol (3):2-methyl-2,4-pentanediol (4) = 3:1									
0.0000	0.0052	0.9753	0.0194	0.0000	0.6475	0.0814	0.2710	-	-
0.0004	0.0057	0.9631	0.0308	0.1407	0.5731	0.0694	0.2168	3.498	0.010
0.0009	0.0056	0.9469	0.0466	0.3737	0.4298	0.0362	0.1603	5.410	0.013
0.0016	0.0059	0.9273	0.0652	0.6200	0.2438	0.0127	0.1236	9.378	0.024
0.0023	0.0061	0.8769	0.1147	0.7632	0.1154	0.0096	0.1118	17.540	0.053
0.0059	0.0063	0.9033	0.0884	0.8960	0.0282	0.0023	0.0735	33.927	0.223
glycerol (3):2-methyl-2,4-pentanediol (4) = 1:1									
0.0000	0.0074	0.9036	0.0890	0.0000	0.3577	0.1802	0.4621	-	-
0.0015	0.0080	0.9107	0.0798	0.2234	0.2815	0.1442	0.3509	4.233	0.028
0.0020	0.0079	0.9197	0.0705	0.3568	0.2526	0.1105	0.2801	5.579	0.031
0.0046	0.0091	0.8652	0.1211	0.4455	0.2216	0.0810	0.2519	3.977	0.041
0.0033	0.0071	0.9174	0.0722	0.5753	0.1957	0.0512	0.1779	6.325	0.036
0.0030	0.0072	0.9149	0.0749	0.6736	0.1674	0.0294	0.1296	9.657	0.043
0.0025	0.0067	0.9152	0.0756	0.7656	0.1186	0.0189	0.0969	17.30	0.056
0.0039	0.0076	0.9013	0.0872	0.8750	0.0698	0.0075	0.0477	24.43	0.109
glycerol (3):2-methyl-2,4-pentanediol (4) = 1:3									
0.1287	0.1089	0.3961	0.3663	0.6374	0.1722	0.0413	0.1491	3.132	0.632
0.0925	0.0827	0.4816	0.3433	0.6586	0.1571	0.0325	0.1519	3.748	0.526
0.0814	0.0606	0.4596	0.3984	0.6961	0.1261	0.0298	0.1480	4.110	0.481
0.0685	0.0469	0.4885	0.3962	0.7197	0.1100	0.0215	0.1487	4.480	0.426
0.0409	0.0234	0.5191	0.4166	0.7844	0.0706	0.0151	0.1299	6.357	0.331
0.0252	0.0109	0.5999	0.3641	0.8349	0.0355	0.0135	0.1162	10.173	0.307
0.0151	0.0049	0.6068	0.3732	0.8804	0.0202	0.0105	0.0889	14.143	0.243

[a] Expanded uncertainties U are $U(T)$ = 0.1 K, $U(P)$ = 1 kPa, $U(x_i)$ = 0.004 for the solvent-rich phase, and $U(x_i)$ = 0.007 for the alkane-rich phase (0.95 level of confidence, k = 2) (Taylor & Kuyatt, 1994)

Table 3.10. NRTL and UNIQUAC T-dependent interaction parameters and root mean square deviations (RMSD) for the *n*-heptane (1) + toluene (2) + 1,4-butanediol (3) system at (298.2, 313.2 and 333.2) K and 0.1 MPa.

Component		NRTL						UNIQUAC					
i	*j*	a_{ij}	a_{ji}	b_{ij}/K	b_{ji}/K	α_{ij}	RMSD	A_{ij}	A_{ji}	B_{ij}/K	B_{ji}/K	RMSD
1	2	11.31	-7.875	-3457	2546	0.3		-5.459	3.426	1598	-1011	
1	3	1.625	2.221	735	199.8	0.2	2.12×10^{-4}	-0.856	-0.196	-188.6	-28.52	8.9×10^{-2}
2	3	-0.268	0.899	1612	-41.1	0.2		0.344	-0.432	-612	132.8	

Table 3.11. NRTL and UNIQUAC T-dependent interaction parameters and root mean square deviations (RMSD) for the *n*-heptane (1) + toluene (2) + glycerol (3) system at (298.2, 313.2 and 333.2) K and 0.1 MPa.

Component		NRTL						UNIQUAC					
i	*j*	a_{ij}	a_{ji}	b_{ij}/K	b_{ji}/K	α_{ij}	RMSD	A_{ij}	A_{ji}	B_{ij}/K	B_{ji}/K	RMSD
1	2	1.388	-5.294	-611.7	2507	0.3		-1.952	4.169	736.7	-1609	
1	3	-0.939	-0.374	1526	1335	0.2	2.09×10^{-4}	-0.094	0.287	-445.4	-254.9	1.1×10^{-2}
2	3	2.184	1.586	722.6	124.1	0.2		-0.397	-0.472	-358.1	19.14	

Table 3.12. T-dependent binary interaction parameters for the NRTL and UNIQUAC models with root mean square deviations (RMSD) for the *n*-nonane (1) + *o*-xylene (2) + butane-1,4-diol (3) system at (298.2, 313.2 and 333.2) K and 0.1 MPa.

Component		NRTL						UNIQUAC				
i	*j*	a_{ij}	a_{ji}	b_{ij}/K	b_{ji}/K	α_{ij}	RMSD	a_{ij}	a_{ji}	b_{ij}/K	b_{ji}/K	RMSD
1	2	3.830	-9.605	-701.1	3021	0.3		-4.786	3.750	1170	-1026	
1	3	4.378	6.584	139.5	-979.0	0.2	2.68×10^{-3}	-1.372	-0.592	-184.0	147.2	2.82×10^{-3}
2	3	-0.184	-0.348	1167	432.5	0.2		-0.160	0.275	-344.0	-88.73	

Table 3.13. T-dependent binary interaction parameters for the NRTL and UNIQUAC models with root mean square deviations (RMSD) for the *n*-nonane (1) + o-xylene (2) + glycerol (3) system at (298.2, 313.2 and 333.2) K and 0.1 MPa.

Component		NRTL						UNIQUAC					
i	*j*	a_{ij}	a_{ji}	b_{ij}/K	b_{ji}/K	α_{ij}	RMSD	a_{ij}	a_{ji}	b_{ij}/K	b_{ji}/K	RMSD
1	2	5.926	-9.079	-1054	3021	0.3		-4.163	2.883	872.7	-761.7	
1	3	6.281	5.484	-592.4	-263.1	0.2	8.16×10^{-4}	-2.326	-0.443	135.0	23.67	8.84×10^{-4}
2	3	1.710	0.144	445.4	888.3	0.2		-0.716	0.212	-110.1	-251.1	

Table 3.14. NRTL and UNIQUAC T-dependent interaction parameters and root mean square deviations (RMSD) for the *n*-heptane (1) + toluene (2) + 1,4-butanediol (3) + 2-methyl-2,4-pentanediol (4) system at (298.2 and 313.2) K and 0.1 MPa.

		NRTL				UNIQUAC		
i	*j*	a_{ij}	a_{ji}	α_{ij}	RMSD	a_{ij}	a_{ji}	RMSD
				T = 298.2 K				
1	2	-2.346	4.237	0.20		-0.050	-0.395	
1	3	-10.95	-2.570	0.28		-0.147	-1.082	
1	4	109.8	3.146	0.34	0.0091	-1.107	-0.573	0.029
2	3	-9.902	2.188	0.38		-0.092	-0.791	
2	4	5.353	0.498	0.35		0.546	-2.411	
3	4	2.620	16.90	0.20		1.126	-18.51	
				T = 313.2 K				
1	2	-2.454	3.775	0.20		-2.336	1.084	
1	3	-12.48	-11.07	0.42		-0.253	-0.736	
1	4	2.958	2.995	0.45	0.01	-0.812	-0.601	0.025
2	3	-9.305	2.256	0.40		-0.410	-0.534	
2	4	4.743	0.893	0.43		0.222	-0.488	
3	4	1.376	18.54	0.20		1.443	-17.48	

Table 3.15. NRTL and UNIQUAC model T-dependent interaction parameters together with root mean square deviations (RMSD) for the system *n*-heptane (1) + toluene (2) + glycerol (3) + 2-methyl-2,4-pentanediol (4) at (298.2 and 313.2) K and 0.1 MPa.

		NRTL						UNIQUAC					
i	*j*	a_{ij}	a_{ji}	α_{ij}	RMSD	AAD	% AARD	a_{ij}	a_{ji}	RMSD	AAD	% AARD
							T = 298.2 K						
1	2	-1.025	2.427	0.20				1.440	-2.464				
1	3	3.768	3.563	0.47				-1.006	-0.707				
1	4	3.384	3.104	0.43	0.012	0.009	16.0	-1.205	0.365	0.013	0.008	23.4	
2	3	3.378	9.404	0.33				-0.926	-0.97				
2	4	2.123	0.802	0.20				-0.682	0.334				
3	4	2.960	3.309	0.41				-0.716	0.096				
							T = 313.2 K						
1	2	-0.139	3.687	0.33				0.885	-1.390				
1	3	4.715	4.872	0.43				-1.383	-0.322				
1	4	3.074	2.626	0.43	0.009	0.007	11.6	-0.156	-0.546	0.011	0.007	13.2	
2	3	3.271	7.533	0.34				-0.532	-1.152				
2	4	1.800	1.161	0.20				0.681	-1.173				
3	4	2.398	2.433	0.41				-0.632	0.038				

Table 3.16. Structural parameters for the UNIQUAC model: r (relative molecular volume) together with q (relative molecular surface area) (Aspen Plus, 2004)

I	r_i	q_i
n-Heptane	5.174	4.396
n-Nonane	6.523	5.476
Toluene	3.923	2.968
o-Xylene	4.658	3.536
1,4-Butanediol	3.757	3.328
Glycerol	3.386	3.060
2-Methyl-2,4-Pentanediol	4.574	3.896

Table 3.17. Comparison of binary interaction parameters from binary, ternary, and quaternary data for the NRTL and UNIQUAC models for at 298.2 K for the system *n*-heptane (1) + toluene (2) + glycerol (3)

		Binary				Ternary				Quaternary			
		NRTL		UNIQUAC		NRTL		UNIQUAC		NRTL		UNIQUAC	
i	*j*	τ_{ij}	τ_{ji}	τ_{ij}	τ_{ji}	τ_{ij}	τ_{ji}	τ_{ij}	τ_{ji}	τ_{ij}	τ_{ji}	τ_{ij}	τ_{ji}
1	2	-0.428	1.132	0.134	-0.260	-0.664	3.115	-0.099	0.035	-1.025	2.427	1.440	-2.464
1	3	5.721	5.071	-1.996	-0.729	4.179	4.104	-1.489	-0.292	3.768	3.563	-1.006	-0.707
2	3	4.077	3.295	-3.517	-0.484	4.608	2.002	-1.709	0.013	3.378	9.404	-0.926	-0.970

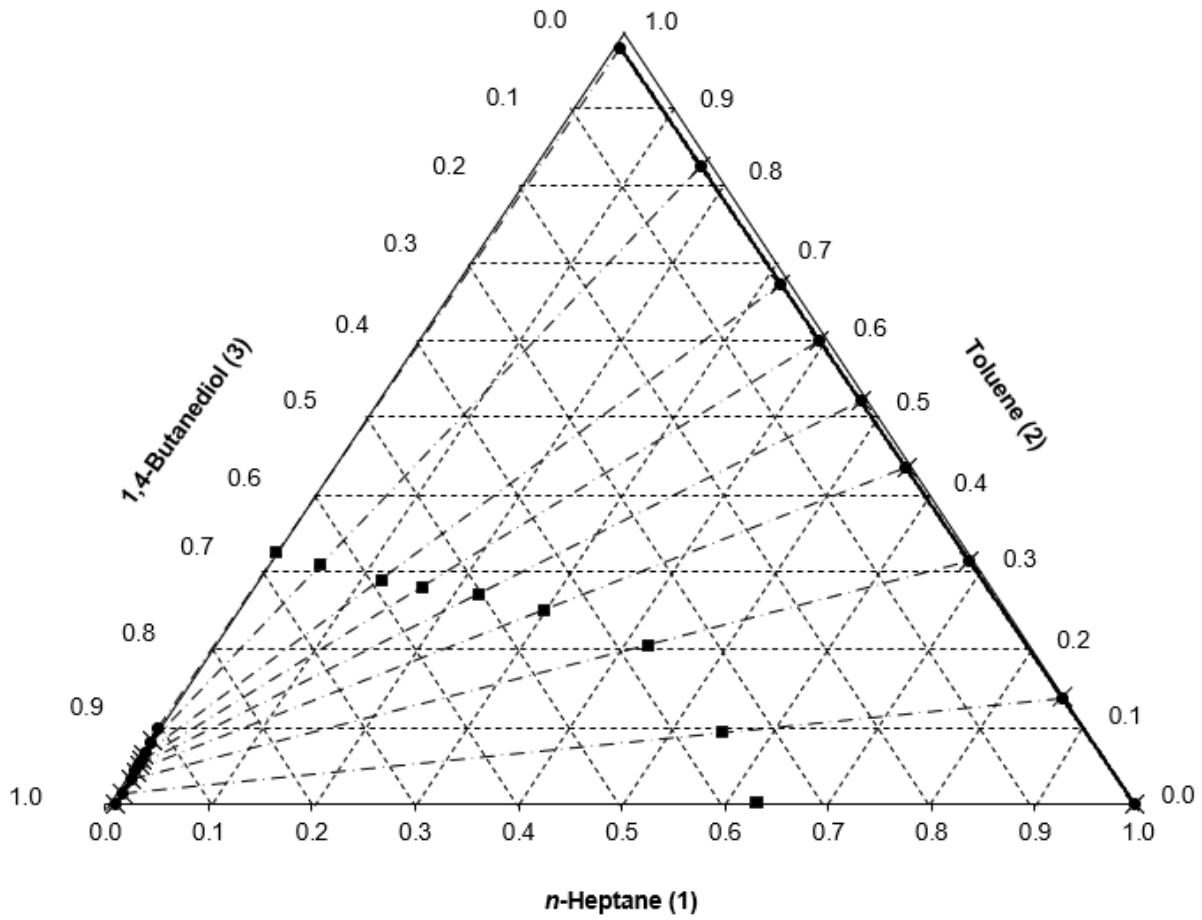

Figure 3.3. Liquid-liquid equilibrium mole composition data for the *n*-heptane (1) + toluene (2) + 1,4-butanediol (3) system at 298.2 K and 0.1 MPa. × – experimental (this study); -●- – NRTL model; ■ – tie -line feed composition

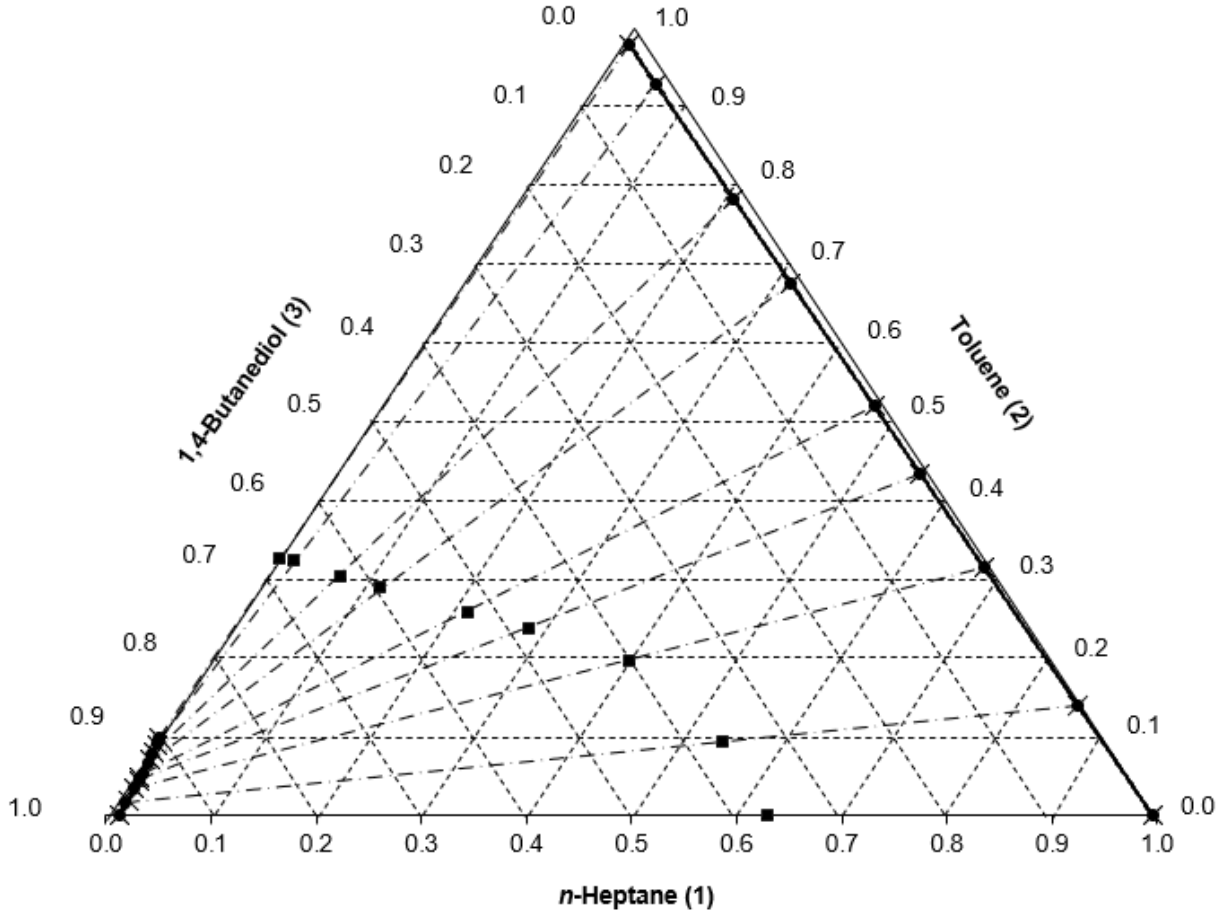

Figure 3.4. Liquid-liquid equilibrium mole composition data for the *n*-heptane (1) + toluene (2) + 1,4-butanediol (3) system at 313.2 K and 0.1 MPa. × – experimental (this study); -●- – NRTL model; ■ – tie -line feed composition

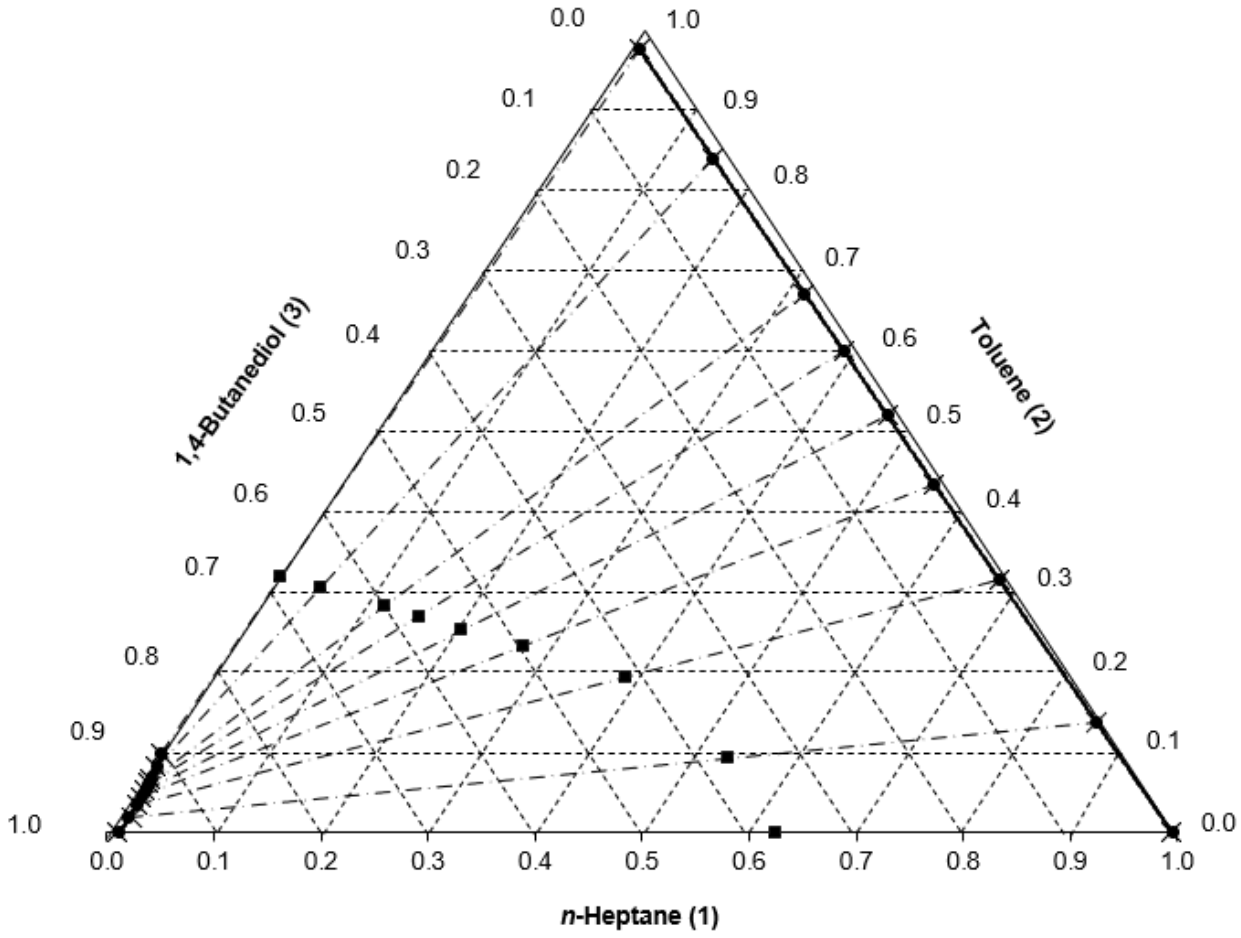

Figure 3.5. Liquid-liquid equilibrium mole composition data for the *n*-heptane (1) + toluene (2) + 1,4-butanediol (3) system at 333.2 K and 0.1 MPa. × – experimental (this study); -●- – NRTL model; ■ – tie -line feed composition

.

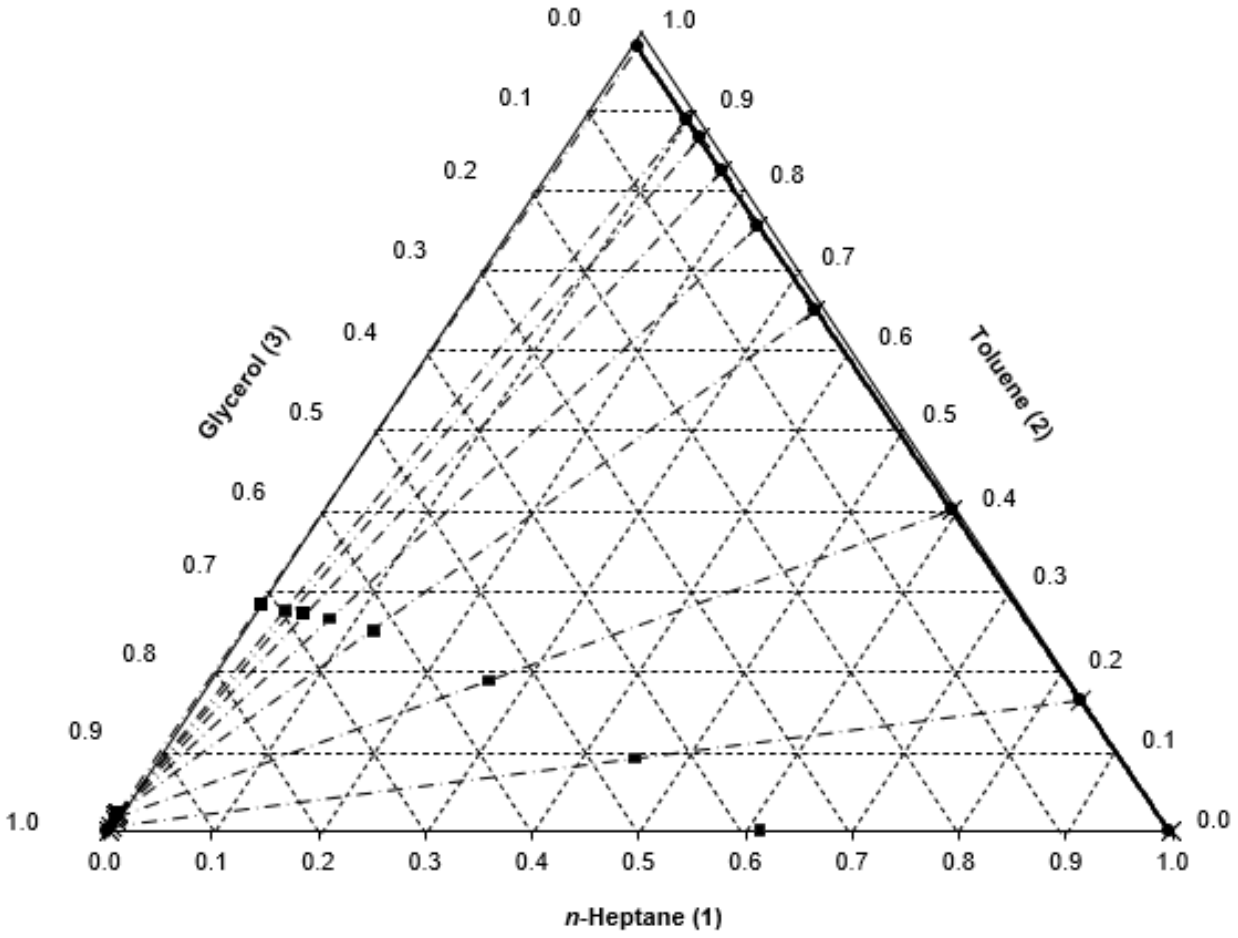

Figure 3.6. Liquid-liquid equilibrium mole composition data for the *n*-heptane (1) + toluene (2) + glycerol (3) system at 298.2 K and 0.1 MPa. × – experimental (this study); -●- – NRTL model; ■ – tie-line feed composition

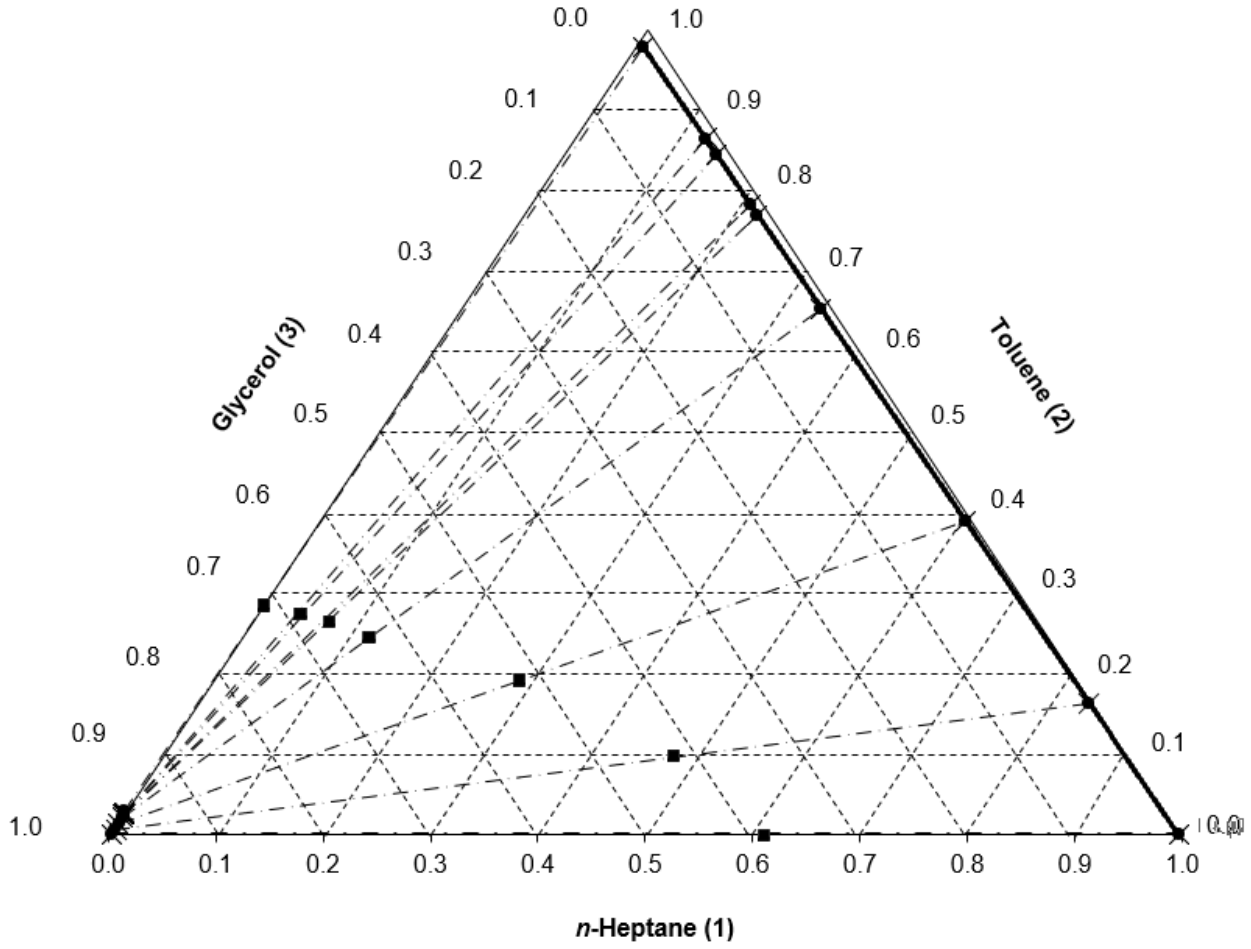

Figure 3.7. Liquid-liquid equilibrium mole composition data for the *n*-heptane (1) + toluene (2) + glycerol (3) system at 313.2 K and 0.1 MPa. × – experimental (this study); -●- – NRTL model; ■ – tie-line feed composition

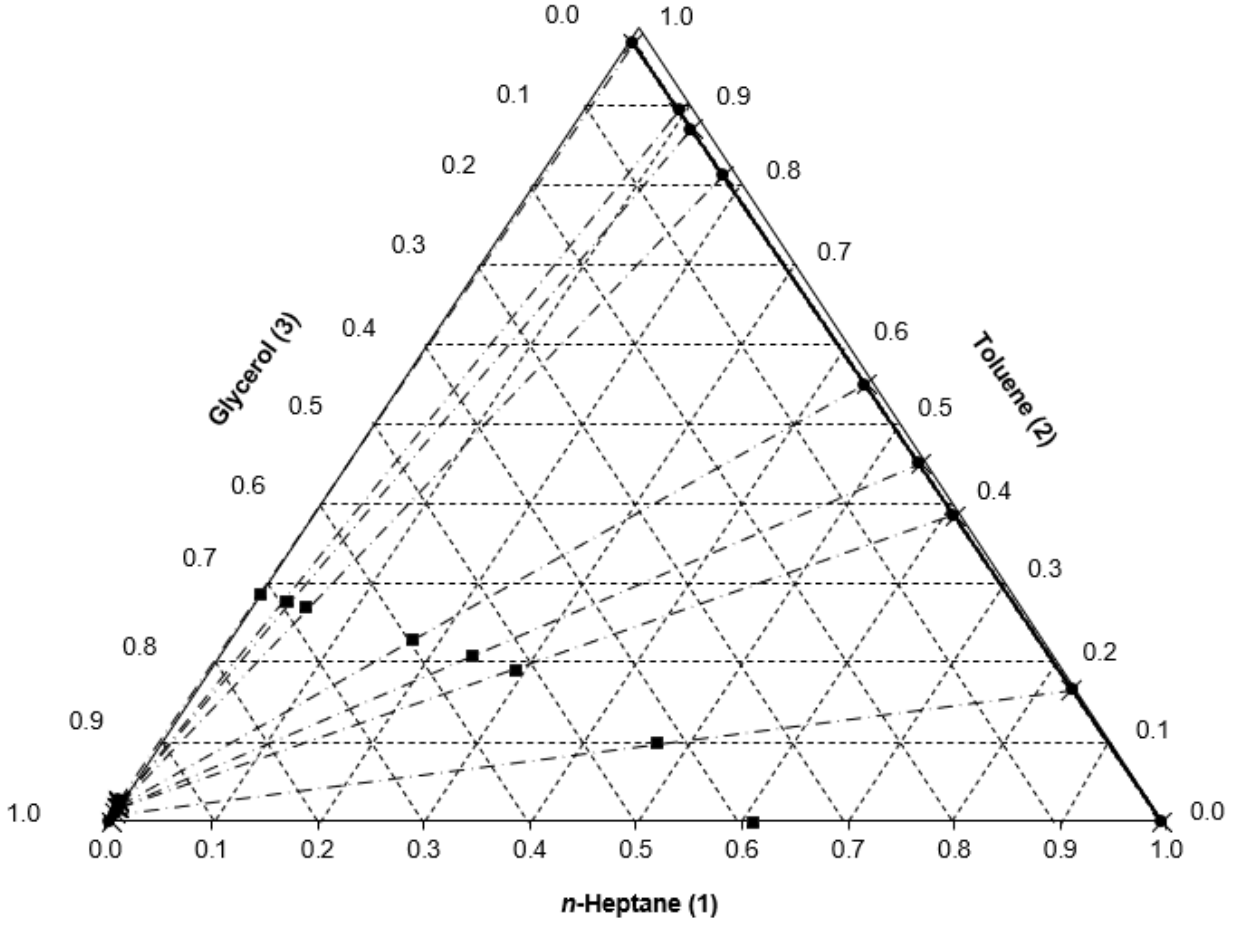

Figure 3.8. Liquid-liquid equilibrium mole composition data for the *n*-heptane (1) + toluene (2) + glycerol (3) system at 333.2 K and 0.1 MPa. × – experimental (this study); -●- – NRTL model; ■ – tie-line feed composition

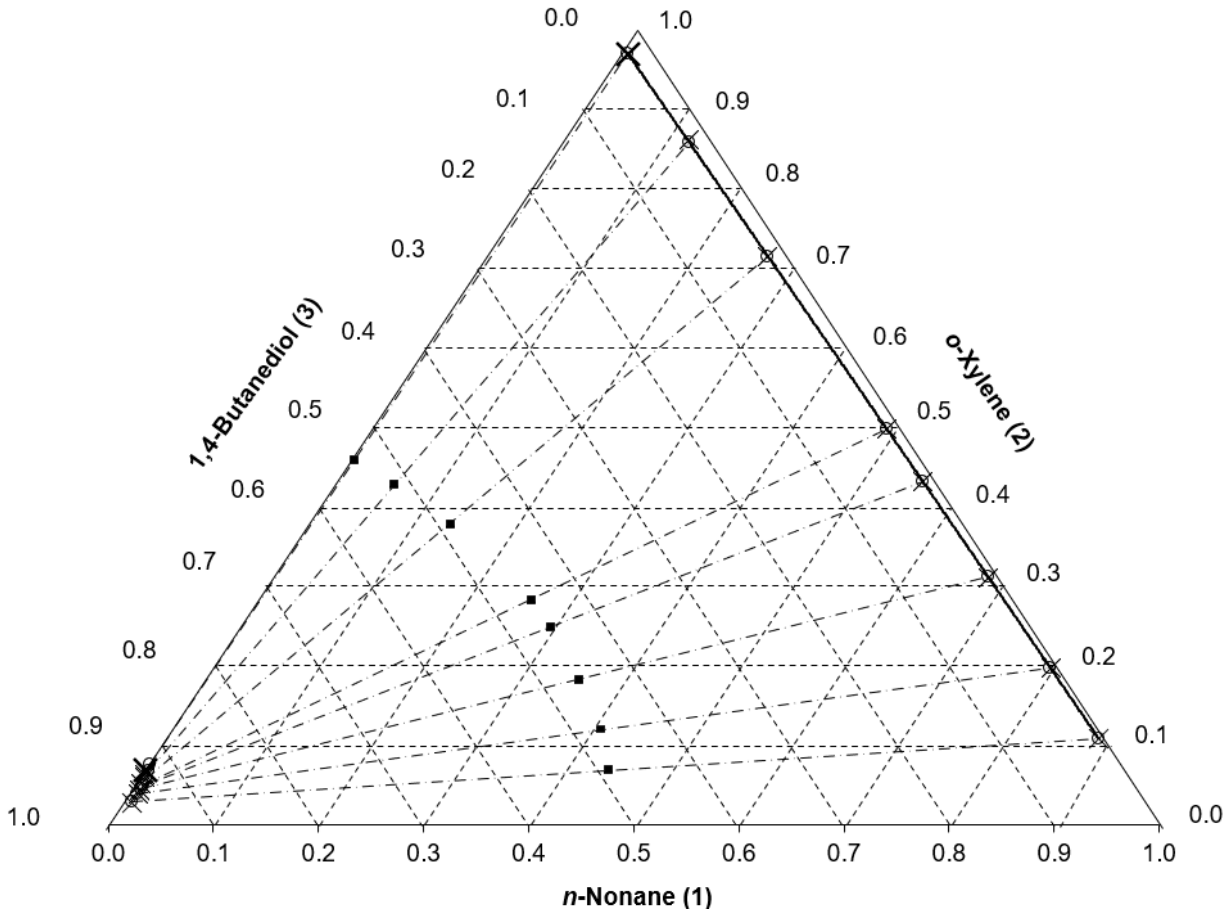

Figure 3.9. Ternary liquid-liquid equilibrium data (mole basis) for the *n*-nonane (1) + *o*-xylene (2) + butane-1,4-diol (3) system at 298.2 K and 0.1 MPa. × – experimental (this study); -○- – NRTL model; ■ – tie -line feed composition

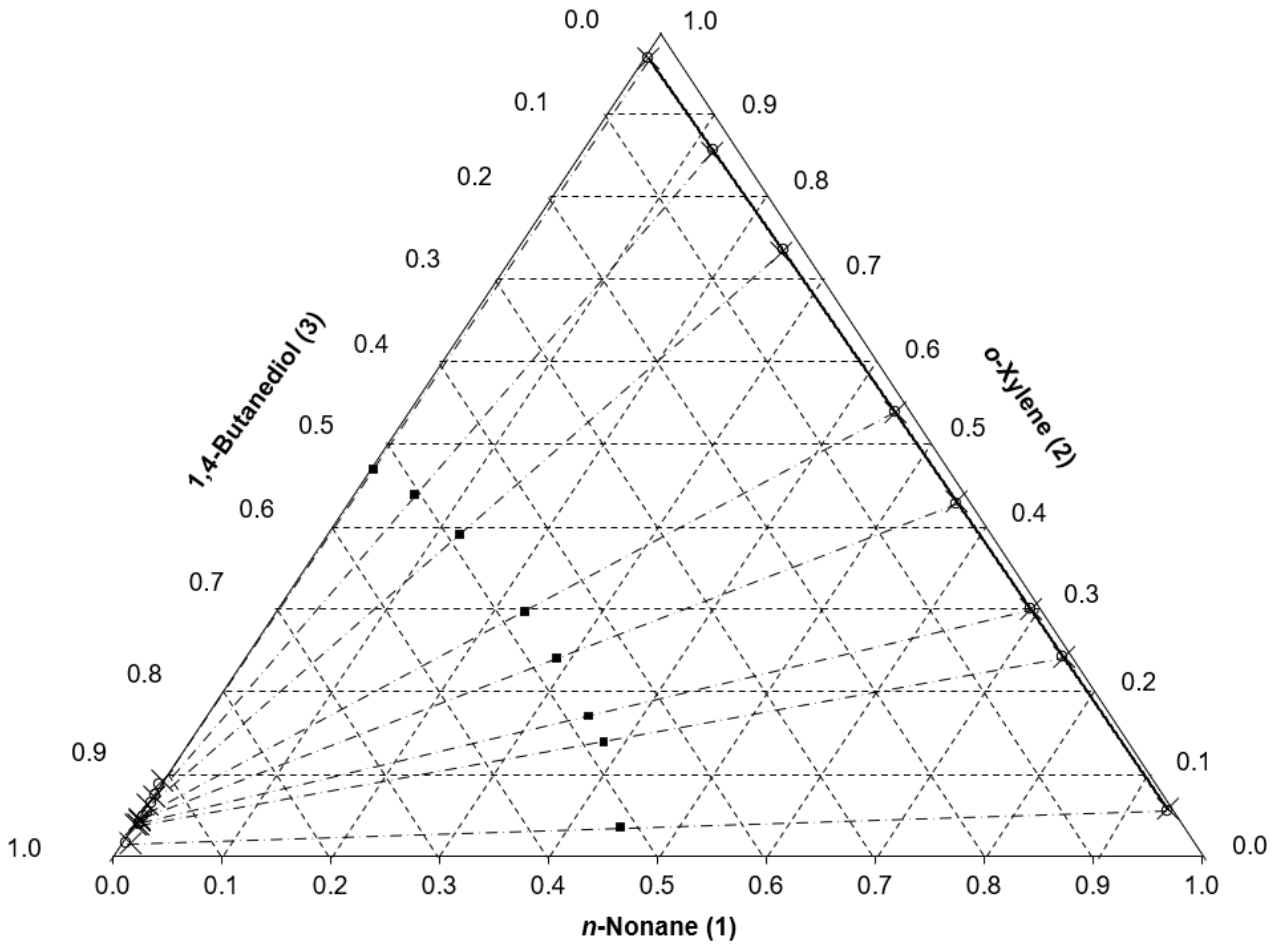

Figure 3.10. Ternary liquid-liquid equilibrium data (mole basis) for the *n*-nonane (1) + *o*-xylene (2) + butane-1,4-diol (3) system at 313.2 K and 0.1 MPa. × – experimental (this study); -○- – NRTL model; ■ – tie -line feed composition

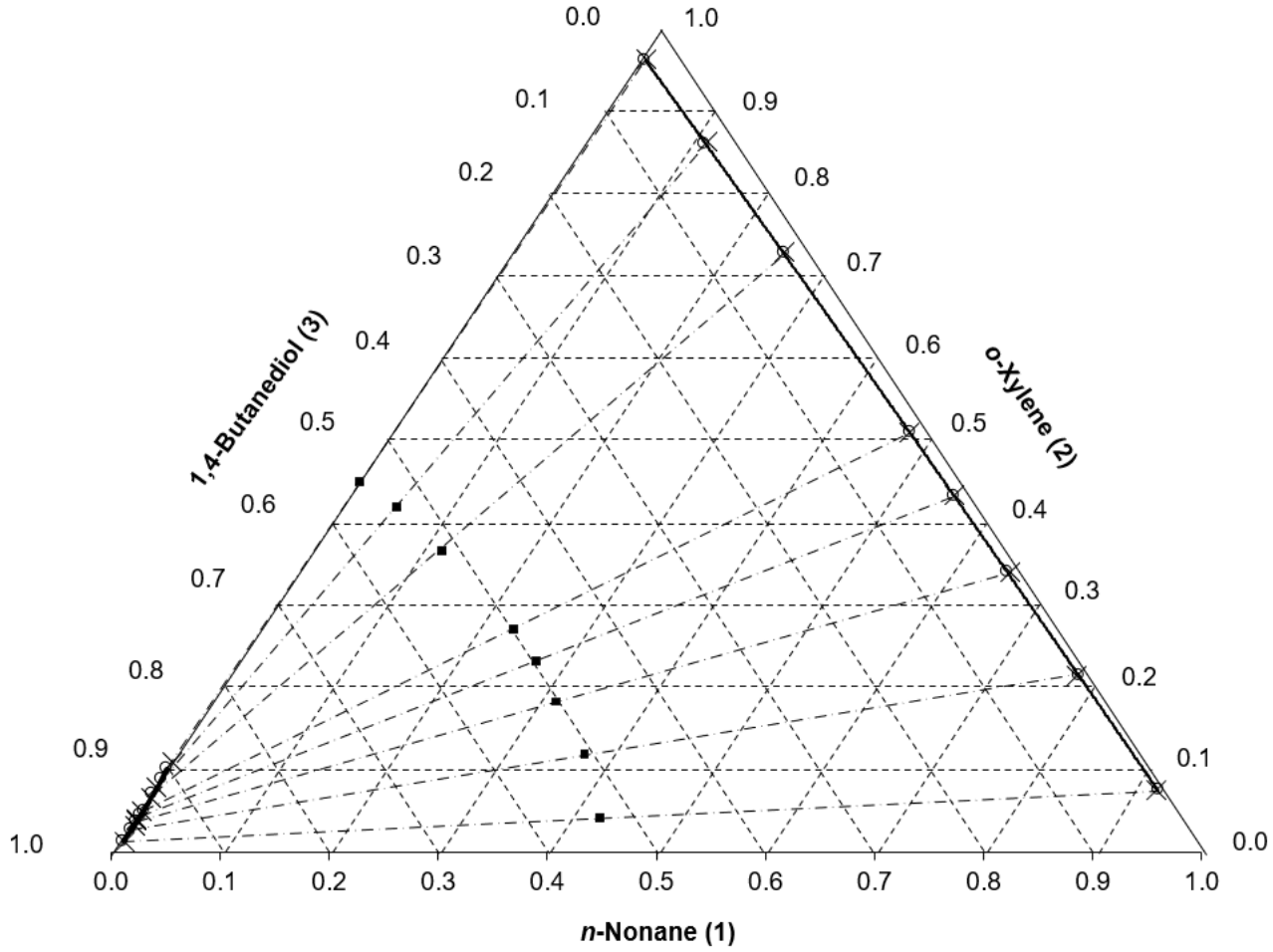

Figure 3.11. Ternary liquid-liquid equilibrium data (mole basis) for the *n*-nonane (1) + *o*-xylene (2) + butane-1,4-diol (3) system at 333.2 K and 0.1 MPa. × – experimental (this study); -○- – NRTL model; ■ – tie -line feed composition

.

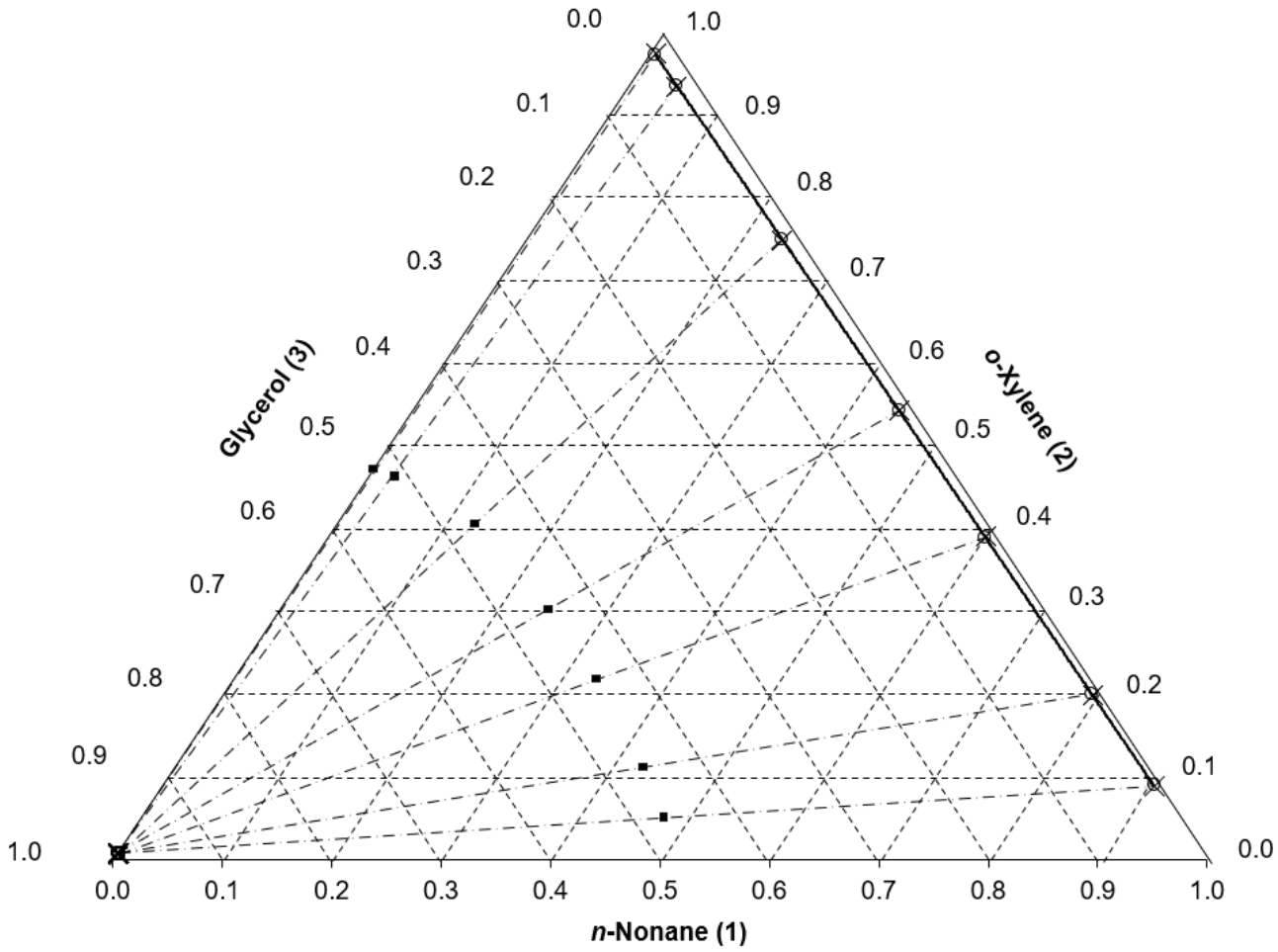

Figure 3.12. Ternary liquid-liquid equilibrium data (mole basis) for the *n*-nonane (1) + *o*-xylene (2) + glycerol (3) system at 298.2 K and 0.1 MPa. × – experimental (this study); -○- – NRTL model; ■ – tie-line feed composition

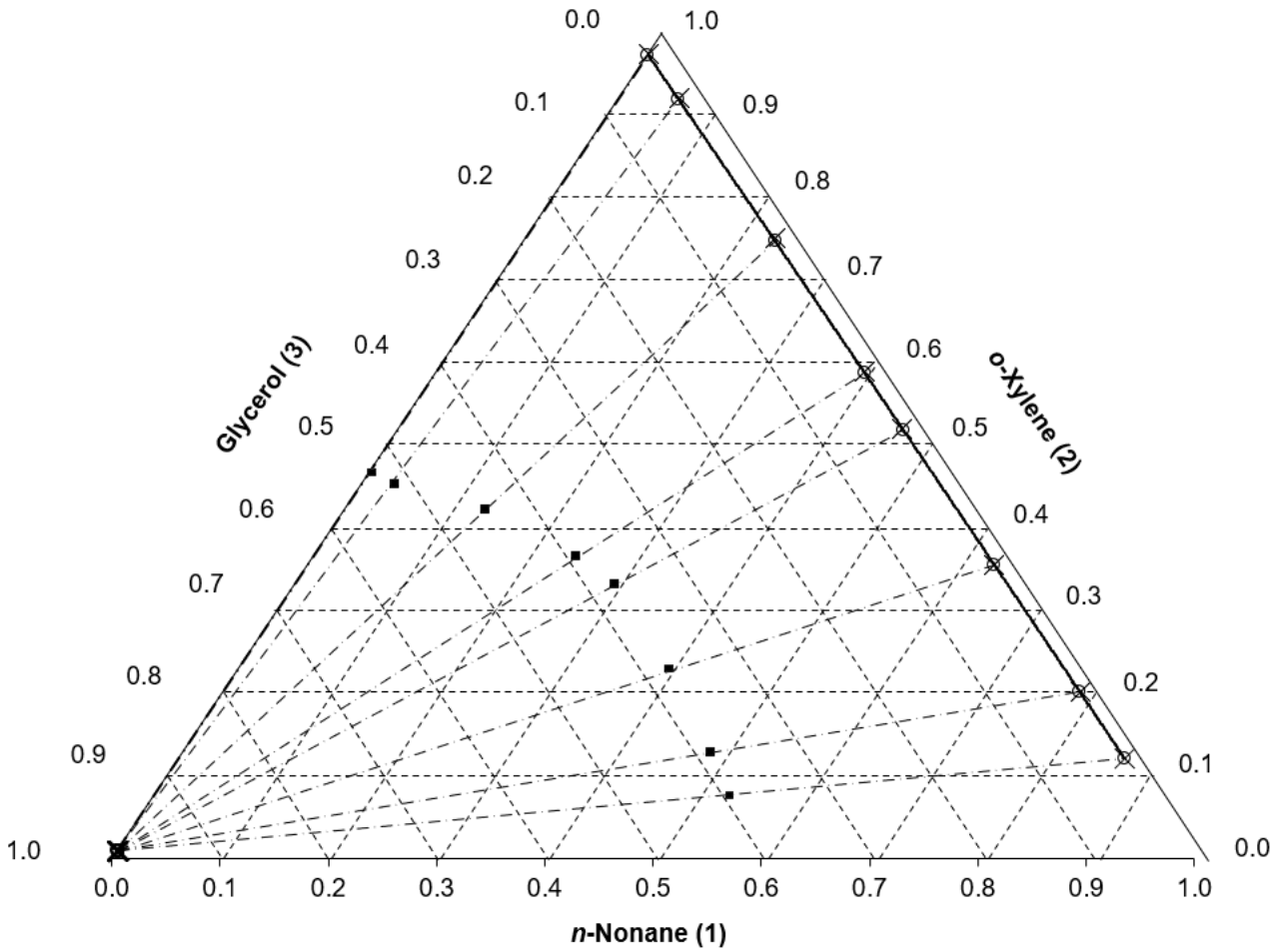

Figure 3.13. Ternary liquid-liquid equilibrium data (mole basis) for the *n*-nonane (1) + *o*-xylene (2) + glycerol (3) system at 313.2 K and 0.1 MPa. × – experimental (this study); -○- – NRTL model; ■ – tie-line feed composition

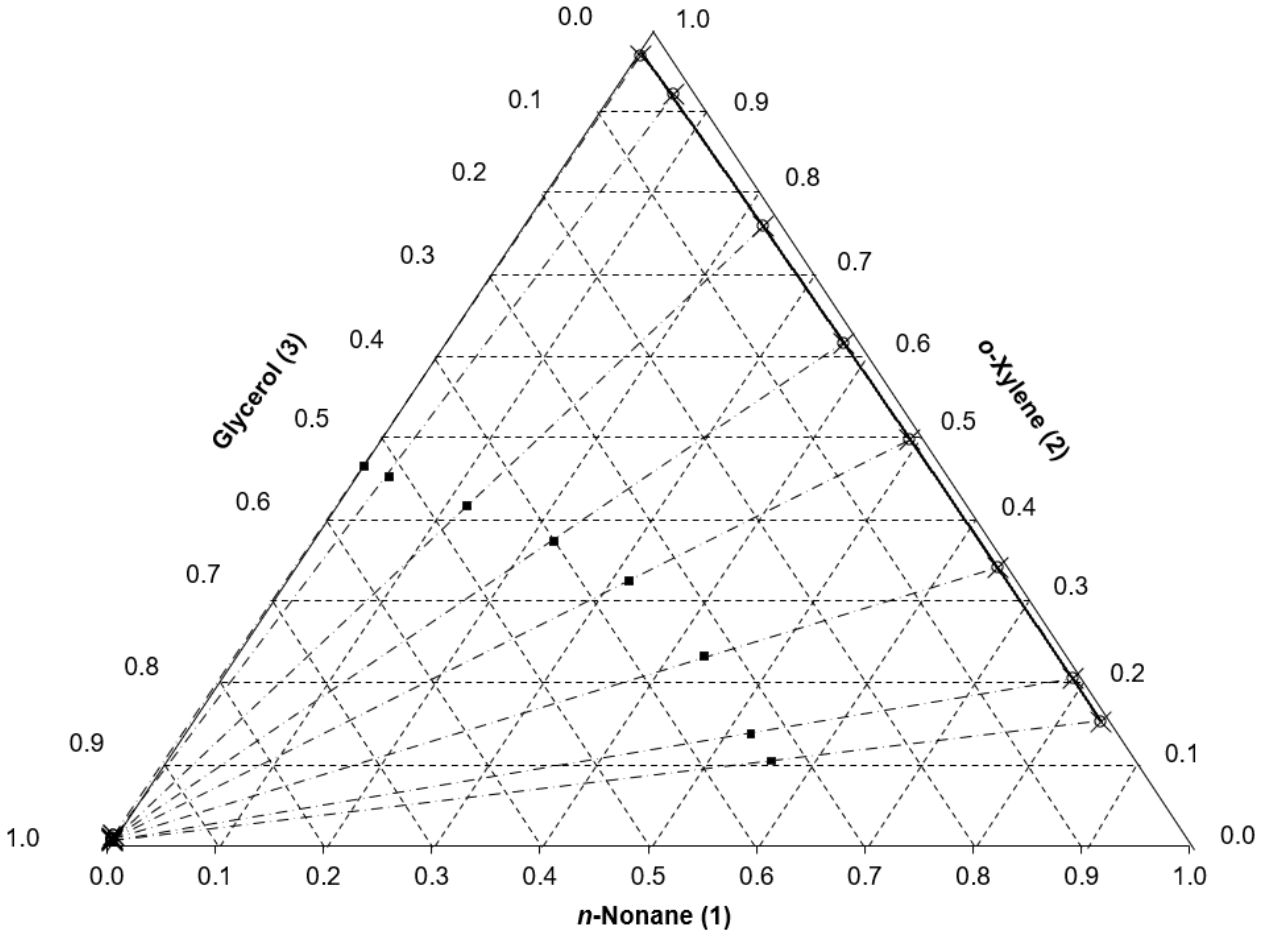

Figure 3.14. Ternary liquid-liquid equilibrium data (mole basis) for the *n*-nonane (1) + *o*-xylene (2) + glycerol (3) system at 333.2 K and 0.1 MPa. × – experimental (this study); -○- – NRTL model; ■ – tie-line feed composition

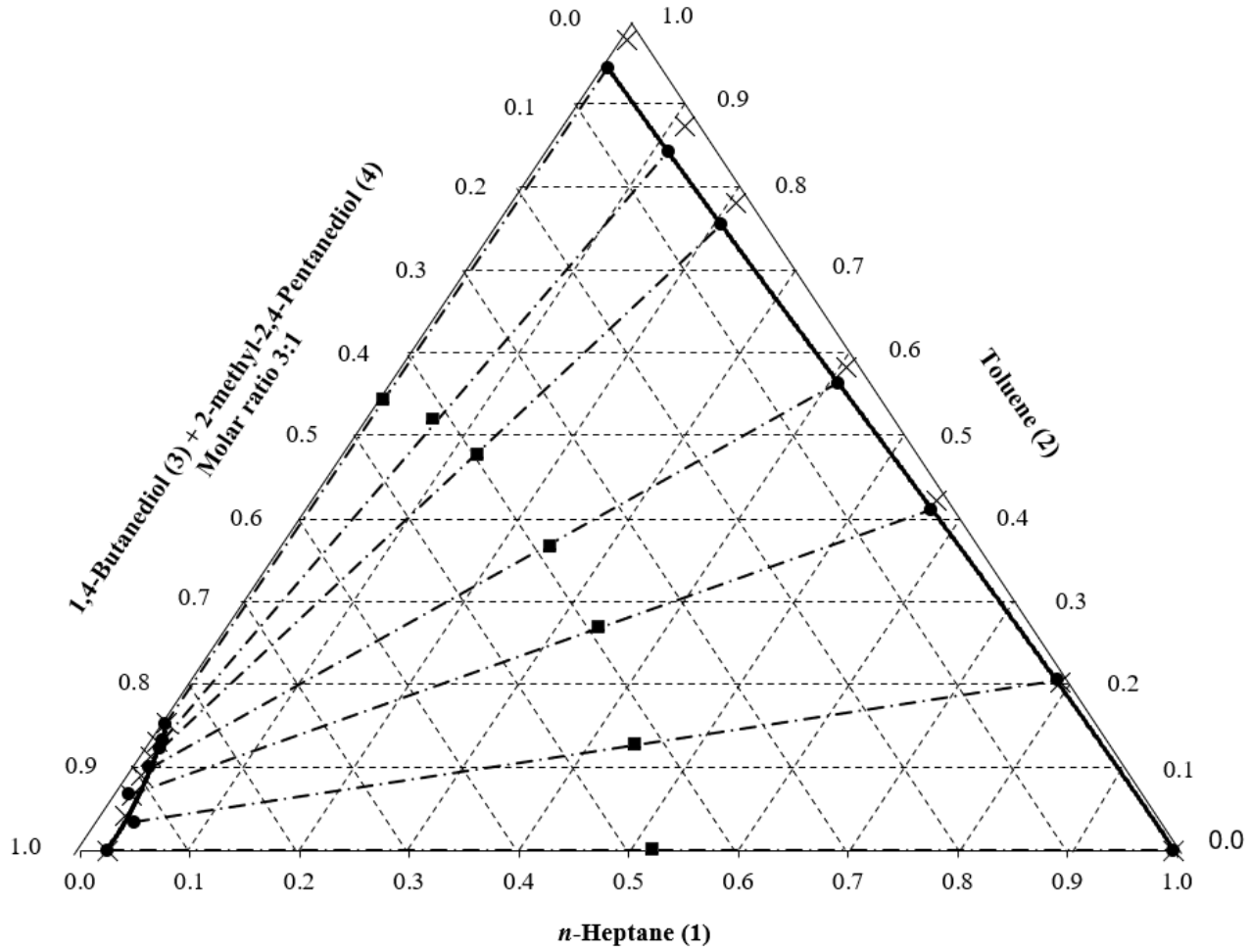

Figure 3.15. Pseudo ternary liquid -liquid equilibrium mole composition data for the *n*-heptane (1) + toluene (2) + 1,4-butanediol (3) + 2-methyl-2,4-pentanediol (4) system at 298.2 K and 0.1 MPa for 3:1 solvent: co-solvent ratio. × – experimental (this study); -●- – NRTL model; ■ – tie -line feed composition

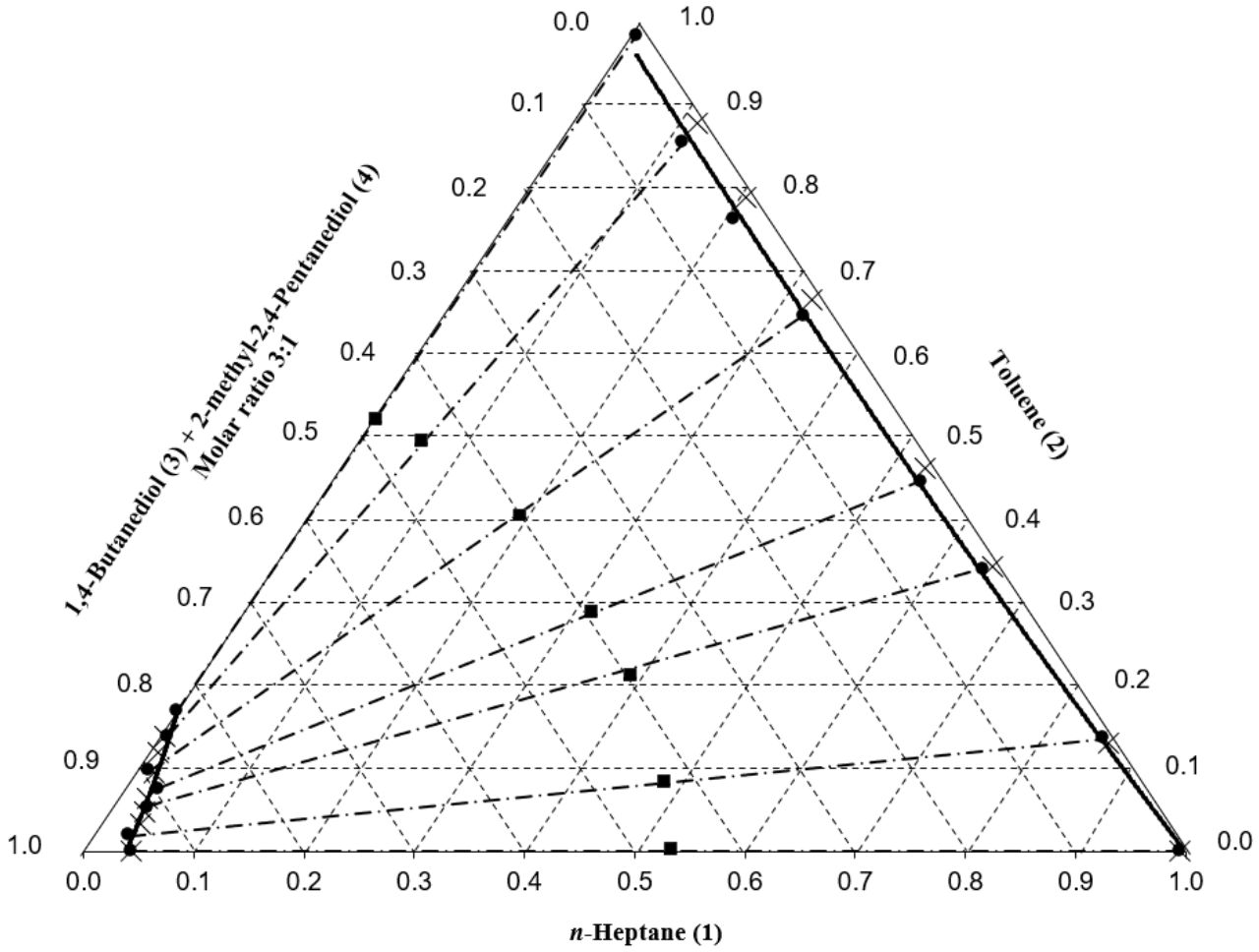

Figure 3.16. Pseudo ternary liquid -liquid equilibrium mole composition data for the *n*-heptane (1) + toluene (2) + 1,4-butanediol (3) + 2-methyl-2,4-pentanediol (4) system at 313.2 K and 0.1 MPa for 3:1 solvent: co-solvent ratio. × – experimental (this study); -●- – NRTL model; ■ – tie -line feed composition

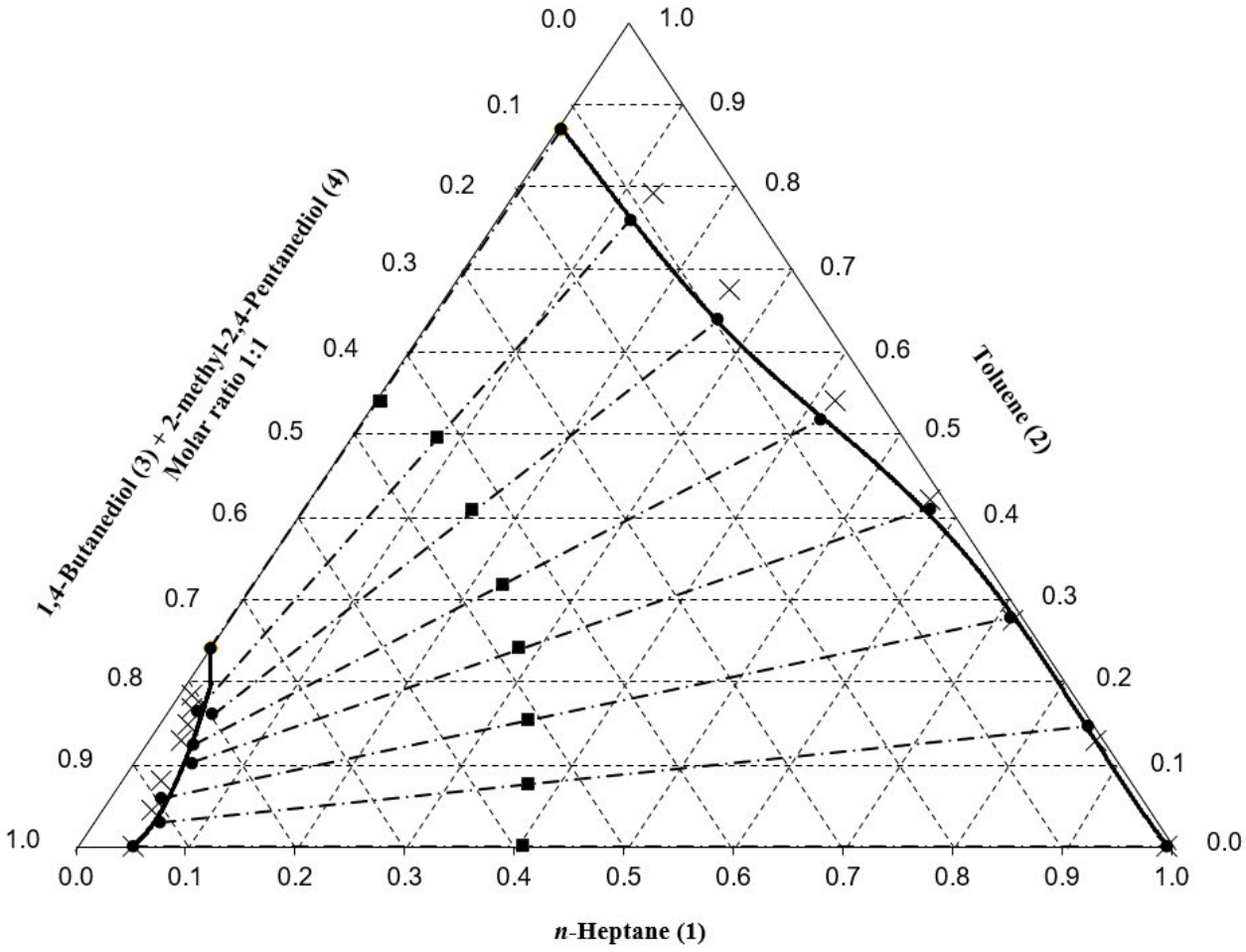

Figure 3.17. Pseudo ternary liquid -liquid equilibrium mole composition data for the *n*-heptane (1) + toluene (2) + 1,4-butanediol (3) + 2-methyl-2,4-pentanediol (4) system at 298.2 K and 0.1 MPa for 1:1 solvent: co-solvent ratio. × – experimental (this study); -●- – NRTL model; ■ – tie -line feed composition

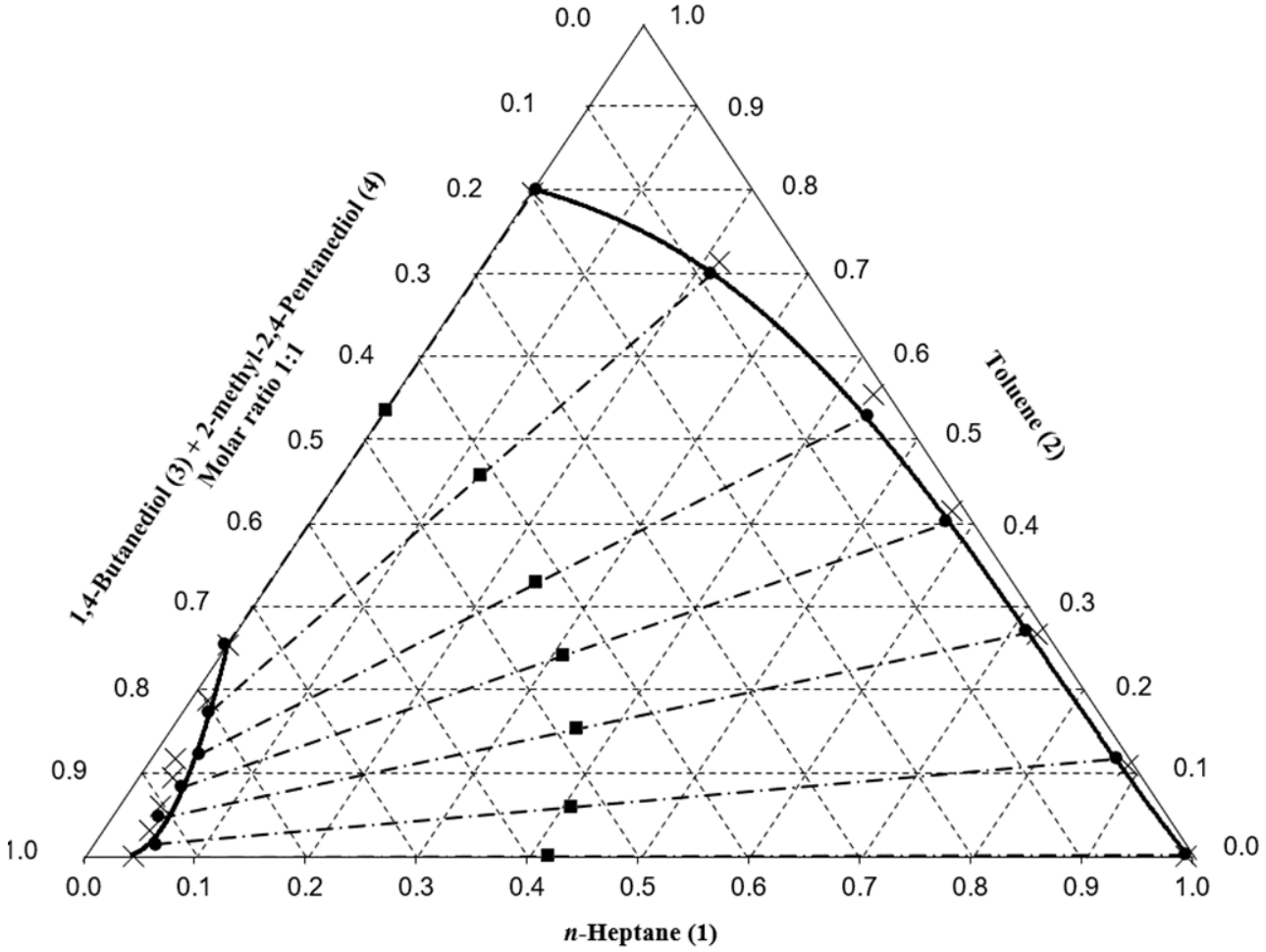

Figure 3.18. Pseudo ternary liquid -liquid equilibrium mole composition data for the *n*-heptane (1) + toluene (2) + 1,4-butanediol (3) + 2-methyl-2,4-pentanediol (4) system at 313.2 K and 0.1 MPa for 1:1 solvent: co-solvent ratio. × – experimental (this study); -●- – NRTL model; ■ – tie -line feed composition

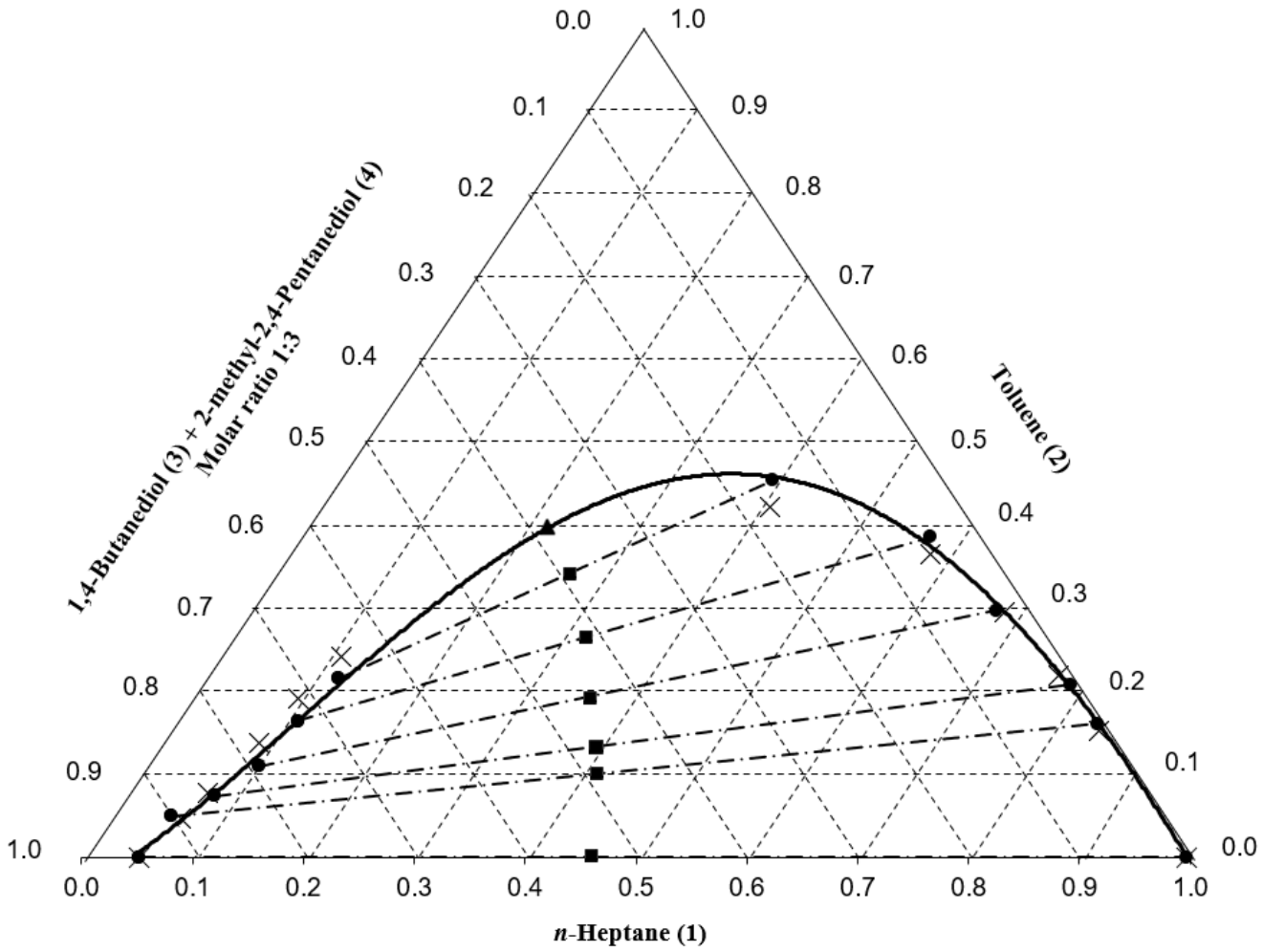

Figure 3.19. Pseudo ternary liquid -liquid equilibrium mole composition data for the *n*-heptane (1) + toluene (2) + 1,4-butanediol (3) + 2-methyl-2,4-pentanediol (4) system at 298.2 K and 0.1 MPa for 1:3 solvent: co-solvent ratio. × – experimental (this study); -●- – NRTL model; ■ – tie-line feed composition; ▲- plait point

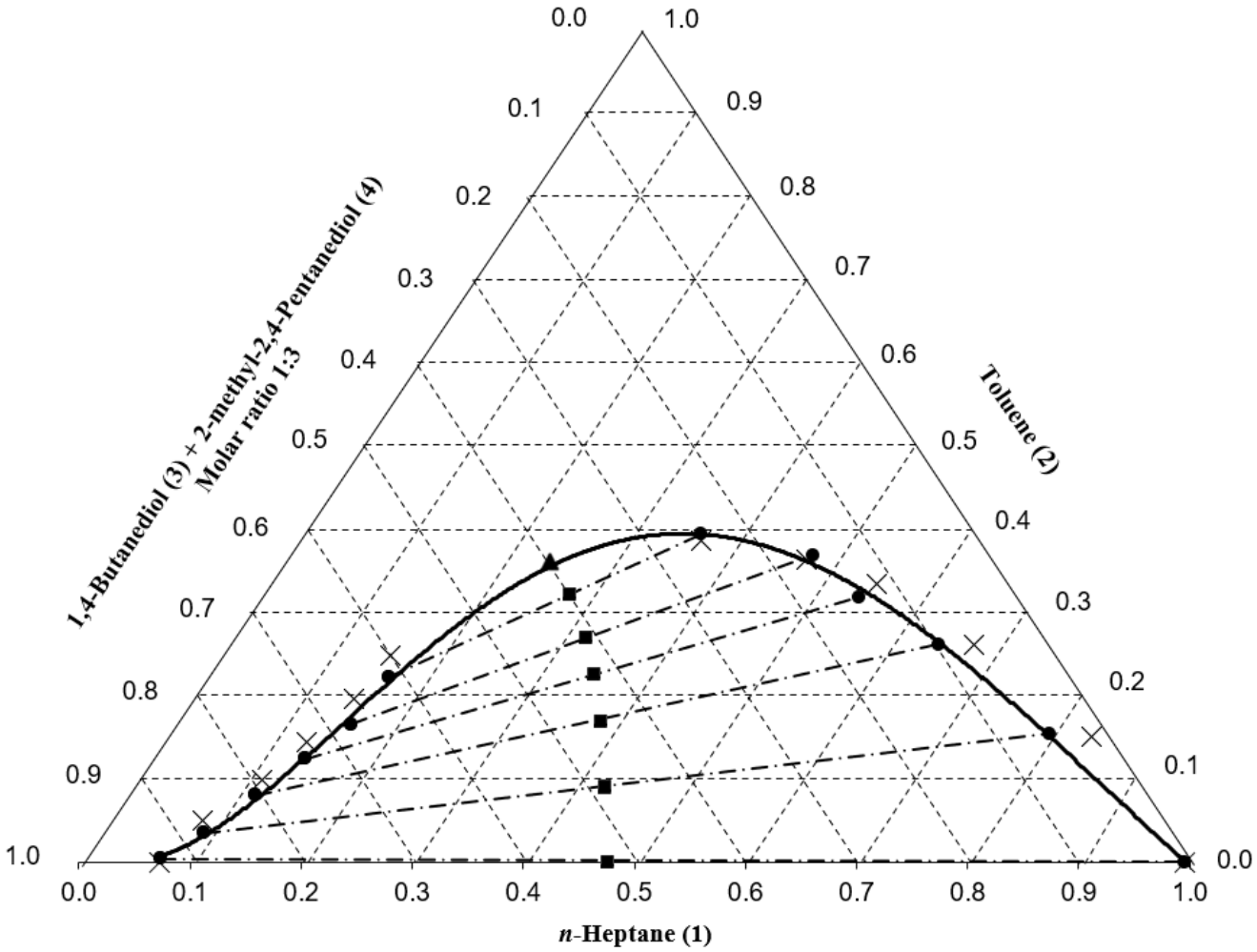

Figure 3.20. Pseudo ternary liquid-liquid equilibrium mole composition data for the *n*-heptane (1) + toluene (2) + 1,4-butanediol (3) + 2-methyl-2,4-pentanediol (4) system at 313.2 K and 0.1 MPa for 1:3 solvent: co-solvent ratio. × – experimental (this study); -●- – NRTL model; ■ – tie-line feed composition; ▲ - plait point

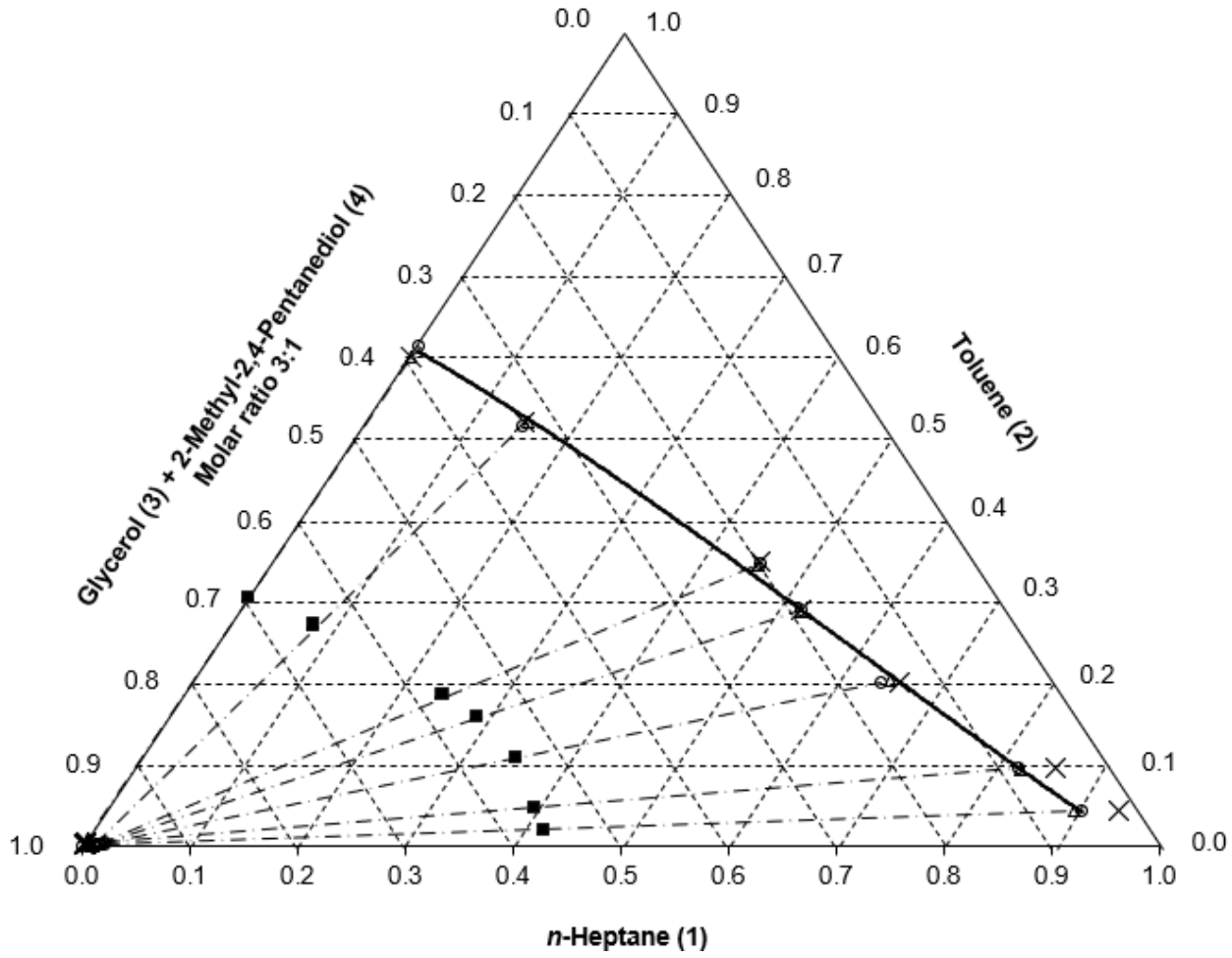

Figure 3.21. Liquid-liquid equilibrium (pseudo ternary) mole composition data for the system *n*-heptane (1) + toluene (2) + glycerol (3) + 2-methyl-2,4-pentanediol (4) at 298.2 K and 0.1 MPa for 3:1 solvent: co-solvent ratio. × – experimental (this study); -○- – NRTL model; △ - UNIQUAC model; ■ – tie -line feed composition

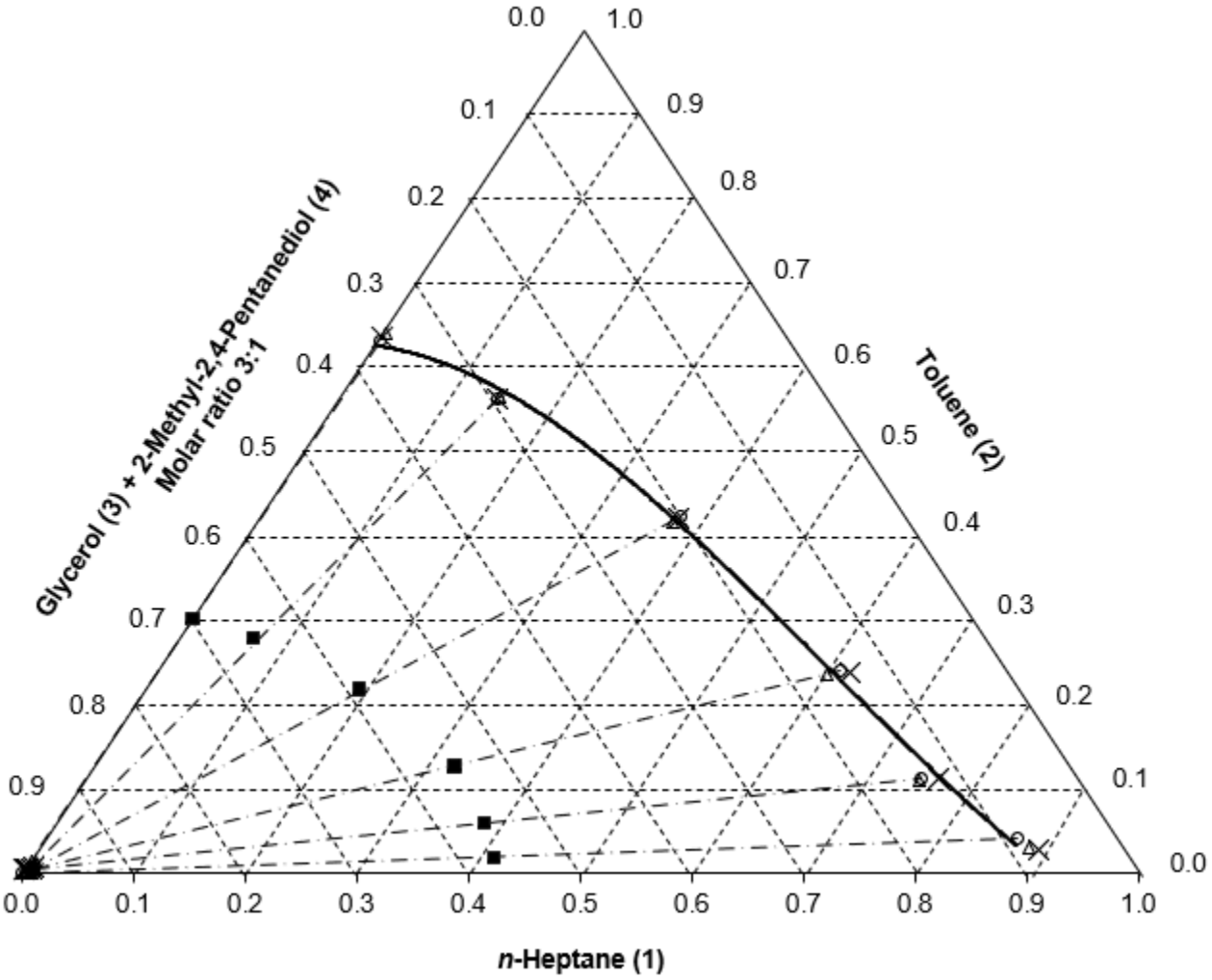

Figure 3.22. Liquid-liquid equilibrium (pseudo ternary) mole composition data for the system *n*-heptane (1) + toluene (2) + glycerol (3) + 2-methyl-2,4-pentanediol (4) at 313.2 K and 0.1 MPa for 3:1 solvent: co-solvent ratio. × – experimental (this study); -○- – NRTL model; △ - UNIQUAC model; ■ – tie -line feed composition

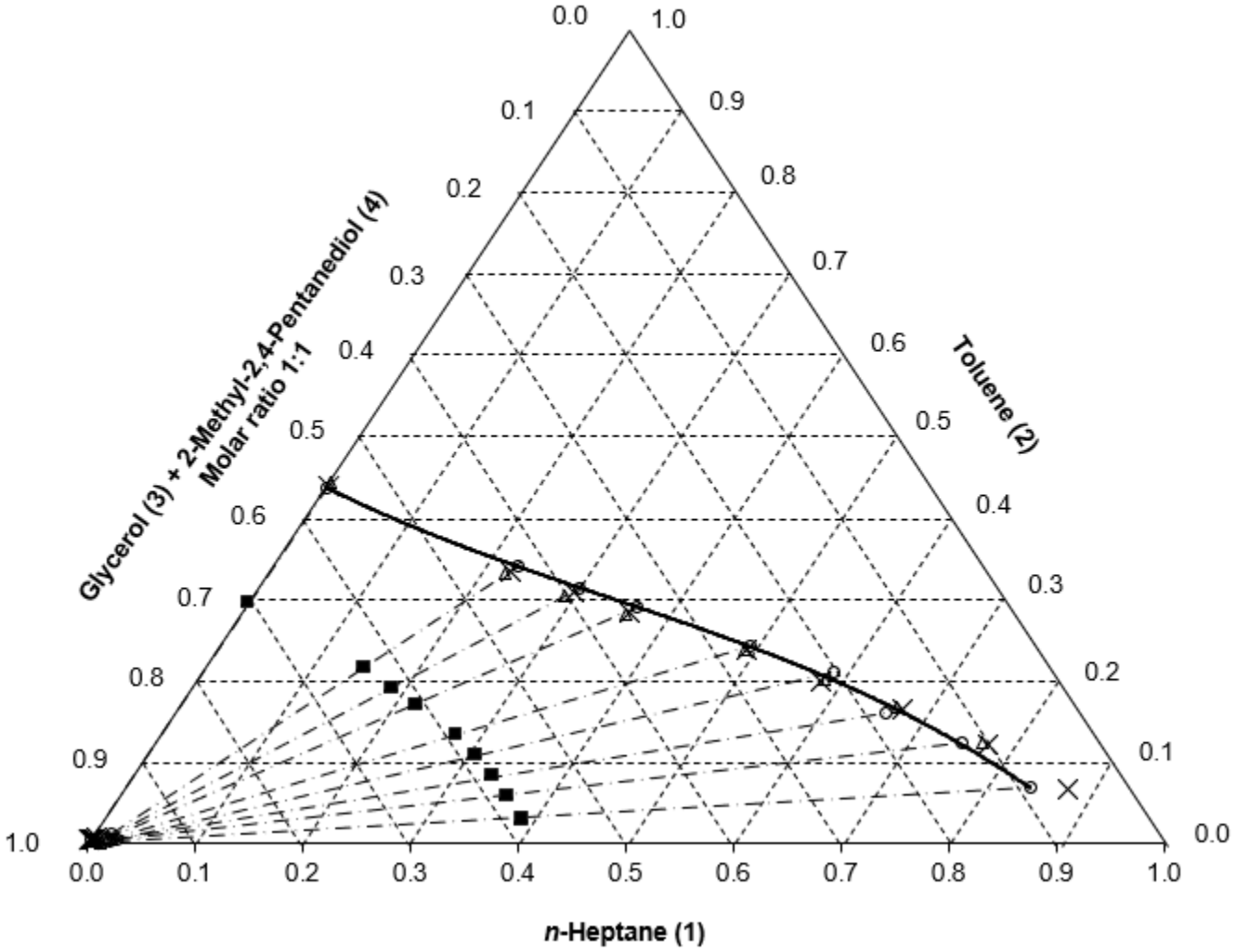

Figure 3.23. Liquid-liquid equilibrium (pseudo ternary) mole composition data for the system *n*-heptane (1) + toluene (2) + glycerol (3) + 2-methyl-2,4-pentanediol (4) at 298.2 K and 0.1 MPa for 1:1 solvent: co-solvent ratio. × – experimental (this study); -○- – NRTL model; △ - UNIQUAC model; ■ – tie -line feed composition

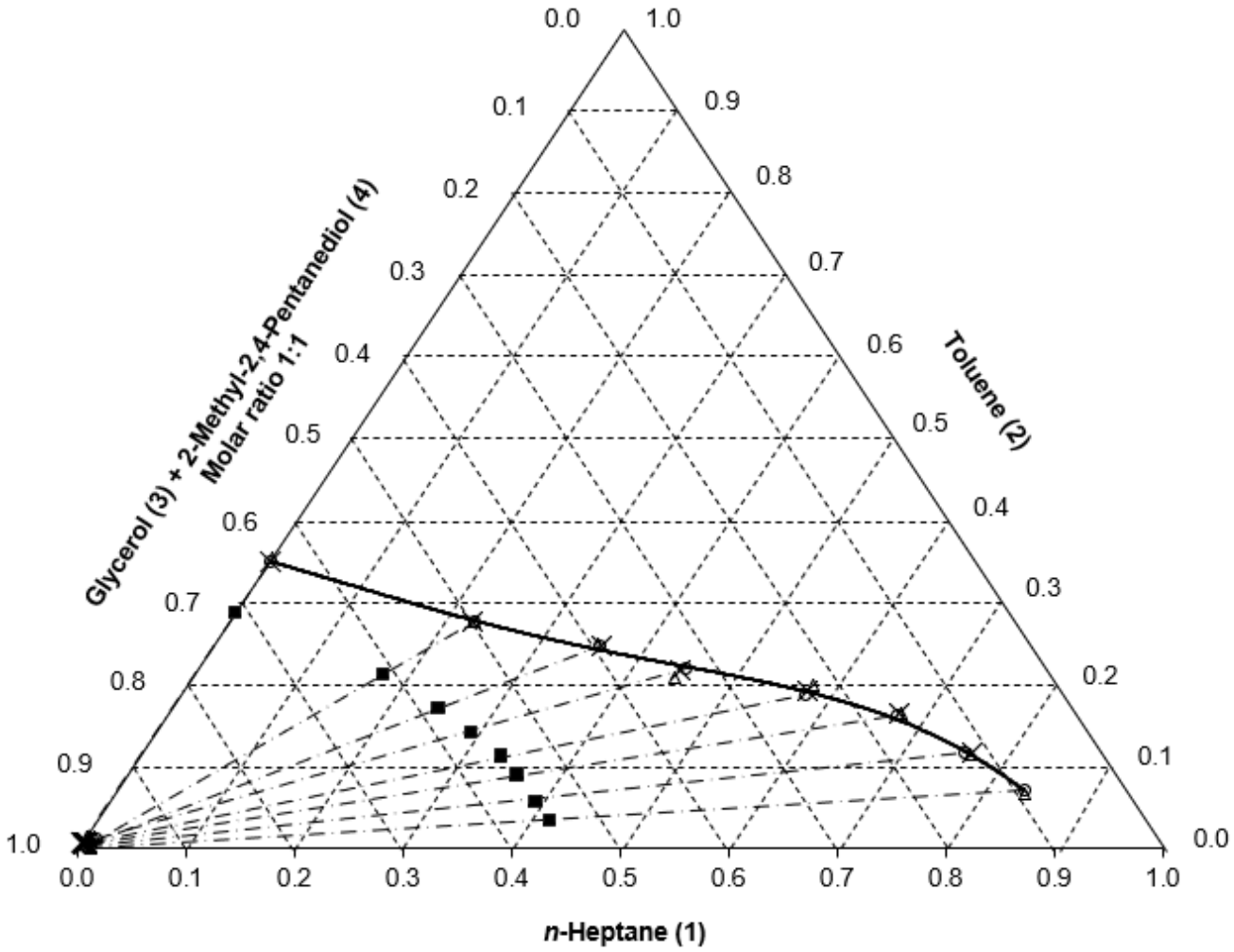

Figure 3.24. Liquid-liquid equilibrium (pseudo ternary) mole composition data for the system *n*-heptane (1) + toluene (2) + glycerol (3) + 2-methyl-2,4-pentanediol (4) at 313.2 K and 0.1 MPa for 1:1 solvent: co-solvent ratio. × – experimental (this study); -○- – NRTL model; △ - UNIQUAC model; ■ – tie -line feed composition

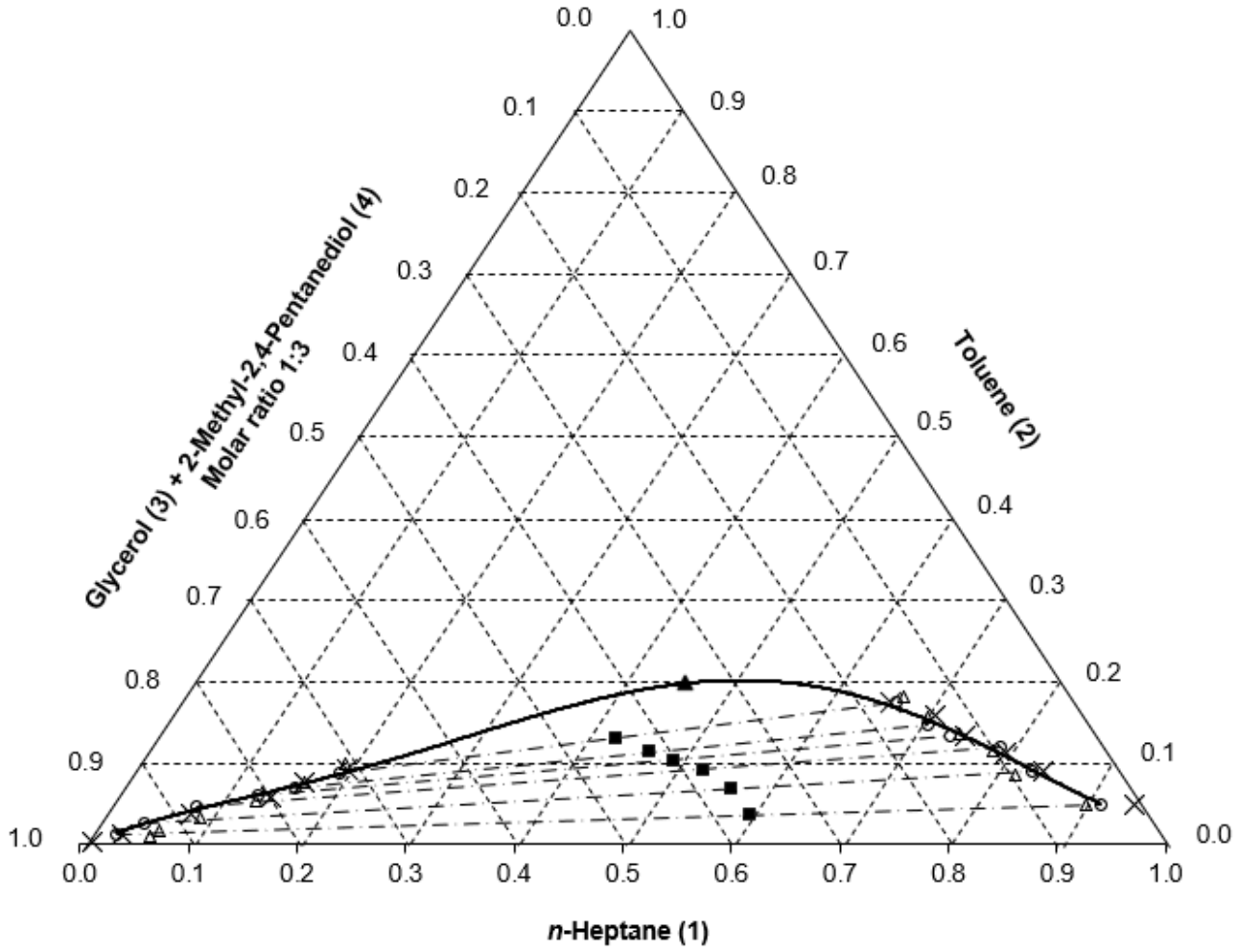

Figure 3.25. Liquid-liquid equilibrium (pseudo ternary) mole composition data for the system *n*-heptane (1) + toluene (2) + glycerol (3) + 2-methyl-2,4-pentanediol (4) at 298.2 K and 0.1 MPa for 1:3 solvent: co-solvent ratio. × – experimental (this study); -○- – NRTL model; △ - UNIQUAC model; ■ – tie-line feed composition; ▲- plait point

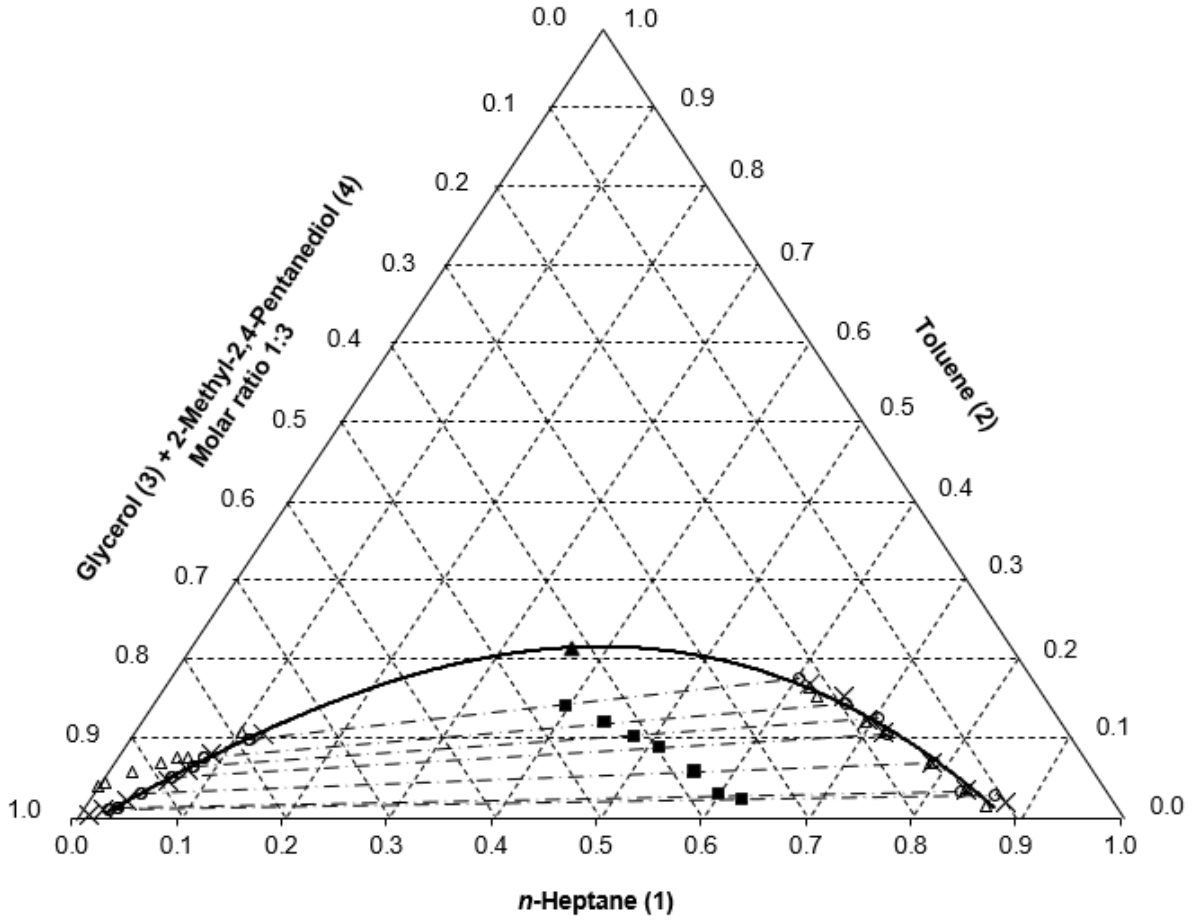

Figure 3.26. Liquid-liquid equilibrium (pseudo ternary) mole composition data for the system *n*-heptane (1) + toluene (2) + glycerol (3) + 2-methyl-2,4-pentanediol (4) at 313.2 K and 0.1 MPa for 1:3 solvent: co-solvent ratio. × – experimental (this study); -○- – NRTL model; △ - UNIQUAC model; ■ – tie-line feed composition; ▲ - plait point

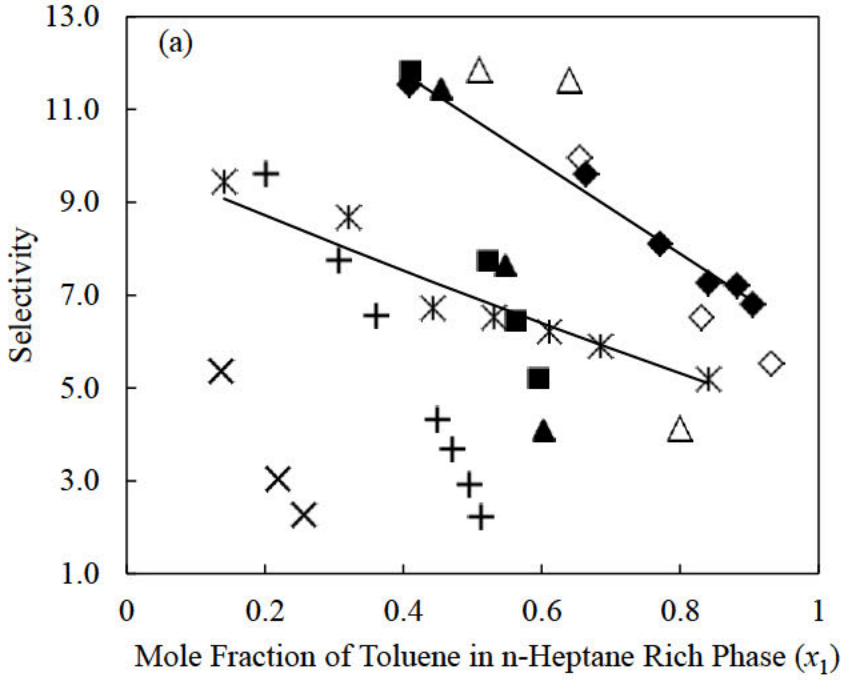
(a)
Selectivity
13.0
11.0
9.0
7.0
5.0
3.0
1.0
0
0.2
0.4
0.6
0.8
1
Mole Fraction of Toluene in n-Heptane Rich Phase (x_1)

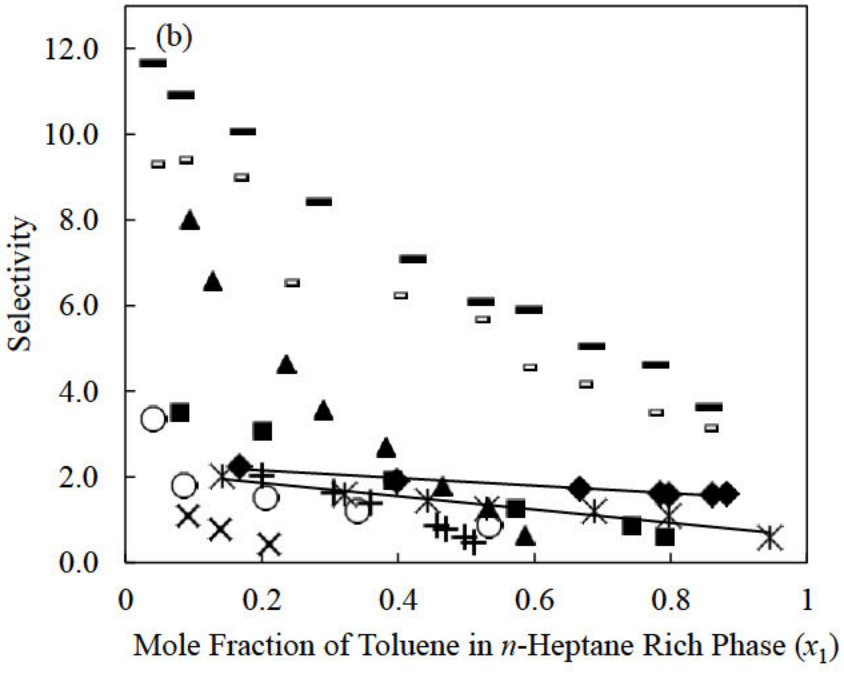
(b)
Selectivity
12.0
10.0
8.0
6.0
4.0
2.0
0.0
0
0.2
0.4
0.6
0.8
1
Mole Fraction of Toluene in *n*-Heptane Rich Phase (x_1)

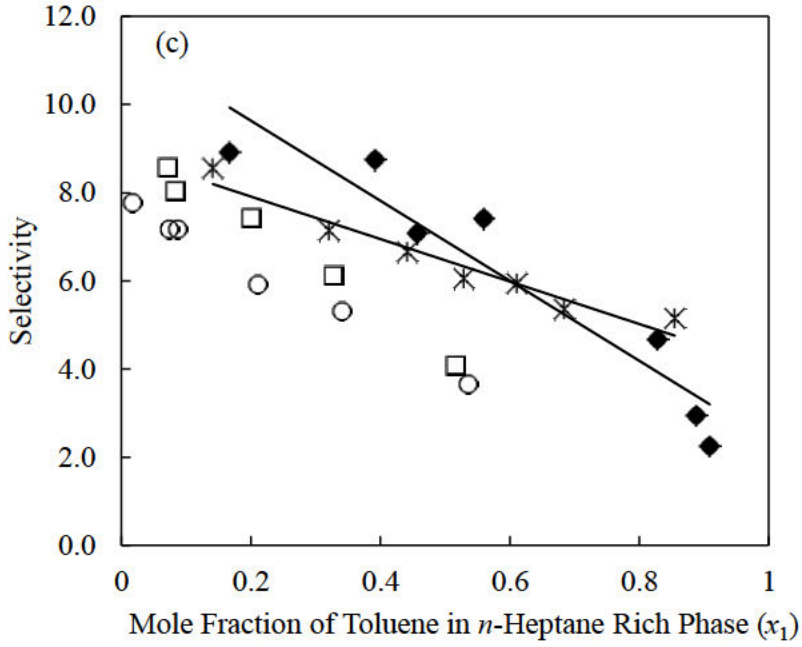

Figure 3.27. Selectivity comparison with respect to toluene content in the alkane-rich phase for the ternary system *n*-heptane (1) + toluene (2) + solvent (3) at:

(a) 298.15 K and 0.1 MPa; × – NMP (Nagpal & Rawat, 1981); ▲–Sulfolane (Tripathi et al., 1975); + – NFM (DongChu, HongQi, & Hao, 2007); ■ – DMSO (Farghi & Kaddami, 2008); △-1-methyl-3-octylimidazolium tetrafluoroborate (Shaahmadi et al., 2018); ◇ - 1-ethyl-3-methylimidazolium bis{(trifluoromethyl)sulfonyl}amide (Arce et al., 2008); ✳ – 1, 4-butanediol (this work); ♦ – glycerol (this work); black line – NRTL prediction

(b) 313.15 K and 0.1 MPa; × – NMP (Nagpal & Rawat, 1981); ▲–sulfolane (Tripathi et al., 1975); + – NFM (DongChu, HongQi, & Hao, 2007); ■ – tetraethylene glycol (Saha et al., 1998a); ○ - ethylene glycol and tetrabutylphosphonium (Kareem et al., 2012); ▬ - 1-ethyl-3-methylimidazolium 1,1,2,2-tetrafluoroethanesulfonate (García et al., 2011); ▭ - 1-ethyl-3-methylimidazolium trifluoromethanesulfonate (García et al., 2011); ✳ – 1, 4-butanediol (this work), ♦ - glycerol (this work); black line – NRTL prediction

(c) 333.15 K and 0.1 MPa × – NMP (Nagpal & Rawat, 1981); ▲–Sulfolane (Tripathi et al., 1975); + – NFM (DongChu, HongQi, & Hao, 2007); ■ – DMSO (Farghi & Kaddami, 2008); □ - sulfolane and tetratbutylphosphonium (Kareem et al., 2012); ○ - ethylene glycol and tetrabutylphosphonium (Kareem et al., 2012); ✳ – 1, 4-butanediol (this work); ♦ – glycerol (this work); black line – NRTL prediction

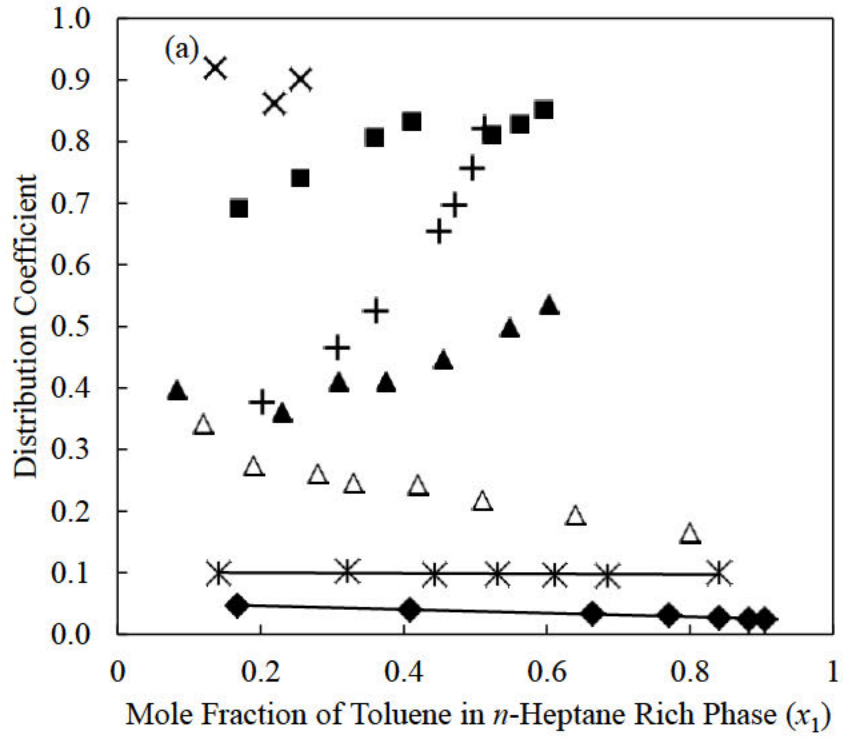
(a)
Distribution Coefficient
1.0
0.9
0.8
0.7
0.6
0.5
0.4
0.3
0.2
0.1
0.0
0
0.2
0.4
0.6
0.8
1
Mole Fraction of Toluene in n-Heptane Rich Phase (x_1)

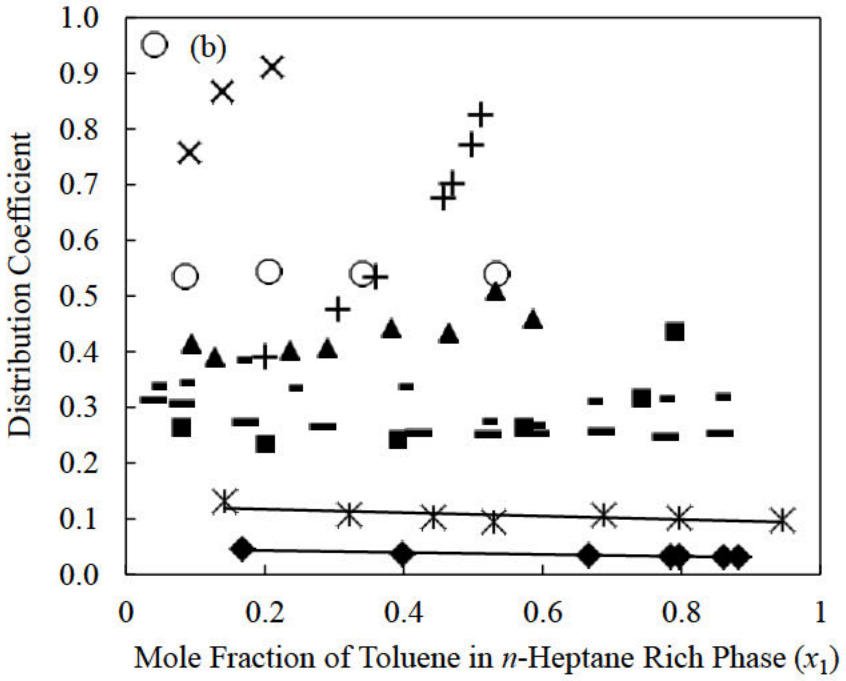
(b)
Distribution Coefficient
1.0
0.9
0.8
0.7
0.6
0.5
0.4
0.3
0.2
0.1
0.0
0
0.2
0.4
0.6
0.8
1
Mole Fraction of Toluene in n-Heptane Rich Phase (x_1)

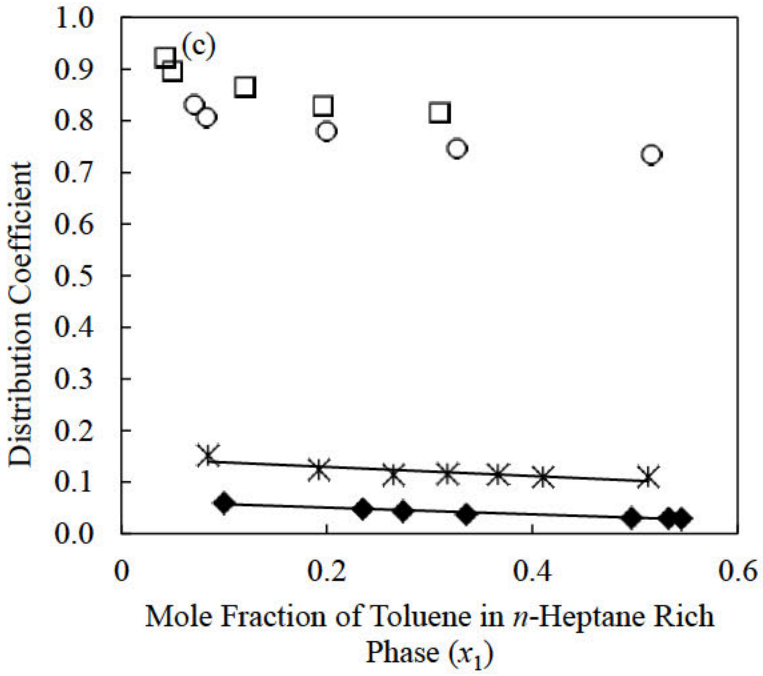

Figure 3.28. Solvent capacity comparison with respect to toluene content in the alkane-rich phase for the ternary system *n*-heptane (1) + toluene (2) + solvent (3) at:

(a) 298.15 K and 0.1 MPa; × – NMP (Nagpal & Rawat, 1981); ▲–Sulfolane (Tripathi et al., 1975); + – NFM (DongChu, HongQi, & Hao, 2007); ■ – DMSO (Farghi & Kaddami, 2008); △-1-methyl-3-octylimidazolium tetrafluoroborate (Shaahmadi et al., 2018); ◇ - 1-ethyl-3-methylimidazolium bis{(trifluoromethyl)sulfonyl}amide (Arce et al., 2008); ✳ – 1, 4-butanediol (this work); ♦ – glycerol (this work); black line – NRTL prediction

(b) 313.15 K and 0.1 MPa; × – NMP (Nagpal & Rawat, 1981); ▲–sulfolane (Tripathi et al., 1975); + – NFM (DongChu, HongQi, & Hao, 2007); ■ – tetraethylene glycol (Saha et al., 1998a); ○ - ethylene glycol and tetrabutylphosphonium (Kareem et al., 2012); ▬ - 1-ethyl-3-methylimidazolium 1,1,2,2-tetrafluoroethanesulfonate (García et al., 2011); ▭ - 1-ethyl-3-methylimidazolium trifluoromethanesulfonate (García et al., 2011); ✳ – 1, 4-butanediol (this work), ♦ - glycerol (this work); black line – NRTL prediction

(c) 333.15 K and 0.1 MPa × – NMP (Nagpal & Rawat, 1981); ▲–Sulfolane (Tripathi et al., 1975); + – NFM (DongChu, HongQi, & Hao, 2007); ■ – DMSO (Farghi & Kaddami, 2008); □ - sulfolane and tetratbutylphosphonium (Kareem et al., 2012); ○ - ethylene glycol and tetrabutylphosphonium (Kareem et al., 2012); ✳ – 1, 4-butanediol (this work); ♦ – glycerol (this work); black line – NRTL prediction

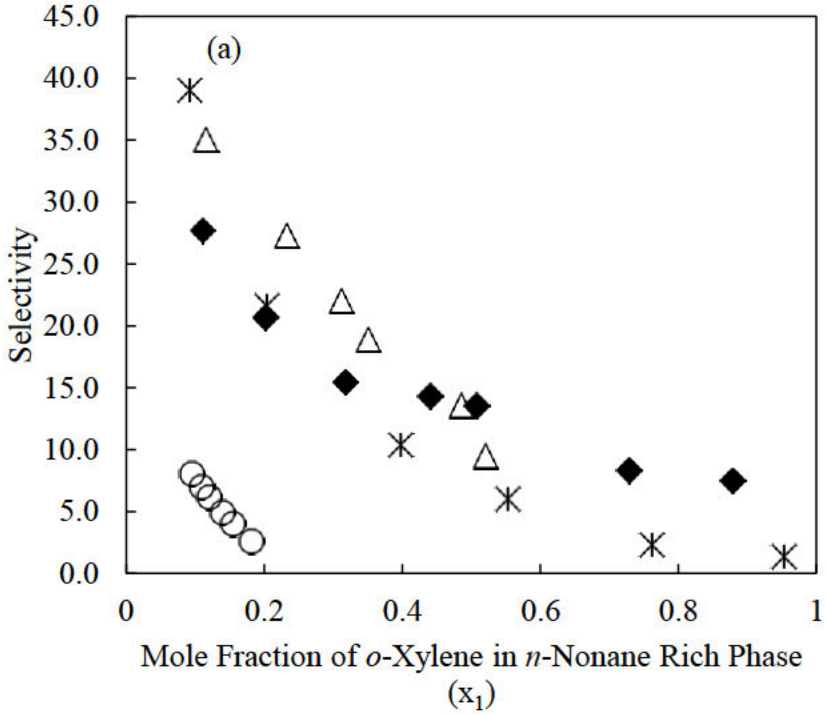
(a)
Selectivity
45.0
40.0
35.0
30.0
25.0
20.0
15.0
10.0
5.0
0.0
0
0.2
0.4
0.6
0.8
1
Mole Fraction of o-Xylene in n-Nonane Rich Phase
(x1)

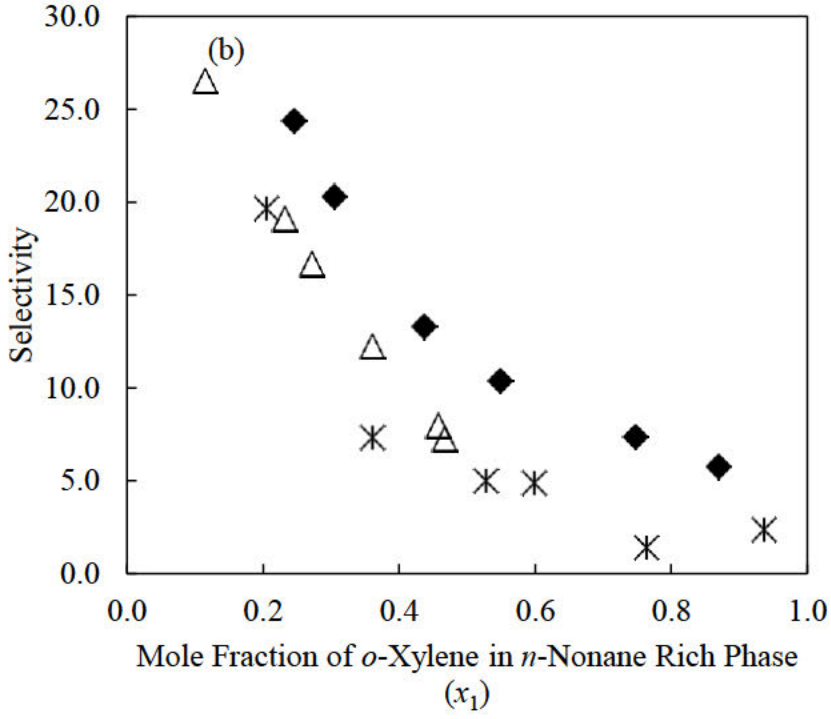
(b)
Selectivity
30.0
25.0
20.0
15.0
10.0
5.0
0.0
0.0
0.2
0.4
0.6
0.8
1.0
Mole Fraction of o-Xylene in n-Nonane Rich Phase
(x1)

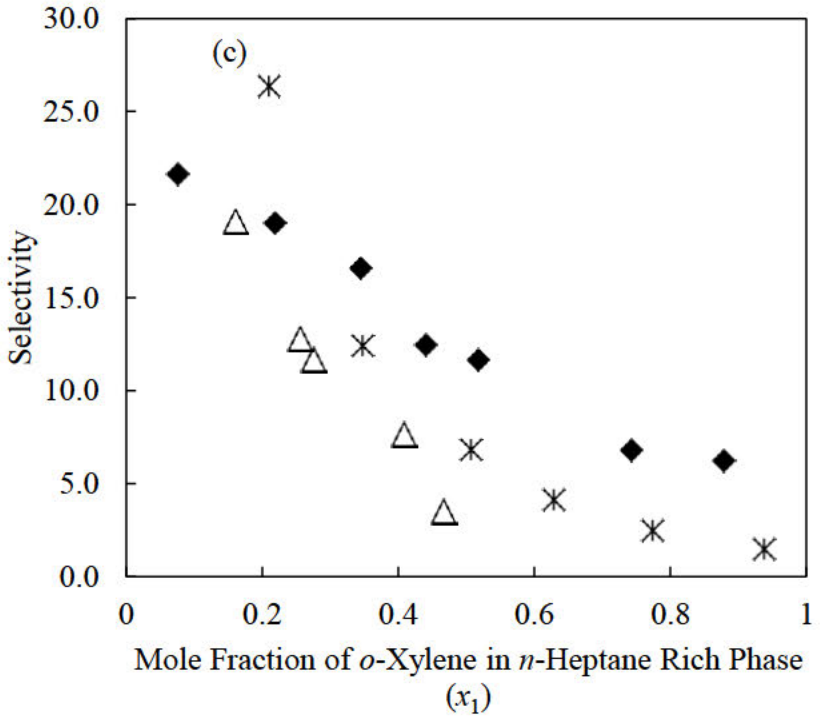

Figure 3.29. Selectivity comparison for the ternary systems:

(a) ✳ – *n*-nonane (1) + *o*-xylene (2) + 1, 4-butanediol (3) at 298.15 K and 0.1 MPa (this work); ♦ – *n*-nonane (1) + *o*-xylene (2) + glycerol (3) at 298.15 K and 0.1 MPa (this work); ○ – *n*-nonane (1) + toluene (2) + NMP (3) 298.15 K and 0.1 MPa (M. Letcher & K. Naicker, 1998); △ – *n*-nonane (1) + toluene (2) + NFM (3) at 303.15 K and 0.1 MPa (Brijmohan & Narasigadu, 2020)

(b) ✳ – *n*-nonane (1) + *o*-xylene (2) + 1, 4-butanediol (3) at 313.15 K and 0.1 MPa (this work); ♦ – *n*-nonane (1) + *o*-xylene (2) + glycerol (3) at 313.15 K and 0.1 MPa (this work); △ – *n*-nonane (1) + toluene (2) + NFM (3) at 323.15 K and 0.1 MPa (Brijmohan & Narasigadu, 2020)

(c) ✳ – *n*-nonane (1) + *o*-xylene (2) + 1, 4-butanediol (3) at 333.15 K and 0.1 MPa (this work); ♦ – *n*-nonane (1) + *o*-xylene (2) + glycerol (3) at 333.15 K and 0.1 MPa (this work; △ – *n*-nonane (1) + toluene (2) + NFM (3) at 343.15 K and 0.1 MPa (Brijmohan & Narasigadu, 2020)

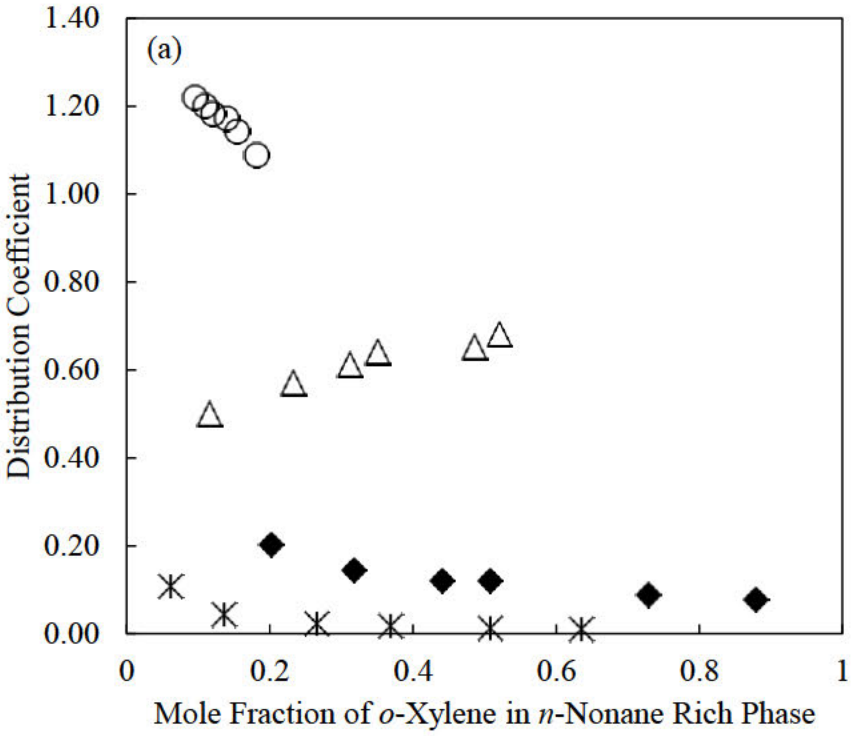
(a)
Distribution Coefficient
1.40
1.20
1.00
0.80
0.60
0.40
0.20
0.00
0
0.2
0.4
0.6
0.8
1
Mole Fraction of o-Xylene in n-Nonane Rich Phase

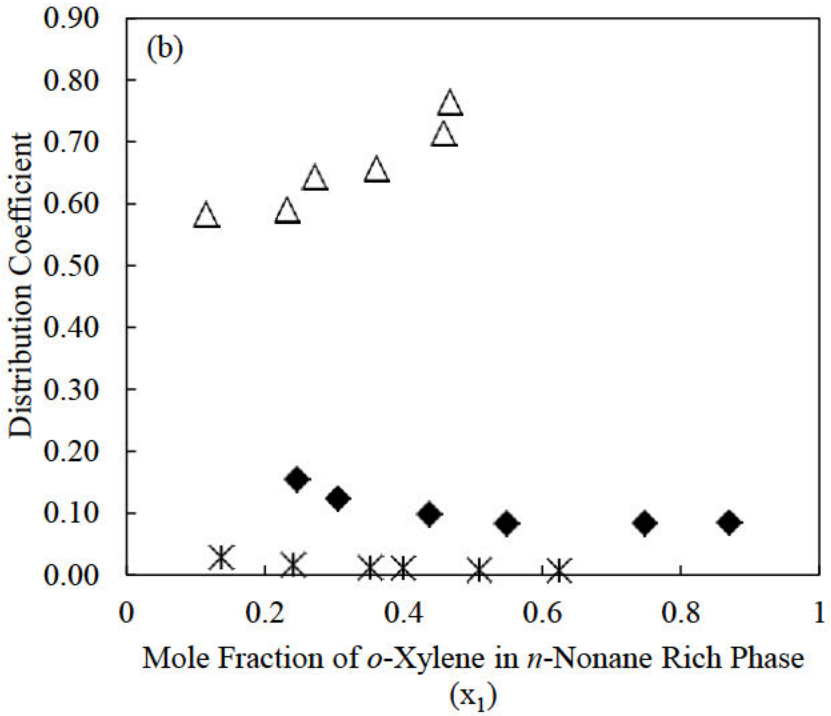
(b)
Distribution Coefficient
0.90
0.80
0.70
0.60
0.50
0.40
0.30
0.20
0.10
0.00
0
0.2
0.4
0.6
0.8
1
Mole Fraction of o-Xylene in n-Nonane Rich Phase
(x1)

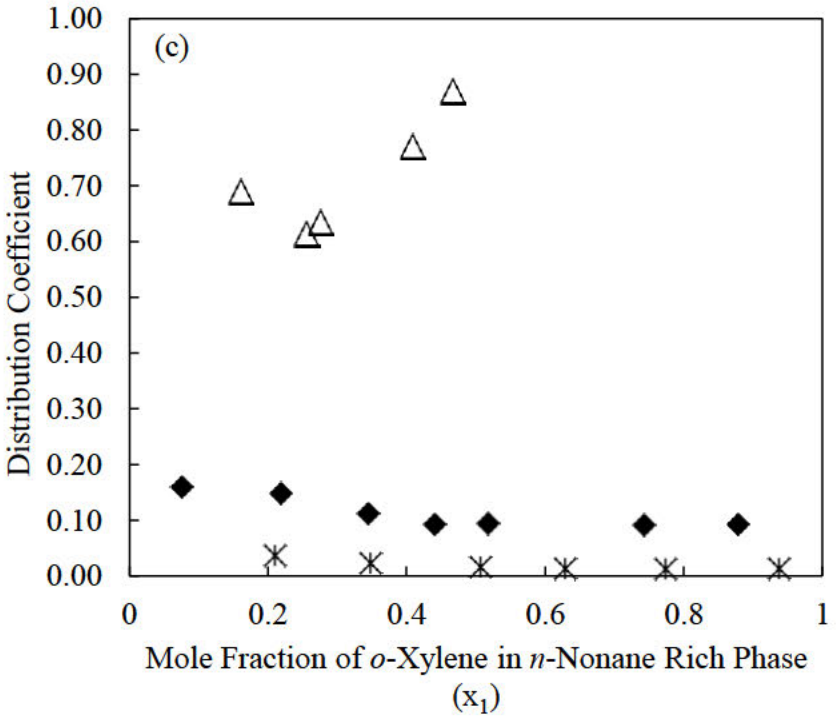

Figure 3.30. Distribution coefficient (capacity) comparison for the ternary systems:

(a) ✳ – *n*-nonane (1) + *o*-xylene (2) + 1, 4-butanediol (3) at 298.15 K and 0.1 MPa (this work); ♦ – *n*-nonane (1) + *o*-xylene (2) + glycerol (3) at 298.15 K and 0.1 MPa (this work); ○ – *n*-nonane (1) + toluene (2) + NMP (3) 298.15 K and 0.1 MPa (M. Letcher & K. Naicker, 1998); △ – *n*-nonane (1) + toluene (2) + NFM (3) at 303.15 K and 0.1 MPa (Brijmohan & Narasigadu, 2020)

(b) ✳ – *n*-nonane (1) + *o*-xylene (2) + 1, 4-butanediol (3) at 313.15 K and 0.1 MPa (this work); ♦ – *n*-nonane (1) + *o*-xylene (2) + glycerol (3) at 313.15 K and 0.1 MPa (this work); △ – *n*-nonane (1) + toluene (2) + NFM (3) at 323.15 K and 0.1 MPa (Brijmohan & Narasigadu, 2020)

(c) ✳ – *n*-nonane (1) + *o*-xylene (2) + 1, 4-butanediol (3) at 333.15 K and 0.1 MPa (this work); ♦ – *n*-nonane (1) + *o*-xylene (2) + glycerol (3) at 333.15 K and 0.1 MPa (this work; △ – *n*-nonane (1) + toluene (2) + NFM (3) at 343.15 K and 0.1 MPa (Brijmohan & Narasigadu, 2020)

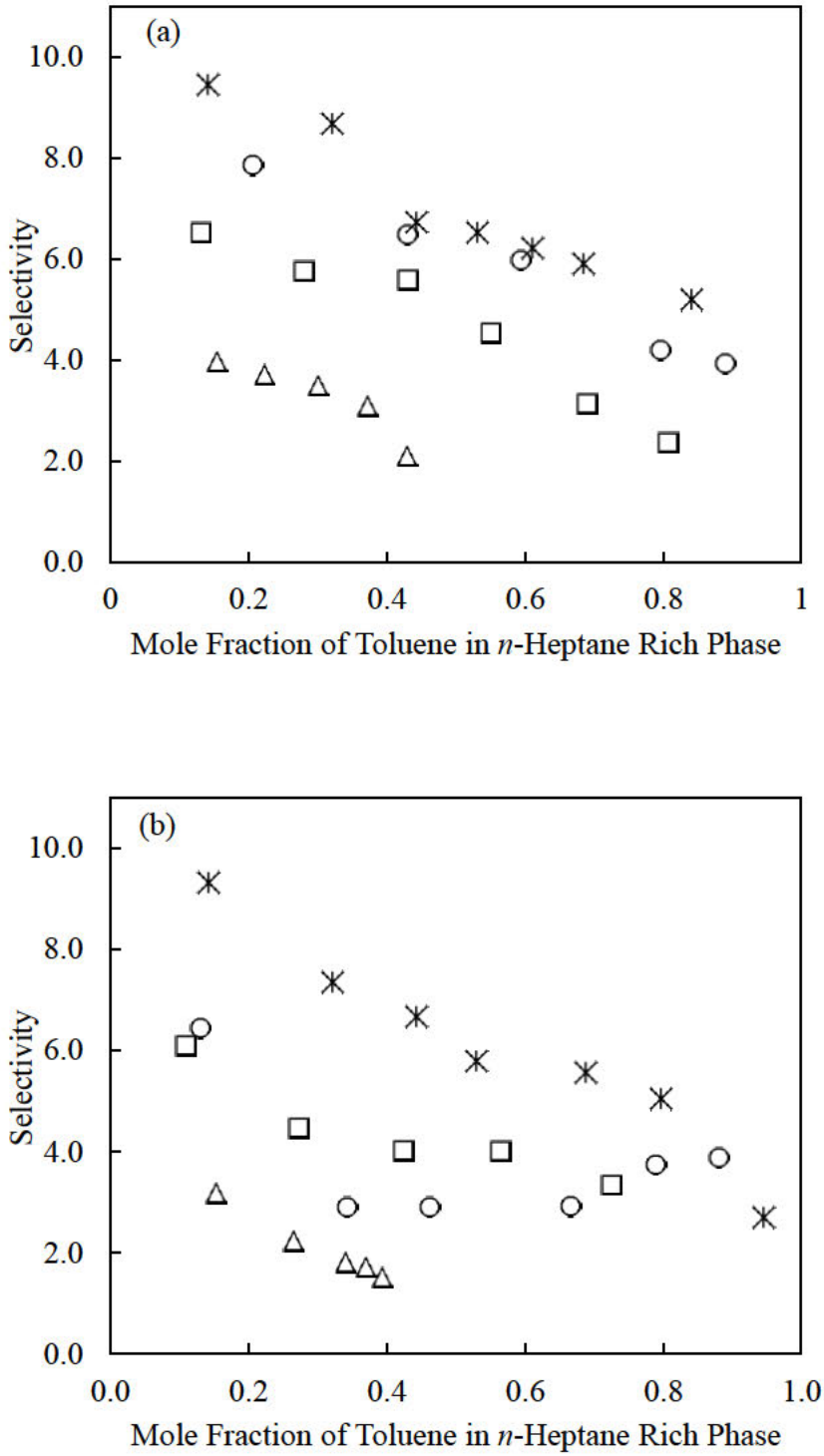

Figure 3.31. Selectivity comparison for the *n*-heptane (1) + toluene (2) + 1,4-butanediol (3) + 2-methyl-2,4-pentanediol (4) system with respect to toluene content in the alkane-rich phase at (a) 298.2 K and 0.1 MPa, and (b) 313.2 K and 0.1 MPa; ✳ - pure 1,4-butandiol (this work), ○ - 3:1 ratio (this work); □ - 1:1 ratio (this work); △ - 1:3 ratio (this work)

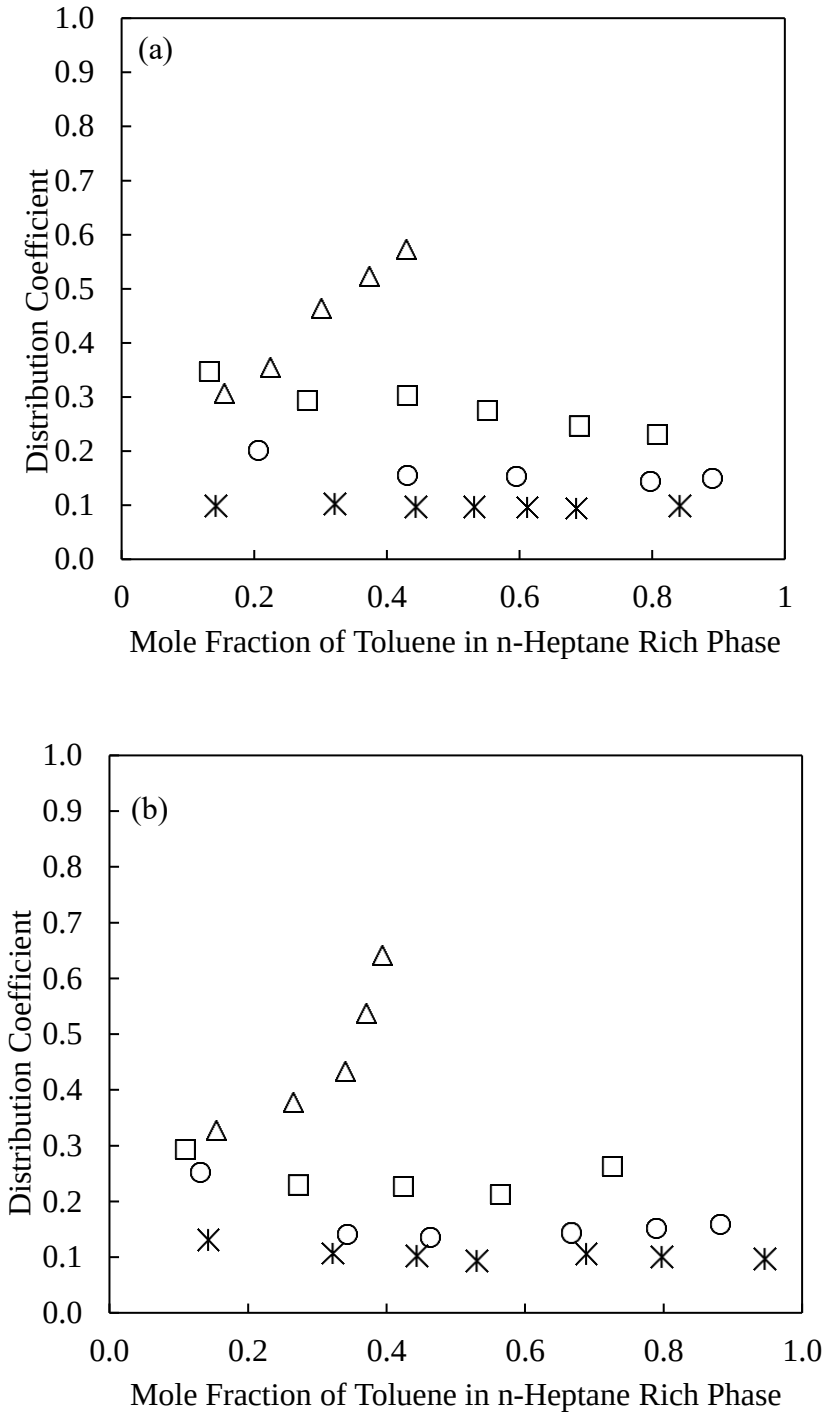

Figure 3.32. Distribution coefficient comparison for the *n*-heptane (1) + toluene (2) + 1,4-butanediol (3) + 2-methyl-2,4-pentanediol (4) system with respect to toluene content in the alkane-rich phase at (a) 298.2 K and 0.1 MPa, and (b) 313.2 K and 0.1 MPa; ✳ - pure 1,4-butandiol (this work), ○ - 3:1 ratio (this work); □ - 1:1 ratio (this work); △ - 1:3 ratio (this work)

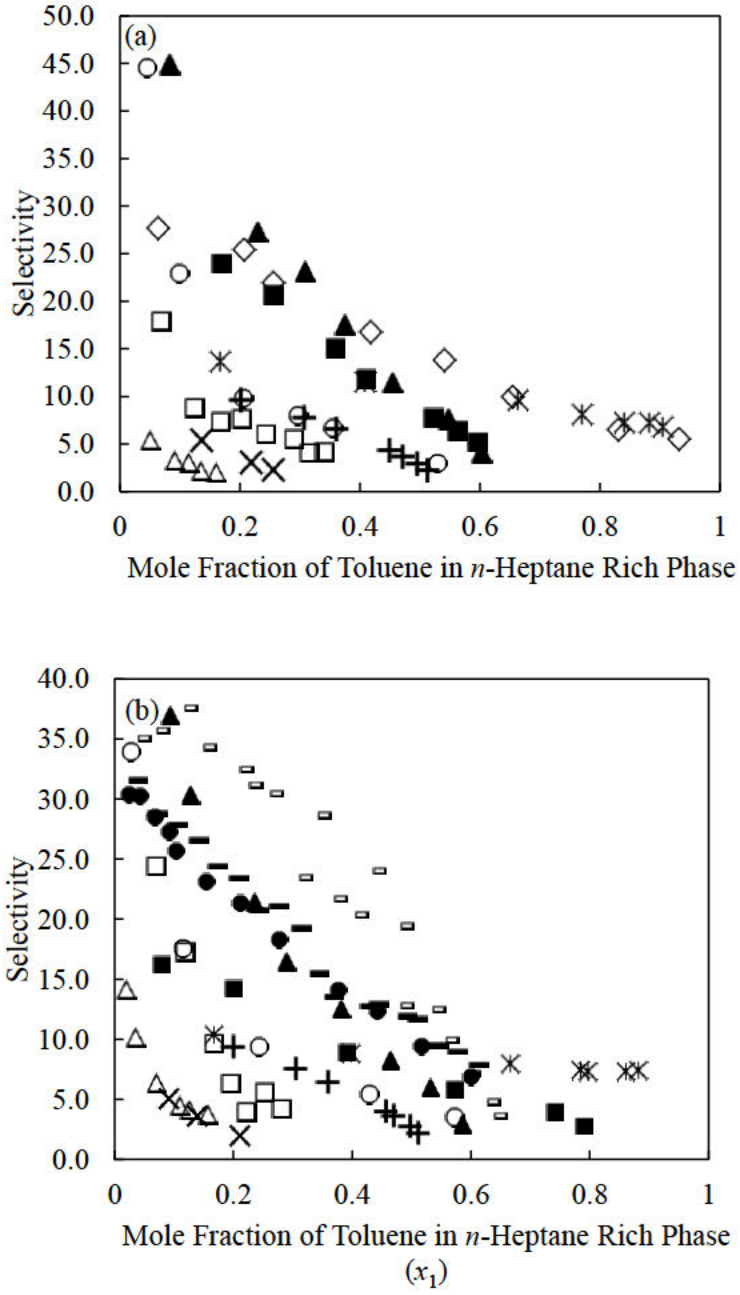

Figure 3.33. Comparison of selectivities for the system *n*-heptane (1) + toluene (2) + glycerol (3) + 2-methyl-2,4-pentanediol (4) at (a) 298.2 K and 0.1 MPa, and (b) 313.2 K and 0.1 MPa; ✳ - pure glycerol (this work); × – NMP (Nagpal & Rawat, 1981); ▲–Sulfolane (Tripathi et al., 1975); **+ – NFM (DongChu, HongQi, & Hao, 2007); ■ – DMSO (Farghi & Kaddami, 2008); ● - [mebupy]BF_4** (Meindersma et al., 2006); **▬ - [emim]$C_2H_5SO_4$** (Meindersma et al., 2006); **▭ - [mmim]$C_2H_5SO_4$** (Meindersma et al., 2006); **○ - 3:1 ratio (this work); □ - 1:1 ratio (this work); △ - 1:3 ratio (this work)**

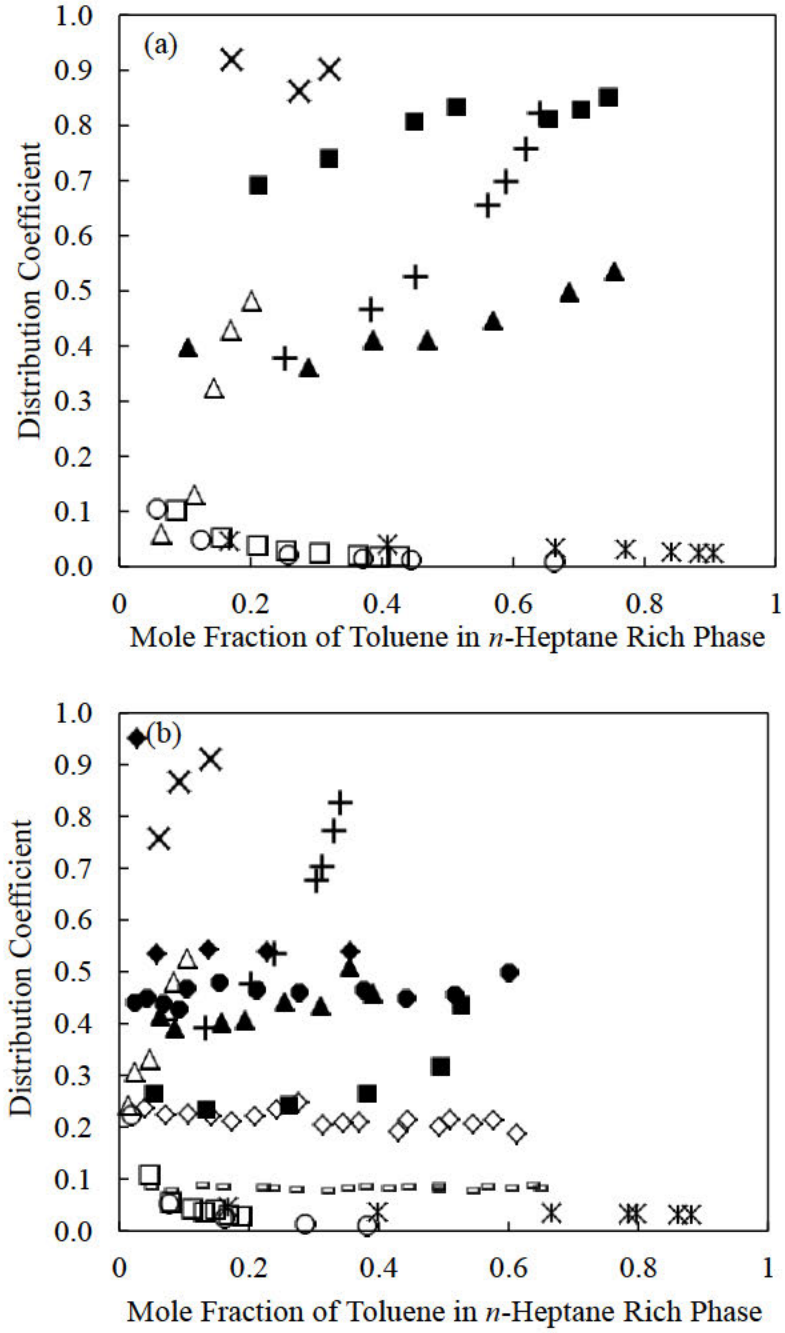

Figure 3.34. Comparison of distribution coefficients for system the *n*-heptane (1) + toluene (2) + glycerol (3) + 2-methyl-2,4-pentanediol (4) at (a) 298.2 K and 0.1 MPa, and (b) 313.2 K and 0.1 MPa; ✳ - pure glycerol (this work); × – NMP (Nagpal & Rawat, 1981); ▲– Sulfolane (Tripathi et al., 1975); **+ – NFM (DongChu, HongQi, & Hao, 2007); ■ – DMSO (Farghi & Kaddami, 2008); ● -[mebupy]BF_4** (Meindersma et al., 2006); ◇ - **[emim]$C_2H_5SO_4$** (Meindersma et al., 2006); ▭ - **[mmim]$C_2H_5SO_4$** (Meindersma et al., 2006); ○ - **3:1 ratio (this work); □ - 1:1 ratio (this work); △ - 1:3 ratio (this work)**

Ternary system (*n*-heptane + toluene + 1,4-butanediol or glycerol):

These systems are observed to exhibit type 2 ternary LLE behavior at all measured temperatures (Treybal, 1963). The phase behaviour with glycerol and 1,4-butanediol as the solvent are highly similar in that there is little transfer of alkanes to the solvent-rich phase and negligible solvent present in the alkane-rich phase. However, 1,4-butanediol has a higher solubility of the aromatic component (toluene) in the solvent phase as compared to glycerol. The low compositions of toluene in the glycerol-rich phase indicates a low distribution coefficient and therefore commercial applications would require an unfeasible, large solvent-to-feed ratio. Thus, in order for glycerol to be made practically viable, its use would need to be considered in conjunction with a co-solvent. The selectivity for all systems measured were significantly greater than unity, implying that the extraction of toluene from alkanes using 1,4-butanediol or glycerol as the solvent is feasible. Selectivity was noted to decrease slightly with temperature while the distribution of toluene in the solvent-rich phase increased with temperature. The NRTL and UNIQUAC models were able to adequately correlate the experimental data for all systems studied, as evidenced by the low RMSD values reported in Tables 3.10 and 3.13. The NRTL model produced significantly low RMSD values and is able to provide a better representation of the data. The coherence of the regressed parameters was validated with the use of a GUI-MATLAB tool developed by Marcilla et al. (2017).

While the selectivity values in Tables 3.2 and 3.3 indicate that selectivity is lower at higher temperatures, due to the average values between temperatures showing a decreasing trend, the optimal extraction temperature depends on several factors' characteristic of specific process requirements. Selectivity clearly depends on the overall toluene content, which indicates that feed composition plays a significant role in solvent choice as well as operating temperatures. Thus, the optimal process conditions depend on the trade-off between higher selectivities at lower temperatures (indicating reduced capital costs), and greater solvent capacities at higher temperatures which would result in lower solvent-to-feed ratios and lower energy costs but greater capital investment.

Figures 3.27a – 3.27c illustrate the selectivity compared to conventional solvents employed in this process in industry. The selectivities for 1,4-butanediol and glycerol are competitive in that they are comparable to solvents currently used – both solvents have selectivities superior to NFM and

NMP across most of the composition range. Figures 3.28a – 3.28c illustrate the solvent capacity (distribution coefficient) for the solvents studied in this work compared to conventional solvents. 1,4-Butanediol and glycerol have poor solvent capacities compared to conventional solvents and would require significantly higher solvent-to-feed ratios. Use of these solvents would have to be considered in conjunction with a co-solvent to increase solvent capacity.

Ternary system (*n*-nonane + *o*-xylene + 1,4-butanediol or glycerol):

The experimental data for the *n*-nonane + *o*-xylene + 1,4-butanediol or glycerol also shows that the systems demonstrate type 2 ternary LLE behavior. In using butane-1,4-diol or glycerol as a solvent, there would be low costs associated with recovering higher alkanes spilled-over to the extract due to their low concentrations in the solvent-rich phase. Butane-1,4-diol has a significantly higher solubility of *o*-xylene compared to glycerol, and this manifests in higher distribution coefficients, indicating this solvent would require lower solvent-to-feed ratios. While glycerol offers benefits in terms of health, safety, and environmental impact compared to conventional solvents, it has unfeasible solvent capacities for higher alkane and aromatic feedstocks (diesel fractions). All selectivities were greater than one, indicating that the solvents studied are appropriate for this application. The phase behaviour for the two solvents studied are similar with the only significant difference being the higher solubility of *o*-xylene demonstrated by butane-1,4-diol. There are no significant changes in phase behaviour associated with higher temperatures. The solvents may be easily recovered downstream using conventional distillation as is usually done in solvent extraction processes. The low affinity of the solvent for the alkane-rich phase suggests that there would be capital and operating cost savings resulting from not needing to account for additional process steps that are usually required to recover solvent losses to the raffinate.

There is limited LLE data from literature for the phase behaviour of heavier alkanes with heavier aromatics with different solvents. The most similar systems available in literature is that of *n*-nonane + toluene + NFM as well as *n*-nonane + toluene + NMP. Figures 3.29 and 3.30 also compares the selectivity and distribution coefficients for the systems against that of these similar systems from literature. Comparison to the system *n*-nonane + toluene + NFM shows that NFM with toluene has similar selectivities to the solvents studied in this work with *o*-xylene, although

with significantly higher solvent capacity. NMP on the other hand has significantly lower selectivities with toluene, but substantively higher distribution coefficients.

The experimental data was successfully correlated with the NRTL and UNIQUAC models as indicated by the low RMSD values reported in Tables 3.12 and 3.13. Both models produced similarly low RMSD, suggesting that either would be a suitable choice in modelling the phase behaviour at various temperatures. A GUI-MATLAB tool created by Marcilla et al. (2017) was used to test and validate the coherence of the regressed parameters.

Quaternary system (*n*-heptane + toluene + 1,4-butanediol + 2-methyl-2,4-pentanediol):

For solvent to co-solvent ratios of 3:1 and 1:1, type 2 pseudo ternary systems are observed, whereas type 1 pseudo ternary systems occur for the 1:3 ratio. The effect of transition between different types of LLE systems may present challenges to column design if different molar ratios of solvent:co-solvent are used. A type 1 system limits the effective number of stages at the plait point, which may result in significant overdesign or under-design depending on the aromatic concentration in the feed if column specifications were initially made for a type 2 system. The type 2 systems demonstrate little transfer of alkanes to the solvent-rich phase, and trace amounts of solvent present in the alkane-rich phase. This is desirable as there would be little solvent loss with using 2-methyl-2,4-pentanediol in these concentrations, reducing capital requirements for recovering solvent from the raffinate. The extent of ingress of alkanes in the solvent-rich phase appears to increase as the proportion of 2-methyl-2,4-pentanediol is increased.

Table 3.14 reports RMSDs of 0.0091and 0.01 for the NRTL model at 298.2 K and 313.2 K, as well as 0.029 and 0.025 for the UNIQUAC model at 298.2 K and 313.2 K. This highlights that both models are able to produce reasonable approximations of this system's quaternary phase behavior, with the NRTL model seemingly demonstrating superior correlative capability.

The solvent mixtures studied were all suitable for extraction of toluene as selectivities were greater than unity. Figures 3.31a – 3.31b show the impact of 2-methyl-2,4-pentanediol concentration on selectivity. Selectivity decreased with increasing temperature and increasing concentrations of 2-methyl-2,4-pentanediol. Figures 3.32a – 3.33b highlight the effect on distribution coefficient by increasing the molar ratio of 2-methyl-2,4-pentanediol in the solvent mixture. The distribution coefficients mostly increased with higher temperatures and greater concentrations of 2-methyl-

2,4-pentanediol. At the highest co-solvent concentration, the type 1 system produced the effect of exponentially increasing the distribution coefficient, which in certain composition ranges resulted in the solvent capacity increasing more than 6 times compared to using 1,4-butanediol alone. There is a reduction in selectivity associated with this effect, which would manifest in a higher capital requirement due to the increased number of stages in the extraction column. However, the energy and cost savings associated with substantially reducing the solvent to feed ratio is likely to produce a net benefit. Ultimately, the optimal process conditions as well as solvent composition depends on specific process requirements as the selectivity and distribution coefficient are both dependent on the overall toluene content, indicating that feed composition plays a significant role in the overall design.

Quaternary system (*n*-heptane + toluene + glycerol + 2-methyl-2,4-pentanediol):

Type 2 pseudo ternary systems appear to form for solvent to co-solvent ratios 3:1 and 1:1 for the quaternary system *n*-heptane + toluene + glycerol + 2-methyl-2,4-pentanediol. However, type 1 pseudo ternary system is observed for 1:3 molar ratio. This indicates that a solvent extraction system would have to be designed for a specific molar ratio or a particular range of molar ratios to avoid operational complexities in the industrial environment. The impact of operating the column at different molar ratios would entirely change the dynamics of the operation if the system were to transition from a type 2 to a type 1 system, or vice versa. Column specifications and design parameters made for a type 2 system may not be effective and may limit the separation at the plait point if molar ratios for a type 1 system are used. There is little ingress of alkanes to the solvent-rich phase for the type 2 systems. Solvent recovery costs would be reduced at these concentrations of 2-methyl-2,4-pentanediol due to the lower capital requirement associated with recovering alkane spill-over to the raffinate. The concentration of alkane in the raffinate phase increases as the molar ratio of 2-methyl-2,4-pentanediol is increased. This increase ultimately results in the solvent mixture becoming entirely miscible with toluene, resulting in the type 1 system observed. The RMSDs from the activity coefficient modelling are indicated in Table 3.15 and are 0.012 and 0.009 for the NRTL model at 298.2 K and 313.2 K, and 0.013 and 0.011 for the UNIQUAC model at 298.2 K and 313.2 K. This signifies that both models are able to suitably approximate the phase behaviour at these conditions. In general, both models show good representation across

composition ranges, however UNIQUAC demonstrates larger deviations in the alkane-rich phase at 1:3 molar ratios, as seen in Figures 3.25 and 3.26. Different objective functions were also used such as the ordinary least squares, together with alternative initialization methods. There was no observable change in the fitted parameters with changes in the objective function and initialization method. Regarding the NRTL model, larger positive values of the binary interaction parameters tend to indicate unfavourable interactions between species *i* and *j*. A value of zero indicates an ideal solution as the activity coefficient would tend to unity, while negative values are more indicative of favourable interactions (Chen & Song, 2004). For the phase equilibria studied, the interaction parameters for the highly miscible *n*-heptane-toluene pair is negative, which is aligned to the underlying theory of the interaction parameters; the immiscible *n*-heptane-glycerol and toluene-glycerol pairs have larger positive values, which corresponds to the expected unfavourable interactions between these pairs. The toluene-glycerol parameters are less than the *n*-heptane-glycerol pairs (closer to zero), which may highlight why glycerol has a higher selectivity for toluene as a solvent compared to *n*-heptane. Generally, miscibility is favoured between species containing polar groups or hydrogen atoms. The non-polar pair of *n*-heptane and toluene are miscible, while polar glycerol forms immiscible pairs with *n*-heptane and toluene. A comparison of the UNIQUAC structural parameters indicates that *n*-heptane and 2-methyl-2,4-pentanediol have significantly higher relative molecular surface areas compared to toluene and glycerol. This may suggest that the probability of greater occurrences of Van der Waals forces on the larger molecular areas of 2-methyl-2,4-pentanediol enables it to form positive interactions with non-polar molecules, highlighting the observed miscibility between 2-methyl-2,4-pentanediol and *n*-heptane and the observed immiscibility between glycerol and *n*-heptane due to the small relative molecular surface area of glycerol.

Table 3.17 compares the binary interaction parameters for various component pairs obtained from binary, ternary, and quaternary data. This comparison highlights significant differences in parameters depending on the number of species in a system, reducing the extent to which the parameters may be generalized in different multicomponent mixtures. However, the ranges of values in all cases indicate that the parameters are consistent with the observed phenomena. In general, the parameter values for the immiscible pairs reduce when the number of components comprising the system increases, suggesting that more positive intermolecular interactions are likelier.

The selectivities for all solvent mixtures were greater than one, indicating that the studied systems are appropriate for the extraction of toluene. Figures 3.33a – 3.33b compares the selectivities of the solvent mixtures to that of the previously published pure glycerol as solvent data. Selectivity appears to reduce with increasing concentration of 2-methyl-2,4-pentanediol, as well as with increasing temperature. Figures 3.34a – 3.34b compares the distribution coefficient of the solvent mixtures with that of the distribution coefficient of pure glycerol from literature. In Figures 3.33 and 3.34, each solvent appears to approach a different peak as the solute approaches infinite dilution in the alkane-rich phase. There appears to be exponential growth in selectivity below 0.1 mole fraction, although the comparison depends on availability of data from literature below this point, i.e., some solvents may not have data approaching infinite dilution. For molar ratios of 3:1 and 1:1, which form the type 2 system, there does not appear to be substantial increase in the solvent capacities of glycerol, and therefore would not constitute a significant improvement over using pure glycerol. For the molar ratio of 1:3 (type 1 system) there is an exponential increase in the distribution coefficient; the solvent capacity increases by more than 20 times in certain composition ranges. At high co-solvent concentrations, the type 1 system produces the effect of reduced selectivity, however, substantially increases the solvent capacity. The capacities also appear to increase with temperature. The changes in selectivity and capacity are as a result of the increasing concentration of 2-methyl-2,4-pentanediol. This causes increased miscibility between toluene and 2-methyl-2,4-pentanediol which ultimately results in the type 1 systems observed at high ratios of solvent to co-solvent. The reduced selectivity would increase certain column requirements such as the number of stages, however feasibility is improved with the reduced solvent to feed ratio, which reduces process utilities and distillation energy costs in the solvent recovery section. The selectivity and capacity vary with toluene content, and therefore the optimal process conditions and design characteristics are dependent on the feed composition.

3.5. Conclusion

LLE experimental data were successfully measured at (298.2, 313.2 and 333.2) K and 0.1 MPa for the ternary systems *n*-heptane + toluene + (1,4-butanediol or glycerol) as well as *n*-nonane + *o*-xylene + (1,4-butanediol or glycerol). In order to investigate the influence of 2-methyl-2,4-pentanediol on the solvent capacity of 1,4-butanediol and glycerol in the extraction of toluene from *n*-heptane, LLE experimental data was also measured for the quaternary system *n*-heptane +

toluene + (1,4-butanediol or glycerol) + 2-methyl-2,4-pentanediol at (298.2 and 313.2) K and 0.1 MPa. The direct analytical method was used, with the phase compositions analysed via gas chromatography. All ternary systems studied were found to exhibit type 2 ternary LLE behaviour and were reasonably correlated with the NRTL and UNIQUAC thermodynamic models. Both type 1 and type 2 behavior were observed for the pseudo-ternary systems, with the type 1 system occurring at high concentrations of the co-solvent. The quaternary phase behaviour was found to be suitably represented by the NRTL and UNIQUAC thermodynamic models. The extraction of toluene from *n*-heptane was found to be feasible at all co-solvent ratios studied as the relative selectivity values were greater than unity for all the experimental data. For the molar ratios of 2-methyl-2,4-pentanediol that produced type 2 systems, there did not appear to be significant improvements in solvent capacity. There were substantive increases in solvent capacity with high molar ratios of 2-methyl-2,4-pentanediol, associated with the type 1 system. It is recommended that 2-methyl-2,4-pentanediol be used as a co-solvent to 1,4-butanediol and glycerol in the extraction of toluene from *n*-heptane for the molar ratios that produce type 1 systems, demonstrated at a molar ratio of 1:3 at 298.2 K and 313.2 K.

3.7. References

Abrams, D. S., & Prausnitz, J. M. (1975). Statistical Thermodynamics of Liquid Mixtures: A New Expression for the Excess Gibbs Energy of Partly or Completely Miscible Systems. *AIChE J*, *21*, 116–118.

Alders, L. (1959). *Liquid-Liquid Extraction* (2nd ed.). Elsevier: Amsterdam.

Alkhaldi, K. H. A. E., Fandary, M. S., Al-Jimaz, A. S., Al-Tuwaim, M. S., & Fahim, M. A. (2009). Liquid−liquid Equilibria of Aromatics Removal from Middle Distillate Using NMP. *Fluid Phase Equilib*, *286*, 190−195.

Al-Zayied, T. A., Al-Sahhaf, T. A., & Fahim, M. A. (1990). Measurement of Phase Equilibrium in Multicomponent Systems of Aromatics with N-Methylpyrrolidone and Predictions with Unifac. *Fluid Phase Equilib*, *61*, 131−144.

Arce, A., Earle, M. J., Rodríguez, H., Seddon, K. R., & Soto, A. (2008). 1-Ethyl-3-methylimidazolium bis((trifluoromethyl)sulfonyl)amide as solvent for the separation of aromatic and aliphatic hydrocarbons by liquid extraction – extension to C7- and C8-fractions. *Green. Chem*, *10*, 1294–1300. https://doi.org/10.1039/b807222a

Ashcroft, S. J., Clayton, A. D., & Shearn, R. B. (1982). Liquid-Liquid Equilibriums for Three Ternary and Six Quaternary Systems Containing Sulfolane, N-Heptane, Toluene, 2-Propanol, and Water at 303.15 K. *J. Chem. Eng. Data*, *27*, 148–151.

Aspen Plus (No. 10). (2004). Aspen Technology Incorporation.

Brijmohan, N., Moodley, K., & Narasigadu, C. (2021). Identification and Screening of Potential Organic Solvents for the Liquid–Liquid Extraction of Aromatics. *Org. Process Res. Dev.*, *25*, 2230–2248.

Brijmohan, N., Moodley, K., & Narasigadu, C. (2022a). Ternary Liquid–Liquid Equilibrium Data for the n-Nonane + o-Xylene + (Butane-1,4-diol or Glycerol) Systems at (298.2, 313.2, 333.2) K and 0.1 MPa. *J. Chem. Eng. Data*, *67*, 3468–3475. https://doi.org/10.1021/acs.jced.2c00530

Brijmohan, N., Moodley, K., & Narasigadu, C. (2022b). Ternary Liquid–Liquid Equilibrium Data for the n-Heptane + Toluene + (Butane-1,4-diol or Glycerol) Systems at 298.2, 313.2, and 333.2 K and 0.1 MPa. *J. Chem. Eng. Data*, *67*(4), 975–983. https://doi.org/10.1021/acs.jced.2c00011

Brijmohan, N., Moodley, K., & Narasigadu, C. (2022c). Liquid–Liquid Extraction of Toluene from n-Heptane Using Butane-1,4-diol + 2-Methyl-pentane-2,4-diol Liquid Mixtures. *J. Chem. Eng. Data*, *67*(0), 3177–3185. https://doi.org/10.1021/acs.jced.2c00498

Brijmohan, N., Moodley, K., & Narasigadu, C. (2023). Use of Glycerol + 2-Methylpentane-2,4-diol Liquid Mixtures in the Separation of Toluene from n-Heptane via Liquid–Liquid Extraction. *J. Chem. Eng. Data*. https://doi.org/10.1021/acs.jced.3c00041

Brijmohan, N., & Narasigadu, C. (2020). Ternary Liquid–Liquid Equilibrium Data for the N-Formylmorpholine + Toluene + {n-Nonane or n-Decane} Systems at (303.2, 323.2, and 343.2) K and 101.3 kPa. *J. Chem. Eng. Data*, *65*, 788–792. https://doi.org/10.1021/acs.jced.9b01011

Britt, H. I., & Luecke, R. H. (1973). The Estimation of Parameters in Nonlinear, Implicit Models. *Technometrics*, *15*, 233–247.

Cassell, G. W., Dural, N., & Hines, A. L. (1989). Liquid-Liquid Equilibrium of Sulfolane-Benzene-Pentane and Sulfolane-Toluene-Pentane. *Ind. Eng. Chem. Res*, *28*, 1369−1374.

Cassell, G. W., Hassan, M. M., & Hines, A. L. (1989). Correlation of the Phase Equilibrium Data for the Heptane-Toluene-Sulfolane and Heptane-Xylene-Sulfolane Systems. *J. Chem. Eng. Data*, *34*, 434−438.

Cassell, G. W., Hassan, M. M., & Junes, A. L. (1989). Phase Equilibria of the Cylohexane-Toluene-Sulfolane and Hexane-Toluene-Sulfolane Ternary Systems. *Chem. Eng. Commun*, *85*, 233−243.

Chen, C.-C., & Song, Y. (2004). Solubility Modeling with a Nonrandom Two-Liquid Segment Activity Coefficient Model. *Ind. Eng. Chem. Res.*, *43*, 8354–8362. https://doi.org/10.1021/ie049463u

Chen, D., Ye, H., & Hao, W. (2007). Liquid + Liquid Equilibria of heptane + Xylene + N-Formylmorpholine Ternary System. *J. Chem. Thermodyn*, *39*, 1571−1577.

Chen, J., Duan, L. P., Mi, J. G., Fei, W. Y., & Li, Z. C. (2000). Liquid-liquid equilibria of multi-component systems including n-hexane, n-octane, benzene, toluene, xylene and sulfolane at 298.15 K and atmospheric pressure. *Fluid Phase Equilib*, *173*, 109−119.

Chen, J., Li, Z., & Duan, L. (2000). Liquid−Liquid Equilibria of Ternary and Quaternary Systems Including Cyclohexane, 1-Heptene, Benzene, Toluene, and Sulfolane at 298.15 K. *J. Chem. Eng. Data*, *45*, 689−692.

Chen, Q. L., Wang, Q., Zhang, B. J., He, C., & He, C. C. (2017). Optimal Design of a New Aromatic Extractive Distillation Process Aided by a Co-Solvent Mixture. *Energy Procedia*, *105*, 4927–4934.

Cho, J., Ko, M. S., Na, S., & Kim, H. (2002). Simulation of the Aromatic Recovery Process by Extractive Distillation. *Korean J. Chem. Eng*, *19*, 996–1000.

de Fré, R. M., & Verhoeye, L. A. (1976). Phase Equilibria in Systems Composed of an Aliphatic and an Aromatic Hydrocarbon and Sulpholane. *J. Appl. Chem. Biotechnol*, *26*, 469−487.

Delancey, G. (2013). *Principles of Chemical Engineering Practice*. John Wiley & Sons.

Deming, W. E. (1943). *Statistical adjustment of data.* John Wiley & Sons: New York

DongChu, C., HongQi, Y., & Hao, W. (2007). (Liquid + liquid) equilibria of three ternary systems: (heptane + benzene + N-formylmorpholine), (heptane + toluene + N-formylmorpholine), (heptane + xylene + N-formylmorpholine) from T = (298.15 to 353.15) K. *J. Chem. Thermodyn*, *39*, 1182−1188.

Fan, W., Yan, H., Huang, H., Ma, Y., Gao, J., Xu, D., & Wang, Y. (2021). Measurement and Thermodynamic Modeling of Ternary Liquid–Liquid Equilibrium for Extraction of 2,6-Xylenol from Aromatic Hydrocarbon Mixtures with Different Solvents. *J. Chem. Eng. Data*, *66*, 330–337. https://doi.org/10.1021/acs.jced.0c00718

Farghi, F., & Kaddami, M. (2008). Phase Diagrams of Ternary and Quaternary Systems Containing Heptane, Toluene, Dimethylsulfoxide, Methanol, and Ethanol at 298.15 K. *Russ. J. Phys. Chem.*, *92*, 2502–2506.

Ferreira, P. O., Ferreira, J. B., & Medina, A. G. (1984). Liquid-liquid equilibria for the system N-methylpyrrolidone + toluene + n-heptane: UNIFAC interaction parameters for N-methylpyrrolidone. *Fluid Phase Equilib*, *16*, 369−379.

García, S., García, J., Larriba, M., S. Torrecilla, J., & Rodríguez, F. (2011). Sulfonate-Based Ionic Liquids in the Liquid–Liquid Extraction of Aromatic Hydrocarbons. *J. Chem. Eng. Data*, *56*, 3188–3193. https://doi.org/10.1021/je200274h

Hadj-Kali, M. K., Salleh, Z., Ali, E., Khan, R., & Hashim, M. A. (2017). Separation of aromatic and aliphatic hydrocarbons using deep eutectic solvents: a critical review. *Fluid Phase Equilib*, *448*, 152–167.

Hernández, E., Santiago, R., Moya, C., Navarro, P., & Palomar, J. (2021). Multiscale evaluation of CO2-derived cyclic carbonates to separate hydrocarbons: Drafting new competitive processes. *Fuel Process Technol.*, *212*, 106–639.

Kareem, M. A., Mjalli, F. S., Hashim, M. A., Hadj-Kali, M. K. O., Bagh, F. S. G., & Alnashef, I. M. (2012). Phase equilibria of toluene/heptane with tetrabutylphosphonium bromide based deep eutectic solvents for the potential use in the separation of aromatics from naphtha. *Fluid Phase Equilib*, *333*, 47–54. https://doi.org/10.1016/J.FLUID.2012.07.020

Larriba, M., Ayuso, M., Navarro, P., Delgado-Mellado, N., Gonzalez-Miquel, M., García, J., & Rodríguez, F. (2018). Choline Chloride-Based Deep Eutectic Solvents in the Dearomatization of Gasolines. *Sustainable Chem. Eng.*, *6*, 1039–1047.

Lesek, F., & Mandík, L. (1982). Liquid-liquid equilibrium in binary glycols-toluene and glycols-xylenes systems. *Collect. Czech. Chem. Commun*, *47*, 1686–1694.

Li, J., Zhao, Q., Tang, X., Xiao, K., & Yuan, J. (2014). Liquid−Liquid Equilibria for the Systems: Heptane + Benzene + Solvent (Propylene Carbonate, N,N-Dimethylformamide, or Mixtures) at Temperature from (303.2 to 323.2) K. *J. Chem. Eng. Data*, *59*, 3307−3313.

Lide, D. R. (2006). *CRC Handbook of Chemistry and Physics* (86th ed.). Taylor and Francis Group: London.

M. Letcher, T., & K. Naicker, P. (1998). Ternary Liquid−Liquid Equilibria for Mixtures of an n-Alkane + an Aromatic Hydrocarbon + N-Methyl-2-pyrrolidone at 298.2 K and 1 atm. *J. Chem. Eng. Data*, *43*, 1034–1038. https://doi.org/10.1021/je980114e

Marcilla, A., Reyes-Labarta, J. A., & Olaya, M. M. (2017). Should we trust all the published LLE correlation parameters in phase equilibria? Necessity of their assessment prior to publication. *Fluid Phase Equilib*, *433*, 243−252.

Meindersma, G. W., Podt, A. J. G., & de Haan, A. B. (2006). Ternary liquid–liquid equilibria for mixtures of toluene + n-heptane + an ionic liquid. *Fluid Phase Equilib*, *247*, 158–168. https://doi.org/10.1016/J.FLUID.2006.07.002

Moodley, K., Rarey, J., & Ramjugernath, D. (2018). Model evaluation for the prediction of solubility of active pharmaceutical ingredients (APIs) to guide solid–liquid separator design. *Asian J. Pharm. Sci.*, *13*, 265–278. https://doi.org/10.1016/J.AJPS.2017.12.004

Nagpal, J. M., & Rawat, B. S. (1981). Liquid-Liquid Equilibria for Toluene-Heptane-N-Methyl Pyrrolidone and Benzene-Heptane Solvents. *J. Chem. Technol. Biotechnol*, *31*, 146−150.

Narasigadu, C., Naidoo, M., & Ramjugernath, D. (2014). Ternary Liquid–Liquid Equilibrium Data for the Water + Acetonitrile + {Butan-1-ol or 2-Methylpropan-1-ol} Systems at (303.2, 323.2, 343.2) K and 1 atm. *J. Chem. Eng. Data*, *59*, 3820–3824. https://doi.org/10.1021/je5007218

Raal, J. D., & Mühlbauer, A. L. (1998). *Phase Equilibria: Measurement and Computation*. Taylor and Francis: Bristol.

Rawat, B. S., & Prasad, G. (1980). Liquid-Liquid Equilibria for Benzene-N-Heptane Systems with Triethylene Glycol, Tetraethylene Glycol, and Sulfolane Containing Water at Elevated Temperatures. *J. Chem. Eng. Data*, *25*, 227−230.

Renon, H., & Prausnitz, J. M. (1968). Local Compositions in Thermodynamic Excess Functions for Liquid Mixtures. *AIChE J*, *14*, 135–144.

Saha, M., Rawat, B. S., Khanna, M. K., & Nautiyal, B. R. (1998a). Liquid−Liquid Equilibrium Studies on Toluene + Heptane + Solvent. *J. Chem. Eng. Data*, *43*, 422−426.

Saha, M., Rawat, B. S., Khanna, M. K., & Nautiyal, B. R. (1998b). Liquid−Liquid Equilibrium Studies on Toluene + Heptane + Solvent. *J. Chem. Eng. Data*, *43*, 422−426.

Seyedein Ghannad, S. M., Lotfollahi, M. N., & Haghighi Asl, A. (2011). Measurement of (liquid + Liquid) Equilibria for Ternary Systems of. *J. Chem. Thermodyn*, *43*, 938−942.

Shaahmadi, F., Hashemi Shahraki, B., & Farhadi, A. (2018). Liquid–liquid extraction of toluene from its mixtures with aliphatic hydrocarbons using an ionic liquid as the solvent. *Sep. Sci. Technol*, *53*, 2409–2417. https://doi.org/10.1080/01496395.2018.1449859

Taylor, B. N., & Kuyatt, C. E. (1994). *Guidelines for Evaluating and Expressing the Uncertainty of NIST Measurement Results*. NIST: Gaithersburg, MD.

Treybal, R. E. (1963). *Liquid Extraction* (2nd ed.). McGraw-Hill: New York.

Tripathi, R. P., Ram, A. R., & Rao, P. B. (1975). Liquid-Liquid Equilibriums in Ternary System Toluene-N-Heptane-Sulfolane. *J. Chem. Eng. Data*, *20*, 261−264.

Walas, S. M. (1985). *Phase Equilibrium in Chemical Engineering*. Butterworth: Boston.

Wang, Z., Xia, S., & Ma, P. (2012). (Liquid + Liquid Equilibria for the Ternary System of (N-Formylmorpholine + Ethylbenzene + 2,2,4-Trimethylpentane) at Temperatures (303.15 , 313.15, and 323.15) K. *Fluid Phase Equilib*, *328*, 25−30.

Weissermel, K., & Arpe, H. (2003). *Industrial Organic Chemistry*. Wiley. https://doi.org/10.1002/9783527619191

Werner, S., Haumann, M., & Wasserscheid, P. (2010). Ionic Liquids in Chemical Engineering. *Annu. Rev. Chem. Biomol. Eng*, *1*, 203–230.

4

CHAPTER FOUR

Technoeconomic Analysis and Feasibility of Co-Solvent Mixtures in the Liquid-Liquid Extraction of Aromatics

Abstract

It is desired to improve the efficiency of liquid-liquid extraction processes in the fuel industry by reducing energy consumption and operational costs as well as reducing risk to health, safety and the environment. Co-solvent mixtures for extraction consisting of butane-1,4-diol, propane-1,2,3-triol (glycerol), and 2-methylpentane-2,4-diol (hexylene glycol) were assessed in terms of capital costs, operating costs and total annual costs relative to a baseline process that is employed for the liquid-liquid extraction of toluene from *n*-heptane. Commercial solvents such as sulfolane, morpholine-4-carbaldehyde (NFM), and dimethyl sulfoxide (DMSO) were used for the baseline processes that were simulated in ASPEN Plus V10. The capital costs ranged between 5.8-6.2 million US dollars, while the energy intensity ranged between 1000 - 1400 kJ/kg. The total annual costs for all solvents studied varied between 2.4 - 2.6 million dollars. The results highlighted that these co-solvent mixtures may offer some benefits in terms of total annual cost when the impact of solvent choice is holistically considered.

4.1. Introduction

The production of aromatic compounds such as benzene, toluene and xylene occur as a result of their separation from intermediate petroleum-based streams such as pyrolysis gasoline and reformate. These

compounds are used as feedstocks to the plastics industry (Chen et al., 2017). Traditional distillation is not a feasible method of separation due to the azeotropes that form between the aliphatic and aromatic components, therefore liquid-liquid extraction is utilized when feedstocks are low in aromatic content (Cho et al., 2002). Extractive and azeotropic distillation are used for higher concentrations of aromatics in the feed.

Liquid-liquid extraction involves contacting the feed in a packed or trayed column with a solvent, which the solute (aromatic component) has a greater affinity towards. The solvent is selectively chosen such that there is a formation of two immiscible phases (Treybal, 1963). The raffinate is the stream rich in aliphatics, while the extract is rich in the solvent and aromatics. The solvent is then separated from the extract via traditional distillation and recycled.

The practical suitability of a solvent is generally assessed with experimental liquid-liquid equilibrium (LLE) measurements, and the resulting analysis of the phase behaviour. Ternary systems with an alkane such as *n*-heptane representing the carrier liquid and an aromatic such as toluene representing the solute have been published for decades with a variety of different solvents conventionally used for this application. Phase equilibrium data has been reported for solvents such as sulfolane (Ashcroft et al., 1982; Cassell, Dural, et al., 1989; Cassell, Hassan, & Hines, 1989; Cassell, Hassan, & Junes, 1989; Duan, et al., 2000; J. Chen, Li, et al., 2000; de Fré & Verhoeye, 1976), tetraethylene glycol (Rawat & Prasad, 1980), 1-methylpyrrolidin-2-one (NMP) (Alkhaldi et al., 2009; Al-Zayied et al., 1990; Ferreira et al., 1984), morpholine-4-carbaldehyde (NFM) (D. Chen et al., 2007; Seyedein Ghannad et al., 2011; Wang et al., 2012), N,N-dimethylmethanamide (DMF) (J. Li et al., 2014), and dimethyl sulfoxide (DMSO) (Saha et al., 1998). There has also been a focus on ionic liquids such as 1-methyl-3-octylimidazolium tetrafluoroborate, 1-ethyl-3-methylimidazolium bis{(trifluoromethyl)sulfonyl}amide, tetrabutylphosphonium, 1-ethyl-3-methylimidazolium 1,1,2,2-tetrafluoroethanesulfonate, and 1-ethyl-3-methylimidazolium trifluoromethanesulfonate (Canales & Brennecke, 2016). The difficulties associated with ionic liquids are the costs of large-scale production, the non-renewable feedstocks used, and the disposal method employed (Werner et al., 2010). Deep eutectic solvents have also been considered, obtained from choline chloride, glycerol, and levulinic acid (Hadj-Kali et al., 2017). These present commercial challenges such as having high melting points, and thermal stability regions close to distillation column temperature profiles (Larriba et al., 2018). Cyclic carbonates have been most recently studied as potential solvents due to use of CO_2 and having similar extraction ability compared to sulfolane (Hernández et al., 2021). The performance of the solvent is usually assessed by the selectivity and capacity (distribution coefficient).

In addition to the solvent's requirement to form two phases, it should possess physical properties that are not detrimental in terms of health, safety, and environment. In 2019, the South African government introduced legislation to ban hazardous liquid waste at all landfill sites, motivating the need to study alternative solvents that offer lower risks to health and safety. The solvent should also minimize impact on operating costs such as utilities. Continuous improvement necessitates the identification of new solvents. In a previous study (Brijmohan et al., 2021), the authors' developed and conducted a consolidated screening exercise that took into consideration all aforementioned factors and determined the impact of solvent choice on these factors, with the aim of identifying new solvents. A database was screened for chemicals that met the physical and thermodynamic requirements for liquid-liquid extraction. New potential organic solvents were then scored in a detailed risk assessment that included indices relating to occupational health, safety, and the environment. Lastly, chemicals which passed this stage were evaluated with process designs using ASPEN Plus to ascertain the impact of retrofitting existing plants with the new solvents identified, in terms of energy consumption, capital costs, and total annual costs.

The authors' then published ternary LLE data for the new solvents (Brijmohan et al., 2022b). The results showed that butane-1,4-diol, propane-1,2,3-triol (glycerol) are technically suitable and offer some advantages in terms of health, safety, and the environment. However, the data indicated high selectivities and low capacities, implying that high solvent-to-feed ratios would be required if these solvents were retrofitted to existing plants. The predictive method used (UNIFAC-LL) also incorrectly predicted immiscibility between 2-methyl-2,4-pentanediol and *n*-heptane. However, subsequent tests showed that 2-methyl-2,4-pentanediol may be a suitable co-solvent to 1,4-butanediol and glycerol at different ratios. The authors then published quaternary LLE data which confirmed this to be case (Brijmohan et al., 2022a), and found that co-solvent mixtures in certain ratios significantly increase capacity, rendering them more feasible for retrofitting.

The objective of this study is to conduct an economic assessment of using the co-solvent mixtures (1,4-butanediol + 2-methyl-2,4-pentanediol and glycerol + 2-methyl-2,4-pentanediol) in molar ratios of 1:3 compared to conventional solvents, with the basis of the work being the authors' published experimental equilibrium data, as opposed to theoretical predictions. This is important because companies considering retrofitting conventional solvents with glycerol or 1,4-butanediol would benefit from a comparative study that shows the impact on process economics when these solvents are used in conjunction with 2-methyl-2,4-pentanediol (hexylene glycol).

4.2. Solvent Extraction – Co-Solvent Mixtures

4.2.1 Process Design

Solvent choice has a significant role in the capital and operating costs of the solvent extraction process. The solvent's characteristics affects infrastructure such as the size of the column and the heating duties required in the recovery columns.

In the authors' previous study (Brijmohan et al., 2021), process simulations for the liquid-liquid extraction of toluene from *n*-heptane was developed using ASPEN Plus V10 for the conventional solvents (sulfolane, NFM, and DMSO) as a benchmark or baseline to which the new potential solvents could be compared to. The base case design consisted of a 1500 kg/hr feed stream made up of 30 wt % toluene and 70 wt % *n*-heptane, contacting the solvent in a trayed counter-current extraction column. The solvent enters the top of the column with the minimum rate determined with the use of a sensitivity analysis; the solvent rate was chosen such that the recovery of aromatics to the extract was maximized while the ingress of aliphatics to the raffinate was minimized. This factor is dependent on the aromatic content in the feed, with the selectivity changing at each stage in the column. A large number of stages was initially selected and thereafter minimized in the same manner as the solvent rate, with the use of a sensitivity analysis. The column temperature and pressure profiles were specified to match the feed conditions such that the operation was isothermal and isobaric. The column selectivity profile results in ingress of *n*-heptane to the extract, which is recovered in the distillate of a stripper column and recycled to the extraction column together with a portion of toluene. The valuable aliphatics are then almost entirely recovered in the raffinate. A large number of stages was initially specified in the stripper and then optimized using a sensitivity analysis. Stripper specifications such as the reflux ratio and distillate-to-feed ratio were done using the design spec functionality. The stripper bottoms consisting almost entirely of the solvent and toluene is transported to the solvent recovery column, which uses traditional distillation to separate the solvent and the aromatic component and recycle the solvent to the extraction column. The loss of solvent to the raffinate is recovered using another extraction column which uses water as the solvent. This method is the industrial norm in this process, with the water and solvent mixture recovered downstream via a decanter. The columns utilized in ASPEN V10 were the rigorous 'Extract' and 'Radfrac' models for the extraction and distillation columns respectively. The purpose of this current study is to assess the impact of replacing the conventional solvents with the co-solvent mixtures that the authors' have studied. In order for an effective comparison to be made, it is necessary that the conditions under which the baseline was developed be strictly applied to the new proposed solvents.

Input parameters such as the feed composition and results such as the aromatic recovery and stream purity must be kept consistent; the process designs were developed with the objective of achieving a minimum aromatics recovery of 99 wt %. Due to the diversity in feedstock in refineries around the world, different baselines would need to be developed for specific feed conditions. Process flow diagrams of the system together with stream conditions and results are presented for the new co-solvent mixtures in Figures 4.1 and 4.2. Table 4.1 consists of the comparison between the co-solvent simulation results (this work), and the previously published simulation results using conventional solvents (Brijmohan et al., 2021). Tables 4.2 and 4.3 contain equipment specifications (based on standard sizes) for the large process units such as the solvent extraction columns, distillation columns, and heat exchangers. As this is a conceptual design to compare alternatives, more detailed specifications is determined in the detailed design phase.

In practice, the reboiler temperature of the solvent recovery column for the Sulfolane process is often controlled at 200°C to reduce the extent of sulfolane decomposition. This necessitates a more complex column design with greater capital and operating costs to achieve the same aromatic recoveries and purity at a lower reboiler temperature. The simulations in this study are conceptual and preliminary in nature with the process designs kept consistent between the baseline and proposed solvents. The decomposition of sulfolane in reality would require solvent regeneration as an additional step, also increasing capital and operating costs. In either scenario (capped or uncapped reboiler temperature), the economic viability of sulfolane reduces upon inclusion of further design considerations. Therefore, comparison of the new solvents to the conceptual sulfolane design in this work is conservative in its approach and understates the economic impact of the new mixed solvents relative to sulfolane. Additionally, Li et al. (2011) reported actual plant studies that show it is possible to safeguard against and reduce sulfolane decomposition at higher temperatures by limiting air ingress into the extraction system by optimizing the nitrogen sealing on the solvent, feedstock, and back-washing tanks.

Table 4.1: Comparison of Simulation Results for Co-Solvent Mixtures and Conventional Solvents

	Main Extractor Solvent Rate (kg/hr)	Aliphatic Loss Recovery Column					Solvent Recovery Column						Solvent Recycle Cooler Duty (kW)
		Feed Stage	No. of Stages	Condenser Duty (kW)	Reboiler Duty (kW)	Reboiler Temperature (°C)	Feed Stage	No. of Stages	Reflux Ratio	Condenser Duty (kW)	Reboiler Duty (kW)	Reboiler Temperature (°C)	
Sulfolane	4200	10	16	31.04	163.14	156.77	5	13	0.4	140.52	413.04	286.43	415.17
NFM	4000	15	26	17.9	332.51	162.6	10	15	0.51	99.95	276.78	239.44	490.14
DMSO	3000	13	25	19.72	241.54	148.59	11	17	0.85	139.04	184.93	189.92	264.56
1,4-Butanediol + Hexylene Glycol	5580	8	16	4.15	490.63	159.17	8	15	0.9	107.74	253.96	201.37	633.36
Glycerol + Hexylene Glycol	5759	7	15	4.64	456.62	153.38	7	13	0.7	95.98	284.12	204.07	629.59

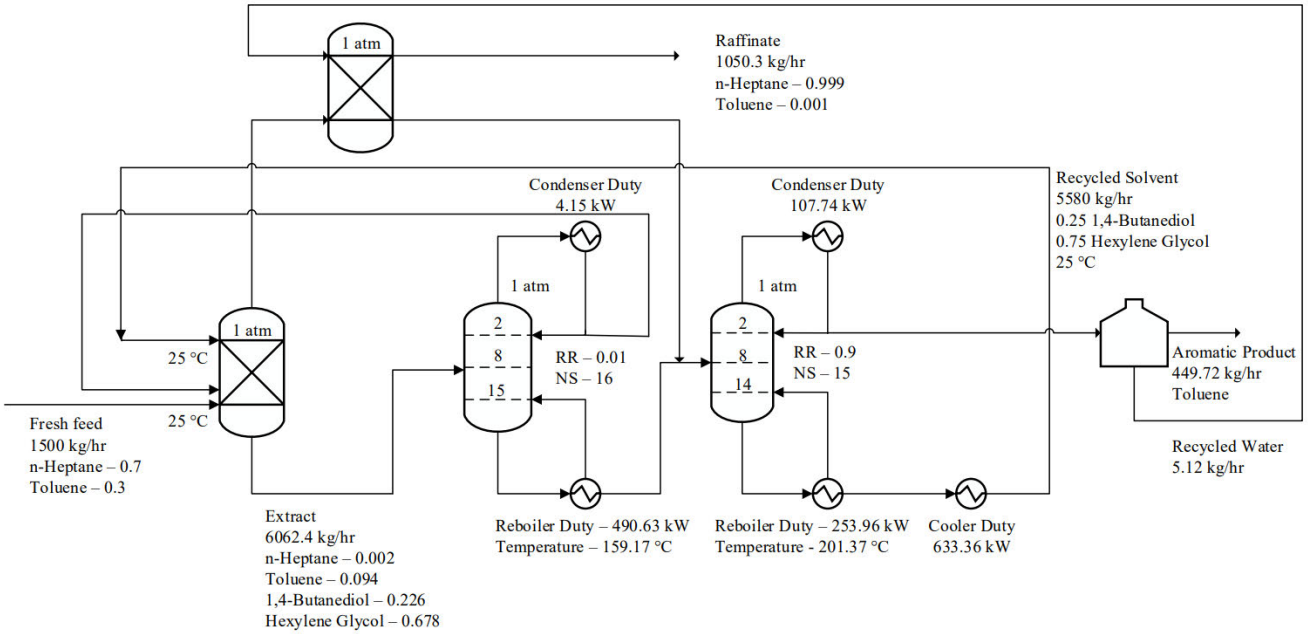

Figure 4.1. Flowsheet for the optimized extraction process with the use of 1,4-butanediol + hexylene glycol as the solvent mixture; compositions reported as wt%.

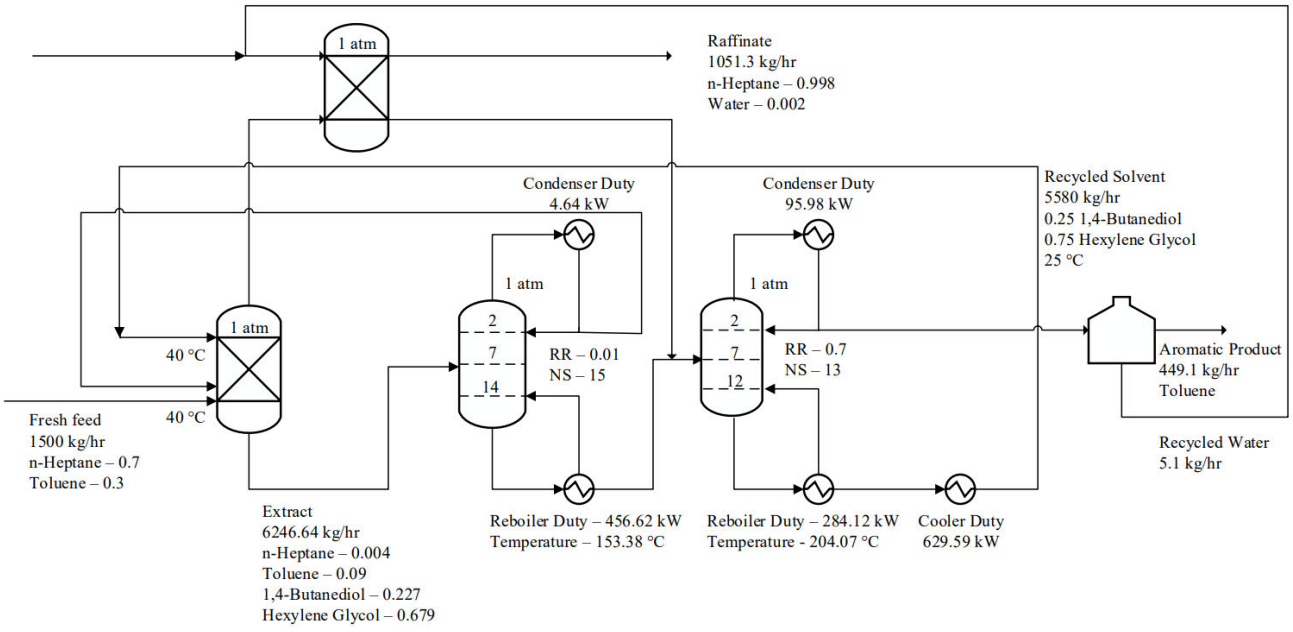

Figure 4.2. Flowsheet for the optimized extraction process with the use of glycerol + hexylene glycol as the solvent mixture; compositions reported as wt%.

Table 4.2: Equipment Specifications of Solvent Extraction and Distillation (Recovery) Columns

	1,4-Butanediol + Hexylene Glycol			
	C1	C2	C3	C4
Diameter (m)	0.762	0.762	0.762	0.457
Tray type	SIEVE	SIEVE	SIEVE	SIEVE
Number of trays	32	7	20	19
Tray spacing (m)	0.6096	0.6096	0.6096	0.6096
Tangent-to-tangent height (m)	25.38	6.27	15.85	15.24
	Glycerol + Hexylene Glycol			
	C1	C2	C3	C4
Diameter (m)	0.762	0.762	0.762	0.457
Tray type	SIEVE	SIEVE	SIEVE	SIEVE
Number of trays	34	7	19	16
Tray spacing (m)	0.6096	0.6096	0.6096	0.6096
Tangent-to-tangent height (m)	27.15	6.27	15.24	13.41

Table 4.3: Equipment Specifications of Heat Exchangers

	1,4-Butanediol + Hexylene Glycol				
	E1	E2	E3	E4	E5
Heat transfer area (m^2)	3.28	47.79	2.30	14.87	55.46
Tube outside diameter (m)	0.0254	0.0254	0.0254	0.0254	0.0254
Tube length extended (m)	0.03175	0.03175	0.03175	0.03175	0.03175
Tube pitch (m)	6.096	6.096	6.096	6.096	6.096
Number of tube passes	1	2	1	2	1
Number of shell passes	1	1	1	1	1
	Glycerol + Hexylene Glycol				
	E1	E2	E3	E4	E5
Heat transfer area (m^2)	1.84	29.96	2.01	18.14	24.56
Tube outside diameter (m)	0.0254	0.0254	0.0254	0.0254	0.0254
Tube length extended (m)	6.096	6.096	6.096	6.096	6.096
Tube pitch (m)	0.03175	0.03175	0.03175	0.03175	0.03175
Number of tube passes	1	2	1	2	1
Number of shell passes	1	1	1	1	1

4.2.2 Thermodynamic Modeling

The liquid phases were modelled with the Non-Random Two Liquid (NRTL) equation (Renon & Prausnitz, 1968), while the Redlich-Kwong (RK) equation of state was used to model the vapour phase. The NRTL model is commonly used to represent deviations from ideality for organic solvents studied in ternary phase equilibrium measurements of systems containing aromatics and aliphatics. For the conventional solvents, binary interaction parameters are generally readily available in the APV100 LLE-ASPEN databank. The new co-solvent mixtures did not have parameters available in the databank and were manually inputted using the authors' published regressed parameters from quaternary data (Brijmohan et al., 2022a). Parameters from binary or ternary LLE data are not available for aliphatic or aromatic systems with hexylene glycol, as these form single phases across the composition range. The aforementioned study highlighted a good correlation between the regressed and experimental data with the Root Mean Square Deviation (RMSD) and Absolute Average Deviation (AAD), thus validating the use of the NRTL model.

Table 4.4 indicates the binary interaction parameters used in this study. The ratio of solvent to co-solvent was chosen based on selectivity and capacity as illustrated in Figures 4.3 and 4.4. A brief overview of selectivity and capacity together with the NRTL model is presented herewith.

Capacity, or distribution coefficient, is the extent to which the solvent is able to extract the aromatic component and highlights the distribution of the solute between the immiscible phases.

$$K_i = \frac{x_i^I}{x_i^{II}} \tag{4.1}$$

The superscripts *I* and *II* represent the solvent-rich and aliphatic-rich phases, while *i* denotes the aromatic component; *x* is the equilibrium molar composition.

The ratio of the distribution coefficients of the aromatic and aliphatic components (*j*) is the selectivity, which has to be greater than unity for a solvent to be effective.

$$S_{ij} = \frac{K_i}{K_j} = \frac{x_i^I x_j^{II}}{x_i^{II} x_j^I} \tag{4.2}$$

The NRTL activity coefficient model was developed by (Renon & Prausnitz, 1968) as a local composition model based on the assumption of non-randomness.

$$\ln(\gamma_i) = \frac{\sum_{j=1}^{n} \tau_{ji} G_{ji} x_j}{\sum_{k=1}^{n} G_{ki} x_k} + \sum_{j=1}^{n} \frac{\sum_{j=1}^{n} G_{ij} x_j}{\sum_{k=1}^{n} G_{kj} x_k} \left(\tau_{ij} - \frac{\sum_{r=1}^{n} \tau_{rj} G_{rj} x_r}{\sum_{k=1}^{n} G_{kj} x_k} \right) \tag{4.3}$$

$$G_{ij} = \exp(-\alpha_{ij} \tau_{ij}) \tag{4.4}$$

$$\tau_{ij} = \frac{g_{ij} - g_{ji}}{RT} \tag{4.5}$$

The activity coefficient in each liquid phase is represented by γ, while *x* is the molar composition of species *i* or *j* in phases *I* and *II* respectively. The level of randomness in the system is designated by α_{ij}, with 0 representing complete randomness. The terms ($g_{ij} - g_{jj}$) and ($g_{ji} - g_{ii}$) are the binary interaction parameters and are regressed from phase equilibrium measurements. *R* and *T* are the ideal gas constant and system temperature respectively.

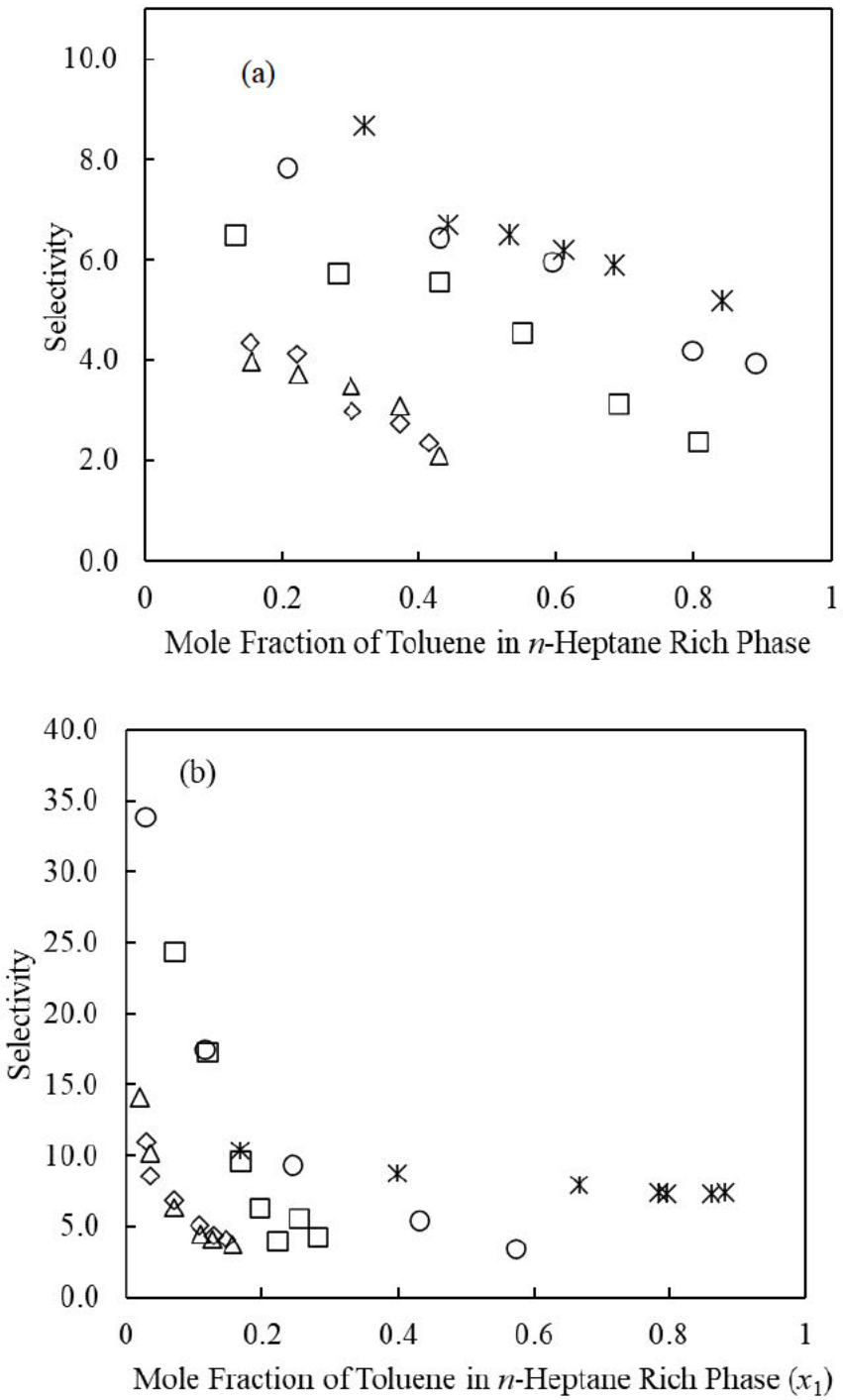

Figure 4.3. Comparison of experimental selectivity data for the systems:

a) *n*-heptane + toluene + 1,4-butanediol + 2-methyl-2,4-pentanediol at 298.2 K and 0.1 MPa;(Brijmohan et al., 2022a) ✳ - pure 1,4-butanediol (Brijmohan et al., 2022b);○ - 3:1 ratio; □ - 1:1 ratio ; △ - 1:3 ratio, ◇ - NRTL model

b) *n*-heptane + toluene + glycerol + 2-methyl-2,4-pentanediol at 313.2 K and 0.1 MPa (Brijmohan et al., 2023); ✳ - pure glycerol (Brijmohan et al., 2022b); ○ - 3:1 ratio; □ - 1:1 ratio ; △ - 1:3 ratio, ◇ - NRTL model

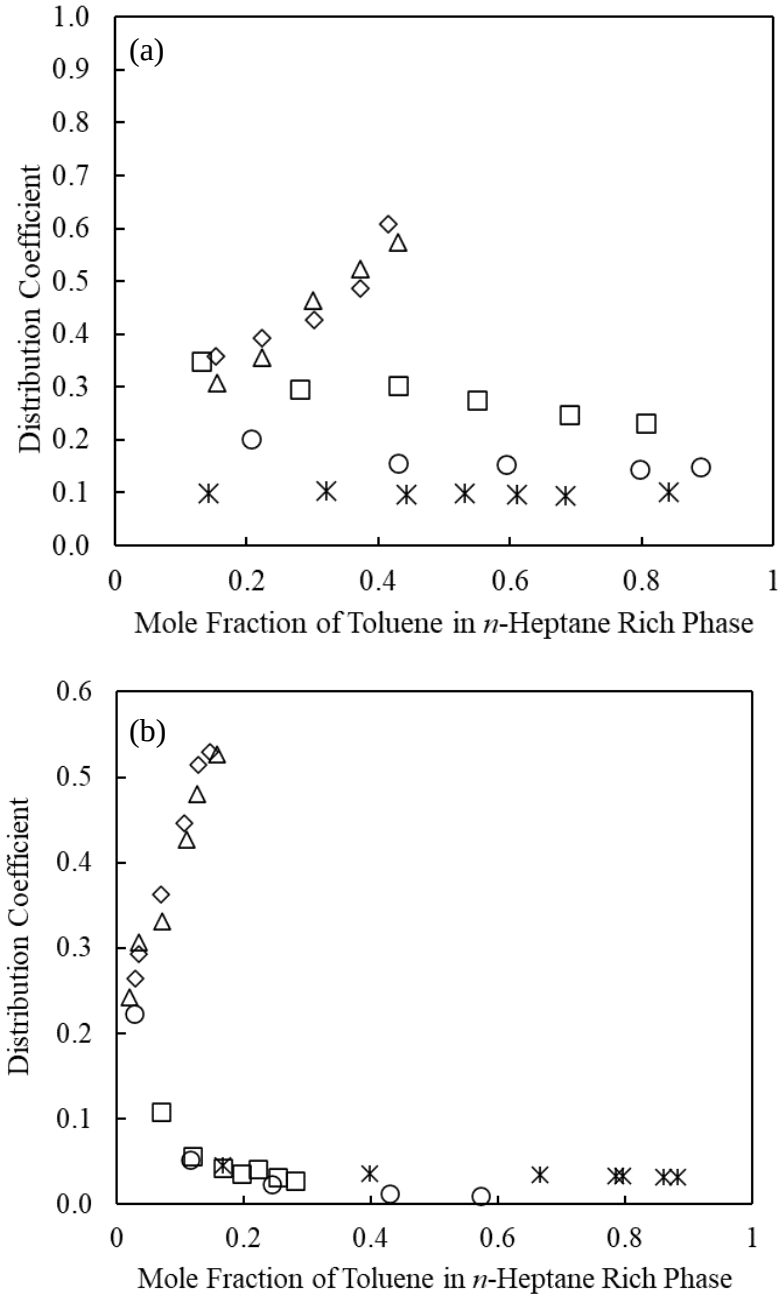

Figure 4.4. Comparison of experimental capacity data for the systems:

a) *n*-heptane + toluene + 1,4-butanediol + 2-methyl-2,4-pentanediol at 298.2 K and 0.1 MPa; ✳ - pure 1,4-butanediol (Brijmohan et al., 2022b); ○ - 3:1 ratio; □ - 1:1 ratio ; △ - 1:3 ratio, ◇ - NRTL model

b) *n*-heptane + toluene + glycerol + 2-methyl-2,4-pentanediol at 313.2 K and 0.1 MPa; ✳ - pure glycerol (Brijmohan et al., 2022b); ○ - 3:1 ratio; □ - 1:1 ratio ; △ - 1:3 ratio, ◇ - NRTL model

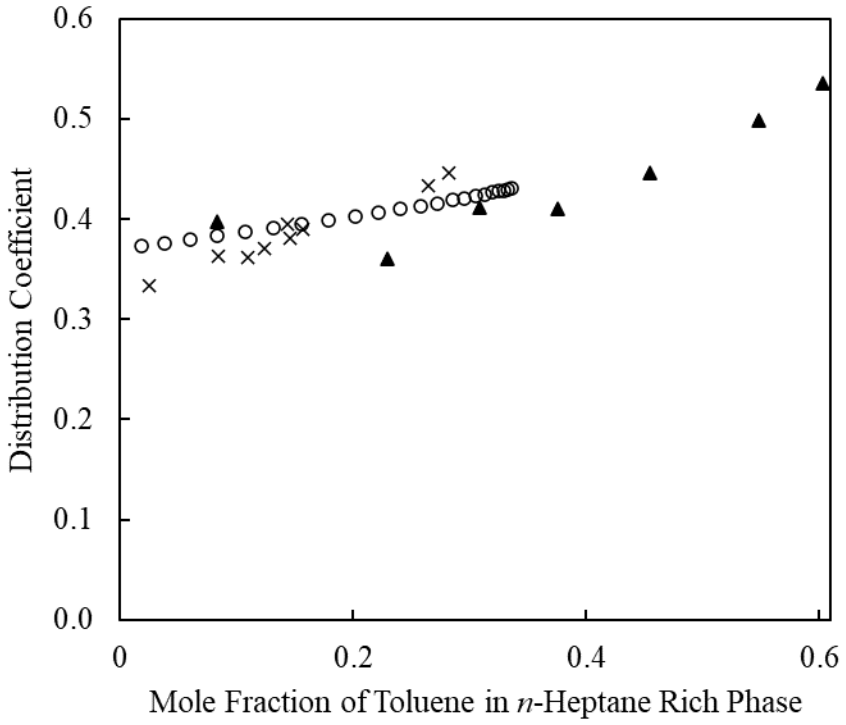

Figure 4.5. Validation of Sulfolane process by comparison of ASPEN Plus V10 simulated data against experimental data for the system *n*-heptane + toluene + sulfolane at 298.2 K and 101.3 kPa; × - Ashcroft et al. (1982); ▲ - Tripathi et al. (1975); ○ - ASPEN simulated extraction column profile

Table 4.4: Binary interaction parameters for the NRTL model

n-Heptane (1) + Toluene (2) + 1,4-Butanediol (3) + Hexylene Glycol (4) at 298.2 K				
i	*j*	τ_{ij}	τ_{ji}	α
1	2	-0.381	-1.169	0.3
1	3	20.27	129.2	0.2
2	3	1.854	11.89	0.2
1	4	4.098	29.98	0.3
2	4	5.610	32.47	0.3
3	4	-0.625	-0.257	0.48
n-Heptane (1) + Toluene (2) + Glycerol (3) + Hexylene Glycol (4) at 313.2 K				
i	*j*	τ_{ij}	τ_{ji}	α
1	2	-0.445	1.056	0.3
1	3	4.124	3.161	0.2
2	3	1.384	2.933	0.2
1	4	4.098	6.633	0.3
2	4	5.610	0.513	0.3
3	4	-0.625	3.302	0.48

The LLE experimental data for the ternary system *n*-heptane + toluene + sulfolane at 298.2 K and 101.3 kPa was used to validate the Sulfolane process to verify the accuracy and simulation capacity of ASPEN Plus, by comparison with the simulated composition profile for the raffinate and extract. Figure 4.5 shows the distribution coefficient calculated using the simulated extract and raffinate compositions for each column stage, compared to the distribution coefficients determined using experimental data. There is agreement between the ASPEN simulated data and experimental data thus indicating that the protocol followed is suitable for the intended purpose.

4.2.3 Process Economics

The nature of the solvent's interaction with the aromatic component influences the solvent to feed ratio which in turn affects infrastructure requirements such as number of stages (column length) and size of heat exchangers. The choice of solvent therefore plays a role in the overall capital cost. Operating costs are affected primarily in terms of utility costs, which the solvent rate is directly

proportional to. However, other factors must be considered such as process conditions like column temperatures and pressures, as well as characteristics of the solvent such as heat capacity and viscosity. These aspects have to be holistically considered in order for effective comparisons to be made.

In this current study, the objective is to consider the impact of using co-solvent mixtures on the process economics of the extraction process compared to conventional solvents. To this end, the capital and operating costs for the process was determined using each solvent, for the conventional as well as proposed co-solvent mixtures. Aspen Process Economic Analyzer (APEA) was used to obtain estimates of the capital and operating costs. The costing done is a preliminary costing and does not contain the numerous complexities and nuances associated with comprehensive costing exercises that would be conducted at the detailed design stage, which is a specialized profession. The purpose of preliminary costing is to assess the impact of different design alternatives, which in essence is what solvent choice amounts to. APEA is a built-in functionality in Aspen Plus and generates results using information provided by construction, procurement and engineering firms. The capital costs consist of the various equipment utilized in the process such as the heat exchangers (preheaters, reboilers, condensers, coolers etc.), reflux drums and pumps, as well as column costs of the liquid-liquid extractors and distillation columns. This is the direct purchase cost of the equipment together with installation costs. The capital costs also include indirect costs such as construction expenses, engineering and supervision costs, as well as legal fees. APEA utilizes a process within ASPEN V10 – after the simulation is completed, the flowsheet models have to be mapped to actual real-world equipment. The next step is the sizing of the equipment according to the specifications made in the simulation together with the process conditions. While this is done by the software, it is critical that the user verifies the default mapping and intervenes if there is any incorrect sizing and resulting erroneous costing models utilizing practical engineering considerations. The user must manually input a particular mapping and sizing if the default contains errors. The costs are then generated as the last evaluation step. APEA also estimates utility costs using the electricity requirement for the various pumps, the cooling mediums used in the condensers and coolers, as well as the heating mediums in the reboilers (low and medium pressure steam). Make-up streams for solvent losses and water are also included as part of the operating costs using bulk market prices.

The Total Annual Cost (TAC) is given in Equation (4.6) and was used as an indicator of the preliminary process economics to be compared for each solvent (Haydary, 2018). The payback time is regarded as the time taken (in years) for the sales of the recovered aromatics to exceed the initial capital investment.

$$\text{TAC} = \frac{\text{Capital Cost}}{\text{Payback Time}} + \text{Utilities} \tag{4.6}$$

$$\text{Payback Time} = \frac{\text{Capital Cost}}{\text{Annual Aromatic Sales}} \tag{4.7}$$

Figure 4.6 compares the capital costs and payback times of the conventional solvents and new proposed co-solvent mixtures. The proposed solvents possess capital costs on par with the conventional solvents. The costs range between 5.8-6.2 million US dollars. As the process design in terms of equipment requirements is the same between all solvents studied, it is expected that the comparative capital requirements fall within a narrow range. The proposed solvents appear to have slightly lower capital costs in the order of 5-8%, as a net effect of differences in column specification throughout the process. However, this analysis is dependent to the baseline used, and would differ depending on the scale of process and the nature of the design in terms of the feed and product specifications. The payback times are inversely proportional to the capital costs and reflect the close ranges of the capital costs between the conventional and proposed solvents. While payback time may be a quick measure, it is not an effective decision-making tool as it uses only the capital costs and does not incorporate the utilities and other operating costs.

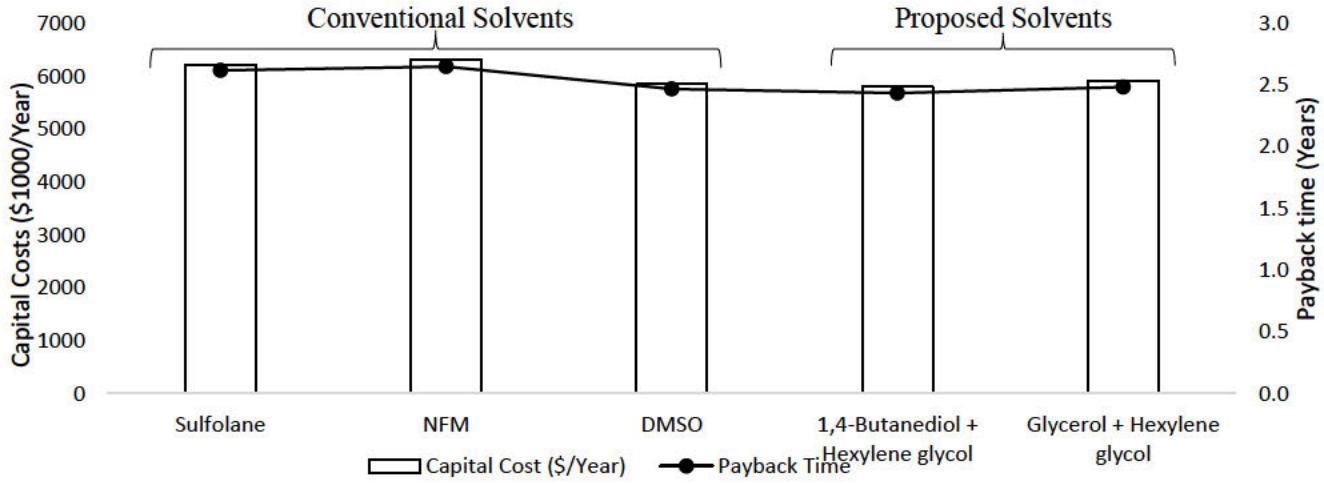

Figure 4.6. Payback times and capital costs for proposed co-solvent mixtures with conventional solvents.

TAC is an indicator that may be more effective in making comparisons as it incorporates capital as well as annual operating costs. Figures 4.7 and 4.8 compares TACs for the conventional and proposed solvents before and after heat integration. Heat recovery was implemented using Aspen Energy Analyzer for both the conventional and proposed solvents, with the heat recovery potentials shown in Figure 4.10 (together with carbon emissions). Figure 4.9 reports the energy intensity (kJ/kg) of the conventional and proposed solvents, which follows the same trend as that of the operating costs. The values range between 1000 – 1400 kJ/kg. Meyers (2016) reports the Sulfolane process as having an energy intensity between 1151 – 1255 kJ/kg. However, energy intensity is a measure that is strongly influenced by economies of scale. It is imperative for throughput rates to be of the same order of magnitude for consistent comparisons to be made. The co-solvent mixtures had TACs comparative to the conventional solvents, indicating that a process using the studied solvents would incur operational costs comparable to the conventional solvents. The heat recovery potential is the total percentage energy saved in the process with the inclusion of heat recovery. The result of this was that the co-solvent mixtures had an overall lower energy consumption (20-38%). The co-solvent mixtures had higher heat recovery potentials due to the location of additional heat in the solvent recovery column reboiler, allowing more MP steam to offset cooling medium requirements in the product cooler. The emissions were determined for two energy sources (coal and natural gas) to generate the LP and MP steam used in the reboilers. This was calculated by using the annual fuel utilization factor, together with the net calorific value and boiler efficiencies to convert the annual energy consumption into the annual amount of coal or natural gas required using each energy source, and thereafter the resulting emissions. The emissions correlate well with the energy consumption, however little correlation is observed with solvent rates or capacity. This highlights the fact that it is important for a holistic and integrated perspective to be applied in the decision-making of these processes.

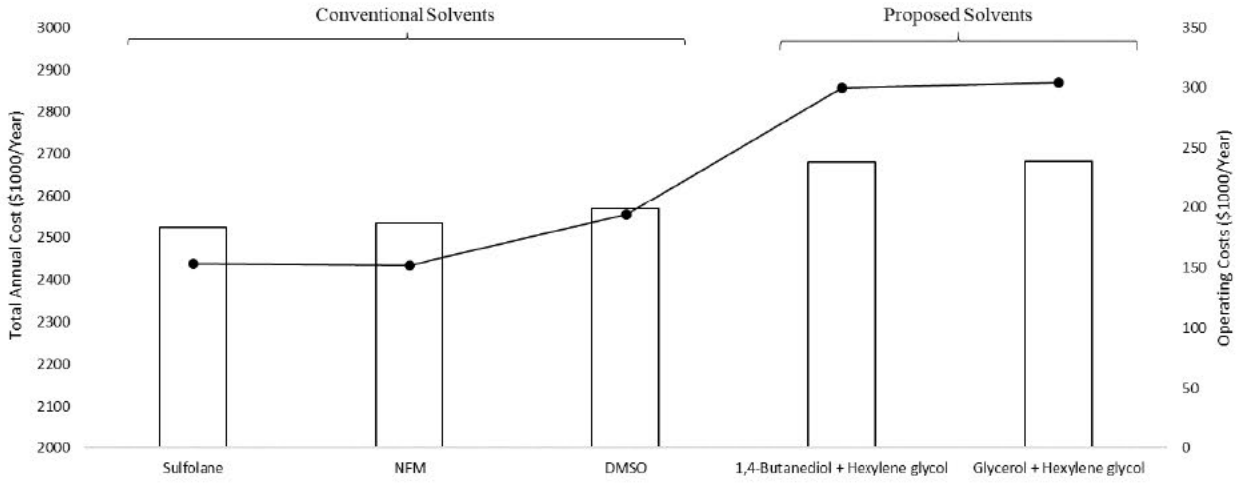

Figure 4.7. Total annual costs and utilities (operating costs) for proposed co-solvent mixtures with conventional solvents prior to heat integration.

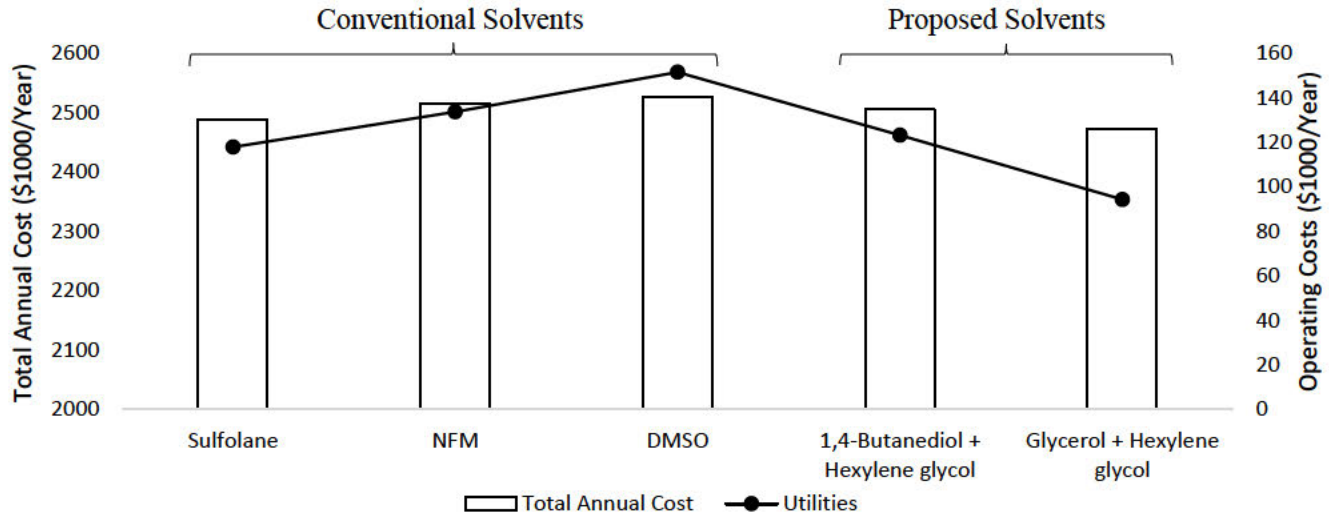

Figure 4.8. Total annual costs and utilities (operating costs) for proposed co-solvent mixtures with conventional solvents.

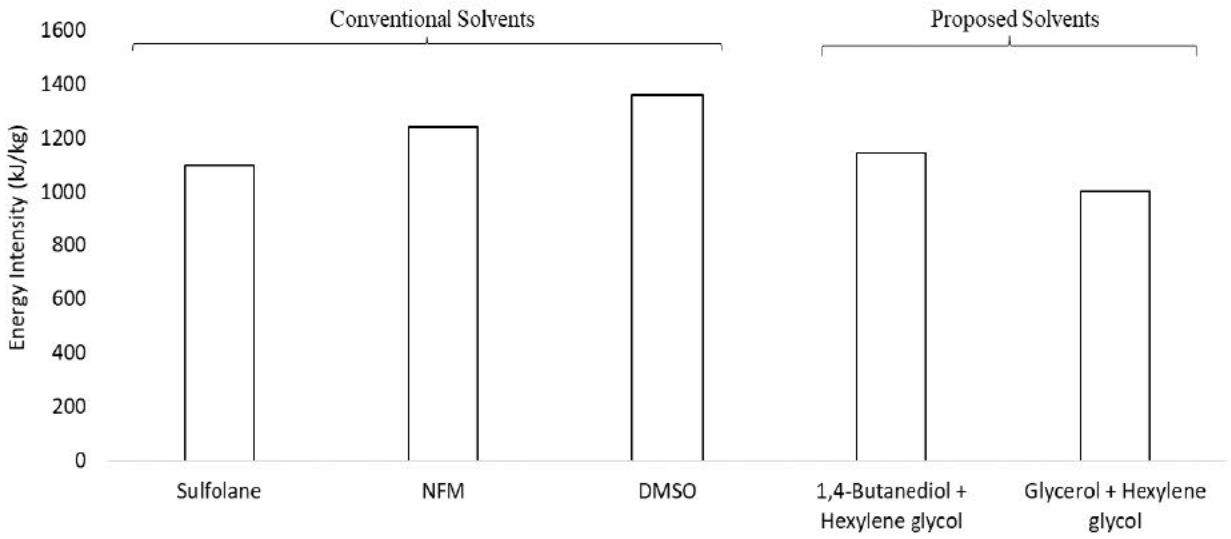

Figure 4.9. Energy intensity (kJ/kg) for proposed co-solvent mixtures with conventional solvents

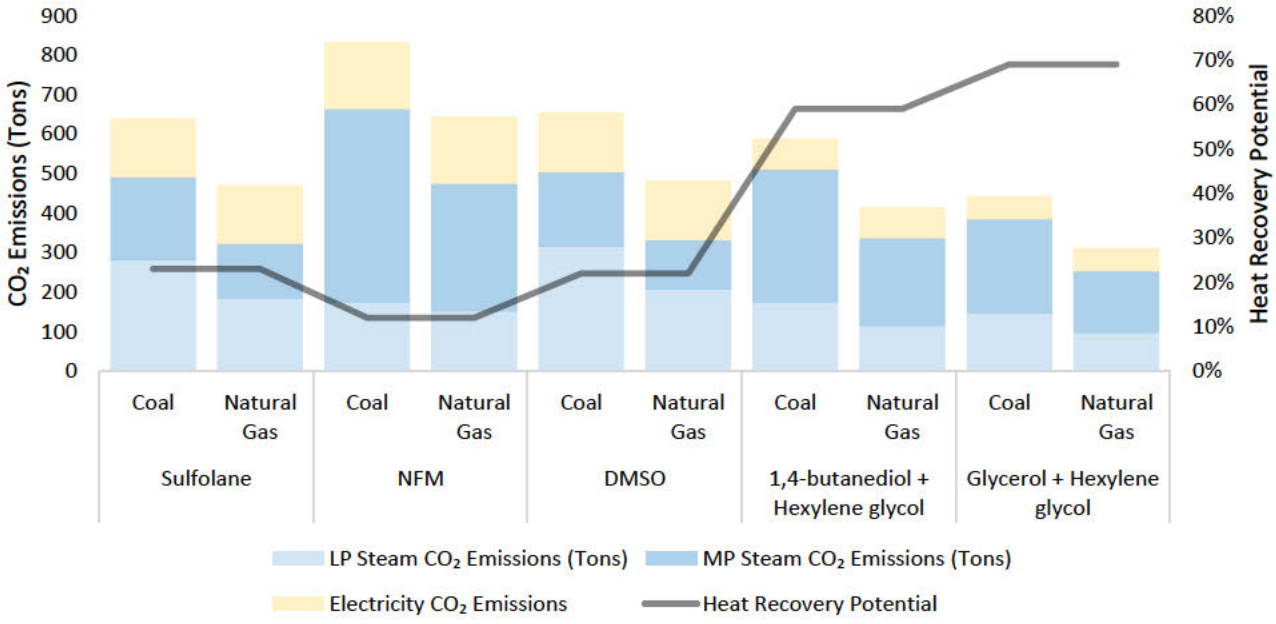

Figure 4.10. Carbon emissions associated with energy consumption together with heat recovery potential for co-solvent and conventional solvents.

4.3. Conclusion

An economic comparison of an aromatic extraction process was conducted for the proposed co-solvent mixtures 1,4-butanediol + hexylene glycol and glycerol + hexylene glycol, against that of conventional and commercial solvents used for this application. Indicators such as energy consumption, capital costs, operating costs and total annual costs were used to make an assessment with the process simulations performed in ASPEN Plus ®. For all solvents studied, the energy intensity varied between 1000 – 1400 kJ/kg, while the capital costs ranged between 5.8 – 6.2 million dollars, and the total annual costs between 2.4 – 2.6 million dollars. The results indicated that the co-solvent mixtures may offer benefits in reducing total annual cost.

4.6. References

Alkhaldi, K. H. A. E., Fandary, M. S., Al-Jimaz, A. S., Al-Tuwaim, M. S., & Fahim, M. A. (2009). Liquid−liquid Equilibria of Aromatics Removal from Middle Distillate Using NMP. *Fluid Phase Equilib, 286*, 190−195.

Al-Zayied, T. A., Al-Sahhaf, T. A., & Fahim, M. A. (1990). Measurement of Phase Equilibrium in Multicomponent Systems of Aromatics with N-Methylpyrrolidone and Predictions with Unifac. *Fluid Phase Equilib*, *61*, 131−144.

Ashcroft, S. J., Clayton, A. D., & Shearn, R. B. (1982). Liquid-Liquid Equilibriums for Three Ternary and Six Quaternary Systems Containing Sulfolane, N-Heptane, Toluene, 2-Propanol, and Water at 303.15 K. *J. Chem. Eng. Data*, *27*, 148–151.

Brijmohan, N., Moodley, K., & Narasigadu, C. (2021). Identification and Screening of Potential Organic Solvents for the Liquid–Liquid Extraction of Aromatics. *Org. Process Res. Dev., 25*, 2230–2248.

Brijmohan, N., Moodley, K., & Narasigadu, C. (2022a). Liquid–Liquid Extraction of Toluene from *n*-Heptane Using Butane-1,4-diol + 2-Methyl-pentane-2,4-diol Liquid Mixtures. *J. Chem. Eng. Data*, *67*, 3177–3185.

Brijmohan, N., Moodley, K., & Narasigadu, C. (2022b). Ternary Liquid–Liquid Equilibrium Data for the *n*-Heptane + Toluene + (Butane-1,4-diol or Glycerol) Systems at 298.2, 313.2, and 333.2 K and 0.1 MPa. *J. Chem. Eng. Data*, *67*(4), 975–983.

Brijmohan, N., Moodley, K., & Narasigadu, C. (2023). Use of Glycerol + 2-Methylpentane-2,4-diol Liquid Mixtures in the Separation of Toluene from *n* -Heptane via Liquid–Liquid Extraction. *Journal of Chemical & Engineering Data*.

Canales, R. I., & Brennecke, J. F. (2016). Comparison of Ionic Liquids to Conventional Organic Solvents for Extraction of Aromatics from Aliphatics. *J. Chem. Eng. Data*, *61*, 1685–1699.

Cassell, G. W., Dural, N., & Hines, A. L. (1989). Liquid-Liquid Equilibrium of Sulfolane-Benzene-Pentane and Sulfolane-Toluene-Pentane. *Ind. Eng. Chem. Res*, *28*, 1369−1374.

Cassell, G. W., Hassan, M. M., & Hines, A. L. (1989). Correlation of the Phase Equilibrium Data for the Heptane-Toluene-Sulfolane and Heptane-Xylene-Sulfolane Systems. *J. Chem. Eng. Data*, *34*, 434−438.

Cassell, G. W., Hassan, M. M., & Junes, A. L. (1989). Phase Equilibria of the Cylohexane-Toluene-Sulfolane and Hexane-Toluene-Sulfolane Ternary Systems. *Chem. Eng. Commun*, *85*, 233−243.

Chen, D., Ye, H., & Hao, W. (2007). Liquid + Liquid Equilibria of heptane + Xylene + N-Formylmorpholine Ternary System. *J. Chem. Thermodyn*, *39*, 1571−1577.

Chen, J., Duan, L. P., Mi, J. G., Fei, W. Y., & Li, Z. C. (2000). Liquid-liquid equilibria of multi-component systems including n-hexane, n-octane, benzene, toluene, xylene and sulfolane at 298.15 K and atmospheric pressure. *Fluid Phase Equilib*, *173*, 109−119.

Chen, J., Li, Z., & Duan, L. (2000). Liquid−Liquid Equilibria of Ternary and Quaternary Systems Including Cyclohexane, 1-Heptene, Benzene, Toluene, and Sulfolane at 298.15 K. *J. Chem. Eng. Data*, *45*, 689−692.

Chen, Q. L., Wang, Q., Zhang, B. J., He, C., & He, C. C. (2017). Optimal Design of a New Aromatic Extractive Distillation Process Aided by a Co-Solvent Mixture. *Energy Procedia*, *105*, 4927–4934.

Cho, J., Ko, M. S., Na, S., & Kim, H. (2002). Simulation of the Aromatic Recovery Process by Extractive Distillation. *Korean J. Chem. Eng*, *19*, 996–1000.

de Fré, R. M., & Verhoeye, L. A. (1976). Phase Equilibria in Systems Composed of an Aliphatic and an Aromatic Hydrocarbon and Sulpholane. *J. Appl. Chem. Biotechnol*, *26*, 469−487.

Ferreira, P. O., Ferreira, J. B., & Medina, A. G. (1984). Liquid-liquid equilibria for the system N-methylpyrrolidone + toluene + *n*-heptane: UNIFAC interaction parameters for N-methylpyrrolidone. *Fluid Phase Equilib*, *16*, 369−379.

Hadj-Kali, M. K., Salleh, Z., Ali, E., Khan, R., & Hashim, M. A. (2017). Separation of aromatic and aliphatic hydrocarbons using deep eutectic solvents: a critical review. *Fluid Phase Equilib*, *448*, 152–167.

Haydary, J. (2018). *Chemical Process Design and Simulation*. John Wiley & Sons, Inc.

Hernández, E., Santiago, R., Moya, C., Navarro, P., & Palomar, J. (2021). Multiscale evaluation of CO2-derived cyclic carbonates to separate hydrocarbons: Drafting new competitive processes. *Fuel Process Technol.*, *212*, 106–639.

Larriba, M., Ayuso, M., Navarro, P., Delgado-Mellado, N., Gonzalez-Miquel, M., García, J., & Rodríguez, F. (2018). Choline Chloride-Based Deep Eutectic Solvents in the Dearomatization of Gasolines. *Sustainable Chem. Eng.*, *6*, 1039–1047.

Li, D., Li, H., & Liu, D. (2011). Factors Affecting Decomposition of Sulfolane Solvent in Aromatic Extraction Units and Countermeasures. *Zhongwai Nengyuan*, *16*(2), 95–99.

Li, J., Zhao, Q., Tang, X., Xiao, K., & Yuan, J. (2014). Liquid−Liquid Equilibria for the Systems: Heptane + Benzene + Solvent (Propylene Carbonate, N,N-Dimethylformamide, or Mixtures) at Temperature from (303.2 to 323.2) K. *J. Chem. Eng. Data*, *59*, 3307−3313.

Meyers, R. A. (2016). *Handbook of petroleum refining processes*. McGraw-Hill Education.

Rawat, B. S., & Prasad, G. (1980). Liquid-Liquid Equilibria for Benzene-N-Heptane Systems with Triethylene Glycol, Tetraethylene Glycol, and Sulfolane Containing Water at Elevated Temperatures. *J. Chem. Eng. Data*, *25*, 227−230.

Renon, H., & Prausnitz, J. M. (1968). Local Compositions in Thermodynamic Excess Functions for Liquid Mixtures. *AIChE J*, *14*, 135–144.

Saha, M., Rawat, B. S., Khanna, M. K., & Nautiyal, B. R. (1998). Liquid−Liquid Equilibrium Studies on Toluene + Heptane + Solvent. *J. Chem. Eng. Data*, *43*, 422−426.

Seyedein Ghannad, S. M., Lotfollahi, M. N., & Haghighi Asl, A. (2011). Measurement of (liquid + liquid) equilibria for ternary systems of (N-formylmorpholine + benzene + cyclohexane) at temperatures (303.15, 308.15, and 313.15) K. *J. Chem. Thermodyn*, *43*, 938−942.

Treybal, R. E. (1963). *Liquid Extraction* (2nd ed.). McGraw-Hill: New York.

Tripathi, R. P., Ram, A. R., & Rao, P. B. (1975). Liquid-Liquid Equilibriums in Ternary System Toluene-N-Heptane-Sulfolane. *J. Chem. Eng. Data*, *20*, 261−264.

Wang, Z., Xia, S., & Ma, P. (2012). (Liquid + Liquid Equilibria for the Ternary System of (N-Formylmorpholine + Ethylbenzene + 2,2,4-Trimethylpentane) at Temperatures (303.15 , 313.15, and 323.15) K. *Fluid Phase Equilib, 328*, 25−30.

Werner, S., Haumann, M., & Wasserscheid, P. (2010). Ionic Liquids in Chemical Engineering. *Annu. Rev. Chem. Biomol. Eng, 1*, 203–230.

5

CHAPTER FIVE

The *A Priori* Screening of Potential Organic Solvents Using Artificial Neural Networks

Abstract

A QSPR model using artificial neural networks was constructed to estimate the binary interaction parameters for the temperature-dependent form of the NRTL model with the objective of using it as a supplement to assist limitations of group contribution methods in the screening of potential solvents for liquid-liquid extraction processes. Parameters were regressed using experimental LLE and VLE data and checked for consistency. Molecule structures were drawn and descriptors determined with the use of Materials Studio. The QSPR model uses 31 descriptors as input and produced absolute average deviations of 0.23 and 0.19 for each pair of binary interaction parameters respectively. The development of this model is shown to be effective in improving the robustness of solvent screening processes.

5.1. Introduction

Liquid-liquid extraction is commonly used when traditional distillation is not a viable separation method due to azeotropes that form between components that need to be separated in a liquid mixture. In the case study involving the separation of aromatics from aliphatics, liquid-liquid extraction is a feasible method that uses a solvent such as sulfolane to contact the mixture and form two immiscible phases, selectively blending with the aromatic components in the denser phase in an extraction column. The solvent and aromatics can thereafter be separated downstream via traditional distillation (Cho et al., 2002).

The choice of solvent plays an important role in the performance of the process in terms of economics, energy consumption, emissions, health, and safety. The solvent should possess characteristics that fundamentally serve to facilitate the formation of separate phases in the column, but at the same time should minimize risk to the health of workers and limit impact on the environment. The solvent should also optimize profits by reducing capital and operating costs. Solvent selectivity for the solute component impacts the design of the column in terms of dimensions and thereby influences capital costs, whereas solvent capacity determines solvent rates which has a downstream impact on utilities and other operating costs. The authors in a previous study (Brijmohan et al., 2021), consolidated all aforementioned factors such as health, safety, environment, process economics, solvent properties etc, into a screening process that identifies and assesses the suitability of a solvent for a particular liquid-liquid extraction application. A database of chemicals was created for which each chemical was evaluated in terms of thermodynamic criteria (selectivity) using UNIFAC-LLE, followed by a detailed risk assessment that consisted of various indices related to occupational health, safety, and the environment. The last stage of the screening process was the creation of process designs in ASPEN Plus V10 to determine if new potential solvents had superior performance in terms of process economics (capital, operating, and total annual costs) compared to a base case involving conventional solvents.

For the case study of the extraction of aromatics from aliphatics, the authors followed up the solvent screening results with experimental liquid-liquid equilibrium data that compared solvent phase behaviour with conventional solvents (Brijmohan et al., 2022a). Some solvents such as butane-1,4-diol and propane-1,2,3-triol (glycerol) offered benefits in terms of health and safety, but possessed poor solvent capacities, requiring large solvent-feed ratios. The predictive model used in the screening process (UNIFAC) (Fredenslund et al., 1975), was not suitable for certain options such as 2-methyl-2,4-pentanediol, as it incorrectly predicted immiscibility with *n*-heptane. However, it was later determined that 2-methyl-2,4-pentanediol serves as an effective co-solvent (Brijmohan et al., 2022b).

The objective of this study is to address the shortcomings in the screening process, which depends on predictive activity coefficient models such as UNIFAC-LLE. It is difficult to reliably predict liquid-liquid equilibrium, and it would benefit researchers to have additional methods to supplement the predictions from the aforementioned model to improve the robustness of the screening process. UNIFAC-LLE also depends on structural parameters of functional groups that are regressed from experimental data. This means that predictions can only be made for molecules which possess functional groups that have structural parameters available. As a result, a large number of potential organic solvents cannot be screened.

Machine learning tools are increasingly being considered as alternatives in the estimation of thermodynamic properties. Recently, Rittig et al. (2023) developed a graph neural network (GNN) applied to molecular properties, as advanced by Coley et al. (2017), that produces high-quality predictions of infinite dilution activity coefficients (temperature-dependent) for a variety of solutes in ionic liquids. This approach represents molecules, specifically the solute and solvent, as a molecular graph in which the atoms are nodes and the bonds edges. The molecular graphs of component molecules are condensed into a single vector used to represent the solution mixture. Sanchez Medina et al. (2022) have also used GNNs to predict constant temperature limiting activity coefficients and have also incorporated this machine learning approach for error-correction in the models UNIFAC and COSMO-RS (Klamt, 1995). The deep-learning model DeepGamma by Felton et al. (2022) uses GNNs trained on COSMO-RS calculations to provide activity coefficient predictions for binary mixtures.

Jirasek et al. (2020) developed a temperature-independent model for infinite-dilution activity coefficients using matrix completion methods, in which a sparse matrix is created with solute-solvent combination activity coefficients as entries, and patterns between rows and columns thereafter used to complete the matrix by filling in the unknown entries. Damay et al. (2021) extended this model to include temperature-dependency using the Gibbs-Helmholtz relation. Another model using matrix completion methods with a neural recommender system was proposed by Chen et al. (2021) to predict temperature-dependent activity coefficients at infinite dilution for solutes in ionic liquids.

Natural language processing has produced the machine learning method of transformers, which when applied to the prediction of molecular properties uses identifiers such as SMILE strings as input and trains artificial neural networks (ANNs) to ascertain relations between the input sequence and the molecular property under consideration (Rong et al., 2020; Schwaller et al., 2019; Weininger, 1988). Recently, A transformer model called SMILES-to-Transformer (SPT) has been developed to predict temperature-dependent limiting activity coefficients using SMILES strings (Winter et al., 2022). A challenge associated with transformer methods is that large datasets are required to train the model in the order of millions of datapoints, which are not readily available for numerous molecular properties. Winter et al. (2022) addressed this with pretraining of the SPT model using synthetic property data (from COSMO-RS calculations) and thereafter fine-tuning of the outputs using experimental data. The amount of data required for pretraining in this approach is computationally demanding and is to an extent subject to limitations in the accuracy of COSMO-RS.

This current study seeks to address challenges in the solvent screening process with the use of a Quantitative-Structure-Property-Relationship (QSPR) model developed in an ANN to produce *a priori*

predictions of binary interaction parameters for the NRTL model, which is known to adequately model phase behaviour. Using machine learning techniques to estimate parameters for established models such as the NRTL model assures a thermodynamically consistent approach (delineated by the Gibbs-Duhem relation), as opposed to prediction of activity coefficients based purely on statistical inferences without physical knowledge. Effectiveness of machine learning methods may also be highly dependent on quality of experimental data used to train the model. This work emphasizes inspection and filtering of literature data used to train ANNs. It is increasingly expected that published NRTL parameters using experimental data be checked for thermodynamic consistency. In this current study checks are performed on the training NRTL parameters to ensure they are thermodynamically consistent for inclusion in the ANN. Previous studies developed ANNs separately for temperature-independent interaction parameters for VLE (Gebreyohannes et al., 2013) and LLE (Gebreyohannes et al., 2014a). This work develops a consolidated temperature-dependent ANN model that is simultaneously trained with both VLE and LLE data with the objective of identifying if a component pair lies in the single or two-phase region, such that a solvent's suitability (from the solvent screening process) may be validated.

5.2. Nonrandom Two-Liquid Activity Coefficient Model

The Nonrandom Two-Liquid (NRTL) model (Renon & Prausnitz, 1968), is extensively used in phase equilibrium studies to represent liquid phase behaviour. It features several adjustable parameters per binary system which may be employed for complex multicomponent streams. This model was chosen as it is capable of providing precise representations of liquid-liquid equilibrium behaviour. However, unlike UNIFAC-LLE, it cannot be generalized to systems which have limited or no data available, which limits its use as a solvent screening tool. The intention is to use the NRTL model as a supplement to UNIFAC-LLE predictions to assist with validation of solvent-screening results.

The model is constructed on the theory of local composition on the assumption of non-randomness. The activity coefficients are represented as shown in Equation (5.1):

$$\ln(\gamma_i) = \frac{\sum_{j=1}^{n} \tau_{ji} G_{ji} x_j}{\sum_{k=1}^{n} G_{ki} x_k} + \sum_{j=1}^{n} \frac{\sum_{j=1}^{n} G_{ij} x_j}{\sum_{k=1}^{n} G_{kj} x_k} \left(\tau_{ij} - \frac{\sum_{r=1}^{n} \tau_{rj} G_{rj} x_r}{\sum_{k=1}^{n} G_{kj} x_k} \right) \tag{5.1}$$

$$G_{ij} = \exp(-\alpha_{ij} \tau_{ij}) \tag{5.2}$$

$$\tau_{ij} = \frac{g_{ij} - g_{ji}}{RT} \tag{5.3}$$

The activity coefficient is designated by γ in each liquid phase, while molar composition is given by x in phases *I* and *II* for species *i* or *j*. The level of randomness in the system is represented by α_{ij}, with complete randomness characterized by a value of 0. The binary interaction parameters (regressed from phase equilibrium measurements) are given by terms ($g_{ij} - g_{jj}$) and ($g_{ji} - g_{ii}$). R and T are the ideal gas constant and system temperature respectively.

5.3. Prediction of Interaction Parameters for Solvent Screening

The first step in developing the artificial neural network (ANN) was creating a database of binary interaction parameters for the NRTL model using VLE and LLE data. This entailed extracting the data and correlating the parameters for each system. The next step was the generation of the set of descriptors. 3D structures for each molecule were drawn in Materials Studio. These structures were optimized in terms of geometry using the Forcite module to minimize the conformation energy. Using the optimized structures, descriptors were calculated using Materials Studio, and thereafter the number of variables were reduced using a correlation matrix. The final set of descriptors was then used to develop the ANN, trained using the regressed parameters. Each of the aforementioned steps are expanded and discussed in detail in the sections that follow.

5.3.1 Creation of Database and Regression of Binary Interaction Parameters

The NIST database was used to identify the systems for which LLE data was published in peer-reviewed journals. This initial list consisted of approximately 6 000 binary systems, which was filtered based on the parameters of the study. Firstly, inorganic systems were excluded from the database as organic chemicals was the primary focus. Despite considerable research on ionic liquids, organic chemicals remain the norm in large-scale industrial processes due to the difficulty and costs associated with bulk production of ionic liquids. Thereafter, the actual LLE data for the remaining systems was individually accessed from NIST via Aspen Plus V10. The database was further reduced by screening of the LLE data. Datasets which had less than four points were not included in the regression. Also excluded, were systems out of a desired temperature range (10 – 80°C). The reduction and validation of the data used was done in

conjunction with the regression of the binary interaction parameters using LLE data, performed using the thermodynamic criterion for equilibrium in terms of fugacity coefficients in solution ($\hat{f}_i$).

$$\left(\hat{f}_i\right)^I = \left(\hat{f}_i\right)^{II} \tag{5.4}$$

$$\left(x_i \gamma_i\right)^I = \left(x_i \gamma_i\right)^{II} \tag{5.5}$$

The molar compositions in each phase are denoted by *x*, the activity coefficients by γ, the particular species by *i*, and the equilibrium phases by *I* and *II* respectively.

Previous studies (Gebreyohannes et al., 2014b) developed ANNs using the temperature-independent form of the NRTL model; the current study includes the temperature dependence by regressing the binary interaction parameter using temperature-dependent parameters a_{ij} and b_{ij} as per Equation (5.6).

$$\tau_{ij} = a_{ij} + \frac{b_{ij}}{T} \tag{5.6}$$

The dimensionless interaction parameter is denoted by τ_{ij}, and temperature by *T*.

As stated, LLE data for each system was extracted from NIST using Aspen Plus V10, and the parameters for each dataset was regressed thereafter in Aspen Plus V10. The regression was performed with the Britt-Leucke algorithm and Deming Initialization method, using a maximum likelihood objective function. The regression was also tested with a non-linear least squares objective function and multiple initial values for the regressed parameters. There were negligible differences observed in the correlation with different objective functions and initial values.

The RMSD (Root Mean Square Deviation) for binary systems was determined for each regression and used to assess the quality of the fit.

$$\mathrm{RMSD} = \left\{ \frac{\sum_a \sum_b \sum_c \left\{ x_{abc}(\mathrm{exp}) - x_{abc}(\mathrm{calc}) \right\}^2}{4k} \right\}^{1/2} \tag{5.7}$$

The database was further reduced upon consideration of the RMSD for each regression – it was observed that the goodness of the fit depended on the experimental method used to measure the data. Actual tie-line data were producing low RMSDs (less than 0.05), while binodal curves without tie-lines (measured by cloud-point or other methods) were producing higher RMSDs (greater than 0.1). On this basis, only datasets which consisted of tie-line data were included in the final database used to train the ANN model.

Preliminary development and testing of the ANN indicated that training the model using only LLE data is insufficient in addressing the stated objectives of improving the robustness of the solvent screening methodology. Previous approaches tended towards separate models for LLE and VLE data, which limits applicability in solvent screening when it is required to determine miscibility between pairs of components. For example, it was not known if previously developed models using LLE data are able to predict interaction parameters for a completely miscible component pair that would otherwise be modelled using VLE data. Testing of preliminary ANNs indicated that training a model using only LLE data results in increased probabilities of the model incorrectly predicting multiple phases for unknown sets of components. If the miscibility of certain chemicals is unknown, it would not be apparent if VLE or LLE data should be the basis to make an *a priori* estimation. It was therefore necessary to develop a single ANN trained simultaneously on both LLE and VLE data such that a distinction could be made between the single and two-phase regions.

Extending the database to include binary interaction parameters from VLE data was done in a manner similar to the process followed for the LLE data. The component list was used to identify the applicable systems for which VLE data was available and then extracted using Aspen Plus V10 in the same manner as per the LLE data. Thereafter the data is regressed using the maximum likelihood function. The criterion for equilibrium used for data correlation is as given in Equation (5.8), assuming an ideal gas in the vapour phase.

$$y_i P = x_i \gamma_i P_i^S \tag{5.8}$$

Total pressure of the system is denoted by P, while P_i^S is the saturated vapour pressure of component i. The vapour phase and liquid phase mole compositions for component i are denoted by y and x respectively. The saturated vapour pressures were determined with the Antoine equation, with parameters taken from the Aspen Plus ® V10 physical property database. The data was checked for thermodynamic consistency in Aspen Plus ® V10 using the equal area consistency test (as part of the regression). Systems that did not pass the consistency test were excluded from the overall database used to train the final ANN model.

The non-randomness parameter α_{ij} was fixed at a value of 0.2 in this study. The phase separation boundary is specific to the value chosen; therefore, it is important that this value is kept constant to ensure that the analysis is consistent. The regressed binary interaction parameters were checked for consistency using the tool developed by Marcilla et al. (2017), and thereafter plotted in Figure 5.1, which shows τ_{ji} as a function

of τ_{ij}. Marcilla et al. (2011) developed the boundary correlations between the single and two-phase regions as a function of the binary interaction parameters for an α_{ij} of 0.2. Figure 5.1 highlights that parameters obtained with VLE data should lie in the single-phase region, while parameters obtained with LLE data should lie in the two-phase region. Systems that did not meet this check were excluded from the final database used to train the ANN. The final dataset consisted of 110 compounds in various binary combinations. The output vector consists of 3180 points of which 1059 is LLE data and 2121 VLE data. Figure 5.2 indicates the percentage distribution of functional groups used in the final model, highlighting that data from a diverse set of functional groups was used to train the ANN.

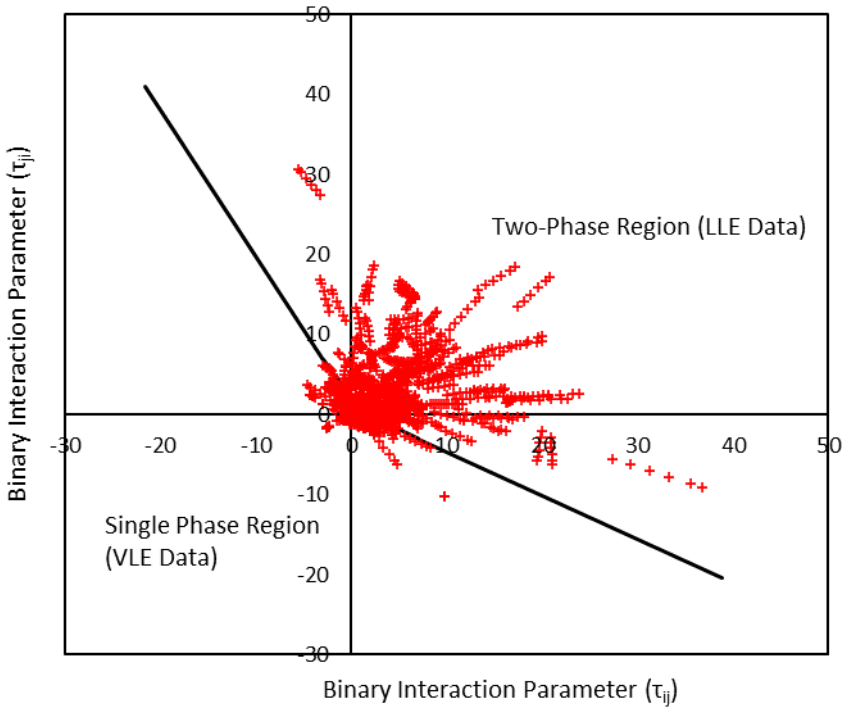

Figure 5.1: Regressed binary interaction parameters of the final dataset represented on miscible and partly miscible regions; solid line indicates phase boundary separation.

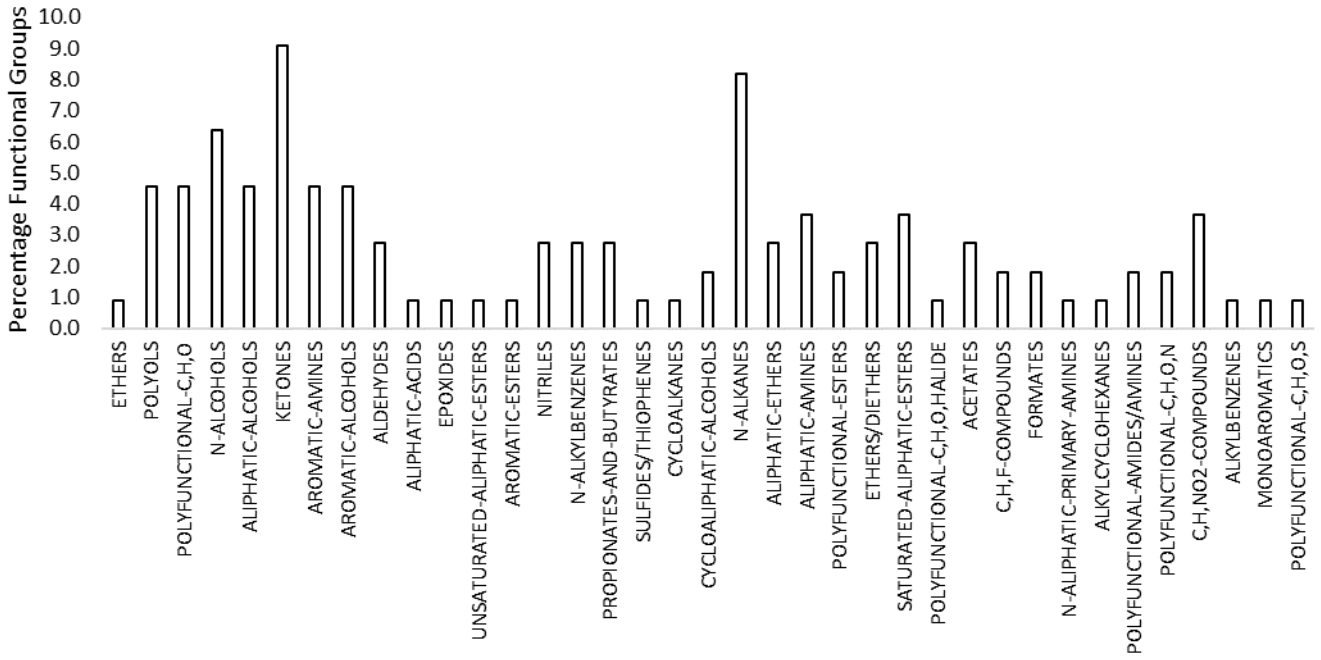

Figure 5.2: Percentage distribution of functional groups for compounds in database

5.3.2 Calculation and Reduction of Descriptors

The descriptors of the QSPR model are properties of the molecule that may be determined only through knowledge of the molecule's structure. The final list of molecules that made up the systems for which the binary interaction parameters were regressed were inputted into Materials Studio. The structures were drawn for each molecule using the sketching tools in Materials Visualizer and thereafter their geometries were optimized using the Forcite module. A classical forcefield is used to represent the potential energy surface on which the atomic nuclei move. The geometry of the structure (in terms of atomic coordinates) is iteratively refined until the potential energy surface is minimized. The "Smart" algorithm was used to conduct the optimization, which is a cascade of the adjusted basis set employing Newton-Raphson, quasi-Newton, and steepest descent methods. The Dreiding forcefield was used, for which the functional form consists of electrostatic interactions described by atomic monopoles and a distance-dependent Coulombic term, and van der Waals interactions and hydrogen bonding by the Lennard-Jones potential (Mayo et al., 2002). Atomic point charges were calculated using the QEq method, which is based on the equilibration atomic electrostatic potentials with respect to a local charge distribution (Rappe and Goddard, 2002). In consideration of other forcefields such as COMPASS and Universal, each have different mathematical forms and have different approaches in modeling intramolecular and intermolecular forces. As a result,

each forcefield results in different total energies for each optimized structure. However, surface potentials were not required as quantum-mechanical descriptors were not used in the final model, and therefore alternative forcefields produces little variation in the molecular descriptors used in this current study. Molecular descriptors were computed for compounds from a variety of functional groups optimized using Universal and COMPASS, and thereafter compared to Dreiding. The results indicated that there was less than 2% variation in descriptors between the forcefields considered. Also, the VAMP routine was used in Materials studio to determine the dipole moment for the optimized structures and this was compared to experimental dipole moments drawn from ASPEN's physical property database (*Aspen Plus*, 2004). Dreiding and COMPASS were observed to more closely agree with measured data.

Dreiding offers a benefit in having a term that accounts for hydrogen bonding on more electronegative atoms. It has been used effectively in various studies involving organic components such as by Pan et al. (2007) in molecular dynamics simulations to determine diffusion coefficients of aromatic compounds in polymer membranes, Zeng et al. (2003) in performing molecular dynamics simulations of organic and inorganic composites, Benitez et al. (2008) in the analysis of density functionals for complex organic molecules such as rotaxanes and catenanes, and by Altintas and Keskin (2016) in adsorption computational screening studies for separation of small hydrocarbons.

The optimized structures were then used to generate descriptors using the QSPR model engine in Materials Studio. Different categories of descriptors available in Materials Studio are given below.

Atom Volumes and Surfaces: volumes and surfaces areas as well as properties based on surface types such as van der Waals, Connolly and Accessible Solvent.

Atomistic: atom-based properties such as the number of atoms, elements, charges, and molecular mass.

Topological: properties that are derived from the molecule's general shape, size, and flexibility. An illustration of a topological descriptor (shadow area and shadow area fraction) used in this study is indicated in Figure 5.3. Shadow area refers to the projection of the molecular surface area on the *x*-*y*, *y*-*z*, and *x*-*z* planes. Shadow area fraction is the ratio of the surface area projection to the area bounded by the rectangle in Figure 5.3. Shadow area and shadow area fraction depend on conformation and orientation of the molecule. As such, these descriptors are calculated after rotating the molecule to align the principal moments of inertia with the *x*, *y*, and *z* axes.

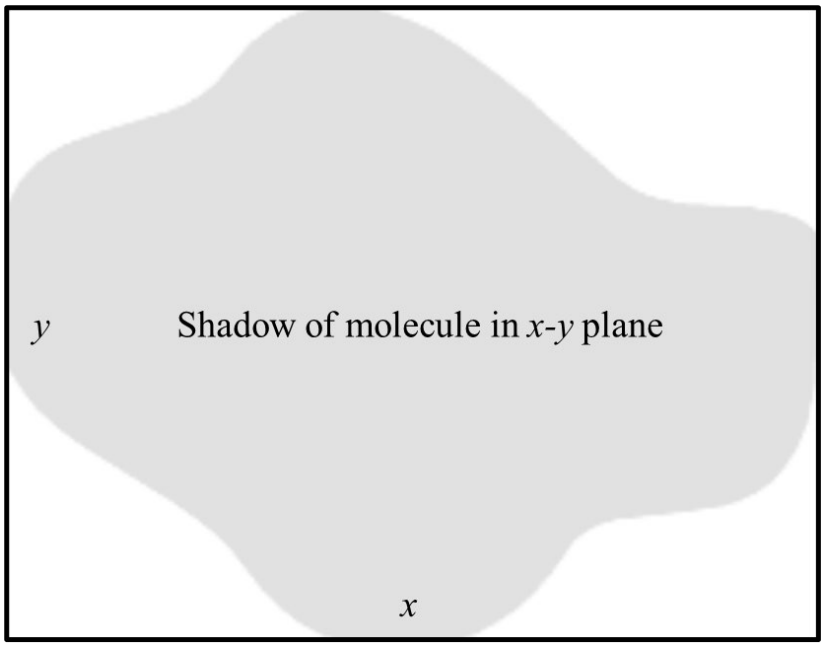

Figure 5.3: Percentage area projection of molecule onto the *x-y* plane

Structural: properties based on the hydrogen bond acceptors and donors, chiral centers and rotatable bonds.

Electrotopological: numerical values (called state keys) that contain information about the electronic interactions and topological environment of an atom, based on graph distances between each atom.

Information-content: descriptors based on informational theory in which structures are partitioned into subsets of equivalent elements.

Thermodynamic: primarily consists of properties that attempt to relate chemical behaviour to structure, mainly in terms of molecular refractivity index and partition coefficient.

Fragment Counts: number of fragments of ranges of hydrocarbon fragments, various functional groups, and different ring fragments.

Jurs Descriptors: sets of properties by which molecules are characterized by shape and electronic information; calculated on individual atoms by mapping partial charges on top of solvent-accessible surface areas.

Spatial: properties based on spatial coordinates and shape, such as moment of inertia, dipole moment, radius of gyration, and molecular density.

Numerous other descriptors may be determined using semi-empirical quantum-mechanical calculations based on wave functions and molecular orbital theory, however these have not been considered due to the complex simulations required for these descriptors to be determined. These calculations often require

specialist software and/or expertise that may be ineffectual for those who may utilize this model to conduct a solvent screening exercise. The descriptors used were limited to those that may be easily computed with knowledge of only a molecule's structure.

In total, 233 descriptors may be generated in the above-mentioned categories in Materials Studio for each molecule. It is required that this number be reduced to limit collinearity between variables, avoid overfitting, and enable sufficient degrees of freedom with respect to the number of data points of the output variable. A correlation matrix was developed to determine which columns of variables are highly correlated with each other. Determining the extent of the correlation between variables determines which may be excluded from further analysis. The correlation coefficient (r) is a good indicator of correlation between variables; it is a function of the covariance (C_{xy}) between any two variables (x and y) and the variance (V) of each individual variable. Values of 1 or -1 for the correlation coefficient indicates a perfect correlation between the variables.

$$r = \frac{C_{xy}}{\sqrt{V_x V_y}} \tag{5.9}$$

The initial 233×233 correlation matrix showed considerable correlation (greater than 0.9) for a major subset of the variables considered, highlighting redundancies that may be excluded from the development of the model without significant loss of information. The number of variables were also reduced in the development of the ANN by considering the sensitivity of a particular variable on the model output. The final set of descriptors consists of 31 input variables, for which the correlation matrix is depicted in Table 5.1. The variable names as well as physical definitions are given in Section 5.4. The number of variables were initially reduced using Genetic Function Approximation (GFA), however it was observed that subsets of variables were being proposed that had some redundancies, with poor model predictions upon development of the ANN.

Table 5.1: Correlation matrix of descriptors used as the input vector to the QSPR model

	X_1	X_2	X_3	X_4	X_5	X_6	X_7	X_8	X_9	X_{10}	X_{11}	X_{12}	X_{13}	X_{14}	X_{15}	X_{16}	X_{17}	X_{18}	X_{19}	X_{20}	X_{21}	X_{22}	X_{23}	X_{24}	X_{25}	X_{26}	X_{27}	X_{28}	X_{29}	X_{30}	X_{31}
X_1	1.00	0.09	0.56	0.15	0.59	0.09	0.46	0.04	0.28	0.25	0.39	0.11	-0.04	0.62	0.24	-0.03	0.13	0.02	0.11	0.05	0.54	0.32	0.34	0.26	0.07	0.07	0.02	0.11	0.15	0.39	0.00
X_2	0.09	1.00	0.10	-0.04	-0.01	0.39	0.45	0.60	-0.13	0.06	0.10	0.52	0.40	0.08	-0.18	-0.07	0.13	0.31	0.04	0.23	-0.02	0.04	-0.11	0.13	0.51	0.14	0.27	0.25	0.08	0.18	0.00
X_3	0.56	0.10	1.00	0.22	0.93	0.33	0.67	0.03	0.28	0.08	0.27	0.01	-0.02	0.75	-0.07	-0.07	-0.03	-0.10	0.28	0.39	0.74	0.23	0.51	0.28	0.09	0.34	0.30	0.50	0.30	0.21	0.00
X_4	0.15	-0.04	0.22	1.00	0.09	0.45	-0.01	0.11	0.15	0.03	0.05	0.04	0.13	0.13	0.21	0.08	-0.13	-0.11	0.90	0.56	0.29	0.55	0.18	0.74	0.32	0.63	0.71	0.53	0.50	0.45	0.00
X_5	0.59	-0.01	0.93	0.09	1.00	0.04	0.64	-0.08	0.34	0.13	0.34	-0.03	-0.14	0.83	-0.04	-0.05	-0.02	-0.12	0.10	0.09	0.81	0.04	0.45	0.21	0.02	0.05	0.04	0.21	0.08	0.01	0.00
X_6	0.09	0.39	0.33	0.45	0.04	1.00	0.29	0.57	-0.01	-0.02	-0.03	0.45	0.40	0.04	-0.11	-0.13	-0.07	0.06	0.57	0.84	0.10	0.54	0.22	0.32	0.33	0.81	0.75	0.83	0.62	0.55	0.00
X_7	0.46	0.45	0.67	-0.01	0.64	0.29	1.00	0.40	0.17	0.10	0.28	0.36	0.16	0.58	-0.13	-0.06	0.07	0.12	0.03	0.10	0.52	-0.05	0.19	0.24	0.22	0.01	0.11	0.21	0.01	0.04	0.00
X_8	0.04	0.60	0.03	0.11	-0.08	0.57	0.40	1.00	-0.01	0.02	0.07	0.71	0.69	-0.03	-0.11	-0.09	-0.03	0.21	0.16	0.25	-0.05	0.12	-0.12	0.27	0.35	0.21	0.28	0.25	0.12	0.19	0.00
X_9	0.28	-0.13	0.28	0.15	0.34	-0.01	0.17	-0.01	1.00	0.15	0.28	0.16	-0.09	0.36	-0.03	-0.10	0.05	0.03	0.09	0.00	0.35	0.03	0.15	0.15	-0.02	0.02	-0.03	0.02	0.01	0.01	0.00
X_{10}	0.25	0.06	0.08	0.03	0.13	-0.02	0.10	0.02	0.15	1.00	0.59	0.10	-0.04	0.36	0.01	-0.01	0.02	0.04	0.02	-0.05	0.28	0.03	0.06	0.20	0.04	-0.03	-0.07	-0.03	-0.07	0.08	0.00
X_{11}	0.39	0.10	0.27	0.05	0.34	-0.03	0.28	0.07	0.28	0.59	1.00	0.06	0.12	0.63	0.03	0.00	-0.07	0.07	0.04	-0.03	0.44	0.02	0.10	0.19	0.04	-0.03	-0.03	0.01	-0.04	0.06	0.00
X_{12}	0.11	0.52	0.01	0.04	-0.03	0.45	0.36	0.71	0.16	0.10	0.06	1.00	0.37	0.01	-0.14	-0.14	0.01	0.16	0.08	0.08	0.02	0.00	-0.06	0.11	0.50	0.04	0.18	0.08	0.01	0.10	0.00
X_{13}	-0.04	0.40	-0.02	0.13	-0.14	0.40	0.16	0.69	-0.09	-0.04	0.12	0.37	1.00	-0.11	0.02	-0.01	-0.05	0.25	0.18	0.26	-0.09	0.21	-0.04	0.22	0.31	0.24	0.28	0.24	0.17	0.29	0.00
X_{14}	0.62	0.08	0.75	0.13	0.83	0.04	0.58	-0.03	0.36	0.36	0.63	0.01	-0.11	1.00	0.01	0.00	-0.02	-0.07	0.13	0.09	0.83	0.05	0.33	0.28	0.05	0.06	0.06	0.18	0.05	0.05	0.00
X_{15}	0.24	-0.18	-0.07	0.21	-0.04	-0.11	-0.13	-0.11	-0.03	0.01	0.03	-0.14	0.02	0.01	1.00	0.47	0.09	-0.01	0.15	-0.02	-0.02	0.28	0.11	0.10	-0.03	0.04	0.06	-0.06	0.17	0.36	0.00
X_{16}	-0.03	-0.07	-0.07	0.08	-0.05	-0.13	-0.06	-0.09	-0.10	-0.01	0.00	-0.14	-0.01	0.00	0.47	1.00	-0.04	0.07	0.02	-0.08	-0.07	-0.11	-0.14	-0.01	-0.04	-0.08	-0.01	-0.09	-0.05	-0.05	0.00
X_{17}	0.13	0.13	-0.03	-0.13	-0.02	-0.07	0.07	-0.03	0.05	0.02	-0.07	0.01	-0.05	-0.02	0.09	-0.04	1.00	0.31	-0.19	-0.03	-0.11	0.08	0.05	-0.17	-0.06	-0.03	-0.10	-0.03	0.08	0.11	0.00
X_{18}	0.02	0.31	-0.10	-0.11	-0.12	0.06	0.12	0.21	0.03	0.04	0.07	0.16	0.25	-0.07	-0.01	0.07	0.31	1.00	-0.14	0.02	-0.14	0.09	0.00	-0.08	0.15	0.01	-0.04	0.01	0.05	0.20	0.00
X_{19}	0.11	0.04	0.28	0.90	0.10	0.57	0.03	0.16	0.09	0.02	0.04	0.08	0.18	0.13	0.15	0.02	-0.19	-0.14	1.00	0.68	0.29	0.58	0.20	0.75	0.37	0.73	0.86	0.64	0.56	0.48	0.00
X_{20}	0.05	0.23	0.39	0.56	0.09	0.84	0.10	0.25	0.00	-0.05	-0.03	0.08	0.26	0.09	-0.02	-0.08	-0.03	0.02	0.68	1.00	0.16	0.72	0.40	0.34	0.23	0.98	0.88	0.99	0.85	0.66	0.00
X_{21}	0.54	-0.02	0.74	0.29	0.81	0.10	0.52	-0.05	0.35	0.28	0.44	0.02	-0.09	0.83	-0.02	-0.07	-0.11	-0.14	0.29	0.16	1.00	0.13	0.48	0.51	0.24	0.15	0.13	0.25	0.13	0.11	0.00
X_{22}	0.32	0.04	0.23	0.55	0.04	0.54	-0.05	0.12	0.03	0.03	0.02	0.00	0.21	0.05	0.28	-0.11	0.08	0.09	0.58	0.72	0.13	1.00	0.52	0.38	0.13	0.78	0.62	0.68	0.84	0.89	0.00
X_{23}	0.34	-0.11	0.51	0.18	0.45	0.22	0.19	-0.12	0.15	0.06	0.10	-0.06	-0.04	0.33	0.11	-0.14	0.05	0.00	0.20	0.40	0.48	0.52	1.00	0.10	0.22	0.37	0.26	0.45	0.62	0.48	0.00
X_{24}	0.26	0.13	0.28	0.74	0.21	0.32	0.24	0.27	0.15	0.20	0.19	0.11	0.22	0.28	0.10	-0.01	-0.17	-0.08	0.75	0.34	0.51	0.38	0.10	1.00	0.34	0.38	0.48	0.34	0.24	0.34	0.00
X_{25}	0.07	0.51	0.09	0.32	0.02	0.33	0.22	0.35	-0.02	0.04	0.04	0.50	0.31	0.05	-0.03	-0.04	-0.06	0.15	0.37	0.23	0.24	0.13	0.22	0.34	1.00	0.20	0.38	0.23	0.15	0.27	0.00
X_{26}	0.07	0.14	0.34	0.63	0.05	0.81	0.01	0.21	0.02	-0.03	-0.03	0.04	0.24	0.06	0.04	-0.08	-0.03	0.01	0.73	0.98	0.15	0.78	0.37	0.38	0.20	1.00	0.87	0.95	0.85	0.71	0.00
X_{27}	0.02	0.27	0.30	0.71	0.04	0.75	0.11	0.28	-0.03	-0.07	-0.03	0.18	0.28	0.06	0.06	-0.01	-0.10	-0.04	0.86	0.88	0.13	0.62	0.26	0.48	0.38	0.87	1.00	0.85	0.75	0.55	0.00

x_{28}	0.11	0.25	0.50	0.53	0.21	0.83	0.21	0.25	0.02	-0.03	0.01	0.08	0.24	0.18	-0.06	-0.09	-0.03	0.01	0.64	0.99	0.25	0.68	0.45	0.34	0.23	0.95	0.85	1.00	0.84	0.63	0.00
x_{29}	0.15	0.08	0.30	0.50	0.08	0.62	0.01	0.12	0.01	-0.07	-0.04	0.01	0.17	0.05	0.17	-0.05	0.08	0.05	0.56	0.85	0.13	0.84	0.62	0.24	0.15	0.85	0.75	0.84	1.00	0.73	0.00
x_{30}	0.39	0.18	0.21	0.45	0.01	0.55	0.04	0.19	0.01	0.08	0.06	0.10	0.29	0.05	0.36	-0.05	0.11	0.20	0.48	0.66	0.11	0.89	0.48	0.34	0.27	0.71	0.55	0.63	0.73	1.00	0.00
x_{31}	0.00	0.00	0.00	0.00	0.00	0.00	0.00	0.00	0.00	0.00	0.00	0.00	0.00	0.00	0.00	0.00	0.00	0.00	0.00	0.00	0.00	0.00	0.00	0.00	0.00	0.00	0.00	0.00	0.00	0.00	1.00

5.3.3 Development of QSPR Model and Artificial Neural Network

Artificial neural networks provide a mechanism that enables representation of nonlinear functions. The structure consists of weighted interconnections between an input layer, hidden layer, and output layer. The weights were obtained through training via back-propagation, which involves iteratively adjusting the weights with the process beginning via the forward pass i.e., the input layer provides an input to each node of the hidden layer which computes an output that becomes an input to the nodes of the output layer, which then determines the model output based on the input vector. Error reduction then occurs via adjustment of weights through the backward pass. Using the output vector, the error values are determined for each node. Thereafter, the error values as a portion of the output nodes are determined for the hidden layers. The weights were adjusted using the Broyden-Fletcher-Goldfarb-Shanno (BFGS) method (Nash & Sofer, 1995), with the random number seed varied to establish that the algorithm was converging on the global minimum, rather than a local minimum.

The input and output vectors were standardized by mean and standard deviation as per Equation (5.10). The input vector itself was taken as the absolute value of the difference in descriptor values of the chemicals that make up a particular binary system. Thus, for a binary system comprising an ideal solution, the limit of the activity coefficient tends to one, which is enabled by a binary interaction parameter of zero. The absolute value is taken as selection of component 1 and component 2 in literature appears to be arbitrary. As temperature is in itself a descriptor, the overall model intercept is nevertheless trained to approach zero when the system approaches ideal solution behaviour, i.e., the imposition of boundary conditions.

$$x_i^{'} = \frac{x_i - \overline{x}}{\sigma} \tag{5.10}$$

The standardized data is $x_i^{'}$ while x_i is the original data. The mean and standard deviation of each vector are given by $\overline{x}$ and σ respectively. The standardized data thus has a standard deviation of one and a mean of zero.

The ANN developed in this work may be generally described by Equation (5.11).

$$y_k = f\left(\sum_{j=1}^{n_H} w_{kj} f\left(\sum_{i=1}^{n_I} w_{ji} x_i^{'} + w_{j0}\right) + w_{k0}\right) \tag{5.11}$$

The model output is given by y_k for the kth output, while the model inputs are given by x_i' for the i^{th} descriptor. The number of nodes in the hidden layer is denoted by n_H, and the number of nodes in the input layer by n_I. The weights between the input and hidden layers are represented by w_{ji} for node j. The terms w_{j0} and w_{k0} are referred to as the bias. The output is determined with the use of the function f, which is the s-shaped Sigmoid transfer function given in Equation (5.12). The purpose of transforming the data with this transfer function is to scale the wide domain of each vector to values within a narrow margin (saturation effect). The resulting smooth and differentiable function expedites convergence.

$$f(z) = \frac{1.2}{1+e^{-z}} - 0.1 \tag{5.12}$$

The ANNs developed for both datasets of binary interaction parameters were of configuration 31-18-1. The number of nodes in the hidden layer were varied with no observable improvement in correlation beyond 18 nodes.

Several techniques were employed to avoid overfitting, such as use of test data, cross validation, and response randomization. The internal test set was formed using 25% of the data rows at random. Cross validation was done using three groups of data, i.e., the data is grouped at random into three subsets and the algorithm is independently run for each subset with the other two omitted. The resulting model is then used to generate predicted values for the omitted data which is compared to the actual values. The formation of the test set was done independently for each cross validation run. Response randomization assesses the statistical significance of the model and involves implementing a random permutation on the output variable data and creating new models for the permuted data (inclusive of test data and cross validation). For each run, correlation measures (R^2) as well as the correlation coefficient between the permuted and unpermuted data, is extracted for 40 random trials, which is the default suggested by Materials Studio. The correlation measures are compared to that of the original model for each random trial. The original model is regarded as statistically significant if the correlation measures for trials with low correlation coefficients are significantly less than unity.

5.4. Model Results and Discussion

Table 5.2 lists the final descriptors used, after the reduction process, together with their definitions. The formation of liquid-liquid equilibrium is as a result of interactions in terms of intermolecular forces between the components of the system. The descriptors used in this work are properties that characterize and contain information about molecules that underlie the physical mechanism of liquid-liquid equilibrium as it relates to polarity from interacting Van der Waal's, hydrogen bonds, and London forces. Spatial descriptors such as the dipole moments and shadow areas and fraction, contain information about molecular shape and structure, integral to the types of intermolecular interactions found in mixtures. Jurs descriptors form a significant part of the final ensemble and are important as they combine information concerning partial atomic charges, molecular surface area, charge scaling factors, and charge distribution, i.e., the properties that are responsible for polar and non-polar intermolecular interactions are specifically encoded into several sets of descriptors. Therefore, the model developed is a function of properties that have physical significance to the formation of liquid-liquid equilibrium. Table 5.3 gives various statistical parameters and correlation measures. The model results were analyzed with the use of the root-mean-square-error (RMSE), average absolute logarithmic ratio (AALN) as well as average absolute deviation (AAD). These indicators are defined in Equations (5.13), (5.14), and (5.15).

$$RMSE = \sqrt{\frac{\sum_{i=1}^{n}\left[y_i(\text{calc}) - y_i(\text{exp})\right]^2}{n}} \tag{5.13}$$

$$AALN \text{ ratio } = \frac{\sum_{i=1}^{n}\left|\ln\left(\frac{y_i(\text{calc})}{y_i(\text{exp})}\right)\right|}{n} \tag{5.14}$$

$$AAD = {}^{1}\!/_{n}\sum_{i=1}^{n}\left|y_i(\text{calc}) - y_i(\text{exp})\right| \tag{5.15}$$

The correlated model results with residuals are given in Figures 5.4 – 5.7, with the cross-validated external set in Figures 5.8 and 5.9, and the response randomization results given in Figures 5.10 and 5.11. The figures highlight good agreement between the parameters determined from experimental data, and those predicted with the ANN. The residual plots show that deviations are randomly scattered around the mean residual, suggesting that little further improvement to the

model can be made. There appears to be a greater concentration of outliers for values of τ_{ij} and τ_{ji} greater than 10 and less than -2, suggesting that larger errors are more likely in these data ranges. The presence of these outliers is possibly due to the quality of the experimental data used to obtain those particular sets of binary interaction parameters. The value of α may also be a factor, i.e., a different value may be more suitable for those datasets. In Figures 5.6 and 5.8, the predicted parameters appear to vary linearly with the residuals. This is apparent for larger predicted values greater than 10. From the data, this subset appears to correspond to systems such as octane + water, benzene + monoethanolamine, benzene + water, *n*-heptane + sulfolane, water + *o*-nitrotoluene, styrene + water, toluene + triethylene glycol, and hexadecane + furfural. Many of these systems contain ringed aromatic structures. While water is a compound frequently occurring in this subset, phase behaviour of systems containing water is frequently measured and forms a substantial part of the dataset. A more significant commonality between these systems is that they are highly nonideal and nearly insoluble. The seemingly linear trend of the residuals is also demonstrated for different temperature values of the same nonideal systems. This suggests that the model may possess an offset for strongly nonideal systems which have parameters more dependent on temperature. The R^2 for both ANNs were around 0.99, highlighting a good correlation between both sets of variables. In addition, both cross validated R^2 values were around 0.95 – this correlation measure is the average of the R^2 for all three groups of data used to train the model, as discussed in the preceding section. The high cross validated R^2 (also noted for the test set), suggests it is likely that overfitting did not occur. The high R^2 values may be due to the fact that the model was developed with binary interaction parameters which were determined from LLE datasets with tie-line data, and checked for consistency. A higher RMSE of 12.43 is noted for τ_{ij} compared to 10.36 for τ_{ji}, while similar AALN ratios as well as AADs are noted for both models. These indicators may be skewed due to the aforementioned outliers and bias term in the model equation. The correlated interaction parameters were checked for consistency using the miscibility boundary illustrated in Figure 5.1, and it was observed that the model was able to correctly identify which component pairs were in the single or two-phase region for 98% of the dataset, indicating that model deviations do not significantly change miscibility predictions. The results of the response randomization in Figures 5.10 and 5.11 indicate that no good ANN model with high R^2 is found for random permutations of the output variable for 40 random trials. Low correlation coefficients

were noted between the unpermuted and permuted data, that does not appear to correlate with the low R^2 of the permuted data. This suggests that the model solution is statistically significant.

Table 5.2: Final list of descriptors used as input to ANN model with definitions

Variable	Descriptor Definition	Descriptor Type	Mean	Standard Deviation
x_1	Log of the octanol/water partition coefficient	Thermodynamic	2.032	1.505
x_2	Balaban index JX	Topological	0.895	0.927
x_3	Wiener index	Topological	75.868	125.150
x_4	Molecular density: ratio of molecular weight to molecular volume	Spatial	0.135	0.137
x_5	Principal moments of inertia (magnitude)	Spatial	1147.440	2029.632
x_6	Principal moment of inertia X	Spatial	62.323	89.150
x_7	Ellipsoidal volume: volume of the ellipsoid of inertia derived from the inertia tensor of the system	Spatial	48.718	41.252
x_8	Shadow area in YZ plane: area of molecular shadow formed by projection of molecular surface on YZ plane	Spatial	5.820	5.038
x_9	Shadow area fraction XY plane: fraction of area of molecular shadow in the xy plane	Spatial	0.047	0.034
x_{10}	Shadow area fraction YZ plane	Spatial	0.073	0.051
x_{11}	Shadow area fraction ZX plane	Spatial	0.075	0.052
x_{12}	Shadow length LY: length of molecule in y dimension	Spatial	1.374	1.050
x_{13}	Shadow length LZ	Spatial	0.768	0.722
x_{14}	Shadow ratio: ratio of largest to smallest dimension	Spatial	0.930	0.862
x_{15}	Dipole moment (magnitude)	Spatial	2.017	1.667

x_{16}	Dipole moment X	Spatial	2.486	2.094
x_{17}	Dipole moment Y	Spatial	1.195	1.247
x_{18}	Dipole moment Z	Spatial	0.642	0.722
x_{19}	Partial negative surface area: sum of the solvent-accessible surface areas of all negatively charged atoms	Jurs	38.617	39.318
x_{20}	Total charge-weighted negative surface area: partial negative surface area multiplied by the total negative charge.	Jurs	72.920	180.653
x_{21}	Atomic charge-weighted positive surface area: sum of the product of the solvent-accessible surface area and partial charge for all positively charged atoms	Jurs	16.743	15.437
x_{22}	Atomic charge-weighted negative surface area: sum of the product of the solvent-accessible surface area and partial charge for all negatively charged atoms.	Jurs	15.961	15.511
x_{23}	Difference in atomic charge-weighted surface areas: atomic charge-weighted positive surface area minus the atomic charge-weighted negative surface area	Jurs	20.822	17.990
x_{24}	Fractional partial positive surface area: partial positive surface area divided by the total molecular solvent-accessible surface area	Jurs	0.182	0.155
x_{25}	Fractional atomic charge-weighted positive surface area: atomic charge-weighted positive surface area	Jurs	0.039	0.030

	divided by the total molecular solvent-accessible area			
x_{26}	Fractional charge-weighted negative surface area: total charge-weighted negative surface area divided by the total molecular solvent-accessible are	Jurs	0.219	0.490
x_{27}	Surface-weighted partial negative surface area: product of the partial negative surface area and the total molecular solvent-accessible surface area	Jurs	11.015	12.999
x_{28}	Surface-weighted charge-weighted negative surface area: product of the total charge-weighted negative surface area and the total molecular solvent-accessible area	Jurs	26.755	67.260
x_{29}	Surface-weighted atomic charge-weighted negative surface area: product of the atomic charge-weighted negative surface area and the total molecular solvent-accessible area	Jurs	4.454	5.384
x_{30}	Total polar surface area: sum of solvent-accessible surface areas of all polar atoms	Jurs	51.700	46.411
x_{31}	Temperature	-	318.976	15.918

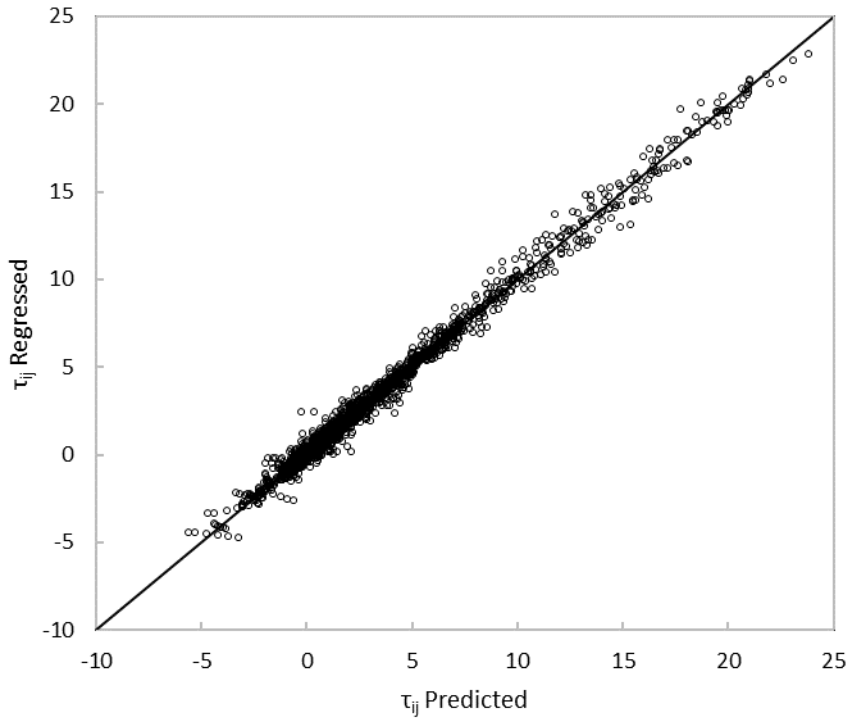

Figure 5.4: Comparison of binary interaction parameter (τ_{ij}) determined from experimental data to correlated parameters

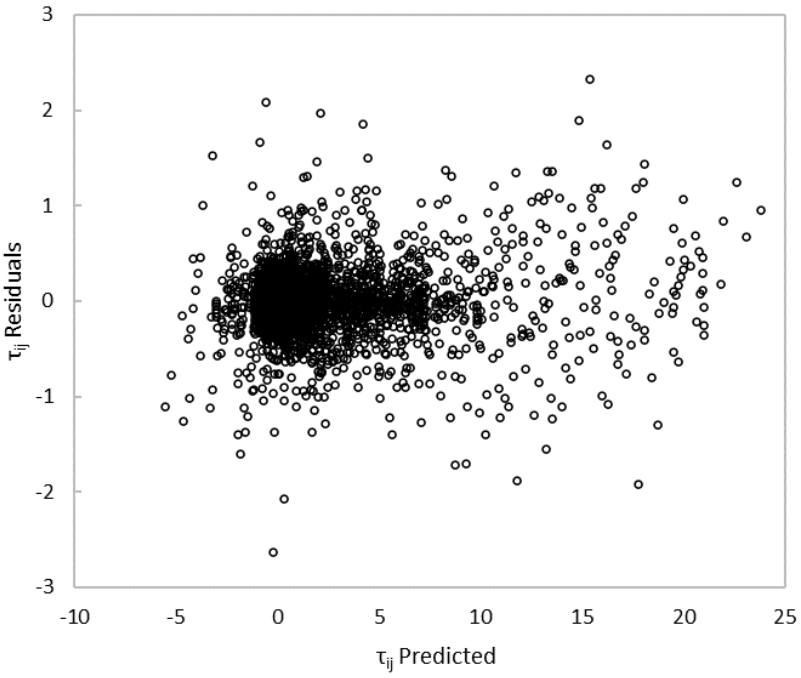

Figure 5.5: Residuals of correlated binary interaction parameter (τ_{ij}) against parameters determined from experimental data

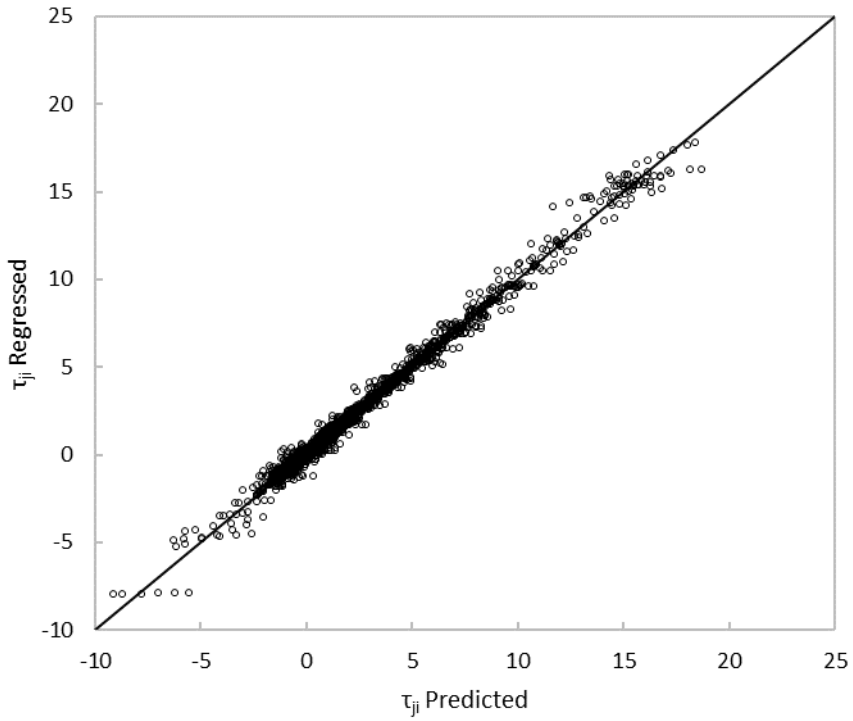

Figure 5.6: Comparison of binary interaction parameter (τ_{ji}) determined from experimental data to correlated parameters

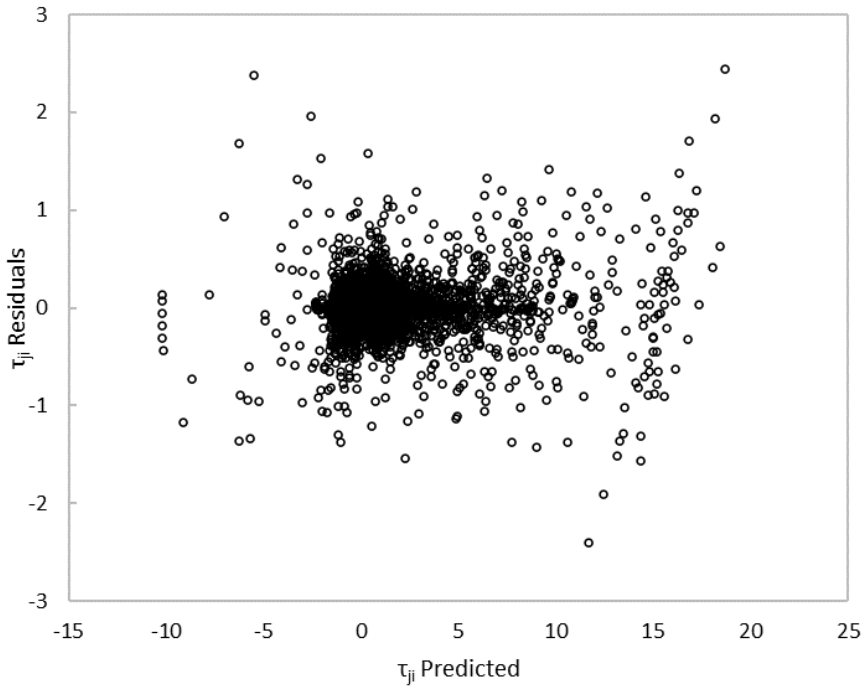

Figure 5.7: Residuals of correlated binary interaction parameter (τ_{ji}) against parameters determined from experimental data

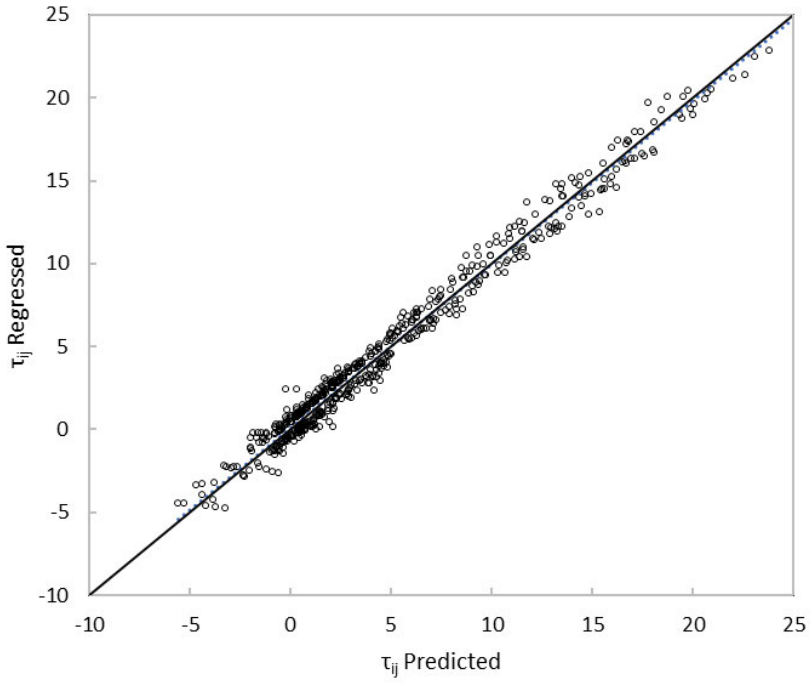

Figure 5.8: Comparison of binary interaction parameter (τ_{ij}) for cross-validated subset (external test set)

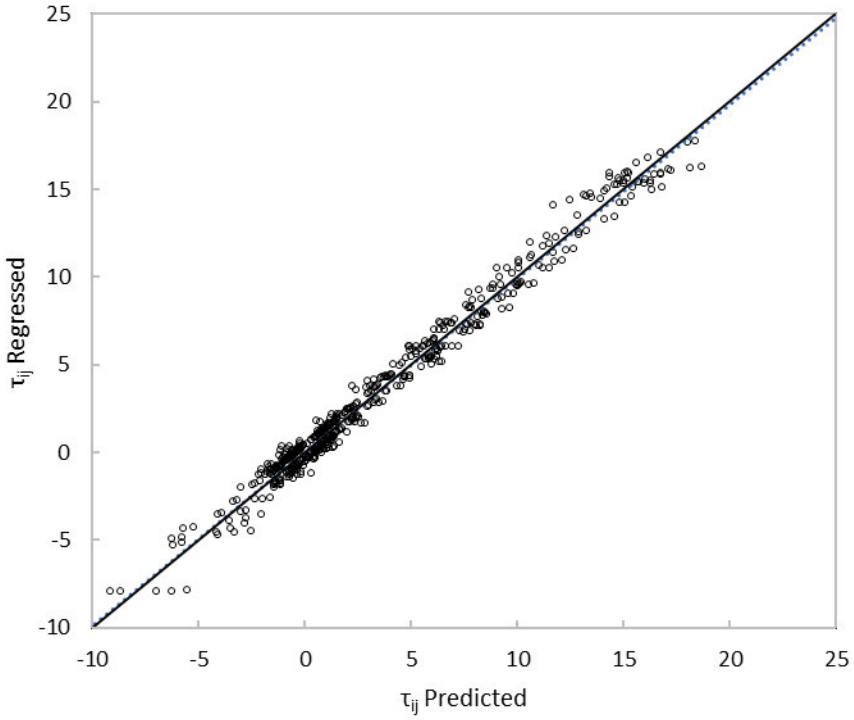

Figure 5.9: Comparison of binary interaction parameter (τ_{ji}) for cross-validated subset (external test set)

Table 5.3: Statistical parameters of AAN model; CV – cross validation

	τ_{ij}	τ_{ji}
R^2	0.9943	0.9941
R^2 (CV)	0.9526	0.9539
R^2 (test set)	0.9876	0.9892
R^2 (CV, test set)	0.9485	0.9408
RMSE	12.43	10.36
AALN Ratio	0.2237	0.2123
AAD	0.2209	0.1839

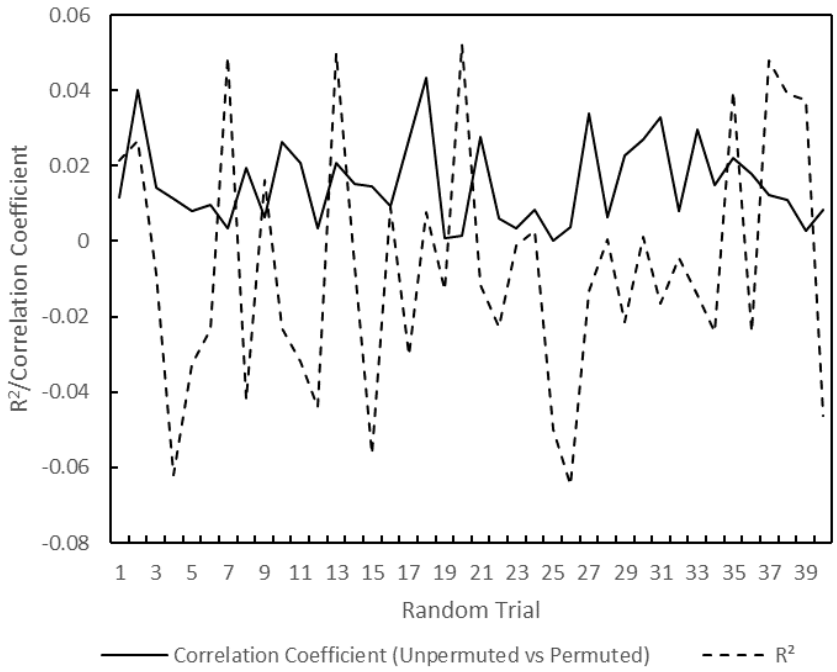

Figure 5.10: Comparison of τ_{ij} R^2 and correlation coefficient (unpermuted and permuted) for randomized vector output of 40 trials

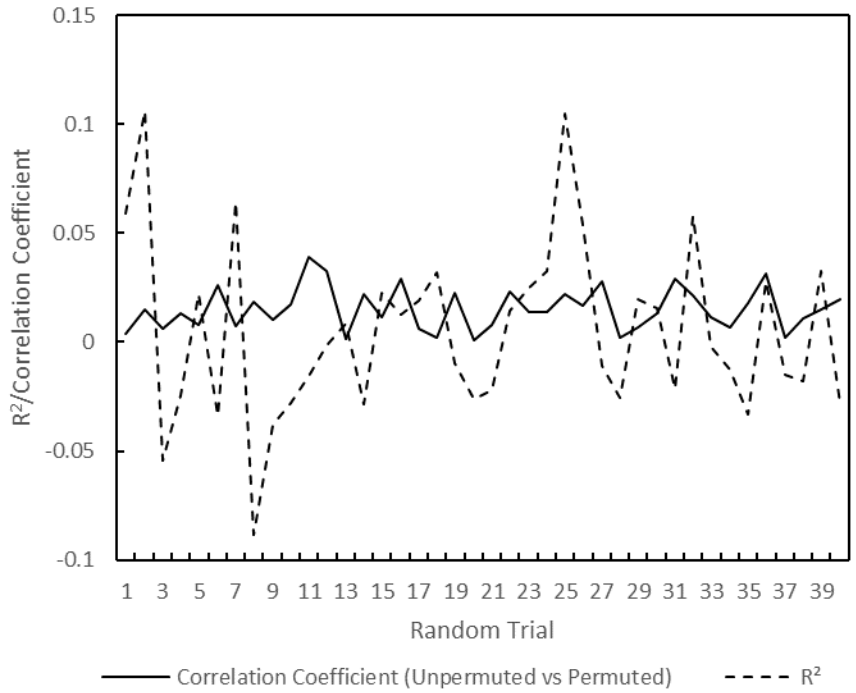

Figure 5.11: Comparison of τ_{ji}, R^2 and correlation coefficient (unpermuted and permuted) for randomized vector output of 40 trials

The model may be used as part of the solvent screening process to improve the robustness of process by considering *a priori* miscibility predictions using the QSPR model developed. For a system consisting of a carrier liquid (1), a solute (2), and solvent (3), infinite dilution activity coefficients may be determined using the NRTL equation, which is a function of only binary interaction parameters after applying the composition limits at a fixed temperature. Estimations of binary interaction parameters with the model in this work therefore enables *a priori* estimations of infinite dilution coefficients. The constraint using a parameter δ in Equation (5.16) is proposed which may assist with solvent screening as a supplement to predictive group contribution methods such as UNIFAC (LLE).

$$\delta = \frac{\tau_{13} - \tau_{23}}{\tau_{13} - \tau_{12}} < 1 \tag{5.16}$$

The solvent-carrier binary pair (τ_{13}) is a highly nonideal pair as the nature of liquid-liquid extraction requires immiscibility between these components; this lies to the right of the phase boundary in the two-phase region. The solute-solvent pair may lie also in the two-phase region

forming a type 2 system; however, it is desired it lie in the single-phase region closer to the carrier-solute pair, which is a highly miscible pair lying to the left of the phase boundary in the single-phase region. This pattern is the motivation for Equation (5.16), as the distance between the solvent-carrier pair and carrier-solute would be greater than that of the solute solvent pair, implying that the ratio would be less than one. The value δ may be greater than one, however this would correspond to the scenario that the solute-solvent pair deviates more from ideality than the carrier-solute pair, which may reduce the appropriateness of the solvent in terms of selectivity. This analysis may be extended to the screening of co-solvent mixtures by considering the solvent and co-solvent interaction as a single pseudo-unit. In the extraction of aromatics, *n*-heptane represents the carrier liquid, and toluene the solute. Table 5.4 presents calculated δ values (all less than one) for this application using the correlated values from the QSPR model for commercial solvents as well as new solvents studied by the authors which were identified in their screening process.

Table 5.4: Calculated δ values for the system *n*-heptane (1)-toluene (2)-solvent (3)

Solvent	τ_{12}	τ_{13}	τ_{23}	δ
Sulfolane	-0.428	18.945	2.077	0.871
N-Formylmorpholine	-0.428	14.752	2.773	0.789
N-Methyl-2-pyrrolidone	-0.428	12.478	0.958	0.893
Diethylene glycol	-0.428	7.002	3.104	0.525
N,N-Dimethylformamide	-0.428	6.532	1.569	0.713
Tetraethylene glycol	-0.428	14.166	12.401	0.121
1,4-Butanediol	-0.428	7.246	5.437	0.236
Glycerol	-0.428	7.214	4.077	0.410

5.5. Conclusion

To improve the robustness of solvent screening processes, a QSPR model as an artificial neural network was developed to produce *a priori* predictions of binary interaction parameters of the NRTL model using regressed parameters checked for consistency from LLE and VLE data that included temperature dependence. This serves as a supplement to predictive group contribution methods that are limited by availability of empirical data or may produce inaccurate immiscibility

estimations. Analysis of the model results indicate it may serve as an effective tool in efficiently directing research focus.

5.6. Acknowledgements

This work used the software Materials Studio for which access was provided by the CHPC (Centre for High Performance Computing).

5.7. Declaration

The authors declare no competing financial interests.

5.8. References

Altintas, C., & Keskin, S. (2016). Computational screening of MOFs for C_2H_6 /C_2H_4 and C_2H_6 /CH_4 separations. *Chemical Engineering Science*, *139*, 49–60. https://doi.org/10.1016/j.ces.2015.09.019

Aspen Plus (10). (2004). Aspen Technology Incorporation.

Benitez, D., Tkatchouk, E., Yoon, I., Stoddart, J. F., & Goddard, W. A. (2008). Experimentally-Based Recommendations of Density Functionals for Predicting Properties in Mechanically Interlocked Molecules. *Journal of the American Chemical Society*, *130*, 14928–14929. https://doi.org/10.1021/ja805953u

Brijmohan, N., Moodley, K., & Narasigadu, C. (2021). Identification and Screening of Potential Organic Solvents for the Liquid–Liquid Extraction of Aromatics. *Org. Process Res. Dev.*, *25*, 2230–2248.

Brijmohan, N., Moodley, K., & Narasigadu, C. (2022a). Liquid–Liquid Extraction of Toluene from n-Heptane Using Butane-1,4-diol + 2-Methyl-pentane-2,4-diol Liquid Mixtures. *J. Chem. Eng. Data*, *67*, 3177–3185. https://doi.org/10.1021/acs.jced.2c00498

Brijmohan, N., Moodley, K., & Narasigadu, C. (2022b). Ternary Liquid–Liquid Equilibrium Data for the n-Heptane + Toluene + (Butane-1,4-diol or Glycerol) Systems at 298.2, 313.2, and 333.2 K and 0.1 MPa. *J. Chem. Eng. Data*, *67*(4), 975–983. https://doi.org/10.1021/acs.jced.2c00011

Chen, G., Song, Z., Qi, Z., & Sundmacher, K. (2021). Neural recommender system for the activity coefficient prediction and UNIFAC model extension of ionic liquid-solute systems. *AIChE Journal*, *67*. https://doi.org/10.1002/aic.17171

Cho, J., Ko, M. S., Na, S., & Kim, H. (2002). Simulation of the Aromatic Recovery Process by Extractive Distillation. *Korean J. Chem. Eng*, *19*, 996–1000.

Coley, C. W., Barzilay, R., Green, W. H., Jaakkola, T. S., & Jensen, K. F. (2017). Convolutional Embedding of Attributed Molecular Graphs for Physical Property Prediction. *Journal of Chemical Information and Modeling*, *57*, 1757–1772. https://doi.org/10.1021/acs.jcim.6b00601

Damay, J., Jirasek, F., Kloft, M., Bortz, M., & Hasse, H. (2021). Predicting Activity Coefficients at Infinite Dilution for Varying Temperatures by Matrix Completion. *Industrial & Engineering Chemistry Research*, *60*, 14564–14578. https://doi.org/10.1021/acs.iecr.1c02039

Felton, K. C., Ben-Safar, H., & Lapkin, A. A. (2022). DeepGamma: A deep learning model for activity coefficient prediction. *1st Annual AAAI Workshop on AI to Accelerate Science and Engineering (AI2ASE)*.

Fredenslund, A., Jones, R. L., & Prausnitz, J. M. (1975). Group-contribution estimation of activity coefficients in nonideal liquid mixtures. *AIChE Journal*, *21*, 1086–1099. https://doi.org/10.1002/aic.690210607

Gebreyohannes, S., J. Neely, B., & A. M. Gasem, K. (2014a). Generalized Nonrandom Two-Liquid (NRTL) Interaction Model Parameters for Predicting Liquid–Liquid Equilibrium Behavior. *Ind. Eng. Chem. Res.*, *53*, 12445–12454. https://doi.org/10.1021/ie501699a

Gebreyohannes, S., J. Neely, B., & A. M. Gasem, K. (2014b). Generalized Nonrandom Two-Liquid (NRTL) Interaction Model Parameters for Predicting Liquid–Liquid Equilibrium Behavior. *Industrial & Engineering Chemistry Research*, *53*(31), 12445–12454. https://doi.org/10.1021/ie501699a

Gebreyohannes, S., Yerramsetty, K., Neely, B. J., & Gasem, K. A. M. (2013). Improved QSPR generalized interaction parameters for the nonrandom two-liquid activity coefficient model. *Fluid Phase Equilib*, *339*, 20–30. https://doi.org/10.1016/J.FLUID.2012.11.020

Jirasek, F., Alves, R. A. S., Damay, J., Vandermeulen, R. A., Bamler, R., Bortz, M., Mandt, S., Kloft, M., & Hasse, H. (2020). Machine Learning in Thermodynamics: Prediction of Activity Coefficients by Matrix Completion. *The Journal of Physical Chemistry Letters*, *11*, 981–985. https://doi.org/10.1021/acs.jpclett.9b03657

Rappe, A., Goddard, W. (2002). Charge equilibration for molecular dynamics simulations. *J. Phys. Chem.*, *95*, 3358–3363. https://doi.org/10.1021/j100161a070

Klamt, A. (1995). Conductor-like Screening Model for Real Solvents: A New Approach to the Quantitative Calculation of Solvation Phenomena. *The Journal of Physical Chemistry*, *99*, 2224–2235. https://doi.org/10.1021/j100007a062

Mayo, S., Olafson, B., Goddard, W. (2002). DREIDING: a generic force field for molecular simulations. *J. Phys. Chem.*, *94*, 8897–8909. https://doi.org/10.1021/j100389a010

Marcilla, A., Reyes-Labarta, J. A., & Olaya, M. M. (2017). Should we trust all the published LLE correlation parameters in phase equilibria? Necessity of their assessment prior to publication. *Fluid Phase Equilib*, *433*, 243−252.

Marcilla Gomis, A., Labarta, J. A., dolores Serrano, M., Del Mar Olaya, M., Antonio Reyes-Labarta, J., Dolores Serrano Cayuelas, M., & del Mar Olaya López, M. (2011). GE Models and Algorithms for Condensed Phase Equilibrium Data Regression in Ternary Systems: Limitations and Proposals. In *The Open Thermodynamics Journal* (Vol. 5). https://www.researchgate.net/publication/264885160

Nash, S., & Sofer, A. (1995). *Linear and Nonlinear Programming*. McGraw-Hill College.

Pan, F., Peng, F., & Jiang, Z. (2007). Diffusion behavior of benzene/cyclohexane molecules in poly(vinyl alcohol)-graphite hybrid membranes by molecular dynamics simulation. *Chemical Engineering Science*, *62*, 703–710. https://doi.org/10.1016/j.ces.2006.07.046

Renon, H., & Prausnitz, J. M. (1968). Local Compositions in Thermodynamic Excess Functions for Liquid Mixtures. *AIChE J*, *14*, 135–144.

Rittig, J. G., Ben Hicham, K., Schweidtmann, A. M., Dahmen, M., & Mitsos, A. (2023). Graph neural networks for temperature-dependent activity coefficient prediction of solutes in ionic liquids. *Computers & Chemical Engineering*, *171*, 108153. https://doi.org/10.1016/j.compchemeng.2023.108153

Rong, Y., Bian, Y., Xu, T., Xie, W., Wei, Y., Huang, W., & Huang, J. (2020). *Self-Supervised Graph Transformer on Large-Scale Molecular Data*.

Sanchez Medina, E. I., Linke, S., Stoll, M., & Sundmacher, K. (2022). Graph neural networks for the prediction of infinite dilution activity coefficients. *Digital Discovery*, *1*, 216–225. https://doi.org/10.1039/D1DD00037C

Schwaller, P., Laino, T., Gaudin, T., Bolgar, P., Hunter, C. A., Bekas, C., & Lee, A. A. (2019). Molecular Transformer: A Model for Uncertainty-Calibrated Chemical Reaction Prediction. *ACS Central Science*, *5*, 1572–1583. https://doi.org/10.1021/acscentsci.9b00576

Sørensen, J. M., & Arlt, W. (1980). Liquid–Liquid Data Equilibrium Collection. *DECHEMA Chemistry Data Series*, *V*.

Weininger, D. (1988). SMILES, a chemical language and information system. 1. Introduction to methodology and encoding rules. *Journal of Chemical Information and Computer Sciences*, *28*, 31–36. https://doi.org/10.1021/ci00057a005

Winter, B., Winter, C., Esper, T., Schilling, J., & Bardow, A. (2022). *SPT-NRTL: A physics-guided machine learning model to predict thermodynamically consistent activity coefficients*.

Winter, B., Winter, C., Schilling, J., & Bardow, A. (2022). *A smile is all you need: Predicting limiting activity coefficients from SMILES with natural language processing*.

Zeng, Q. H., Yu, A. B., Lu, G. Q., & Standish, R. K. (2003). Molecular Dynamics Simulation of Organic−Inorganic Nanocomposites: Layering Behavior and Interlayer Structure of Organoclays. *Chemistry of Materials*, *15*, 4732–4738. https://doi.org/10.1021/cm0342952

6

CHAPTER SIX

CULMINATING DISCUSSION

The outcome of this work may be considered as a superstructure-based process synthesis framework, illustrated in Figure 6.1, that combines Computer-Based Molecular Design (CAMD) using group contribution methods and artificial neural network Quantitative Structure Property Relationship (QSPR) models with Health, Safety, and Environmental (HSE) impacts using a rating-based risk assessment method. These factors culminate in integrated solvent and process designs with relatively fixed configurations that capture the interaction of solvent choice on design alternatives, with the incorporation of sustainability measures.

Chapter 2 presented a systematic solvent screening process that proposed a series of organic chemicals as new potential solvents for the extraction of aromatics from aliphatics, as part of an effort to create a framework linking all steps of Process Systems Engineering (PSE) in order for engineers to improve efficiency of liquid-liquid extraction processes at a macro-level with a characterization of the relationship of process performance and solvent molecular design, within a broader framework of sustainability.

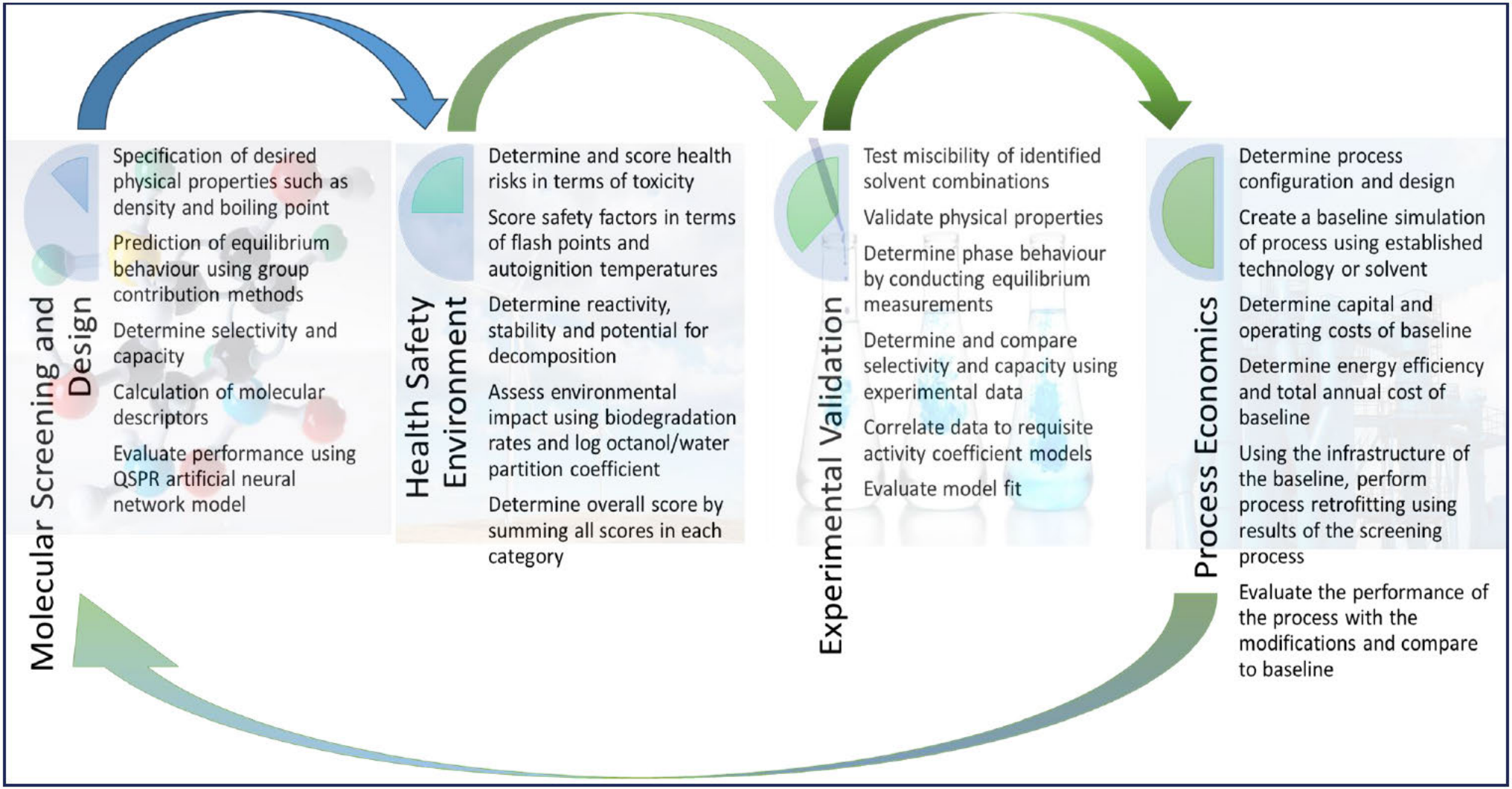

Figure 6.1.: Flowchart illustrating the process synthesis framework that captures the interaction of solvent choice on design alternatives with the incorporation of sustainability measures

The results of the first step reported UNIFAC-LLE predictions of screened solvents due to the abundance of main group and sub-group parameters as well as interaction energies, allowing more chemicals to be screened. An achievement noted was that chemicals were identified as potential solvents that had not been considered for this application, and had no available data in published literature. However, there were several limitations with this first step in that many chemicals could not be evaluated in terms of selectivity and capacity due to lack of availability of structural parameters, and that UNIFAC-LLE predictions were not suitable for the system *n*-heptane + 2-methyl-2,4-pentanediol (hexylene glycol), while subsequent tests showed hexylene glycol to be a more appropriate co-solvent. These limitations highlighted that alternative methods need to be considered as a supplement to predictive models to improve the robustness of this approach, which is the subject of the publication presented in Chapter 5. In this chapter, a QSPR model as an artificial neural network to produce *a priori* predictions of binary interaction parameters of the NRTL model using regressed parameters checked for consistency from LLE and VLE data that included temperature dependence, was presented. A method of solvent screening using the *a priori* NRTL interaction parameters was also presented in which a ratio is defined that incorporates values of the interaction parameters based on extent of ideality for the various binary pairs in a ternary mixture. The outcome was that this was applied to conventional solvents and the new solvent options identified in this work, and the method was found to be a robust supplement to predictive group contribution methods. The limitations of this are that the methodology requires a user to optimize the molecule's geometric structure and compute numerous molecular descriptors. This was done in Materials Studio in this work, and therefore requires access to specialized software and the particular skillset for its use.

A benchmarking in terms of HSE served to further screen the new potential solvents as the second major PSE step due to the fact that it is important for any new feasible alternative to be considered a sustainable replacement. The main HSE risks and hazards were identified for conventional and new potential solvents. The type, number, extent, and impact of the hazards determined the overall and individual HSE scores for each solvent, as well as the category each solvent is placed in (preferred, usable, undesirable). This procedure was performed on the conventional solvents initially in order to set a baseline, to compare to their rating in published solvent guides. This approach is the next achievement of this work, in that HSE aspects of solvent impact in terms of

sustainability, were systematized within the structure. The first step of thermodynamic theoretical predictions using molecular knowledge were related to HSE risk assessments using a benchmarking rating system as the second step in PSE. The methodology in this step possesses some limitations in that HSE and subsequent sustainability evaluations are not clearly deterministic in the rating system as heuristics may need to guide engineers in terms of process requirements, e.g., flammability increasing risk assessment ratings even though this may be a desired property of the liquid (as a fuel) in the process. While this is not the case in liquid-liquid extraction, generalization of this method requires adaption of sustainability indices to the nature of the process. A further limitation is the dependency on HSE data such as log octanol/water partition coefficients, flash points, explosive limits, vapour pressure, toxicity etc. This information may not be readily available for novel chemicals identified in the preceding step and the user may have to rely on empirical models.

Chapter 3 presented liquid-liquid equilibrium (LLE) phase composition experimental measurements and thermodynamic modelling for ternary and quaternary systems at various temperatures. The use of hexylene glycol as a potential co-solvent to butane-1,4-diol and glycerol was also studied. This section highlighted the continuing importance of experimental measurements validating theoretical predictions. While it was confirmed in terms of selectivity that butane-1,4-diol and glycerol are suitable for these applications, there would be limitations with regards to solvent capacity. This limitation was addressed with the use of hexylene glycol as a co-solvent to both butane-1,4-diol and glycerol. As discussed in Chapter 3, the presence of hexylene glycol in certain molar ratios significantly improves solvent capacity and competitiveness with conventional solvents. The interesting result is that the experimental measurements highlighted a solvent mixture as the optimal solution that was not apparent in the initial solvent identification step. This implies that the identification of solvent mixtures should form part of the screening. This was also addressed in Chapter 5, where the *a priori* ANN prediction of a binary interaction parameter can be made for a solvent unit consisting of the solvent and co-solvent as a single pseudo component. This approach may assist researchers and engineers to search for a particular solvent mixture as a “designer” solvent as opposed to attempting to identify a single chemical that has all desired properties for the application under consideration.

ASPEN Plus V10 was used to develop a conceptual design for each of the solvents tested for the extraction and recovery processes for three conventional solvents to set a baseline feasibility to which the potential solvents were compared. This is the final PSE step which links the molecular design and HSE risk assessments to economic performance on a macro level. The choice of solvent affects capital costs as the selectivity influences the column number of stages and therefore length, while volume of solvent required influences recirculation rates, diameter and operating costs. Solvent properties also affect other operational behaviours such as aliphatic spillover to the raffinate and recovery of solvent losses within the system. Combining capital and operational costs into the Total Annual Cost (TAC) measure is effective in analysing the economic impact of solvent choice. Solvent type also affects energy sources consumption and sources used. It is critical to incorporate heat recoveries as quality and location of heat creates varying degrees of potential energy savings. Lastly, converting the energy sources and consumptions to equivalent carbon emissions closes the sustainability loop and associates solvent selection directly with large-scale environmental impact.

Finding an ASPEN V10 simulation iteration that represents the most optimal process design, much like most nonconvex optimization problems, depends on finding a global optimality state in which many interdependent variables across different process units are simultaneously optimized. The sensitivity of arrays of variables may also lead to suboptimal solutions if convergence issues prevent feasible solutions at different states. These computational issues were addressed by specifying conditions for the base case process designs with the conventional solvents by imposing narrow constraints on certain output variables such as aromatic yield and recovery. The optimization of highly sensitive variables such as solvent recirculation rates and distillation reflux ratios thus only function within the constraints specified which increases the probability of effective comparisons with the process designs due to the consistency required in aligning with the baseline methodology.

7

CHAPTER SEVEN

CONCLUSIONS

- Systematic methods incorporating CAMD for the screening of solvents for liquid-liquid extraction processes were developed and applied to the extraction of aromatics from aliphatics.
- Existing solvents and identification of new potential solvents were screened using UNIFAC-LLE, taking into account criteria in terms of physical properties, capacity, selectivity, and performance index.
- The main HSE risks and hazards were identified for conventional and new potential solvents. The type, number, extent, and impact of the hazards determined the overall and individual HSE scores for each solvent using a rating-based system.
- DMF and NMP were ranked as 'Undesirable' with scores of 11 and 10, as a result of their acute and chronic toxicity hazards to humans. Sulfolane and NFM are the best ranking conventional solvents with a score of 7 and rank as 'Usable'.
- Diethanolamine was ranked 'Undesirable' from the potential solvents as it poses serious acute and chronic toxicity hazards to humans, is sensitive to air and light, and has long lasting harmful effects on aquatic life. Diethylenetriamine was ranked 'Undesirable' as it causes severe skin burns and eye damage and is fatal if inhaled.
- Glycerol had the best score of 6 and is the only identified solvent to receive a 'Preferred' rating, as it presents little risk to occupational health and safety and is a renewable bioresource.
- Butane-1,4-diol, and 2-methyl-2,4-pentanediol (hexylene glycol) received the same rating as sulfolane and NFM, and as diols, can be produced in biologically sustainable processes.

- A QSPR model using artificial neural networks was constructed to estimate the binary interaction parameters for the temperature-dependent form of the NRTL model.
- The artificial neural network developed was found to serve as an effective supplement to group contribution methods in the screening of potential solvents for liquid-liquid extraction processes, thus improving the robustness of the overall solvent screening framework.
- Parameters were regressed using experimental LLE and VLE data and checked for consistency with a consistency rate of 98%. Molecule structures were drawn, and descriptors determined with the use of Materials Studio.
- The QSPR model uses 31 descriptors as input and produced absolute average deviations of 0.23 and 0.19 for each pair of binary interaction parameters respectively.
- Novel LLE experimental data were successfully measured at (298.2, 313.2 and 333.2) K and 0.1 MPa for the ternary systems *n*-heptane + toluene + (butane-1,4-diol or glycerol) as well as *n*-nonane + o-xylene + (butane-1,4-diol or glycerol).
- The influence of 2-methyl-2,4-pentanediol on solvent capacity was determined by LLE experimental data for the quaternary system n-heptane + toluene + (butane-1,4-diol or glycerol) + 2-methyl-2,4-pentanediol at (298.2 and 313.2) K and 0.1 MPa.
- All ternary systems studied were found to exhibit type 2 ternary LLE behaviour and were reasonably correlated with the NRTL and UNIQUAC thermodynamic models.
- Both type 1 and type 2 behavior were observed for the pseudo-ternary systems, with the type 1 system occurring at high concentrations of the co-solvent.
- For the molar ratios of 2-methyl-2,4-pentanediol that produced type 2 systems, there did not appear to be significant improvements in solvent capacity, with substantive increases noted with high molar ratios of 2-methyl-2,4-pentanediol, associated with the type 1 system.
- It is recommended that 2-methyl-2,4-pentanediol be used as a co-solvent to 1,4-butanediol and glycerol in the extraction of toluene from n-heptane for the molar ratios that produce type 1 systems, demonstrated at a molar ratio of 1:3 at 298.2 K and 313.2 K.
- An economic comparison of an aromatic extraction process was conducted for the proposed co-solvent mixtures 1,4-butanediol + hexylene glycol and glycerol + hexylene glycol, against that of conventional and commercial solvents used for this application. Indicators such as energy consumption, capital costs, operating costs and total annual costs were used to make an assessment with the process simulations performed in ASPEN Plus V10. The results indicated

that the co-solvent mixtures may offer benefits in reducing total annual cost. The base case design consisted of a 1500 kg,/hr feed stream made up of 30 wt % toluene and 70 wt % *n*-heptane. For all solvents studied in this work, the energy intensity of the process holistically varied between 1000 – 1400 kJ/kg. The capital costs ranged between 5.8 – 6.2 million dollars, and the total annual costs between 2.4 – 2.6 million dollars.

8

CHAPTER EIGHT

LIMITATIONS and RECOMMENDATIONS

Group contribution methods such as UNIFAC-LLE are limited in their application by lack of availability of molecular volume and area parameters. This limits the number of chemicals that can be analysed as new potential solvents. The reliability of liquid-liquid equilibrium predictions using predictive group contribution methods require further development. These models tend to not account for interconnectivity between groups and therefore experience difficulty in accounting for some structural isomers and enantiomers. While this study attempts to address these shortcomings with a QSPR model that provides *a priori* predictions of NRTL parameters, the method is entirely empirical and still dependent on regression of interaction parameters based on published phase equilibrium data. It would add considerable value for future work to focus on the development of activity coefficient models, not from the perspective of group contribution methods, but rather on some of the QSPR descriptors used in this work such as topological indices (that include atom connectivity) and Jurs descriptors.

For the superstructure developed in this work to be effectively utilized by engineering and R&D personnel it would require access to specialized software (such as Materials Studio) and knowledge of various types of models including artificial neural networks to be able to effectively implement. It would be most beneficial for all steps in this framework to be consolidated into a single tool that takes as input the carrier liquid and solute and proposes new and potential solvents by performing the molecular design models, HSE risk assessments, and process economics analysis. This would require creating a large database of chemicals with the molecular descriptors used in this work.

APPENDIX A

Temperature Sensor Calibration

The Pt-100 temperature sensor was calibrated with a Wika CTB 9100 unit. The sensor and standard probe were immersed in an oil liquid bath for which the temperature was varied from 293.2 K to 373.2 K and back to 293.2 K in 5 K increments. The temperature readings were recorded at all setpoint temperatures, and the calibration curve was subsequently developed as shown in Figure A1 with deviations in Figure A2.

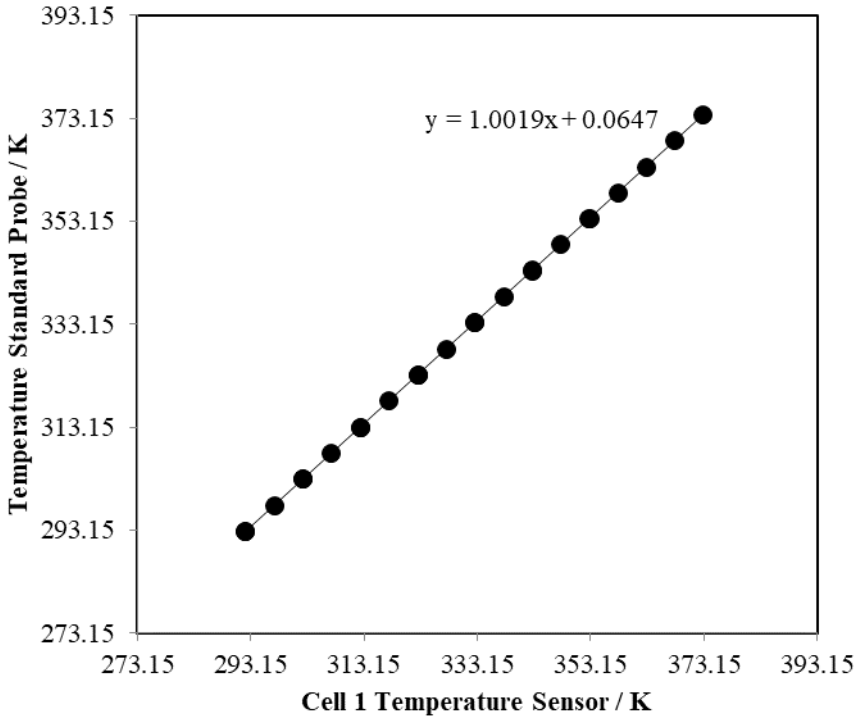

Figure A1: Temperature calibration plot of cell 1 temperature sensor.

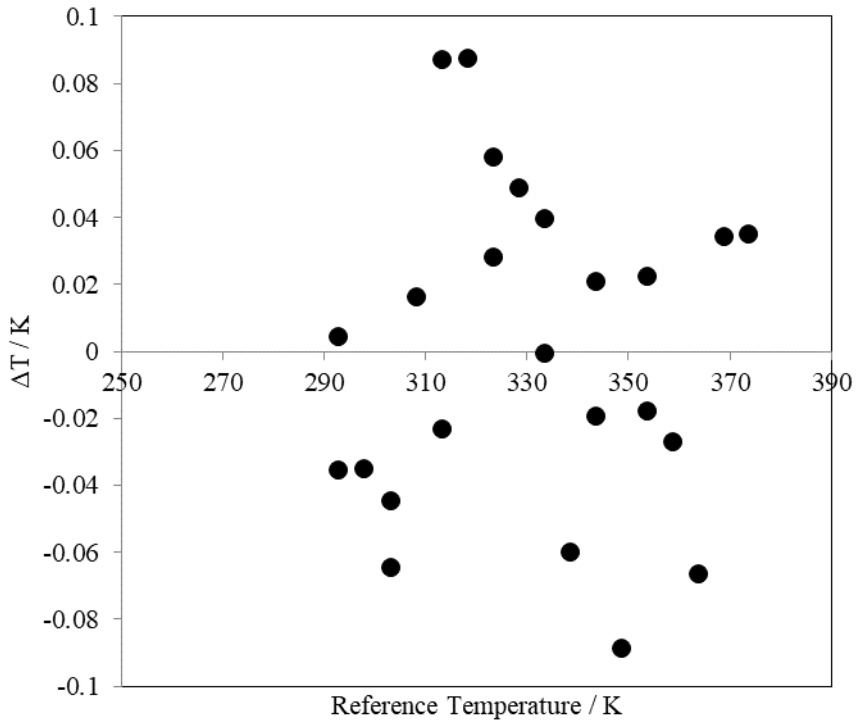

Figure A2: Temperature deviation plot of cell 1 temperature sensor.

The expanded uncertainty in temperature *U(T)* was determined as per the propagation equation by taking into account deviations resulting from the calibration and inherent deviations in the measuring instruments and devices.

$$U(T) = k \times \pm\sqrt{u_{calibration}(T)^2 + u_{instrument}(T)^2 + u_{repeatability}(T)^2} \qquad \text{(A-1)}$$

The coverage factor (*k*) was set to two based on a 95% confidence interval.

Gas Chromatograph Detector Calibrations

Consistency of area ratios were determined by assessing if the standard deviation was within 1% of the mean for a minimum of three samples.

$$u_{repeatability} = \frac{\text{Standard Deviation}}{\text{Average}} \times 100\% \qquad \text{(A-2)}$$

The absolute average deviation (*AAD*) was determined as follows:

$$AAD = \frac{\sum_{i=1}^{k} |\Delta x_1|}{k} \tag{A-3}$$

Where:

$$\Delta x_1 = (x_1)_{calibration} - (x_1)_{standard} \tag{A-4}$$

The expanded uncertainty in composition $U(x_i)$ was determined using the propagation equation in a similar manner to the temperature uncertainty, by accounting for deviations in the calibration, deviations inherent in the measuring devices (weigh scale), uncertainty due to averaging of response areas, and uncertainties from general material handling and evaporation. The coverage factor (*k*) was again specified as two based on a 95% confidence interval.

$$U(x_i) = k \times \pm \sqrt{u_{calibration}(x_i)^2 + u_{instrument}(x_i)^2 + u_{repeatability}(x_i)^2} \tag{A-5}$$

System	Calibration	Dilute Region	AAD (Mole Fraction)
n-Heptane + Toluene + (1,4-Butanediol or Glycerol):			
n-Heptane (1) + Toluene (2)	$\frac{x_1}{x_2} = 0.9737 \left(\frac{A_1}{A_2}\right) + 0.0036$	*n*-Heptane	8.91×10^{-4}
	$\frac{x_2}{x_1} = 1.1427 \left(\frac{A_2}{A_1}\right) + 0.0004$	Toluene	1.56×10^{-3}
Toluene (1) + 1,4-Butanediol (2)	$\frac{x_1}{x_2} = 0.8409 \left(\frac{A_1}{A_2}\right) + 0.0042$	Toluene	2.67×10^{-3}
	$\frac{x_2}{x_1} = 1.1819 \left(\frac{A_2}{A_1}\right) + 0.02$	1,4-Butanediol	1.55×10^{-3}

Toluene (1) + Glycerol (2)	$\frac{x_1}{x_2} = 0.5535 \left(\frac{A_1}{A_2}\right) + 0.0072$	Toluene	1.08×10^{-2}
	$\frac{x_2}{x_1} = 1.8853 \left(\frac{A_2}{A_1}\right) + 0.0293$	Glycerol	1.81×10^{-3}
n-Nonane + *o*-Xylene + (1,4-Butanediol or Glycerol):			
n-Nonane (1) + *o*-Xylene (2)	$\frac{x_1}{x_2} = 0.7162 \left(\frac{A_1}{A_2}\right) + 0.0209$	*n*-Nonane	1.01×10^{-2}
	$\frac{x_2}{x_1} = 1.3246 \left(\frac{A_2}{A_1}\right) + 0.0203$	*o*-Xylene	1.41×10^{-2}
o-Xylene (1) + 1,4-Butanediol (2)	$\frac{x_1}{x_2} = 0.4085 \left(\frac{A_1}{A_2}\right) + 0.0152$	*o*-Xylene	1.35×10^{-2}
	$\frac{x_2}{x_1} = 2.4852 \left(\frac{A_2}{A_1}\right) + 0.0001$	1,4-Butanediol	3.92×10^{-2}
o-Xylene (1) + Glycerol (2)	$\frac{x_1}{x_2} = 0.412 \left(\frac{A_1}{A_2}\right) + 0.0076$	*o*-Xylene	4.9×10^{-3}
	$\frac{x_2}{x_1} = 6.0593 \left(\frac{A_2}{A_1}\right) + 0.023$	Glycerol	6.84×10^{-3}
n-Heptane + Toluene + 1,4-Butanediol + 2-methyl-2,4-pentanediol:			
n-Heptane (1) + Toluene (2)	$\frac{x_1}{x_2} = 0.8645 \left(\frac{A_1}{A_2}\right) - 0.002$	*n*-Heptane	6.26×10^{-4}
	$\frac{x_2}{x_1} = 1.1638 \left(\frac{A_2}{A_1}\right) - 0.002$	Toluene	1.2×10^{-3}
Toluene (1) + 1,4-Butanediol (2)	$\frac{x_1}{x_2} = 0.7011 \left(\frac{A_1}{A_2}\right) + 0.0127$	Toluene	9.23×10^{-3}
	$\frac{x_2}{x_1} = 1.4579 \left(\frac{A_2}{A_1}\right) + 0.049$	1,4-Butanediol	8.25×10^{-3}

Toluene (1) + 2-methyl-2,4-pentanediol (2)	$\frac{x_1}{x_2} = 0.7327 \left(\frac{A_1}{A_2}\right) + 0.0063$	Toluene	9.36×10^{-3}
	$\frac{x_2}{x_1} = 1.3598 \left(\frac{A_2}{A_1}\right) + 0.0854$	2-methyl-2,4-pentanediol	8.67×10^{-3}
n-Heptane + Toluene + glycerol + 2-methyl-2,4-pentanediol:			
n-Heptane (1) + Toluene (2)	$\frac{x_1}{x_2} = 0.8198 \left(\frac{A_1}{A_2}\right) + 0.0645$	*n*-Heptane	6.16×10^{-3}
	$\frac{x_2}{x_1} = 0.9828 \left(\frac{A_2}{A_1}\right) + 0.0041$	Toluene	5.17×10^{-3}
Toluene (1) + glycerol (2)	$\frac{x_1}{x_2} = 0.0009 \left(\frac{A_1}{A_2}\right)^2 + 0.0137 \left(\frac{A_1}{A_2}\right)$	Toluene	9.77×10^{-3}
	$\frac{x_2}{x_1} = 2.4974 \left(\frac{A_2}{A_1}\right) + 0.0019$	Glycerol	1.03×10^{-2}
Toluene (1) + 2-methyl-2,4-pentanediol (2)	$\frac{x_1}{x_2} = -0.0722 \left(\frac{A_1}{A_2}\right)^2 + 0.6726 \left(\frac{A_1}{A_2}\right)$	Toluene	1.2×10^{-2}
	$\frac{x_2}{x_1} = 6.0593 \left(\frac{A_2}{A_1}\right) + 0.023$	2-methyl-2,4-pentanediol	7.16×10^{-3}

n-Heptane + Toluene + (1,4-Butanediol or glycerol):

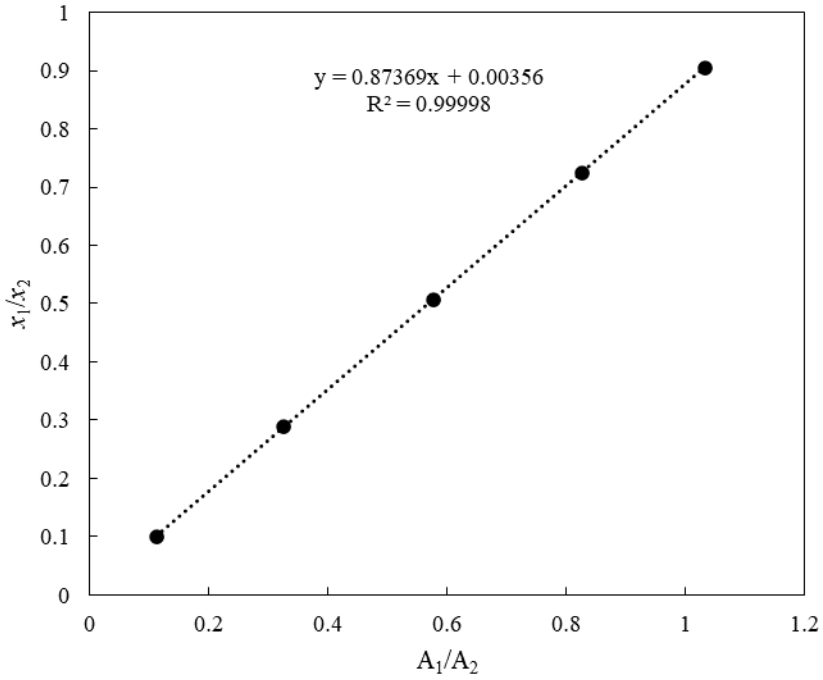

Figure A3: GC detector calibration graph of *n*-heptane (1) + toluene (2) (*n*-heptane dilute region)

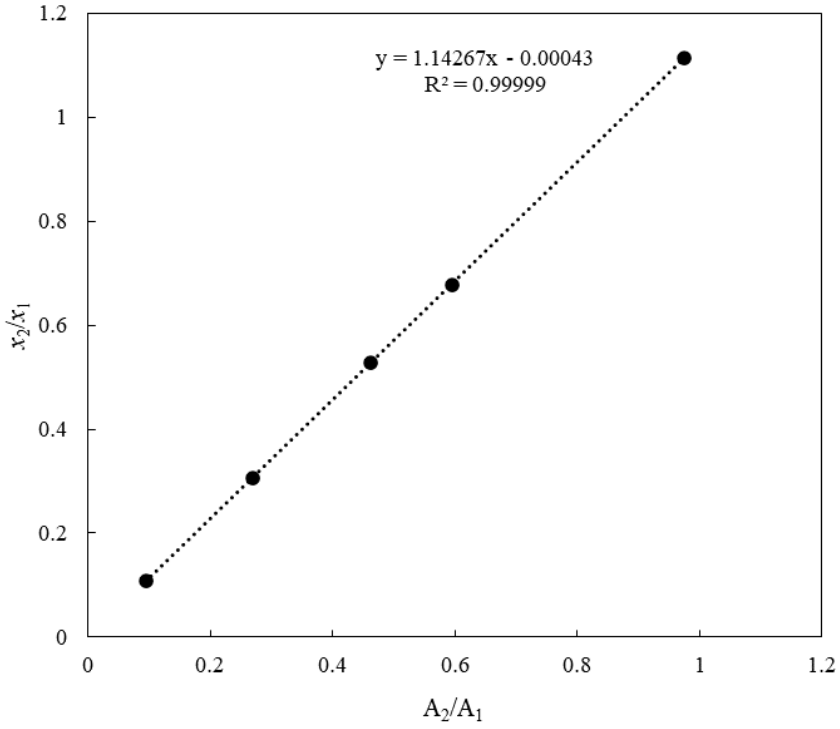

Figure A4: GC detector calibration graph of *n*-heptane (1) + toluene (2) (toluene dilute region)

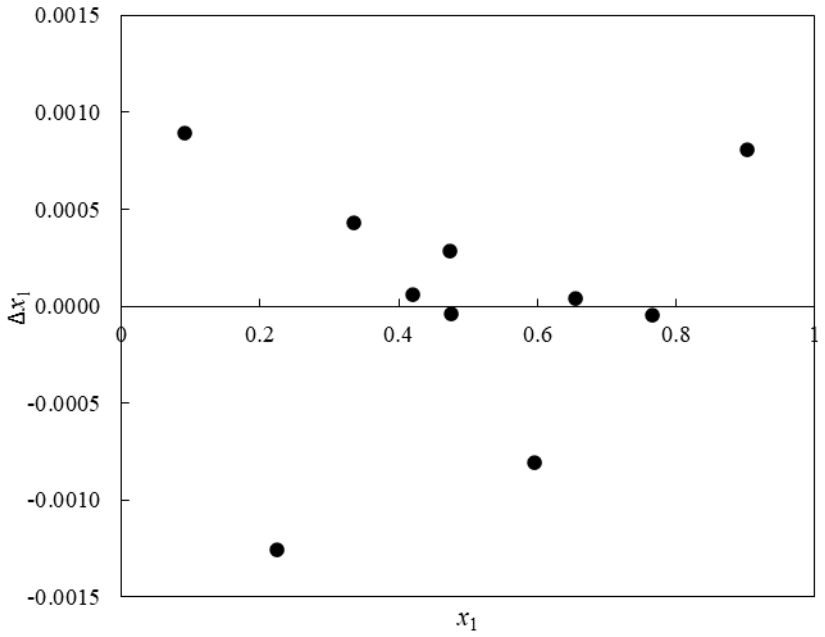

Figure A5: Composition deviation plot for the *n*-heptane (1) + toluene (2) system

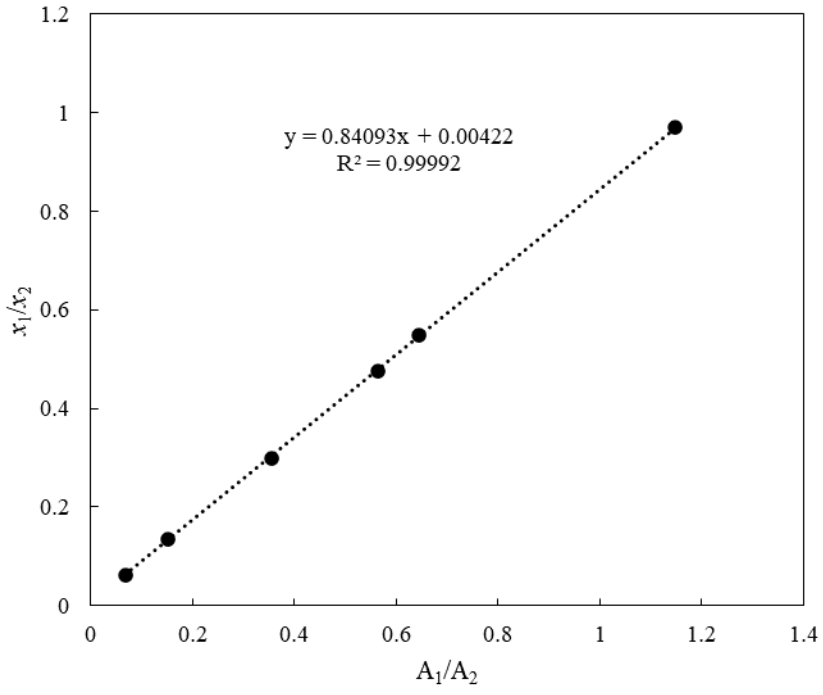

Figure A6: GC detector calibration graph of toluene (1) + 1,4-butanediol (2) (toluene dilute region)

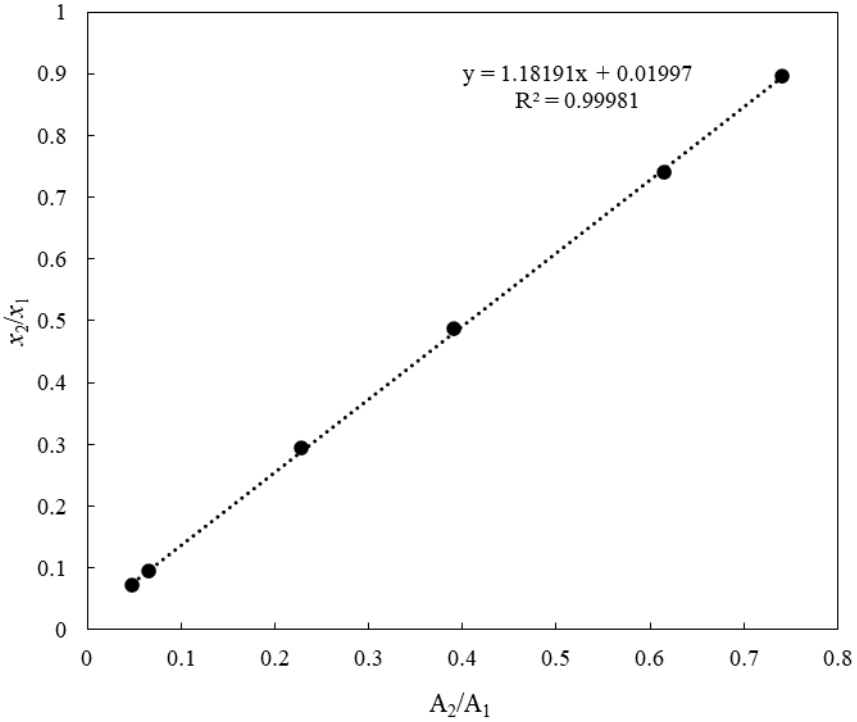

Figure A7: GC detector calibration graph of toluene (1) + 1,4-butanediol (2) (1,4-butanediol dilute region)

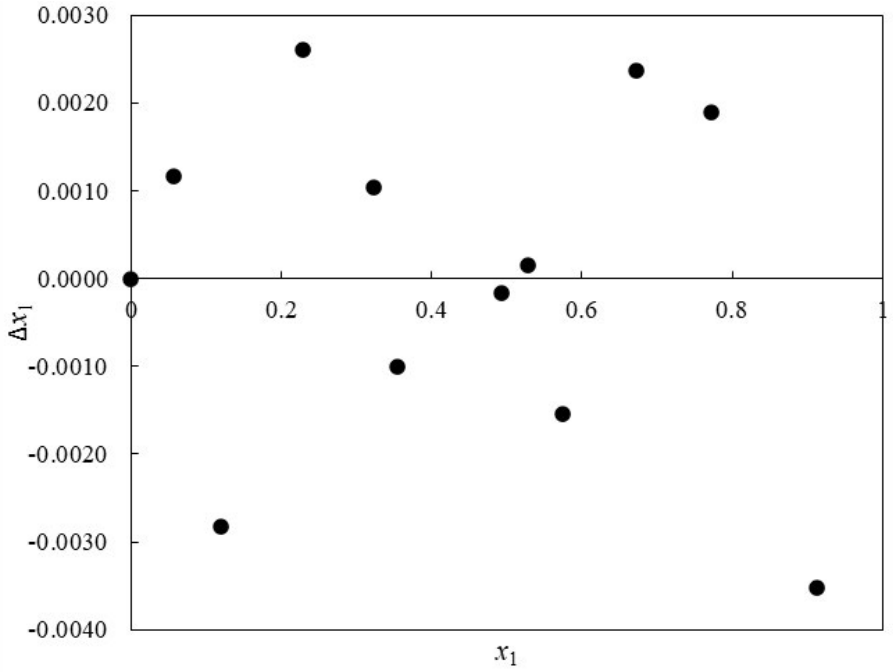

Figure A8: Composition deviation plot for the toluene (1) + 1,4-butanediol (2) system

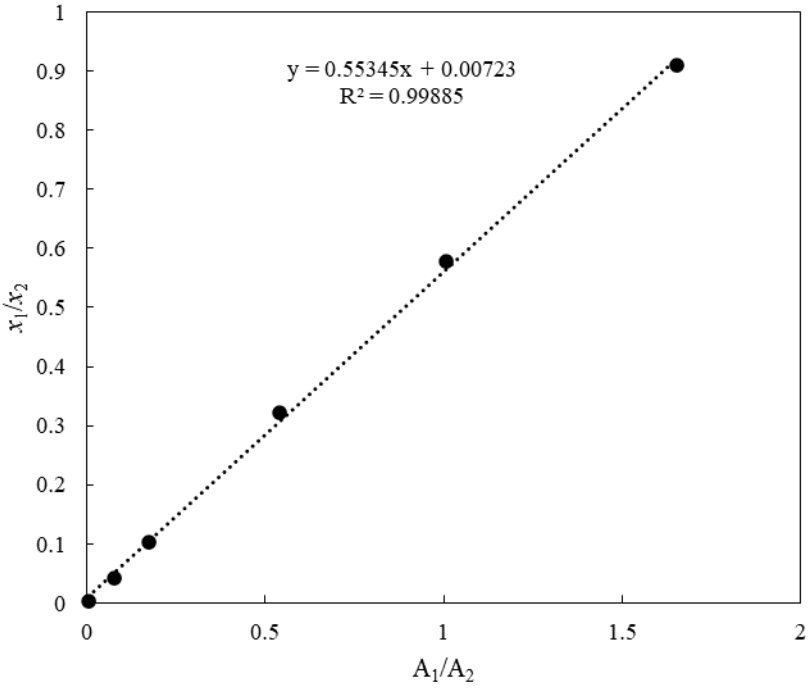

Figure A9: GC detector calibration graph of toluene (1) + glycerol (2) (toluene dilute region)

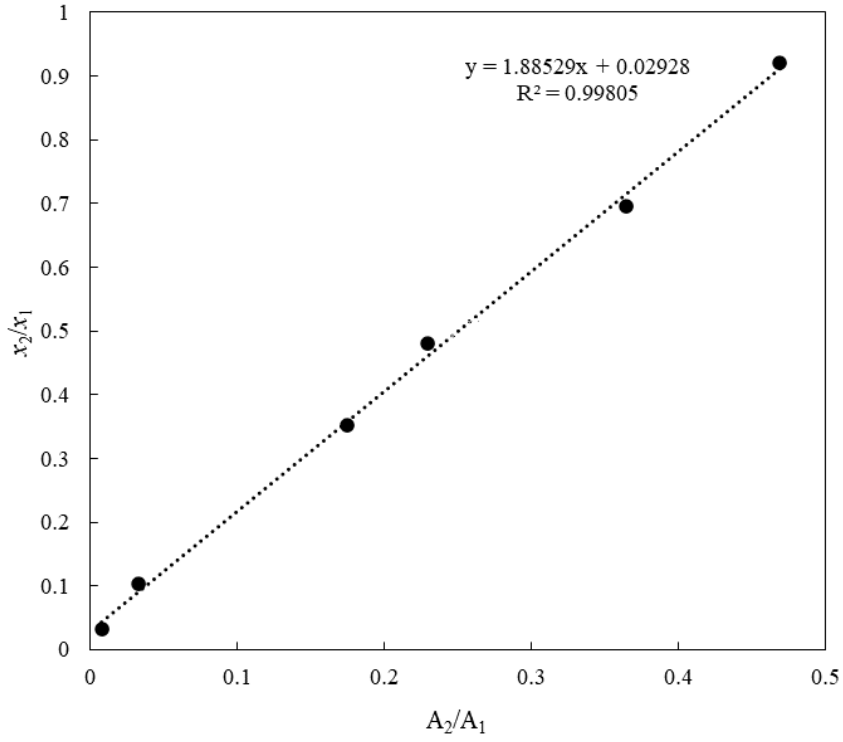

Figure A10: GC detector calibration graph of toluene (1) + glycerol (2) (glycerol dilute region)

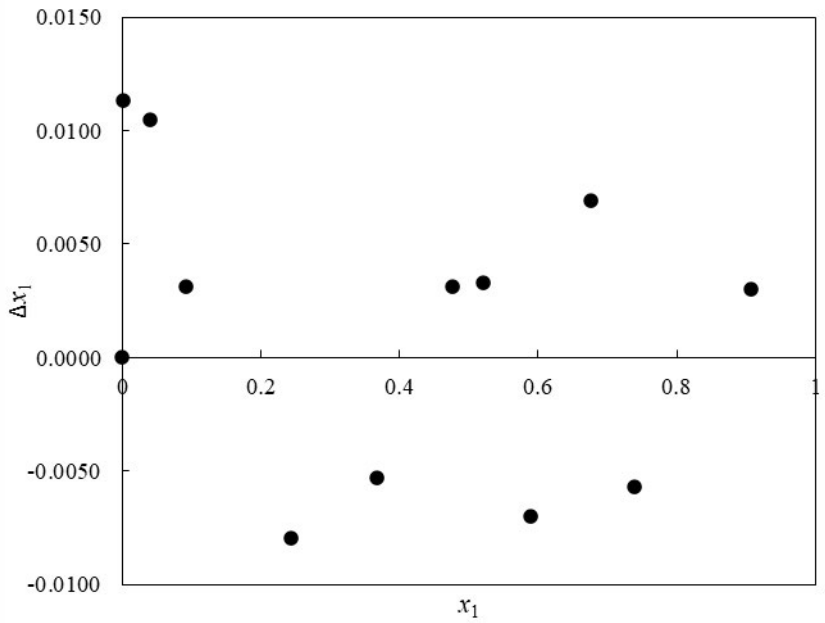

Figure A11: Composition deviation plot for the toluene (1) + glycerol (2) system

n-Nonane + *o*-Xylene + (1,4-Butanediol or glycerol):

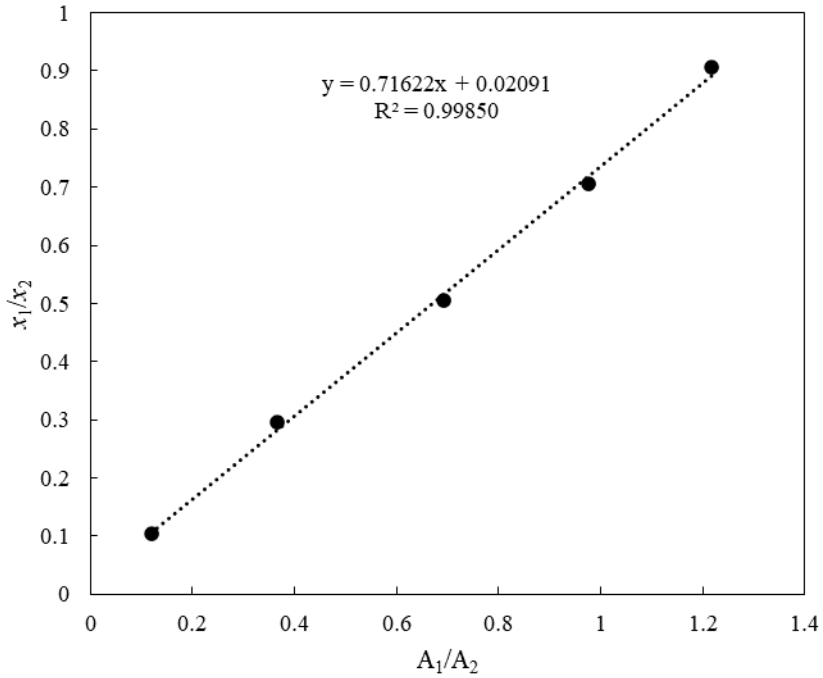

Figure A12: GC detector calibration graph of *n*-nonane (1) + *o*-xylene (2) (*n*-nonane dilute region)

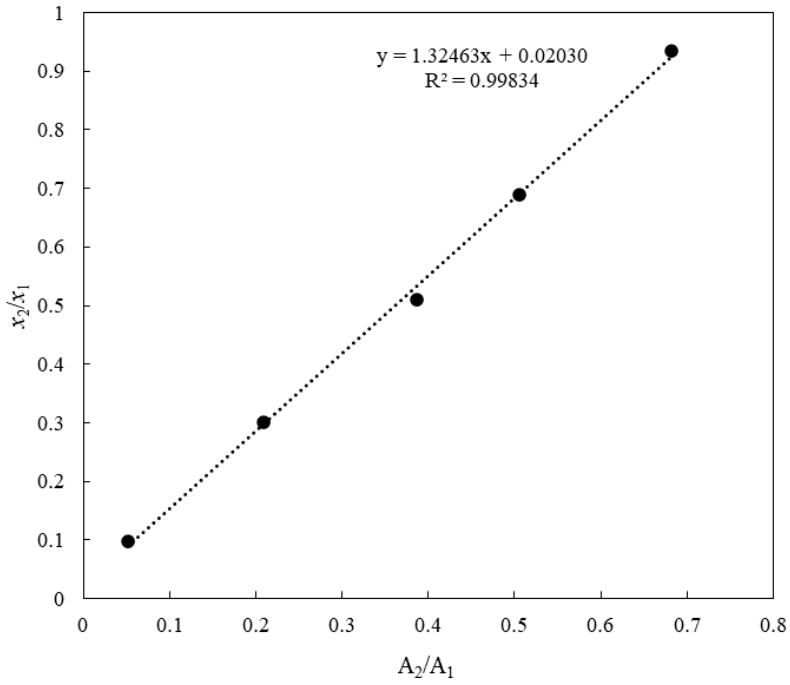

Figure A13: GC detector calibration graph of *n*-nonane (1) + *o*-xylene (2) (*o*-xylene dilute region)

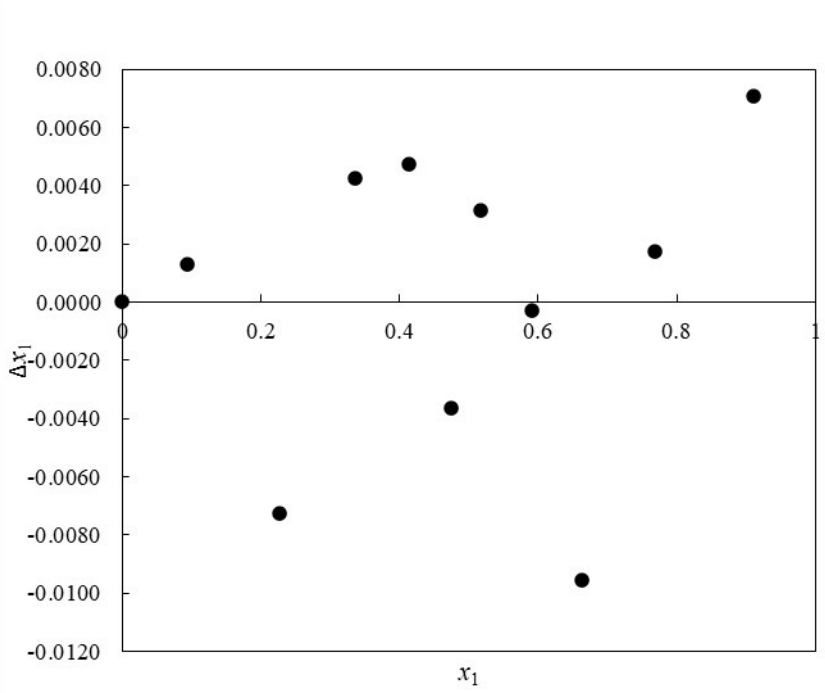

Figure A14: Composition deviation plot for the *n*-nonane (1) + *o*-xylene (2) system

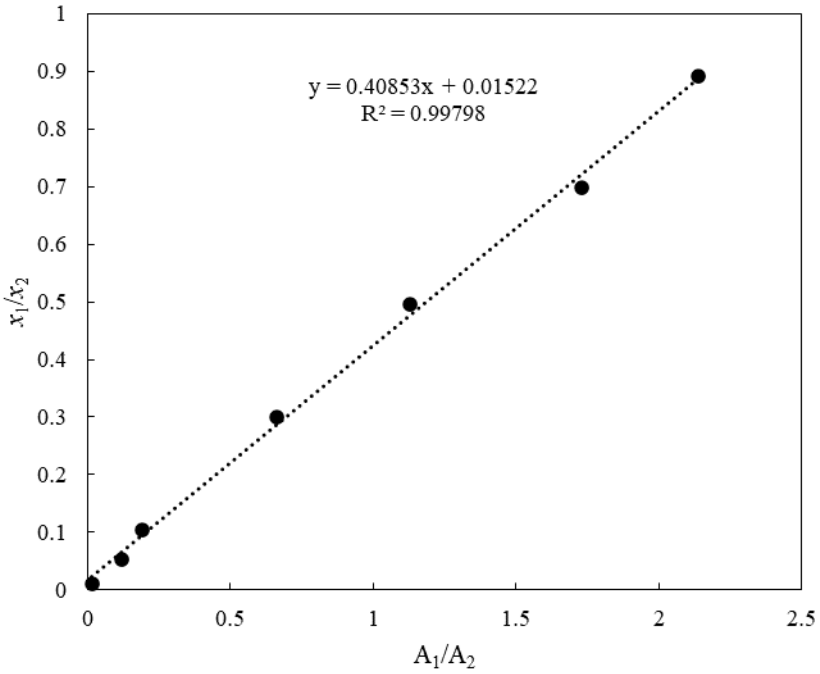

Figure A15: GC detector calibration graph of *o*-xylene (1) + 1,4-butanediol (2) (*o*-xylene dilute region)

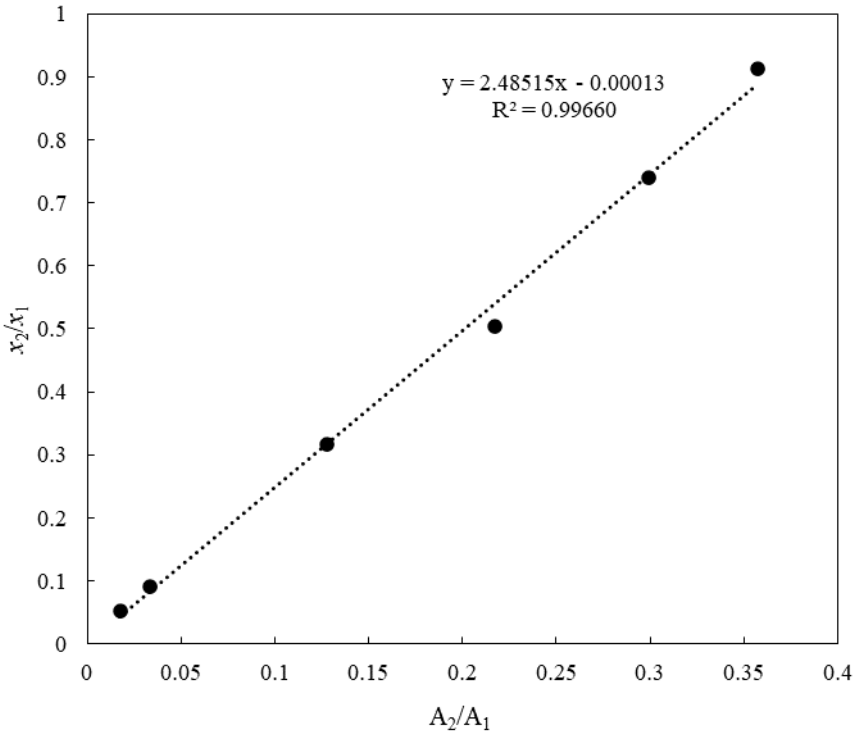

Figure A16: GC detector calibration graph of *o*-xylene (1) + 1,4-butanediol (2) (1,4-butanediol dilute region)

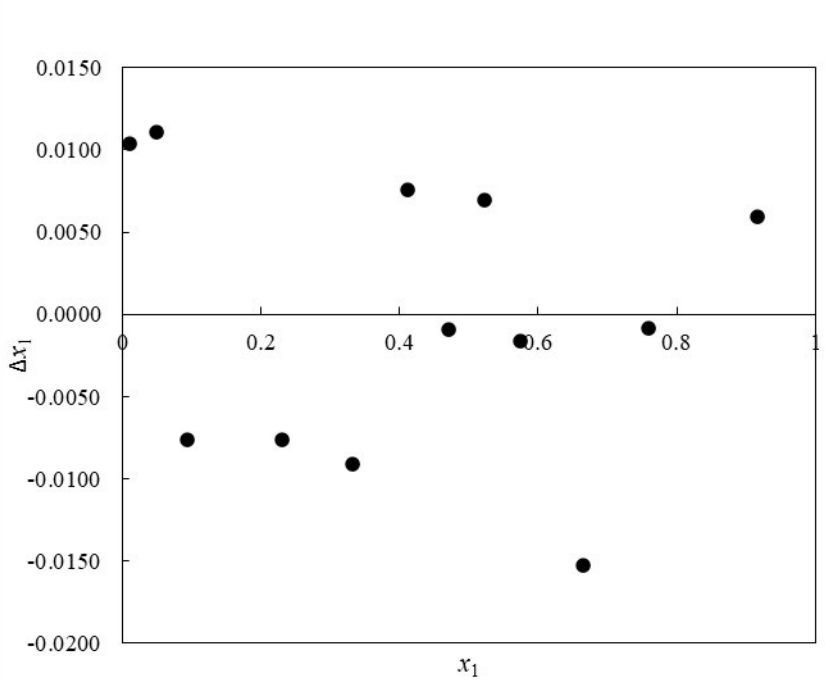

Figure A17: Composition deviation plot for the *o*-xylene (1) + 1,4-butanediol (2) system

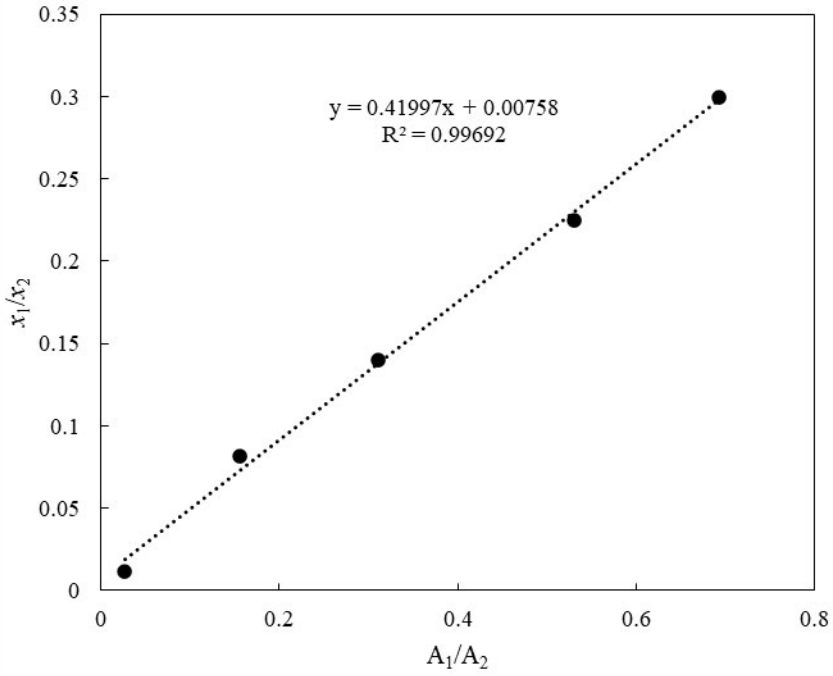

Figure A18: GC detector calibration graph of *o*-xylene (1) + glycerol (2) (*o*-xylene dilute region)

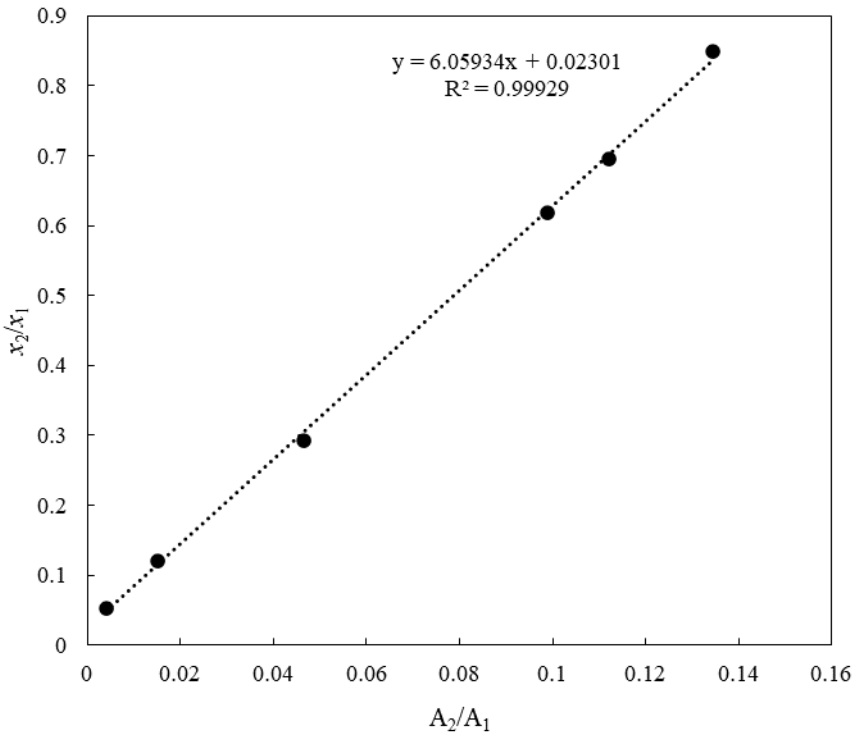

Figure A19: GC detector calibration graph of *o*-xylene (1) + glycerol (2) (glycerol dilute region)

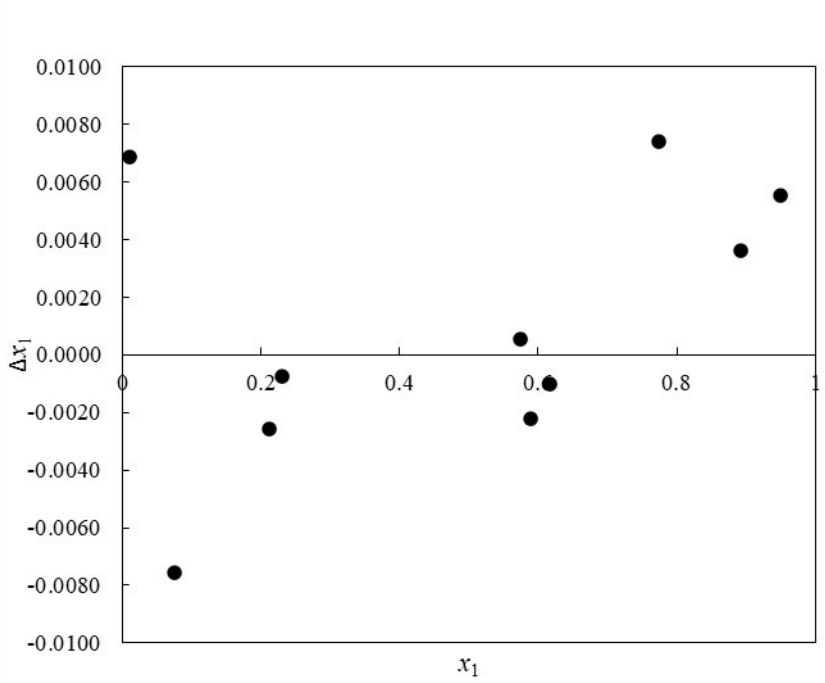

Figure A20: Composition deviation plot for the *o*-xylene (1) + glycerol (2) system

n-Heptane + Toluene + 1,4-Butanediol + 2-methyl-2,4-pentanediol:

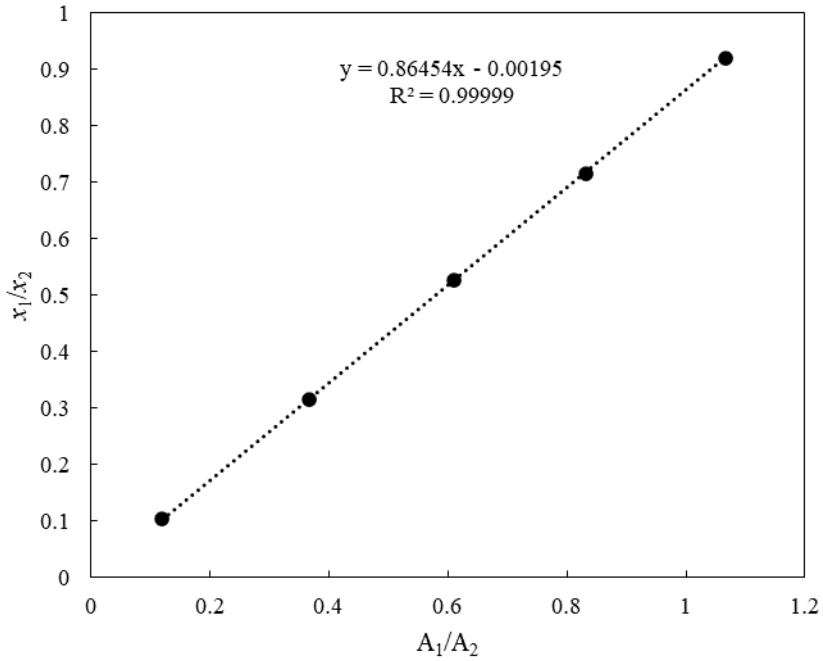

Figure A21: GC detector calibration graph of *n*-heptane (1) + toluene (2) (*n*-heptane dilute region)

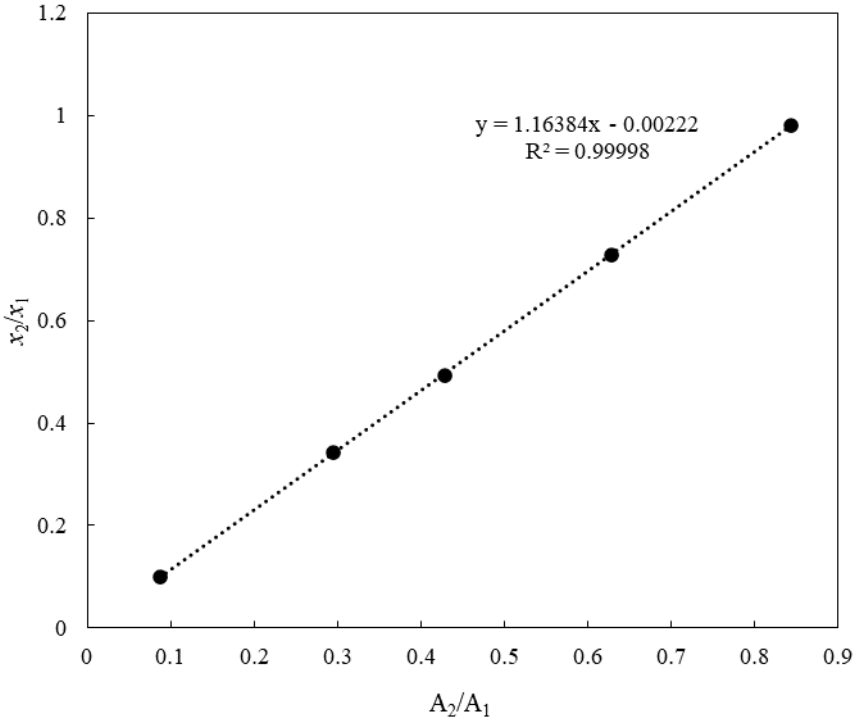

Figure A22: GC detector calibration graph of *n*-heptane (1) + toluene (2) (toluene dilute region)

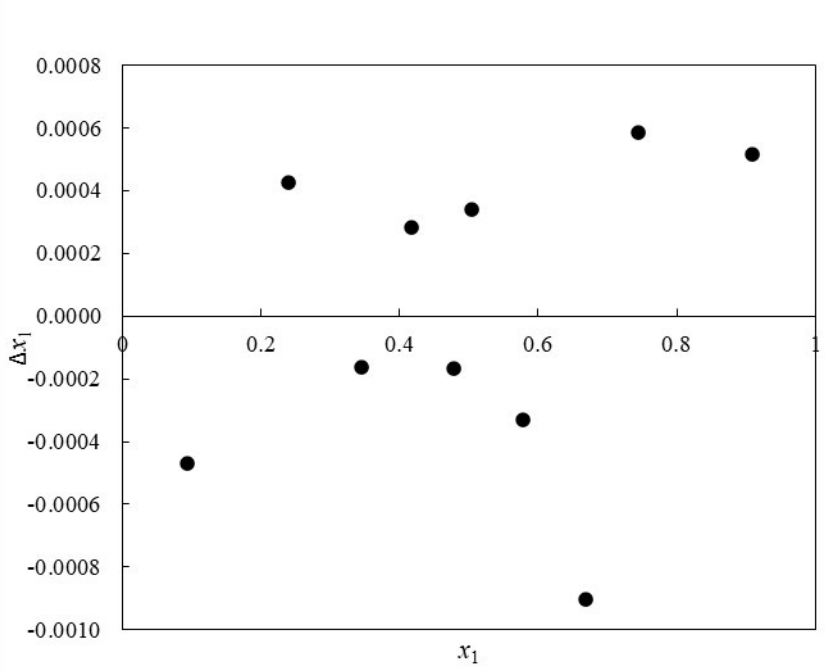

Figure A23: Composition deviation plot for the *n*-heptane (1) + toluene (2) system

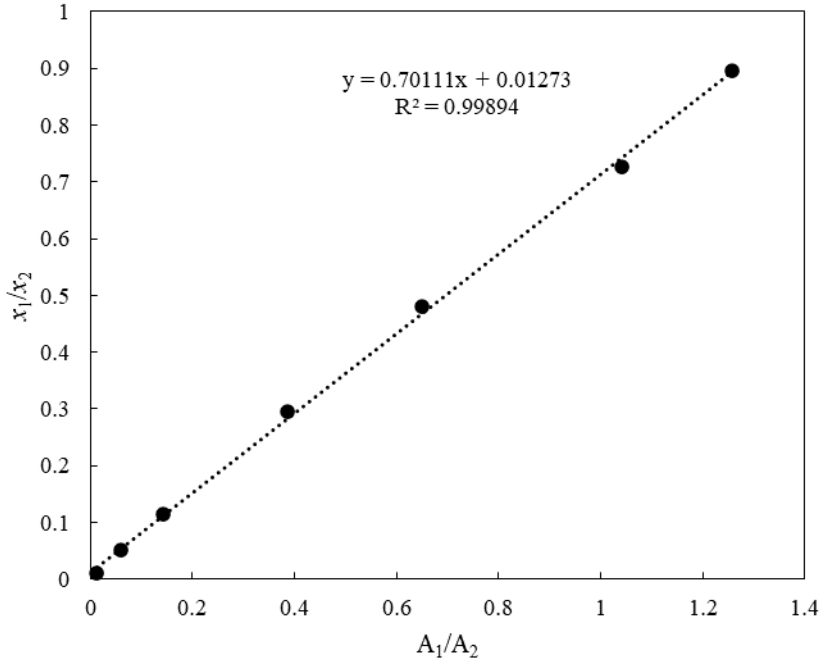

Figure A24: GC detector calibration graph of toluene (1) + 1,4-butanediol (2) (toluene dilute region)

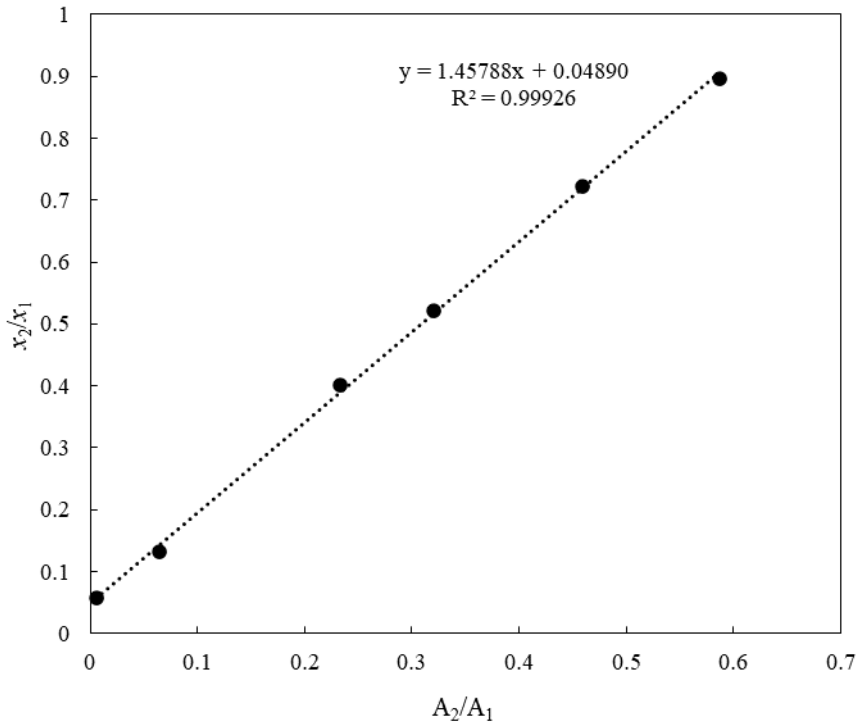

Figure A25: GC detector calibration graph of toluene (1) + 1,4-butanediol (2) (1,4-butanediol dilute region)

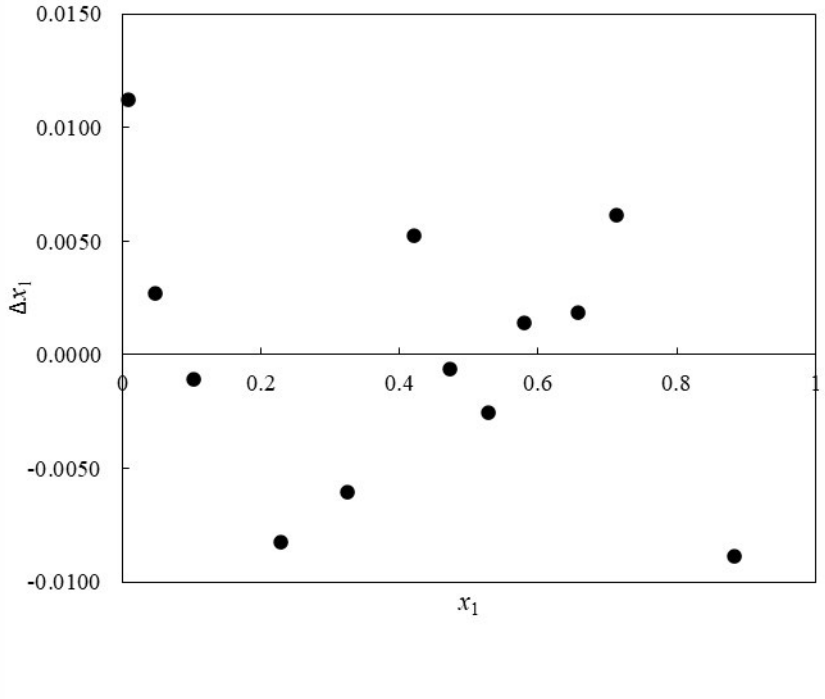

Figure A26: Composition deviation plot for the toluene (1) + 1,4-butanediol (2) system

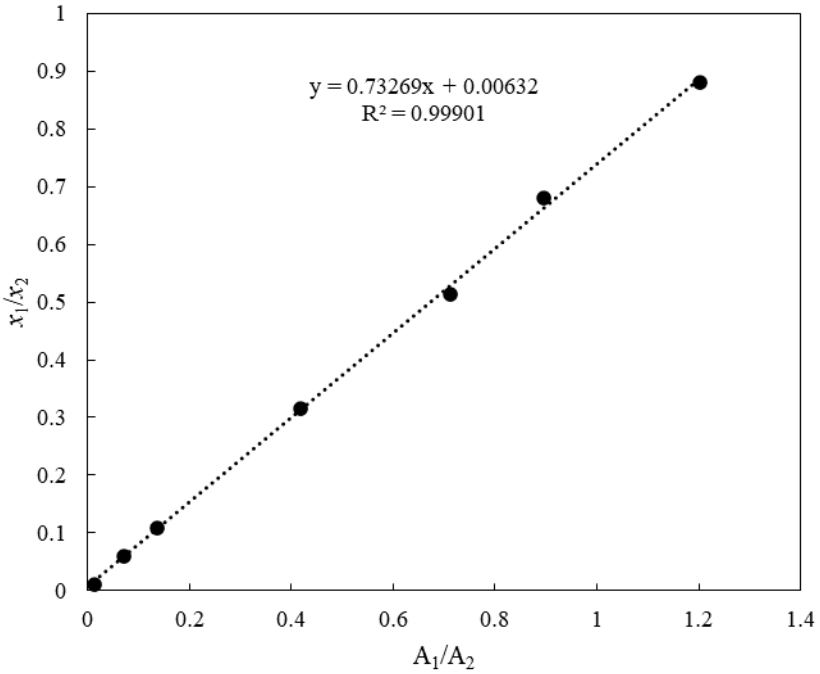

Figure A27: GC detector calibration graph of toluene (1) + 2-methyl-2,4-pentanediol (2) (toluene dilute region)

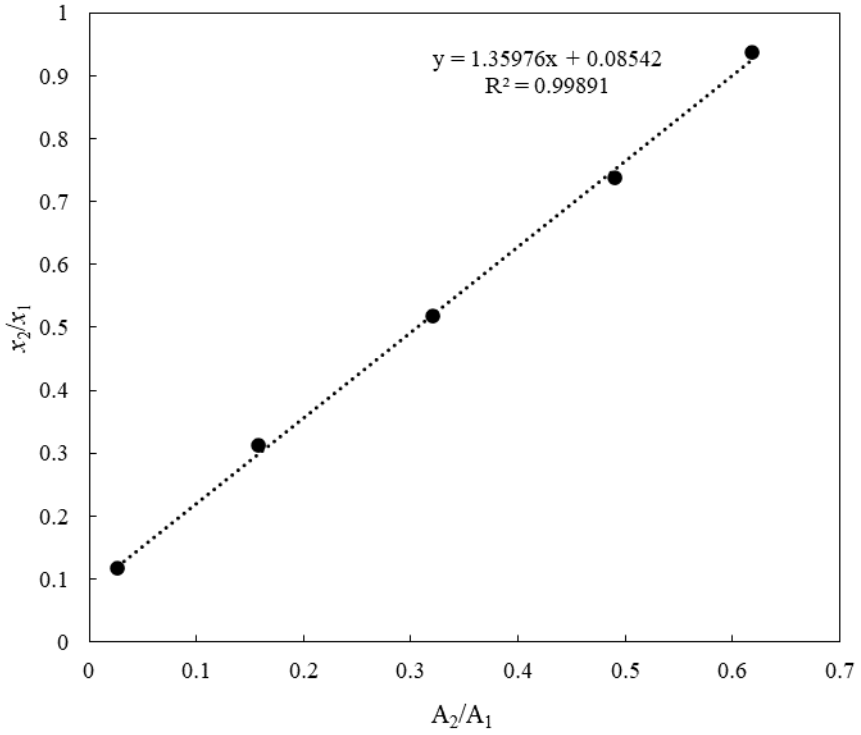

Figure A28: GC detector calibration graph of toluene (1) + 2-methyl-2,4-pentanediol (2) (2-methyl-2,4-pentanediol dilute region)

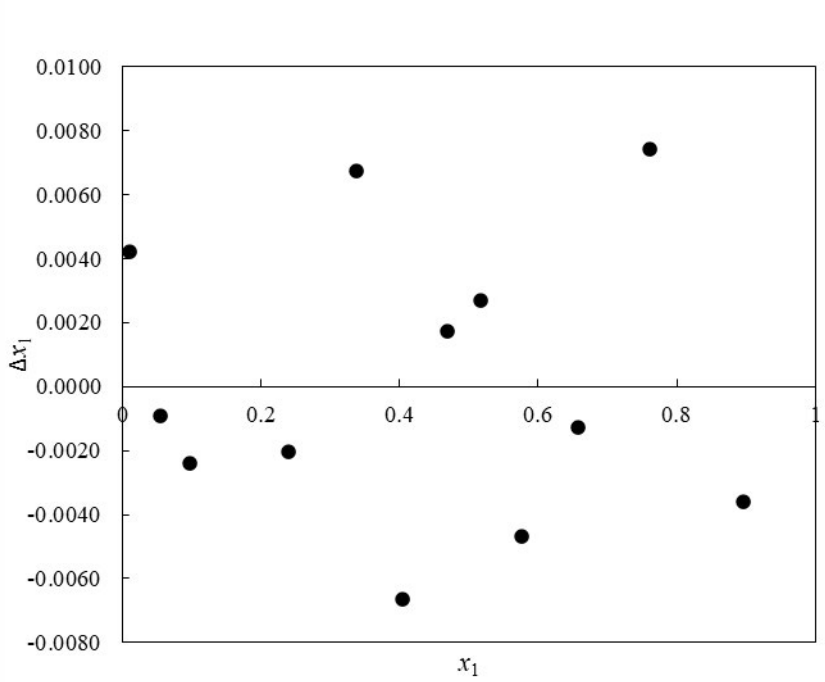

Figure A29: Composition deviation plot for the toluene (1) + 2-methyl-2,4-pentanediol (2) system

n-Heptane + Toluene + Glycerol + 2-methyl-2,4-pentanediol:

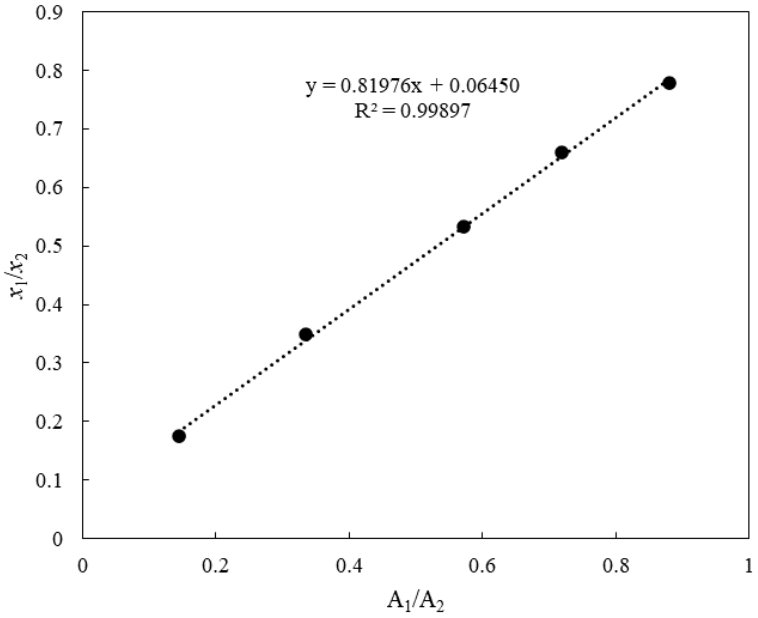

Figure A30: GC detector calibration graph of *n*-heptane (1) + toluene (2) (n-heptane dilute region)

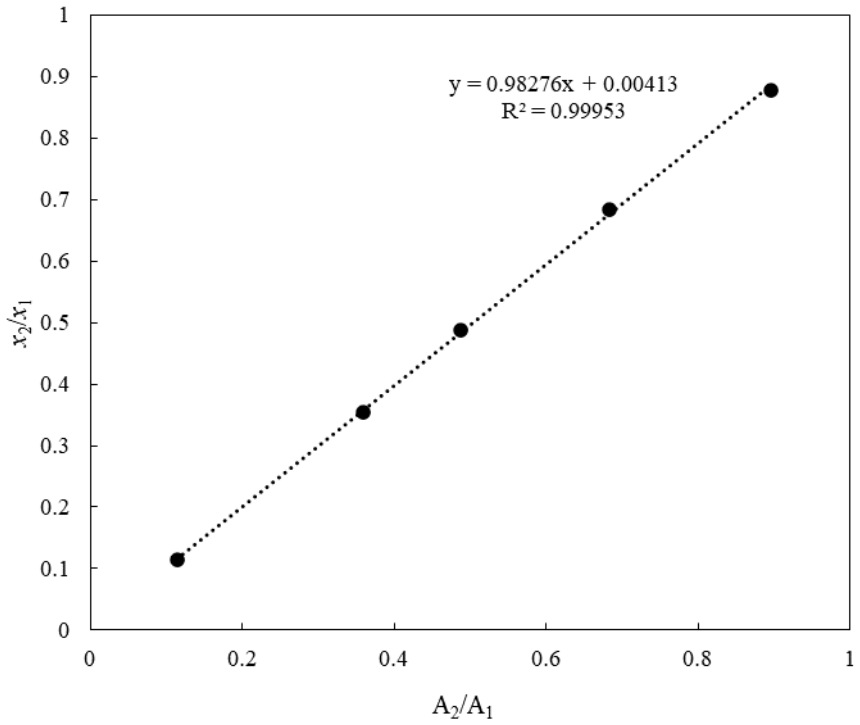

Figure A31: GC detector calibration graph of *n*-heptane (1) + toluene (2) (toluene dilute region)

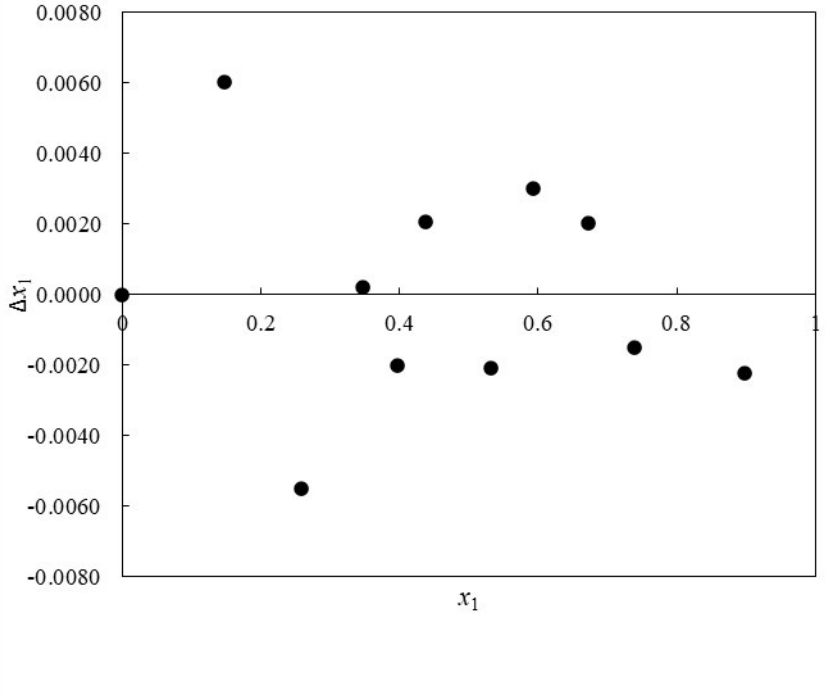

Figure A32: Composition deviation plot for the *n*-heptane (1) + toluene (2) system

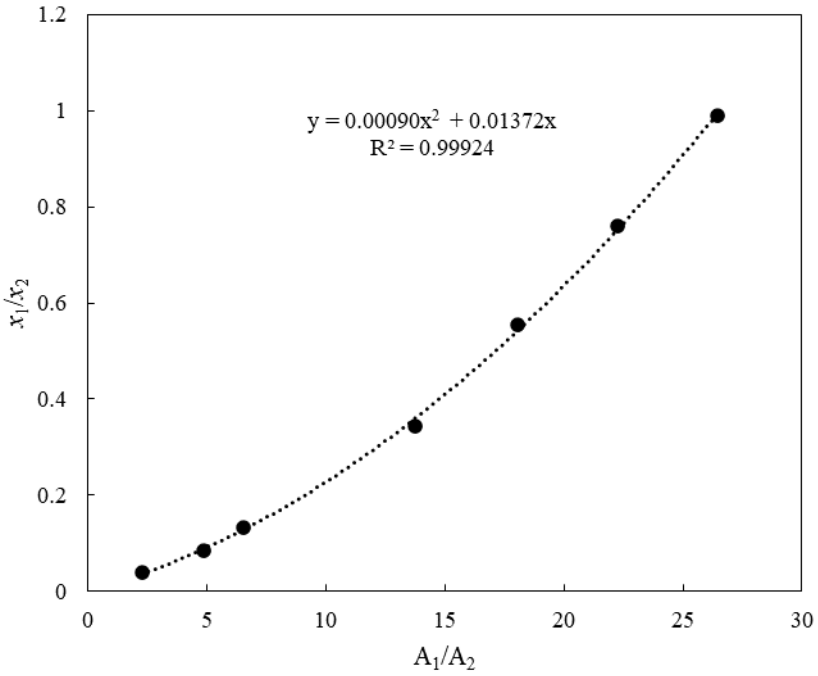

Figure A33: GC detector calibration graph of toluene (1) + glycerol (2) (toluene dilute region)

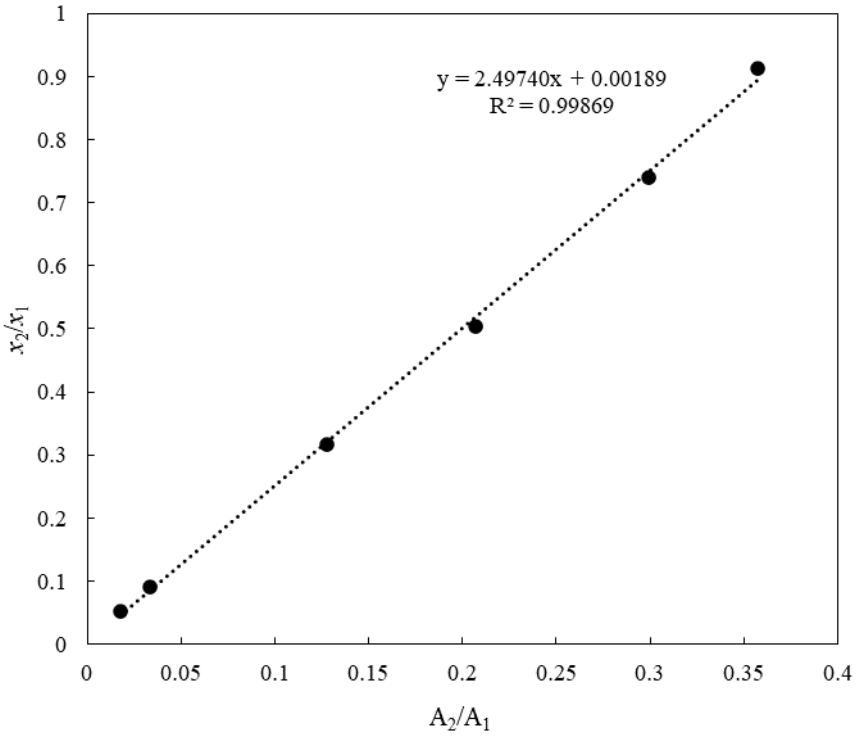

Figure A34: GC detector calibration graph of toluene (1) + glycerol (2) (glycerol dilute region)

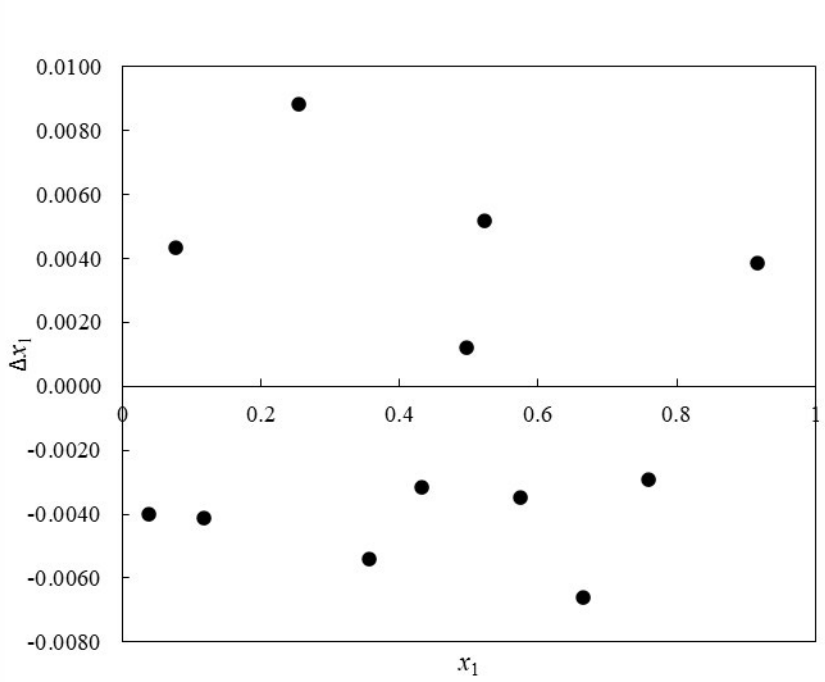

Figure A35: Composition deviation plot for the toluene (1) + glycerol (2) system

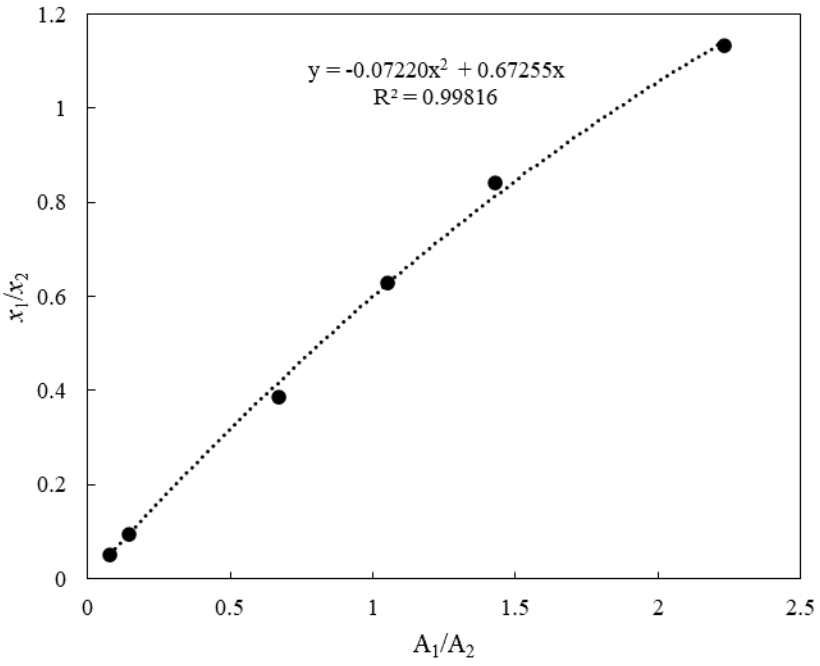

Figure A36: GC detector calibration graph of toluene (1) + 2-methyl-2,4-pentanediol (2) (toluene dilute region)

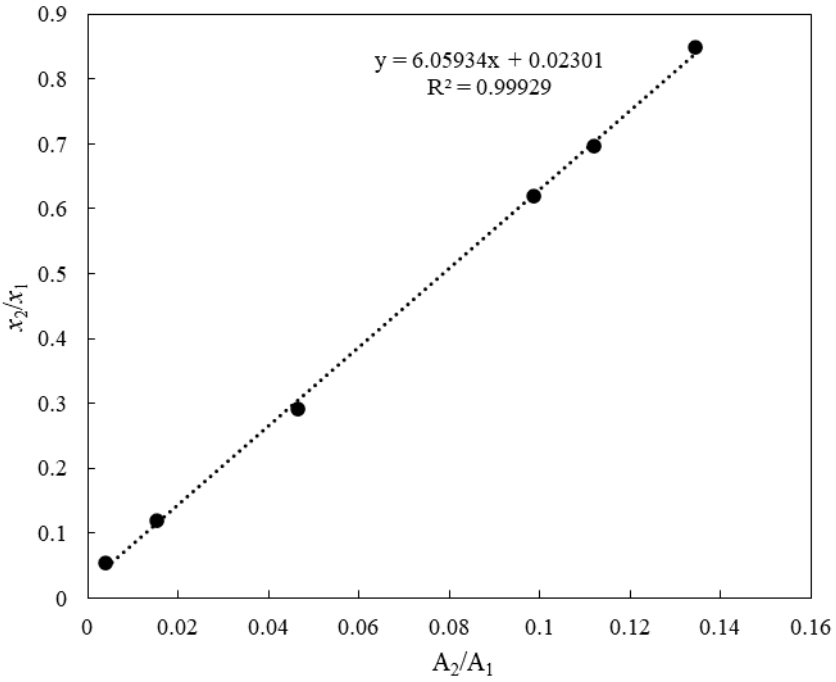

Figure A37: GC calibration graph of toluene (1) + 2-methyl-2,4-pentanediol (2) (2-methyl-2,4-pentanediol dilute region)

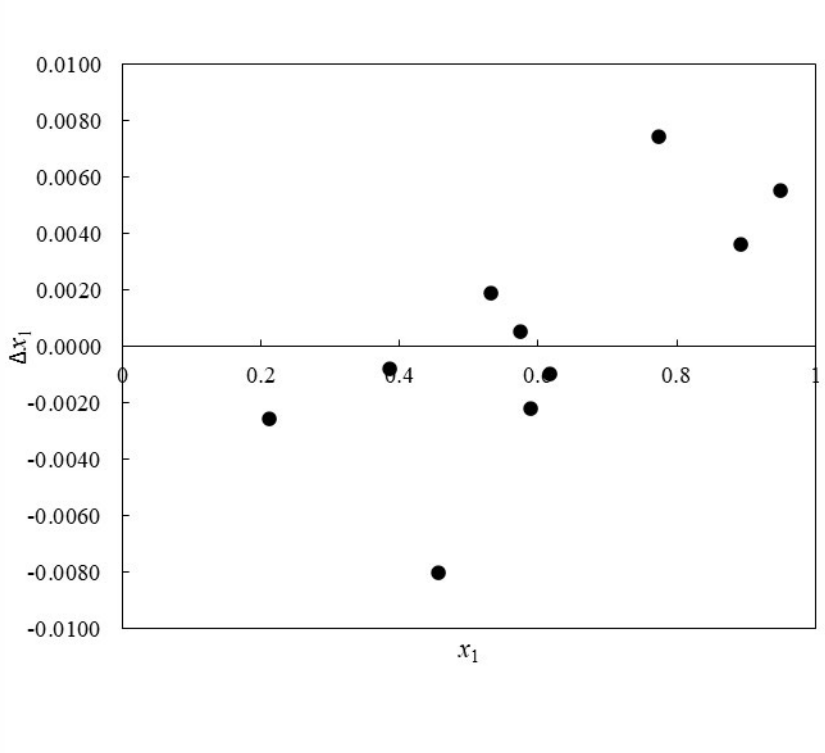

Figure A38: Composition deviation plot for the toluene (1) + 2-methyl-2,4-pentanediol (2) system

APPENDIX B

Table B1: Artificial neural network hidden layer weightings for τ_{ij}

Node	1	2	3	4	5	6	7	8	9	10	11	12	13	14	15	16	17	18
AlogP (Fast Descriptors)	0.39	0.57	0.69	-0.33	0.97	0.21	-0.50	0.08	1.52	1.05	0.91	-1.00	-0.32	0.43	0.10	1.76	0.30	-1.65
Balaban index JX (Fast Descriptors)	0.48	-0.65	0.65	0.15	1.20	0.64	0.20	0.43	-0.89	-1.09	1.14	1.41	-0.86	-0.88	0.55	-1.04	0.46	0.13
Wiener index (Fast Descriptors)	-0.42	1.83	0.32	-0.70	1.40	-0.09	0.18	-0.37	0.22	0.89	0.82	-0.10	1.31	0.64	0.28	-1.48	2.29	-2.71
Molecular density (Spatial Descriptors)	-0.80	-1.02	-0.81	-0.31	-1.25	-1.11	1.02	-0.52	-0.60	-0.49	0.02	1.37	1.23	-0.03	-0.18	0.35	-0.40	-1.05
Principal moments of inertia (magnitude) (Spatial Descriptors)	1.36	-0.22	0.44	1.15	-0.26	-1.82	-0.28	0.98	0.39	1.28	0.86	-0.15	0.88	0.50	0.34	1.11	0.74	-2.13
Principal moment of inertia X (Spatial Descriptors)	0.85	-1.17	-1.04	-0.70	0.74	-0.75	0.27	0.62	0.75	-0.96	-0.50	-1.75	-0.19	-0.11	-0.58	-1.43	-1.40	2.42
Ellipsoidal volume (Spatial Descriptors)	0.97	0.09	-0.10	-0.46	-2.70	-0.88	-1.05	0.24	-0.61	1.44	-1.65	-0.13	1.53	-0.77	-1.42	-0.21	-0.14	1.89
Shadow area: YZ plane (Spatial Descriptors)	-0.47	0.01	-0.46	-0.13	-0.05	-0.21	0.14	-0.38	0.39	-0.11	-0.14	0.06	1.19	-0.37	-1.39	-0.88	0.54	1.15
Shadow area fraction: XY plane (Spatial Descriptors)	-1.09	0.60	-0.39	-0.59	1.69	1.40	-0.31	0.07	-1.18	0.58	-1.42	-0.86	2.07	2.38	-1.74	0.61	0.05	0.27
Shadow area fraction: YZ plane (Spatial Descriptors)	1.12	-1.21	-0.85	0.89	0.29	-0.75	-0.53	0.38	-0.14	-1.51	0.05	0.54	-1.58	-0.75	1.88	0.30	0.47	0.25

Shadow area fraction: ZX plane (Spatial Descriptors)	-1.16	1.34	1.19	0.55	-1.68	-0.48	-0.67	0.27	0.03	-0.04	-1.40	-0.49	-0.50	-0.33	0.46	0.34	0.74	-1.08
Shadow length: LY (Spatial Descriptors)	1.05	-0.28	0.50	0.12	0.97	0.97	0.45	0.20	-0.34	-0.02	1.34	-0.08	-0.83	1.13	0.28	-0.09	-0.42	-3.36
Shadow length: LZ (Spatial Descriptors)	0.02	-0.24	-0.28	0.08	-1.14	0.68	0.02	-0.15	-0.11	0.24	-1.42	-1.32	0.41	1.56	0.01	0.90	-0.20	0.80
Shadow ratio (Spatial Descriptors)	0.23	0.83	0.64	-0.26	-0.81	-0.04	2.41	-2.96	-0.09	1.06	0.06	1.15	0.14	-1.26	1.08	0.00	-1.14	-0.34
Dipole moment (magnitude) (Spatial Descriptors)	0.97	-0.55	-0.97	0.72	-0.13	0.79	0.41	0.41	0.57	0.65	-1.24	-1.76	-1.19	-1.06	-1.12	-1.88	-0.82	1.57
Dipole moment X (Spatial Descriptors)	-0.75	0.52	0.22	-0.50	2.20	-1.02	2.19	-0.85	0.69	0.31	-0.75	-0.51	0.52	-0.22	-1.04	0.20	-1.24	-0.30
Dipole moment Y (Spatial Descriptors)	0.67	0.26	-0.45	0.40	-0.26	0.06	-0.02	0.07	-0.18	0.21	0.77	0.33	-0.12	1.01	0.31	-0.02	-0.22	-0.62
Dipole moment Z (Spatial Descriptors)	0.26	0.39	0.07	-0.27	-0.02	-0.53	-0.50	0.77	0.77	-0.15	-1.03	-0.53	0.94	0.21	-0.53	-0.75	0.00	-0.05
PNSA1 (Jurs Descriptors)	0.16	-1.20	1.53	-0.68	0.51	1.11	-0.11	1.16	0.26	-0.65	-1.74	-1.37	0.86	-2.64	0.56	0.65	-0.26	-0.43
PNSA2 (Jurs Descriptors)	-0.02	0.36	1.22	-2.40	-0.65	0.74	1.29	1.00	-1.14	1.65	0.43	-0.32	-1.65	1.71	1.91	-1.04	-1.47	-1.49
PPSA3 (Jurs Descriptors)	-0.36	0.16	0.21	0.32	0.43	-0.04	0.73	1.19	-0.56	2.13	0.50	0.68	-1.55	-2.73	0.03	-0.85	-0.16	-2.46
PNSA3 (Jurs Descriptors)	0.06	-0.55	0.71	0.46	-1.81	0.29	0.78	-1.40	2.60	1.29	-0.71	3.22	0.71	0.36	1.04	1.21	1.02	0.41
DPSA3 (Jurs Descriptors)	-0.23	-0.05	0.82	-1.66	-0.87	0.11	-1.56	0.98	-1.36	1.22	-0.72	-0.91	1.59	0.34	0.27	-1.44	1.81	1.42
FPSA1 (Jurs Descriptors)	-0.22	-0.05	0.28	-0.63	1.12	-0.11	-0.89	-0.48	-0.24	-3.38	0.43	-0.08	0.45	1.85	-0.59	-2.15	1.12	0.44
FPSA3 (Jurs Descriptors)	-0.28	0.64	0.09	0.78	-0.12	-0.97	0.22	-0.42	0.96	0.11	-1.38	-0.22	-0.75	-0.72	-0.37	0.76	-0.63	-0.33
FNSA2 (Jurs Descriptors)	0.18	2.40	0.29	2.54	1.30	-0.79	-1.47	-0.25	1.04	-0.77	0.94	-0.84	-1.17	-0.46	0.22	1.41	0.56	-0.54
WNSA1 (Jurs Descriptors)	0.00	0.14	-0.86	0.04	0.72	-0.56	-0.34	0.03	-0.21	0.63	-0.20	-1.00	-1.15	0.28	1.05	-1.56	1.46	-1.78
WNSA2 (Jurs Descriptors)	0.26	0.77	-0.51	1.58	-0.74	1.62	-1.88	0.97	0.05	1.12	-1.07	-0.18	1.02	-0.61	-0.50	0.70	0.02	0.19
WNSA3 (Jurs Descriptors)	-0.40	1.27	0.42	0.46	2.26	0.35	0.86	1.57	-0.10	-0.48	3.09	-0.08	-2.05	-1.04	-0.50	-0.25	-1.68	0.46
TPSA (Jurs Descriptors)	-1.39	0.54	0.48	-0.41	0.86	-0.04	0.09	0.79	0.61	-0.61	-1.16	0.37	1.54	0.24	0.50	0.05	0.22	-1.36
Temperature (K)	-0.01	-0.01	-0.04	0.00	-0.03	0.01	-0.03	0.03	-0.20	0.00	0.06	-0.02	-0.01	0.00	-0.01	0.00	-0.01	0.13
Bias	-0.44	1.23	0.38	0.13	0.72	-0.50	1.14	-0.81	-4.59	1.87	0.65	0.43	-0.33	1.21	1.03	0.05	0.61	3.49

Table B2: Artificial neural network hidden layer weightings for τ_{ji}

Node	1	2	3	4	5	6	7	8	9	10	11	12	13	14	15	16	17	18
AlogP (Fast Descriptors)	-0.38	0.62	1.32	0.56	0.55	-0.84	-0.13	0.45	-0.58	0.83	-1.62	1.99	-1.06	0.18	-0.58	-0.05	0.53	-0.31
Balaban index JX (Fast Descriptors)	-1.35	-0.48	-0.50	-1.21	0.72	0.09	0.56	0.19	0.75	-0.50	0.29	-1.40	-1.50	-1.17	0.99	-0.37	-0.51	-1.07
Wiener index (Fast Descriptors)	1.02	0.79	0.01	-2.49	0.05	0.22	-0.08	1.78	-0.93	-0.30	0.53	-1.58	0.03	-1.71	1.68	-1.50	0.86	0.73
Molecular density (Spatial Descriptors)	2.53	1.14	-0.11	1.08	-1.03	-1.98	1.15	1.12	-0.48	-2.98	-0.57	-0.99	-0.74	-1.61	-0.96	-1.61	-1.50	0.97
Principal moments of inertia (magnitude) (Spatial Descriptors)	0.86	-1.19	2.31	1.04	-0.18	0.23	1.03	-0.27	-0.51	-0.40	-0.34	0.16	-0.53	2.28	0.35	0.64	-0.30	-0.21
Principal moment of inertia X (Spatial Descriptors)	2.28	-1.44	0.44	0.51	-0.76	0.05	-1.00	-1.82	-0.13	-0.74	-0.76	-0.02	1.19	-0.01	-0.25	1.32	-0.07	-0.26
Ellipsoidal volume (Spatial Descriptors)	-1.71	0.45	-0.84	0.55	1.23	0.92	-1.87	-2.14	0.27	-0.56	-2.06	-0.33	0.23	1.24	-1.54	0.78	-1.46	-0.50
Shadow area: YZ plane (Spatial Descriptors)	0.82	0.98	0.45	0.01	-0.26	-0.69	1.86	0.67	-0.29	0.47	0.17	0.16	0.87	0.05	-0.95	-1.44	1.34	0.07
Shadow area fraction: XY plane (Spatial Descriptors)	-1.33	0.66	-0.27	0.71	0.34	2.38	-1.47	-2.29	-0.41	0.98	-1.03	1.04	-0.12	0.73	-0.95	0.84	-0.60	-0.77
Shadow area fraction: YZ plane (Spatial Descriptors)	1.41	-0.31	-0.86	-0.77	-0.86	0.25	-1.86	0.22	-1.96	-0.51	-0.06	-1.54	0.25	0.12	2.19	-0.50	0.93	0.06
Shadow area fraction: ZX plane (Spatial Descriptors)	-0.89	-0.69	0.36	-0.09	-0.02	-0.14	0.85	0.09	1.71	-0.22	1.23	0.18	-0.69	-0.43	0.95	-0.19	0.29	-0.26
Shadow length: LY (Spatial Descriptors)	0.34	-2.03	0.28	-0.67	0.94	-0.35	1.43	0.73	0.15	0.12	-0.50	-0.10	-0.98	-0.90	-0.98	0.16	1.48	1.05

Shadow length: LZ (Spatial Descriptors)	0.68	-0.65	-0.88	0.47	-0.03	0.48	-2.22	-0.43	-0.97	-0.08	-1.03	0.22	0.45	-0.09	-1.21	0.55	-0.69	-0.64
Shadow ratio (Spatial Descriptors)	0.20	1.04	-0.01	-0.34	0.29	0.08	0.13	0.47	-0.04	1.51	1.43	1.31	-0.32	-0.25	1.27	1.07	-0.56	-0.08
Dipole moment (magnitude) (Spatial Descriptors)	-0.21	-0.36	0.68	-0.27	1.39	-0.67	0.08	0.51	0.57	0.85	0.13	1.64	-0.52	0.88	0.78	0.74	-0.07	0.13
Dipole moment X (Spatial Descriptors)	0.88	0.65	0.32	-1.14	-0.38	-0.59	-0.47	0.70	-1.20	0.36	0.69	0.34	-0.11	-0.12	1.33	-0.21	-0.59	-0.25
Dipole moment Y (Spatial Descriptors)	1.83	0.05	0.70	0.63	0.42	0.89	0.82	-0.64	1.19	0.09	-0.54	0.93	1.00	-0.06	0.11	0.20	-0.68	-0.31
Dipole moment Z (Spatial Descriptors)	-0.64	0.79	-1.20	0.61	0.34	0.55	-0.83	-0.39	0.96	-0.37	-0.74	-0.63	-0.16	0.18	1.19	-0.11	-0.72	0.14
PNSA1 (Jurs Descriptors)	0.13	3.34	1.82	-0.44	-0.47	-1.03	-1.31	1.61	-1.93	0.23	-0.65	1.04	-2.06	-0.52	-1.49	0.19	-1.60	1.27
PNSA2 (Jurs Descriptors)	0.40	-0.74	-1.10	-0.02	0.61	-0.64	0.81	0.66	-0.45	0.60	-0.09	-1.58	-3.04	1.27	-0.50	-1.88	0.08	0.99
PPSA3 (Jurs Descriptors)	0.82	-1.48	-0.66	0.07	-0.25	-0.51	-1.09	-1.35	1.08	2.02	-1.61	2.53	-0.30	-0.29	-0.34	-0.30	-0.02	-0.18
PNSA3 (Jurs Descriptors)	2.33	-0.43	-0.45	0.24	-0.08	-0.29	0.13	-0.28	0.01	1.89	1.40	2.59	0.05	-0.68	1.42	0.28	-0.28	0.46
DPSA3 (Jurs Descriptors)	-1.37	2.03	-0.91	-0.06	0.32	0.34	-2.06	-0.23	-0.45	-1.69	0.67	-0.51	1.60	1.23	-0.66	-0.10	-1.49	-0.21
FPSA1 (Jurs Descriptors)	-1.41	0.19	-0.99	-0.17	0.51	-0.84	-0.16	0.42	1.39	0.82	1.53	-0.92	2.22	1.78	0.39	1.11	-1.21	-0.88
FPSA3 (Jurs Descriptors)	0.57	1.95	0.33	0.32	-0.23	0.34	1.54	0.38	1.10	0.83	0.88	0.37	0.11	0.01	1.00	-1.27	-0.52	-0.92
FNSA2 (Jurs Descriptors)	-1.80	-0.88	0.56	-0.77	-0.43	-1.10	-2.02	-0.21	0.30	-0.77	1.33	0.29	-0.24	-0.38	-0.66	0.09	0.51	-2.46
WNSA1 (Jurs Descriptors)	0.19	1.42	1.25	-0.33	-0.22	1.49	1.35	-0.68	0.18	-0.32	-0.64	0.67	0.32	0.53	0.03	-1.19	-1.49	-0.31
WNSA2 (Jurs Descriptors)	0.26	1.03	-0.18	0.98	-0.14	0.38	0.87	-0.56	0.30	0.64	1.71	-0.72	1.66	-0.16	1.38	1.54	1.01	0.21
WNSA3 (Jurs Descriptors)	-3.12	1.16	-0.11	0.84	-0.11	0.68	0.41	1.08	1.42	-0.62	-2.05	-1.40	0.39	-0.44	1.33	0.67	-0.73	0.57
TPSA (Jurs Descriptors)	-0.67	1.09	-0.57	0.07	0.35	-0.35	1.05	0.55	1.12	0.57	-1.70	-1.05	0.34	-0.55	-1.39	0.48	-1.35	-0.15
Temperature (K)	-0.05	0.00	0.01	-0.03	0.03	0.02	0.01	0.01	0.00	-0.03	0.03	-0.03	-0.02	0.02	0.09	0.03	0.02	0.06
Bias	0.80	-1.15	0.53	-0.93	1.24	-0.94	1.31	0.97	0.36	1.06	-0.83	0.99	-0.03	-0.45	1.53	0.62	0.41	1.28

Table B3: Artificial neural network output layer weightings

Output Hidden Layer Weights	τ_{ij}	τ_{ji}
Hidden Layer 1 Node 1	3.217	2.184
Hidden Layer 1 Node 2	4.409	4.088
Hidden Layer 1 Node 3	-4.417	-4.206
Hidden Layer 1 Node 4	-5.775	-4.208
Hidden Layer 1 Node 5	-2.084	-5.339
Hidden Layer 1 Node 6	3.162	2.833
Hidden Layer 1 Node 7	4.306	2.883
Hidden Layer 1 Node 8	3.361	3.813
Hidden Layer 1 Node 9	2.288	3.134
Hidden Layer 1 Node 10	-3.704	-4.948
Hidden Layer 1 Node 11	-2.912	-3.128
Hidden Layer 1 Node 12	3.108	4.215
Hidden Layer 1 Node 13	-4.229	-3.548
Hidden Layer 1 Node 14	-1.829	4.191
Hidden Layer 1 Node 15	-2.530	-1.801
Hidden Layer 1 Node 16	3.210	4.564
Hidden Layer 1 Node 17	3.637	4.654
Hidden Layer 1 Node 18	-2.521	-4.400
Bias	2.004	-1.311

Table B4: QSPR descriptors for chemicals used in input vector

Chemical	x_1	x_2	x_3	x_4	x_5	x_6	x_7	x_8	x_9	x_{10}	x_{11}	x_{12}	x_{13}	x_{14}	x_{15}	x_{16}	x_{17}	x_{18}	x_{19}	x_{20}	x_{21}	x_{22}	x_{23}	x_{24}	x_{25}	x_{26}	x_{27}	x_{28}	x_{29}	x_{30}
1,2-Dimethoxybenzene	1.54	2.83	3.01	117	1.03	881	323	183.5	23.1	0.66	0.67	0.77	8.29	4.19	2.15	1.67	-0.01	1.67	0.00	96.0	33.7	-23.2	56.8	0.72	0.10	-0.54	32.7	-63.0	-7.9	37.8
1,2-Ethanediol	-0.71	1.83	2.02	10	1.00	144	34	30.7	16.6	0.72	0.61	0.65	5.18	5.21	1.13	3.66	-1.08	3.31	-1.11	70.1	30.4	-42.3	72.7	0.66	0.15	-0.47	14.6	-20.2	-8.8	128.1
1,2-Propylene glycol 1-monobutylether	1.19	2.61	2.79	114	0.90	1592	89	118.8	18.9	0.68	0.64	0.69	5.78	5.16	2.49	3.91	2.26	3.18	0.02	51.8	49.2	-29.3	78.5	0.86	0.13	-0.37	19.3	-51.5	-10.9	65.3
1-Butanol	0.94	2.13	2.21	20	0.85	373	29	50.2	15.2	0.71	0.77	0.75	4.63	4.25	2.02	3.44	3.21	-0.64	-1.05	45.6	38.5	-27.6	66.2	0.82	0.15	-0.32	11.8	-21.2	-7.2	66.1
1-Dodecanol	4.11	2.74	2.76	364	0.83	6318	78	160.5	15.0	0.77	0.78	0.82	4.58	4.19	4.61	4.70	4.25	-2.00	0.00	42.6	77.3	-25.5	102.8	0.92	0.15	-0.35	21.9	-91.5	-13.1	69.7
1-Heptanol	2.13	2.50	2.54	84	0.84	1500	47	88.0	16.2	0.72	0.79	0.80	4.85	4.23	2.94	4.40	4.23	-0.52	-1.09	46.4	52.5	-28.0	80.4	0.87	0.15	-0.36	16.4	-44.4	-9.9	66.4
1-Nonanol	2.92	2.62	2.66	165	0.84	2900	60	115.6	16.2	0.74	0.79	0.82	4.82	4.22	3.55	5.00	-4.85	-0.59	1.09	48.9	61.9	-28.7	90.6	0.88	0.15	-0.39	20.4	-67.7	-12.0	69.7
1-Octanol	2.53	2.56	2.60	120	0.84	2124	54	105.6	15.3	0.75	0.79	0.81	4.61	4.22	3.25	4.71	-4.54	0.65	-1.10	45.6	57.3	-27.3	84.6	0.88	0.15	-0.36	17.6	-52.8	-10.5	65.7
1-Propoxy-2-propanol	0.79	2.56	2.77	79	0.91	1124	78	130.9	19.6	0.68	0.64	0.69	5.81	5.26	2.19	2.85	0.84	-2.64	-0.65	50.6	45.5	-28.1	73.6	0.85	0.13	-0.34	17.4	-40.9	-9.7	72.3
2,2-Dimethyl-1-propanol	1.45	3.11	3.19	28	0.84	311	116	62.6	25.7	0.65	0.66	0.56	5.79	6.73	1.35	2.06	1.73	0.70	0.88	39.9	35.9	-21.4	57.3	0.86	0.13	-0.26	11.0	-19.9	-5.9	67.6
2,4-Dimethyl-3-pentanone	2.76	3.58	3.67	65	0.87	606	163	106.6	26.3	0.72	0.71	0.72	6.56	5.64	1.58	2.86	0.25	-1.14	2.61	51.3	37.2	-23.0	60.2	0.84	0.12	-0.37	16.5	-38.1	-7.4	51.3
2,4-Pentanedione	0.79	3.19	3.36	48	1.01	487	82	74.8	15.5	0.70	0.69	0.73	5.31	4.24	2.15	5.65	0.00	5.65	0.02	89.0	25.8	-34.3	60.1	0.68	0.09	-0.53	24.7	-40.8	-9.5	99.8
2-Ethylpyridine	1.53	2.78	2.85	64	0.96	548	107	100.3	21.8	0.64	0.61	0.58	6.59	5.44	1.76	0.91	0.16	0.84	-0.32	64.9	27.3	-13.8	41.1	0.78	0.09	-0.30	19.2	-26.0	-4.1	30.8
2-Methyl-1-propanol	0.95	2.47	2.56	18	0.85	255	67	59.7	21.1	0.63	0.64	0.64	6.30	5.22	1.49	2.33	-1.78	-0.86	-1.24	39.9	36.1	-23.1	59.2	0.84	0.14	-0.26	10.1	-16.6	-5.9	67.1
2-Methyl-3-buten-2-ol	0.97	3.36	3.47	28	0.89	281	106	72.0	23.8	0.58	0.62	0.67	6.72	5.70	1.33	2.44	-0.65	1.39	-1.89	66.2	29.1	-28.1	57.1	0.75	0.11	-0.42	17.6	-30.0	-7.5	78.2
2-Methylphenol	2.23	3.09	3.15	60	1.01	475	161	96.3	20.1	0.72	0.66	0.71	7.37	4.17	1.82	1.85	-1.50	1.09	-0.01	85.2	30.3	-25.6	56.0	0.70	0.11	-0.47	24.1	-37.2	-7.2	63.1
2-Methylpropanal	0.61	2.75	2.85	18	0.89	218	67	53.1	21.7	0.64	0.65	0.61	6.37	5.27	1.34	3.58	3.43	0.34	-0.96	55.6	27.6	-25.7	53.4	0.77	0.11	-0.32	13.5	-18.8	-6.2	66.0
2-Methylpropanoic acid	1.02	3.10	3.31	29	0.98	308	99	71.4	22.9	0.57	0.62	0.64	6.75	5.49	1.37	3.74	3.63	-0.57	0.69	80.3	34.8	-44.0	78.9	0.69	0.13	-0.63	21.0	-43.4	-11.5	110.3
2-Methyltetrahydrofuran	0.75	2.09	2.21	26	0.92	279	76	56.3	21.3	0.69	0.70	0.70	5.95	5.11	1.43	2.08	-0.84	1.57	-1.07	32.6	27.9	-13.9	41.9	0.88	0.11	-0.17	8.6	-12.1	-3.7	32.6
2-Nonanol	2.94	2.74	2.78	158	0.84	2466	94	170.4	19.0	0.71	0.64	0.72	5.78	5.14	2.81	2.35	1.09	1.62	1.31	38.7	58.7	-21.8	80.5	0.91	0.14	-0.30	15.9	-51.6	-9.0	71.7
2-Nonanone	2.99	2.80	2.85	158	0.86	2390	82	135.6	17.3	0.69	0.77	0.81	5.33	4.19	3.43	4.36	3.34	-2.80	-0.03	56.5	51.9	-25.7	77.6	0.86	0.13	-0.42	22.8	-68.2	-10.4	62.3
2-Propenoic acid butyl ester	1.08	2.96	3.24	50	1.00	593	61	71.0	17.6	0.63	0.72	0.71	5.86	4.18	2.42	2.18	1.12	-1.87	0.01	90.1	34.3	-33.8	68.1	0.69	0.12	-0.57	26.2	-48.2	-9.8	85.8
3,3-Dimethyl-2-butanone	2.24	3.72	3.82	42	0.88	382	155	69.6	27.8	0.68	0.67	0.60	6.17	6.75	1.25	3.32	2.43	-2.26	-0.09	59.5	30.5	-26.5	57.0	0.79	0.11	-0.41	17.1	-33.7	-7.6	60.9
3,4-Dimethylpyridine	1.67	3.09	3.15	60	0.96	476	161	97.0	21.6	0.70	0.68	0.71	7.57	4.18	1.82	1.62	1.48	0.64	0.00	53.1	25.1	-16.3	41.4	0.81	0.09	-0.24	15.1	-19.3	-4.6	40.0
3,5,5-Trimethyl-2-cyclohexen-1-one	2.65	2.77	2.81	109	0.94	790	335	161.2	33.7	0.63	0.67	0.63	8.08	6.23	1.43	4.54	-1.85	4.15	0.01	77.3	34.7	-32.0	66.7	0.77	0.10	-0.49	26.2	-56.6	-10.8	68.6
3,5-Dimethylpyridine	1.67	3.03	3.09	61	0.96	520	139	96.3	18.8	0.68	0.69	0.72	6.53	4.19	2.18	1.47	0.00	-1.47	0.03	51.5	27.6	-17.1	44.7	0.82	0.09	-0.23	15.1	-19.3	-5.0	42.8
3-Ethylpyridine	1.60	2.79	2.85	64	0.96	551	108	87.4	21.9	0.64	0.61	0.58	6.59	5.42	1.76	1.53	-1.05	1.07	-0.32	60.3	27.1	-15.4	42.5	0.79	0.09	-0.27	17.7	-23.0	-4.5	34.2
3-Heptanone	2.43	2.93	3.01	76	0.87	1054	68	79.1	16.8	0.67	0.75	0.79	5.35	4.18	2.84	2.77	0.88	2.63	0.08	46.2	43.9	-21.1	65.0	0.86	0.13	-0.33	15.7	-37.6	-7.2	50.8
3-Methylphenol	2.23	3.04	3.09	61	1.01	523	138	112.6	21.0	0.62	0.69	0.67	7.26	4.18	2.16	2.58	-1.98	1.60	-0.40	96.6	30.5	-29.6	60.0	0.66	0.11	-0.49	27.8	-40.8	-8.5	73.7
4-Ethylpyridine	1.60	2.79	2.84	64	0.96	551	109	97.4	22.5	0.67	0.61	0.59	6.81	5.41	1.64	1.79	-1.76	0.03	-0.34	55.6	26.6	-14.6	41.2	0.81	0.09	-0.24	16.3	-20.4	-4.3	35.3

4-Heptanol	2.22	2.87	2.94	75	0.84	1054	89	109.4	19.0	0.67	0.64	0.72	5.84	5.10	2.34	2.36	0.05	2.35	-0.06	37.9	49.8	-21.9	71.7	0.89	0.14	-0.30	13.0	-35.2	-7.5	87.8
4-Heptanone	2.43	2.99	3.08	75	0.87	1028	74	93.9	16.3	0.67	0.74	0.79	5.32	4.18	2.83	2.71	0.00	-2.71	-0.05	45.5	45.9	-21.7	67.6	0.87	0.13	-0.32	15.5	-37.6	-7.4	51.1
4-Methylphenol	2.23	2.99	3.05	62	1.01	564	93	78.3	18.1	0.67	0.65	0.71	6.64	4.18	2.17	2.87	2.79	-0.65	0.14	92.2	29.7	-30.0	59.6	0.68	0.10	-0.48	26.4	-39.0	-8.6	72.1
5-Methyl-2-hexanone	2.13	3.00	3.07	74	0.87	888	112	124.0	22.6	0.67	0.65	0.66	6.41	5.39	1.94	3.71	2.53	-2.55	0.95	58.7	38.5	-26.3	64.8	0.82	0.12	-0.40	19.4	-44.1	-8.7	63.7
Acetic acid benzyl ester	1.64	2.37	2.48	174	1.04	1500	161	186.9	26.1	0.65	0.64	0.60	6.83	5.95	1.94	3.54	-3.35	-0.21	-1.13	121.2	30.3	-33.1	63.4	0.66	0.08	-0.62	43.5	-80.1	-11.9	62.7
Acetonitrile	0.17	2.39	2.50	4	0.91	71	3	22.3	10.8	0.70	0.65	0.68	3.96	4.18	1.45	2.21	-2.21	0.10	0.02	67.5	16.8	-17.8	34.6	0.62	0.09	-0.23	12.0	-7.4	-3.2	94.1
Acrolein	0.30	2.63	2.77	10	0.96	161	10	38.9	12.0	0.63	0.67	0.75	5.24	3.40	2.09	3.57	3.44	0.94	0.01	92.9	18.4	-33.7	52.1	0.54	0.09	-0.40	18.9	-16.3	-6.9	96.3
Benzene	2.05	3.00	3.00	27	0.95	219	89	42.6	16.9	0.66	0.74	0.73	6.74	3.40	2.13	0.00	0.00	0.00	0.00	85.3	14.9	-8.3	23.1	0.64	0.06	-0.21	20.4	-11.8	-2.0	0.0
Benzonitrile	2.08	3.03	3.06	64	1.04	518	89	91.9	16.5	0.63	0.73	0.78	6.64	3.40	2.66	3.25	-3.25	0.00	0.02	126.1	17.4	-23.2	40.6	0.53	0.06	-0.36	34.2	-26.8	-6.3	57.7
Benzyl alcohol	1.51	2.80	2.84	64	1.01	553	108	102.8	21.9	0.65	0.60	0.61	6.91	5.25	1.66	3.33	-2.77	1.41	1.21	98.4	27.3	-26.9	54.2	0.65	0.10	-0.42	28.0	-34.0	-7.6	53.5
Butanoic acid butyl ester	2.10	2.91	3.10	150	0.91	2029	107	175.4	19.2	0.61	0.77	0.78	5.98	4.18	3.40	2.39	1.12	2.11	0.03	56.0	56.8	-28.6	85.4	0.86	0.14	-0.44	22.4	-70.1	-11.4	61.6
Butyraldehyde	0.44	2.33	2.42	20	0.89	295	34	44.1	16.4	0.74	0.81	0.73	4.87	4.18	1.83	3.70	-2.97	2.21	-0.02	53.4	29.9	-24.9	54.8	0.78	0.12	-0.31	13.1	-18.9	-6.1	67.4
Carbon disulfide	0.84	2.94	3.18	4	1.42	242	0	0.0	8.6	0.77	0.67	0.77	3.60	3.60	1.91	0.00	0.00	0.00	0.00	169.6	8.9	-30.1	39.0	0.13	0.05	-0.31	33.0	-11.7	-5.9	25.1
Cyclohexane	2.38	2.00	2.00	27	0.83	270	120	49.9	25.1	0.65	0.72	0.67	6.88	5.06	1.46	0.00	0.00	0.00	0.00	10.1	30.8	-2.5	33.2	0.96	0.11	-0.05	2.7	-4.0	-0.7	10.1
Cyclohexanol	1.32	2.09	2.13	42	0.91	411	121	77.0	25.4	0.66	0.71	0.65	6.75	5.26	1.54	2.89	-2.64	-0.78	0.87	33.8	37.6	-20.8	58.4	0.88	0.13	-0.24	9.5	-18.4	-5.8	56.0
Cyclohexanone	1.53	2.21	2.26	42	0.95	367	120	70.6	25.1	0.66	0.71	0.63	6.73	5.22	1.48	4.03	-3.88	0.01	-1.08	54.7	30.7	-24.8	55.6	0.80	0.11	-0.35	15.0	-26.2	-6.8	52.3
Cyclopentanol	0.92	2.14	2.20	26	0.92	289	79	55.0	22.6	0.65	0.67	0.67	6.57	5.11	1.38	3.30	3.19	-0.77	-0.35	38.7	32.3	-22.1	54.4	0.85	0.13	-0.24	9.9	-15.9	-5.7	60.3
Cyclopentanone	1.13	2.32	2.38	26	0.97	260	74	45.6	22.4	0.65	0.73	0.69	6.28	4.88	1.41	3.86	3.86	0.01	0.03	61.5	28.2	-27.0	55.2	0.76	0.11	-0.37	15.5	-23.5	-6.8	65.8
Decane	4.47	2.65	2.65	165	0.79	2868	61	112.7	15.9	0.74	0.80	0.83	4.78	4.18	3.76	0.01	0.01	0.00	0.00	20.3	61.8	-8.6	70.3	0.95	0.14	-0.15	8.8	-29.1	-3.7	20.3
Dibutyl ether	2.43	2.50	2.63	120	0.83	1947	63	132.4	16.9	0.68	0.80	0.79	5.03	4.19	3.38	1.43	0.00	1.43	0.00	27.5	54.2	-12.3	66.5	0.93	0.14	-0.19	10.9	-28.9	-4.9	26.1
Dibutylamine	2.21	2.54	2.61	120	0.81	2002	60	126.1	16.5	0.71	0.79	0.80	4.90	4.24	3.37	0.90	0.00	0.63	-0.65	23.9	57.0	-10.5	67.5	0.94	0.14	-0.18	9.4	-28.0	-4.2	35.8
Diethylene glycol	-0.87	2.25	2.51	56	1.01	943	33	70.3	15.4	0.71	0.79	0.78	4.66	4.19	2.46	0.80	0.00	0.80	0.00	78.2	43.7	-53.9	97.6	0.74	0.15	-0.52	23.5	-46.8	-16.2	126.5
Diethylene glycol monobutyl ether acetate	0.74	2.68	2.95	444	0.97	6389	105	241.4	18.2	0.66	0.78	0.79	5.53	4.20	4.49	5.63	-5.32	1.84	0.00	84.9	63.6	-42.7	106.3	0.83	0.12	-0.61	43.3	-157.8	-21.7	91.0
Dimethoxymethane	0.22	1.92	2.28	20	0.95	237	54	49.1	18.6	0.69	0.77	0.76	5.37	4.48	1.65	0.51	-0.05	-0.51	0.01	54.4	25.2	-22.3	47.4	0.78	0.10	-0.30	13.2	-17.8	-5.4	39.4
Dimethyl adipate	0.48	3.02	3.27	254	1.03	3372	109	104.5	17.8	0.66	0.74	0.79	5.77	4.19	3.61	0.05	0.02	0.02	0.04	113.3	51.8	-50.7	102.5	0.73	0.12	-0.91	47.2	-158.9	-21.1	104.6
Dipropylamine	1.42	2.38	2.47	56	0.81	961	39	67.6	15.7	0.72	0.78	0.79	4.73	4.28	2.72	0.86	0.00	-0.54	-0.67	26.2	48.0	-11.8	59.8	0.92	0.14	-0.18	8.8	-20.9	-4.0	37.5
Dipropylene glycol propyl ether	1.10	3.25	3.54	472	0.99	3067	863	562.7	41.2	0.62	0.68	0.69	10.07	6.03	1.91	5.46	-4.66	2.41	1.51	111.1	49.8	-43.6	93.4	0.78	0.10	-0.77	55.9	-194.7	-21.9	110.4
Dodecane	5.26	2.73	2.73	286	0.79	4912	74	141.6	16.0	0.75	0.80	0.84	4.75	4.22	4.33	0.01	0.01	0.00	-0.01	19.3	71.3	-8.3	79.6	0.96	0.14	-0.15	9.6	-37.5	-4.1	19.3
Epichlorohydrin	0.61	1.85	2.03	17	1.19	374	39	69.9	19.6	0.63	0.64	0.64	5.76	5.33	1.35	2.55	2.54	0.19	-0.22	118.0	18.6	-48.5	67.1	0.50	0.08	-0.47	28.1	-26.4	-11.5	104.5
Ethane	1.30	1.00	1.00	1	0.66	37	6	13.6	13.0	0.75	0.68	0.70	4.27	4.44	1.16	0.00	0.00	0.00	0.00	17.6	25.6	-8.3	33.9	0.90	0.14	-0.09	3.2	-3.0	-1.5	17.6
Ethanol	0.08	1.53	1.67	4	0.86	81	16	27.5	15.1	0.65	0.76	0.68	4.64	4.28	1.40	2.89	2.63	-0.65	1.00	46.3	28.1	-26.7	54.7	0.76	0.14	-0.27	9.1	-10.4	-5.2	65.6
Ethyl acetate	0.21	2.61	2.90	32	0.98	400	59	75.1	18.1	0.62	0.78	0.72	5.58	4.18	2.15	2.54	-1.81	-1.78	-0.01	65.0	32.4	-30.2	62.6	0.76	0.12	-0.41	17.8	-30.8	-8.3	73.0

Ethyl tert-amyl ether	1.66	3.24	3.42	67	0.84	607	217	167.0	32.8	0.61	0.66	0.64	7.88	6.28	1.39	1.04	-0.27	-0.20	-0.98	32.2	35.8	-12.1	47.9	0.90	0.11	-0.22	10.7	-23.7	-4.0	31.2
Ethylbenzene	2.91	2.83	2.83	64	0.91	558	111	100.6	22.7	0.64	0.61	0.59	6.84	5.40	1.77	0.28	0.27	0.01	0.08	72.2	26.6	-10.5	37.1	0.76	0.09	-0.30	21.6	-26.7	-3.1	9.9
Ethylene glycol monoethyl ether acetate	0.04	2.60	2.90	114	0.99	1538	75	123.2	17.5	0.65	0.76	0.76	5.51	4.19	3.02	4.48	2.87	-3.44	-0.10	75.3	42.1	-35.2	77.3	0.79	0.12	-0.49	27.1	-63.2	-12.6	81.8
Fluorobenzene	2.19	2.96	3.05	42	1.10	360	89	72.1	16.5	0.65	0.73	0.75	6.62	3.40	2.30	4.97	4.97	0.00	0.00	117.7	20.5	-35.4	56.0	0.53	0.08	-0.53	29.4	-32.9	-8.9	54.1
Formic acid propyl ester	0.47	2.30	2.55	35	0.97	504	38	63.3	15.5	0.74	0.79	0.73	4.67	4.18	2.15	3.36	-3.21	-0.99	-0.04	66.4	40.1	-34.6	74.7	0.75	0.15	-0.46	17.9	-33.3	-9.3	86.9
Furfural	0.85	2.81	3.01	43	1.15	390	62	65.4	14.4	0.69	0.72	0.77	5.88	3.40	2.38	3.59	-3.57	-0.36	0.00	100.8	23.6	-39.4	63.0	0.59	0.10	-0.52	24.9	-31.5	-9.7	94.7
Glycerol	-1.08	2.57	2.81	31	1.05	409	66	53.7	19.0	0.62	0.63	0.65	5.91	5.11	1.64	4.78	-1.77	3.49	2.74	90.0	38.3	-54.9	93.3	0.64	0.15	-0.71	22.8	-45.3	-13.9	170.6
Heptane	3.28	2.45	2.45	56	0.77	1010	43	76.0	15.0	0.74	0.78	0.80	4.56	4.18	2.84	0.06	0.00	-0.06	0.00	18.1	48.1	-7.8	55.9	0.95	0.14	-0.13	6.2	-14.8	-2.7	18.1
Hexadecane	6.84	2.83	2.83	680	0.80	11508	99	202.7	16.1	0.77	0.79	0.84	4.74	4.32	5.42	0.03	-0.02	0.00	-0.02	20.0	89.9	-8.5	98.4	0.97	0.14	-0.17	12.4	-63.6	-5.3	20.0
Hexane	2.88	2.34	2.34	35	0.76	648	36	59.4	16.2	0.70	0.81	0.79	4.82	4.18	2.52	0.00	0.00	0.00	0.00	18.6	42.9	-8.1	51.0	0.94	0.14	-0.13	5.7	-12.0	-2.5	18.6
Hexanoic acid ethyl ester	2.02	2.92	3.10	150	0.91	2075	98	162.1	18.7	0.61	0.76	0.78	5.91	4.19	3.39	2.35	-1.27	1.98	-0.03	57.3	54.1	-28.5	82.7	0.86	0.14	-0.44	22.8	-69.8	-11.4	62.6
Hexanoic acid methyl ester	1.68	2.84	3.02	110	0.92	1578	72	94.5	16.9	0.69	0.77	0.79	5.27	4.18	3.07	2.49	-2.01	1.47	-0.03	63.5	47.9	-29.3	77.1	0.82	0.13	-0.49	22.9	-63.0	-10.5	60.4
Hexylamine	1.39	2.43	2.45	56	0.81	1000	43	77.0	15.1	0.74	0.78	0.81	4.59	4.18	2.69	2.08	-2.07	-0.23	0.00	32.0	50.1	-17.8	67.9	0.90	0.15	-0.25	10.5	-26.4	-5.8	77.1
Isoamyl formate	1.20	2.67	2.86	79	0.93	904	116	133.4	25.4	0.58	0.68	0.69	6.74	5.51	1.75	4.24	3.96	-1.47	-0.29	71.1	44.0	-36.6	80.5	0.78	0.14	-0.52	22.6	-52.9	-11.6	92.1
Methanol	-0.27	0.88	1.04	1	0.86	30	4	14.5	11.2	0.69	0.63	0.66	4.25	4.18	1.12	2.81	-2.46	-1.28	-0.44	50.3	23.5	-26.8	50.3	0.69	0.14	-0.25	8.3	-6.8	-4.4	65.8
Methoxybenzene	1.79	2.76	2.86	64	1.00	566	99	107.7	19.2	0.61	0.66	0.69	6.96	4.18	2.29	1.34	-0.27	1.32	0.00	91.2	24.4	-17.0	41.4	0.68	0.09	-0.40	26.0	-32.8	-4.9	21.4
Methoxycyclopentane	1.20	2.07	2.16	43	0.90	472	87	78.1	22.4	0.62	0.68	0.70	6.54	5.04	1.75	1.86	-0.70	1.40	-1.01	35.2	32.7	-12.4	45.0	0.88	0.11	-0.21	10.3	-17.6	-3.6	23.1
Methyl acetate	-0.14	2.58	2.93	18	1.01	222	48	47.3	16.4	0.64	0.74	0.71	5.35	4.18	1.85	1.82	-0.78	1.65	0.01	76.0	24.6	-32.2	56.9	0.68	0.10	-0.45	18.1	-25.4	-7.7	72.2
Methyl diethyl amine	0.84	2.63	2.79	31	0.80	410	80	77.0	20.8	0.68	0.63	0.65	6.14	5.37	1.68	0.90	0.00	-0.15	0.88	24.5	33.6	-8.0	41.6	0.92	0.12	-0.14	7.1	-11.7	-2.3	22.3
Methyl propanoate	0.49	2.76	3.06	31	0.98	394	52	48.3	16.6	0.64	0.73	0.74	5.42	4.18	2.17	1.50	-0.08	-1.50	0.00	65.7	33.6	-28.9	62.5	0.76	0.12	-0.44	17.8	-32.1	-7.8	60.8
Methyl tert-amyl ether (TAME)	1.32	3.23	3.40	44	0.84	412	189	115.2	29.6	0.68	0.69	0.68	7.03	6.06	1.24	1.38	0.33	0.24	-1.32	38.0	31.1	-13.1	44.2	0.87	0.10	-0.25	11.4	-22.2	-4.0	29.0
Methyl valerate	1.28	2.83	3.04	76	0.93	1051	66	75.6	16.6	0.67	0.75	0.77	5.34	4.18	2.78	2.04	-1.41	1.48	0.00	65.2	43.2	-29.6	72.8	0.80	0.13	-0.48	21.6	-52.9	-9.8	60.6
Methylcyclohexane	2.71	2.12	2.12	42	0.83	421	123	76.4	25.3	0.68	0.72	0.69	6.73	5.22	1.60	0.27	0.27	0.00	-0.01	15.2	34.7	-5.1	39.8	0.95	0.12	-0.09	4.5	-7.9	-1.5	15.2
Monoethanolamine	-1.06	1.86	2.01	10	0.93	193	18	36.6	15.8	0.64	0.77	0.67	4.80	4.29	1.76	1.72	-1.08	-1.01	-0.89	50.0	38.3	-32.3	70.5	0.77	0.17	-0.34	11.1	-16.8	-7.2	128.9
N,N-Dimethylformamide (DMF)	-0.74	2.60	2.89	18	0.96	219	57	53.3	18.3	0.65	0.71	0.73	6.20	4.18	1.64	3.76	-3.75	-0.28	0.00	64.9	28.9	-27.6	56.5	0.73	0.12	-0.38	15.5	-21.7	-6.6	81.8
N-Formylmorpholine	-1.09	2.07	2.26	64	1.06	539	124	95.0	25.7	0.67	0.66	0.60	7.02	5.51	1.43	2.39	1.73	-1.64	0.18	71.6	30.0	-34.8	64.8	0.75	0.11	-0.41	20.1	-32.2	-9.8	83.0
Nitrobenzene	2.00	2.85	3.02	88	1.17	668	122	102.7	16.5	0.72	0.73	0.77	6.62	3.40	2.53	7.17	-7.17	0.00	0.00	155.1	18.5	-33.1	51.7	0.44	0.07	-0.61	43.2	-47.3	-9.2	94.2
Nitroethane	0.38	2.53	2.95	18	1.11	199	50	42.9	17.7	0.66	0.61	0.58	5.38	5.34	1.30	5.61	-5.42	0.02	-1.45	102.9	19.7	-27.7	47.4	0.54	0.09	-0.43	23.1	-21.7	-6.2	99.8
Nitromethane	-0.08	2.40	2.93	9	1.19	101	37	28.6	13.6	0.71	0.64	0.67	5.11	4.18	1.26	4.72	4.72	-0.01	0.14	112.0	11.8	-25.4	37.1	0.42	0.06	-0.32	21.6	-12.0	-4.9	101.1
N-Methyl-2-pyrrolidone	-0.40	2.36	2.51	40	1.00	359	136	72.8	21.5	0.66	0.78	0.77	6.49	4.26	1.76	3.85	-2.04	3.25	0.28	61.4	31.7	-25.6	57.3	0.78	0.12	-0.40	16.8	-29.6	-7.0	61.9
Nonane	4.07	2.60	2.60	120	0.78	2106	56	103.1	15.0	0.76	0.78	0.82	4.57	4.18	3.45	0.06	0.01	-0.06	0.00	19.1	57.3	-8.1	65.4	0.95	0.14	-0.14	7.7	-23.1	-3.3	19.1
n-Undecane	4.86	2.69	2.69	220	0.79	3798	68	129.9	15.0	0.77	0.78	0.83	4.58	4.19	4.06	0.06	0.01	-0.06	0.01	19.3	66.7	-8.2	74.9	0.96	0.14	-0.15	9.0	-32.5	-3.8	19.3

Octane	3.67	2.53	2.53	84	0.78	1492	49	85.7	16.0	0.72	0.80	0.81	4.80	4.18	3.14	0.01	0.01	0.00	0.00	19.3	52.6	-8.3	60.9	0.95	0.14	-0.14	7.2	-19.5	-3.1	19.3
o-Nitrotoluene	2.47	3.03	3.19	114	1.13	767	217	153.7	23.1	0.66	0.70	0.72	7.90	4.16	2.08	6.84	-6.53	-2.05	-0.13	139.5	23.5	-33.9	57.4	0.54	0.08	-0.66	41.9	-59.3	-10.2	91.9
o-Xylene	2.98	3.13	3.13	60	0.92	483	164	96.4	21.5	0.72	0.68	0.71	7.56	4.18	1.82	0.20	0.20	0.00	0.00	70.5	24.7	-12.6	37.3	0.76	0.08	-0.30	20.6	-25.8	-3.7	16.7
Perfluorohexane	5.47	5.37	6.34	676	1.85	2914	890	129.9	32.4	0.69	0.73	0.74	6.85	6.49	1.55	0.47	-0.01	-0.01	0.47	367.7	0.0	-135.7	135.7	0.00	0.00	-5.26	135.2	-710.7	-49.9	367.7
Phenol	1.76	2.97	3.04	42	1.04	356	90	71.2	16.5	0.66	0.73	0.75	6.64	3.40	2.38	2.48	2.37	0.72	0.00	100.5	24.7	-28.1	52.8	0.61	0.10	-0.47	25.6	-30.5	-7.2	63.6
Propanoic acid propyl ester	1.30	2.81	3.05	76	0.93	1007	68	79.7	17.7	0.65	0.77	0.78	5.55	4.18	2.76	2.18	1.07	1.90	0.00	56.0	46.3	-28.1	74.4	0.83	0.14	-0.42	18.8	-47.1	-9.4	61.3
Propionitrile	0.80	2.38	2.45	10	0.89	155	18	39.6	15.7	0.62	0.79	0.69	4.76	4.18	1.72	2.61	-2.56	-0.51	0.04	67.6	23.5	-19.2	42.7	0.68	0.11	-0.31	14.5	-14.1	-4.1	86.9
Salicylaldehyde	1.44	3.08	3.17	86	1.11	637	196	116.2	20.4	0.61	0.74	0.78	8.06	3.40	2.57	4.52	-4.51	0.31	-0.01	121.5	30.2	-44.6	74.9	0.57	0.11	-0.71	34.4	-57.0	-12.6	115.8
sec-Butyl acetate	1.09	3.05	3.30	71	0.94	661	169	140.8	27.3	0.64	0.68	0.68	7.18	5.57	1.66	3.00	2.60	-0.87	-1.22	61.4	37.0	-27.9	64.9	0.81	0.11	-0.45	19.8	-47.3	-9.0	66.0
Styrene	2.70	2.99	2.99	64	0.95	545	98	102.9	18.3	0.64	0.73	0.76	6.97	3.61	2.66	0.17	-0.17	-0.02	0.03	109.9	19.6	-17.3	36.8	0.62	0.07	-0.36	31.7	-30.2	-5.0	28.0
Sulfolane	-0.66	2.49	2.75	39	1.16	411	143	75.7	26.0	0.66	0.66	0.74	6.85	5.77	1.20	6.72	-6.72	0.00	-0.01	102.4	26.0	-25.7	51.7	0.63	0.09	-0.45	28.2	-34.2	-7.1	94.6
Tetradecane	6.05	2.78	2.78	455	0.80	7747	86	168.2	15.8	0.76	0.79	0.85	4.73	4.20	4.97	0.01	0.01	0.00	0.01	21.3	80.8	-8.7	89.5	0.96	0.14	-0.17	11.9	-53.8	-4.9	21.3
Tetraethylene glycol	-1.20	2.53	2.83	364	1.02	5799	64	135.2	15.5	0.73	0.78	0.77	4.73	4.20	4.37	2.17	-0.01	2.17	0.00	88.3	67.0	-60.6	127.6	0.81	0.14	-0.61	42.1	-138.4	-28.9	146.6
Toluene	2.51	3.02	3.02	42	0.93	363	92	70.5	18.1	0.68	0.65	0.71	6.64	4.18	1.97	0.09	-0.07	-0.02	-0.04	77.8	20.7	-10.8	31.6	0.71	0.08	-0.26	21.1	-19.1	-2.9	9.9
Triethylamine	1.18	2.88	3.03	48	0.80	492	225	132.1	30.3	0.64	0.70	0.70	7.92	5.45	1.52	1.15	-0.04	0.00	-1.15	26.1	37.2	-10.5	47.7	0.92	0.12	-0.16	8.2	-16.2	-3.3	23.7
Triethylene glycol	-1.04	2.43	2.72	165	1.01	2688	48	111.0	15.9	0.71	0.78	0.77	4.77	4.24	3.37	2.20	-1.17	-1.45	1.17	82.5	55.7	-56.8	112.5	0.79	0.14	-0.56	32.2	-85.0	-22.1	136.4
Water	-0.51	0.00	0.00	0	0.91	2	1	2.2	6.5	0.68	0.65	0.65	3.32	3.04	1.30	1.94	1.11	1.12	1.12	53.6	23.1	-36.0	59.1	0.56	0.19	-0.29	6.5	-4.4	-4.4	122.2
1,4-butanediol	-0.21	2.24	2.37	35	0.94	640	31	63.4	16.2	0.68	0.78	0.74	4.87	4.25	2.26	2.19	-1.18	-1.44	1.14	67.4	44.2	-42.9	87.1	0.76	0.16	-0.49	18.6	-37.8	-11.9	115.5